PhD Thesis

Appendix

Dániel Bakonyi
dipl. arch. ing., assistant lecturer

Budapest University of Technology and Economics
Department of Building Constructions

Budapest, 2016

A (Appendix A) – Hot box measurements

A.1 Photos of the hot box apparatus

Fig. 1. – The components of the hot box before painting, assembly and instrumentation

Fig. 2. – The Holten window test rig before hot box installation

Fig. 3. – The pressurization (left) and temperature control (right) system of the window test rig

Fig. 4. – The control unit of the window test rig

Fig. 5. – The black painted baffle of the cold side chamber with the surface temperature sensors already installed

Fig. 6. – The cold side chamber being installed in the window test rig

Fig. 7. – The surround panel at a separate stand with the calibration panel being installed

Fig. 8. – Hoisting the surround panel into place with the crane

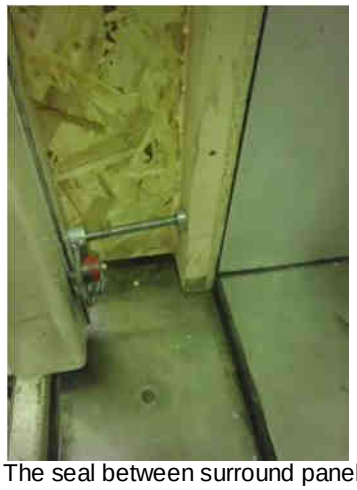

Fig. 9. – The seal between surround panel and the window test rig's wall with adjustable steel bolt

Fig. 10. – the warm side chamber (left) being moved into postition

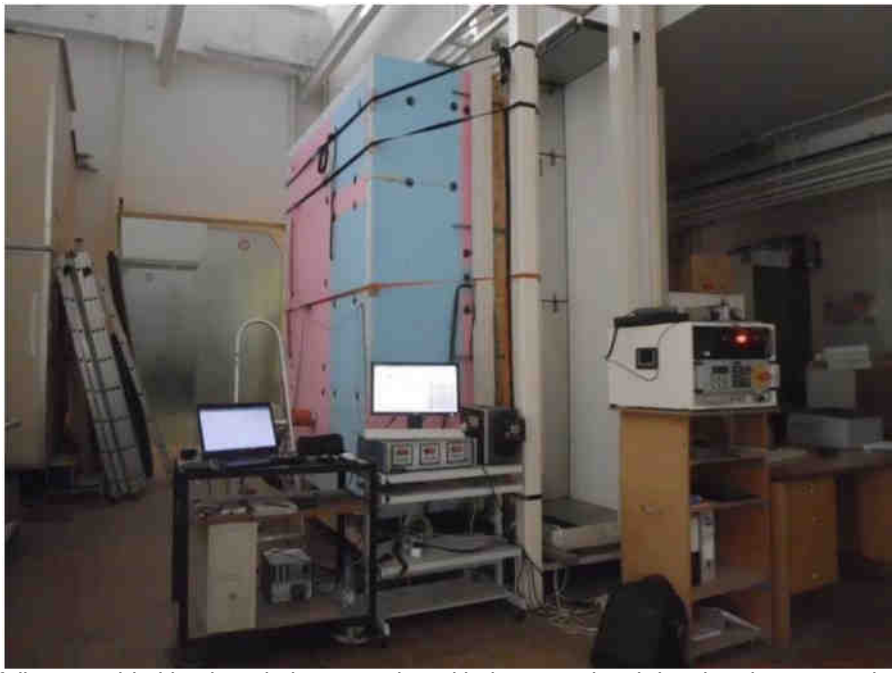

Fig. 11. – The fully assembled hot box during operation with the control and data logging system in the foreground

A.2 Test windows

A.2.1 Window 1

Fig. 12. – Window No. 1 – a typical early 20th century window with fix horizontal transom and a vertical mullion at the top (internal view)

Fig. 13. – Window No. 1 – external view with the roller shutter case not having been removed jet

A.2.2 Window 2

Fig. 14. – Window No. 2 – on a horizontal stand for temperature sensor installation

Fig. 15. – Window No. 2 – a typical mi 20th century box type window without transoms or mullions

A.2.3 Window 2b

Fig. 16. – Window No. 2b – installed in the aperture of the surround panel

Fig. 17. – Window No. 2b – during sensor installation

A.2.4 Window 2c

Fig. 18. – Window No. 2c – the single skin glulam frame being instaled into the old frame of window No. 2

Fig. 19. – Window No. 2c – during sensor installation

A.2.5 Window 3a

Fig. 20. – Window No. 3a – during airtightness testing in the window test rig

Fig. 21. – Window No. 3a – during temperature sensor installation

A.2.6 Window 3b

Fig. 22. – Window No. 3b – during temperature sensor installation

Fig. 23. – Window No. 3b – during installation

A.3 Airtightness measurements

Besides the bot box measurement standard test of airtightness/air permeability, wind resistance and watertightness test were also conducted on all of the test windows. These were not jet used in the current stage of the research documented in this thesis, nevertheless the data is documented here.

window	sashes	T [°C]	dP	a [m^3/hm^2Pa^n]	n [-]	R	class
window 1	all	0	+	6.37	0.821	0.990535	-
	all	20	+	11.79	0.68	0.998846	-
	all	20	-	6.37	0.821	0.990535	-
	external	20	+	20.71	0.667	0.994861	-
	external	20	-	17.91	0.678	0.986804	-
	internal	20	+	13.51	0.734	0.997992	-
	internal	20	-	20.67	0.62	0.992221	-
window 2	all	0	+	9.69	0.593	0.977102	-
	all	0	-	8.35	0.621	0.991531	-
	all	20	+	7.33	0.674	0.991290	-
	all	20	-	7.6	0.628	0.988858	-
	external	20	+	7.97	0.739	0.996978	-
	external	20	-	15.58	0.574	0.993571	-
	internal	20	+	6.0	0.743	0.996915	-
	internal	20	-	10.14	0.586	0.996933	-
window 2b	all	20	+	0.20	0.68	0.995403	III.
	all	20	-	0.05	1.009	0.992840	III.
window 2c	all	20	+	0.21	0.744	0.999299	III.
	all	20	-	0.37	0.608	0.995647	III.
window 3	all	20	+	0.33	0.654	0.997800	III.

A.3.1 Window 1

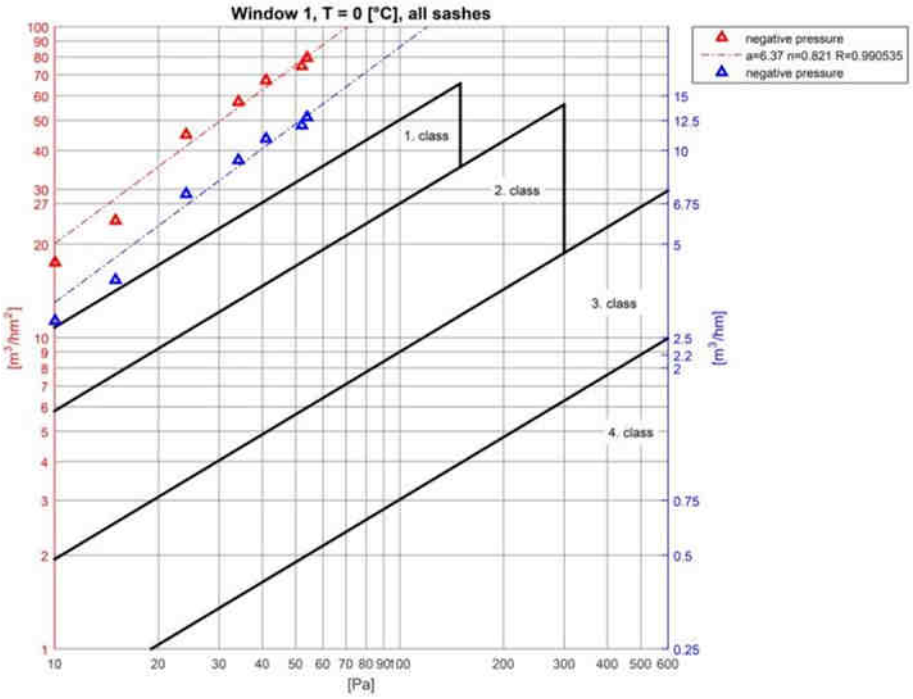

Fig. 24. – Window 1 – airtightness measurements, T=0 [°C], all sashes closed

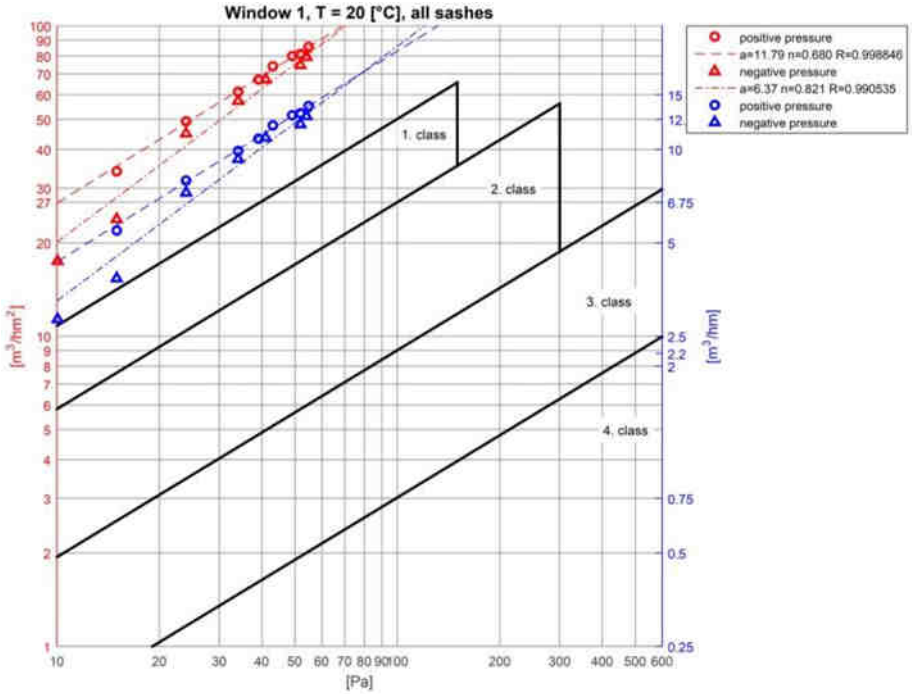

Fig. 25. – Window 1 – airtightness measurements, T=20 [°C], all sashes closed

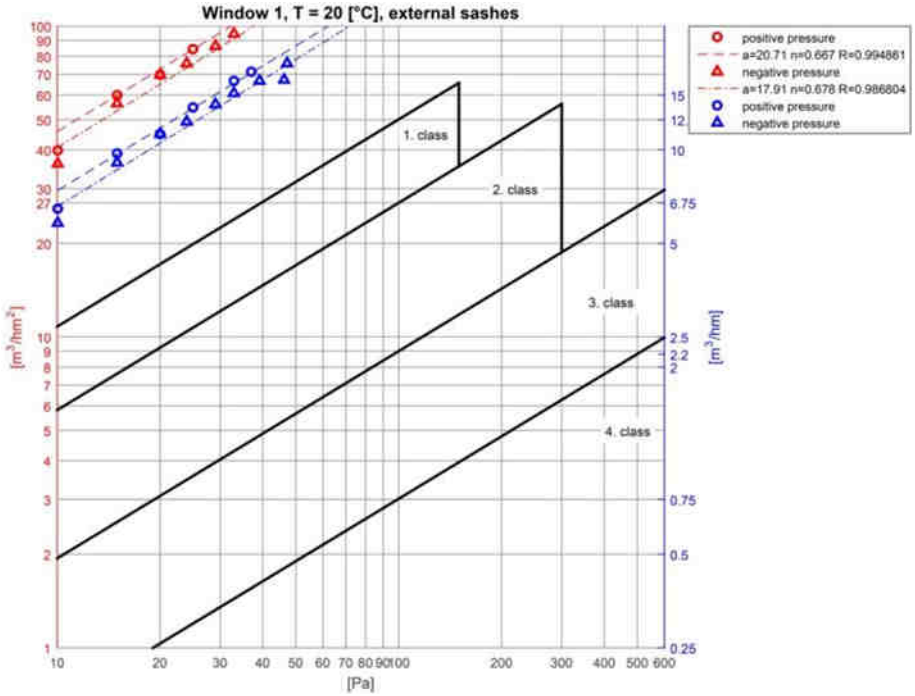

Fig. 26. – Window 1 – airtightness measurements, T=20 [°C], only external sashes closed

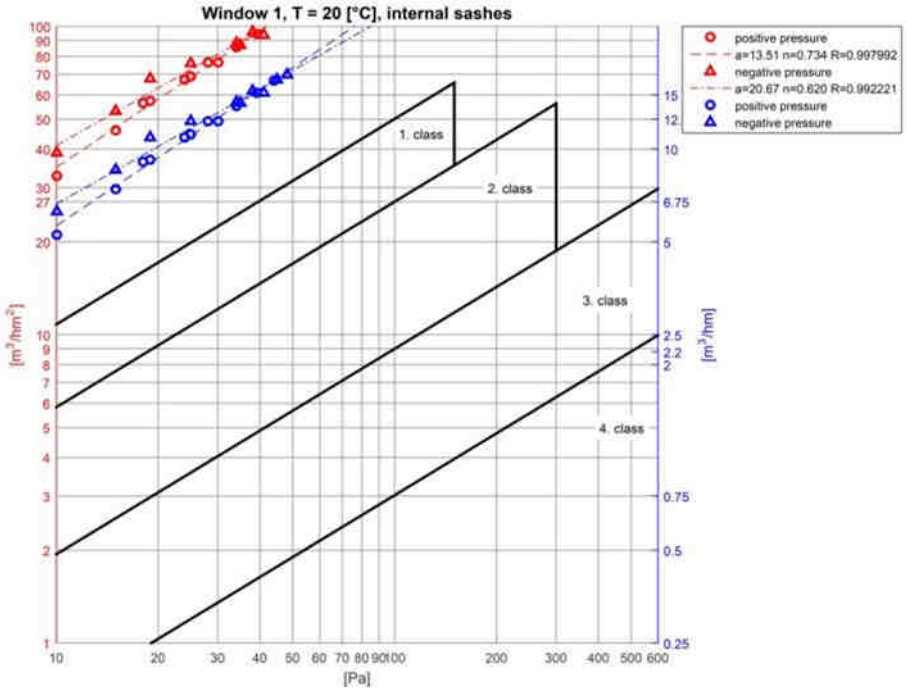

Fig. 27. – Window 1 – airtightness measurements, T=20 [°C], only internal sashes closed

A.3.2 Window 2

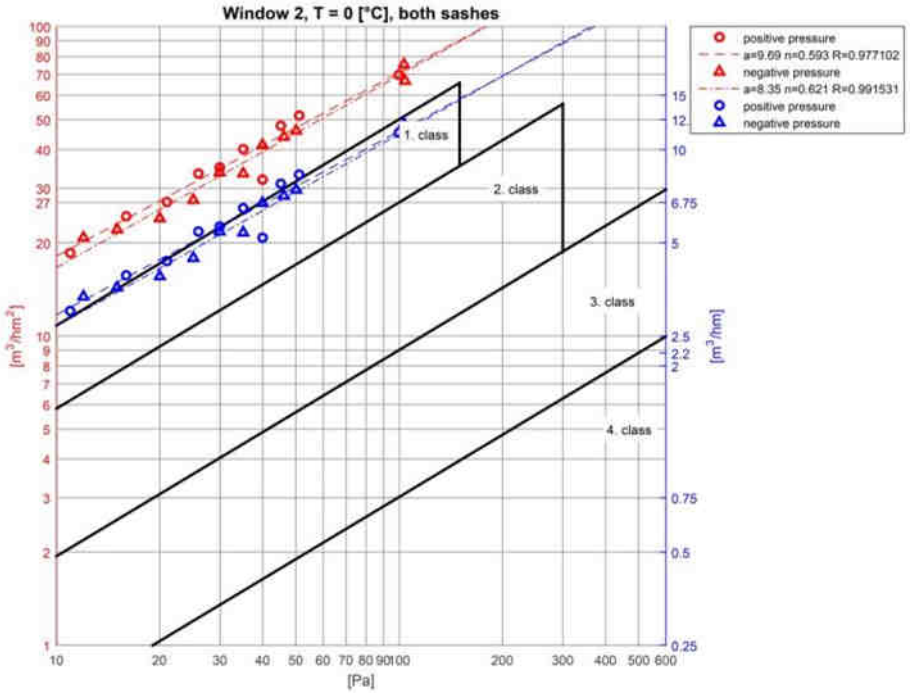

Fig. 28. – Window 2 – airtightness measurements, T=0 [°C], all sashes closed

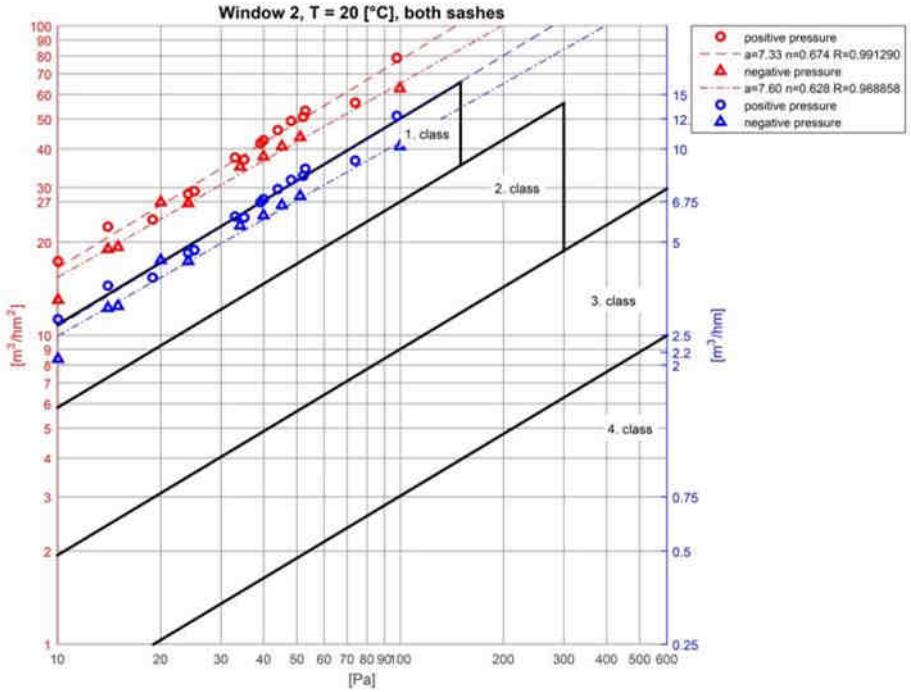

Fig. 29. – Window 2 – airtightness measurements, T=20 [°C], all sashes closed

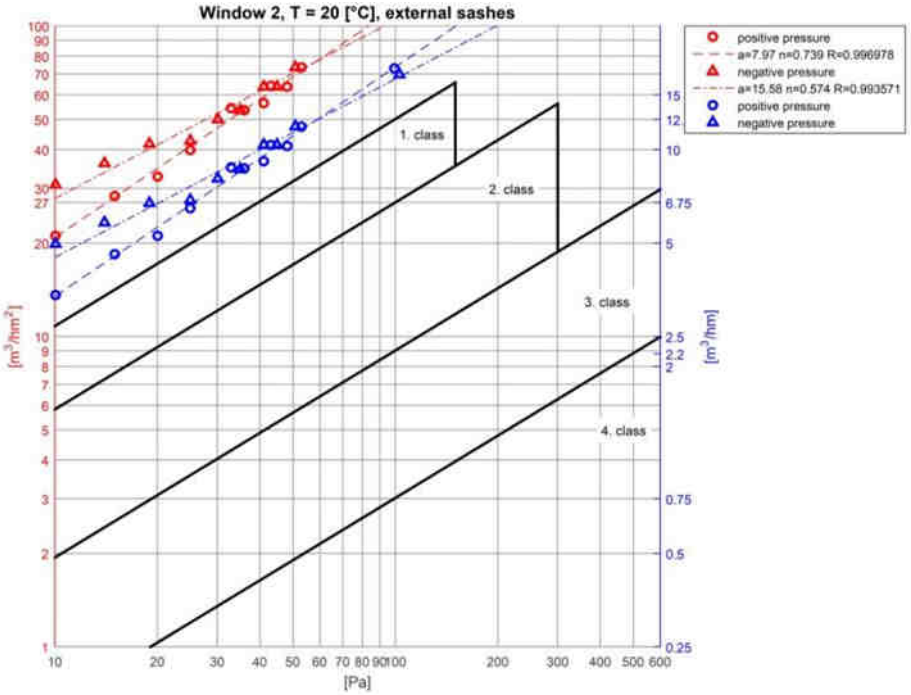

Fig. 30. – Window 2 – airtightness measurements, T=20 [°C], only external sashes closed

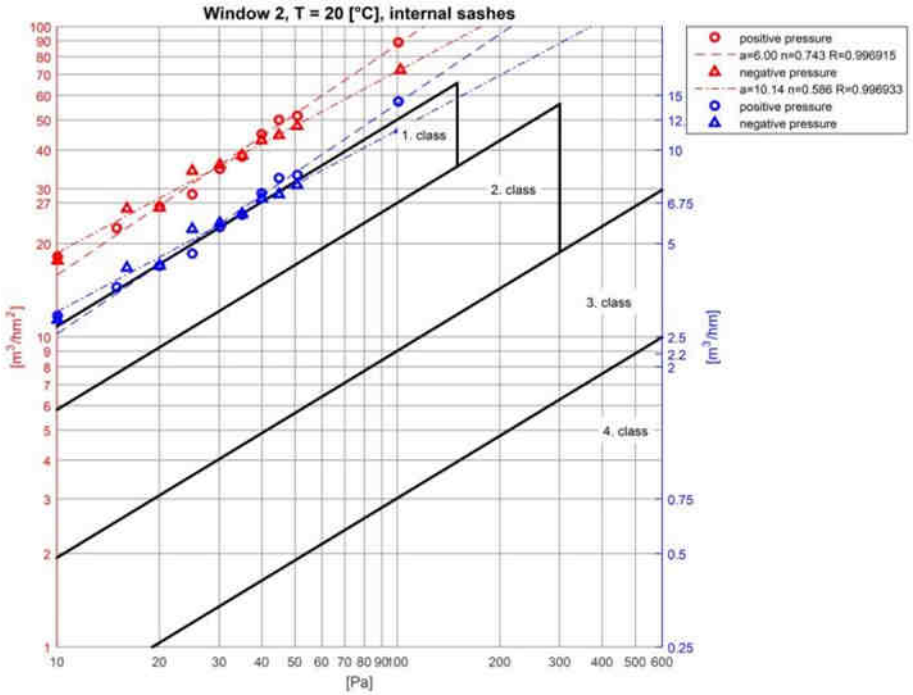

Fig. 31. – Window 2 – airtightness measurements, T=20 [°C], only internal sashes closed

A.3.3 Window 2b

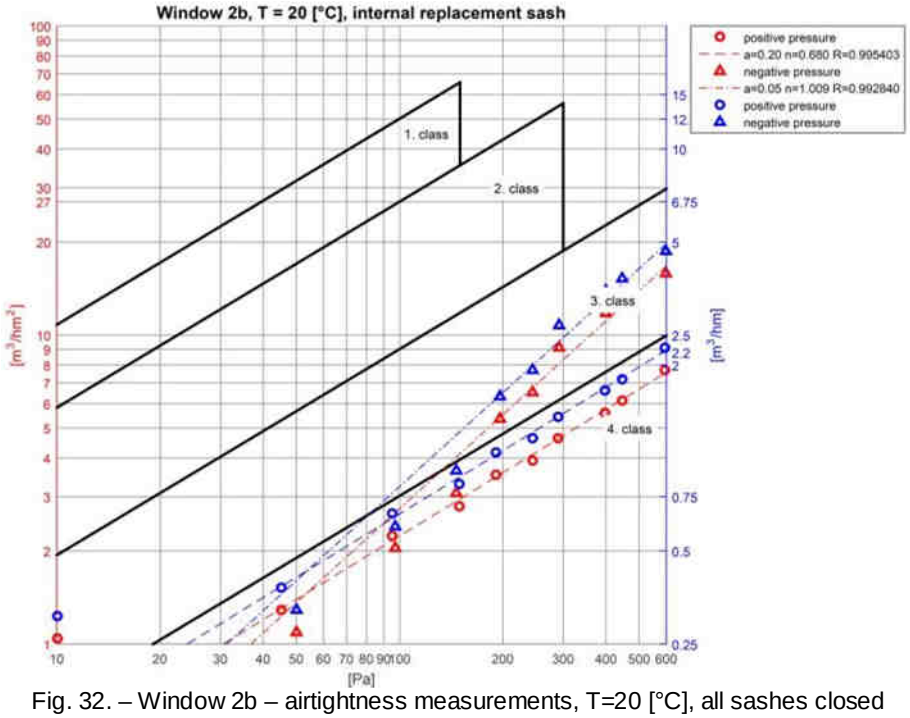

Fig. 32. – Window 2b – airtightness measurements, T=20 [°C], all sashes closed

A.3.4 Window 2c

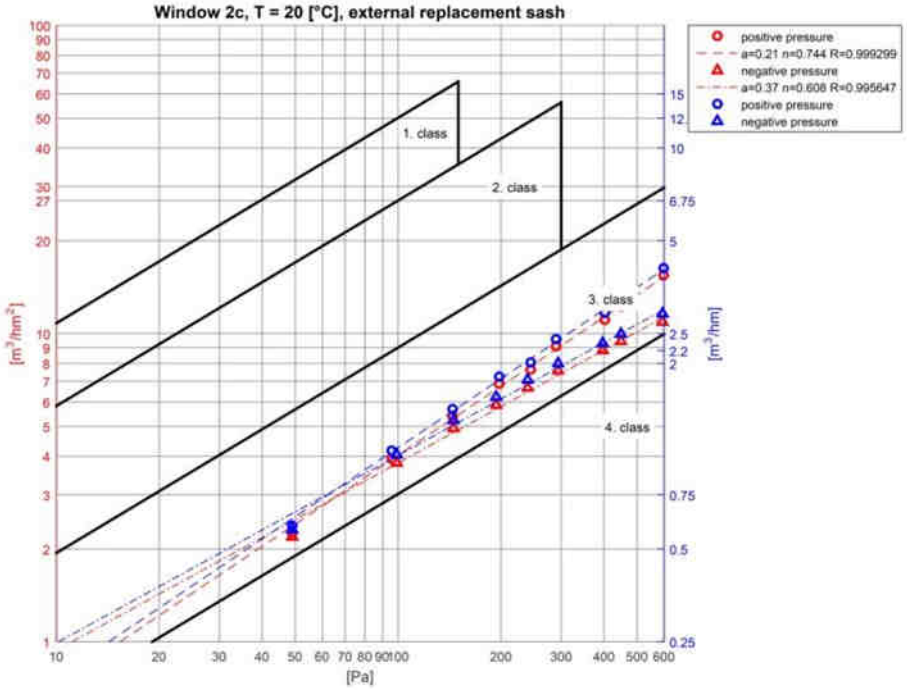

Fig. 33. – Window 2c – airtightness measurements, T=20 [°C]

A.3.5 Window 3a/b

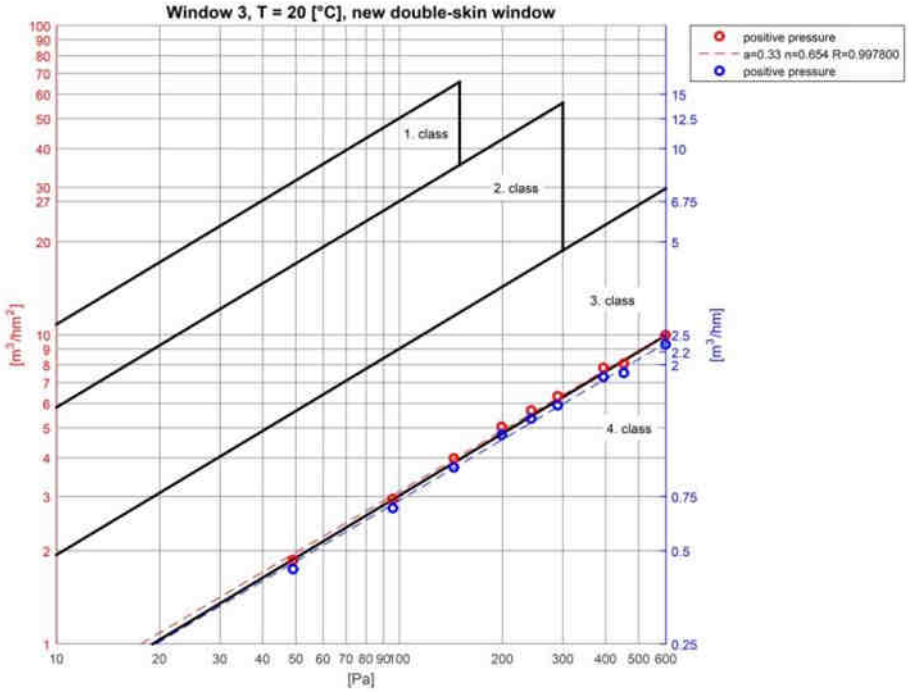

Fig. 34. – Window 3a/b – airtightness measurements, T=20 [°C], all sashes closed

A.4 Hot box measurements

A compressed graphical representation of the bot box measurement is given here: average temperatures during the hot box operation and temperature field measurements in the test windows averaged for the final near-stationary period. The complete detailed dataset is found is found in MATLAB *.mat files enclosed to the thesis.

A.4.1 Window 1

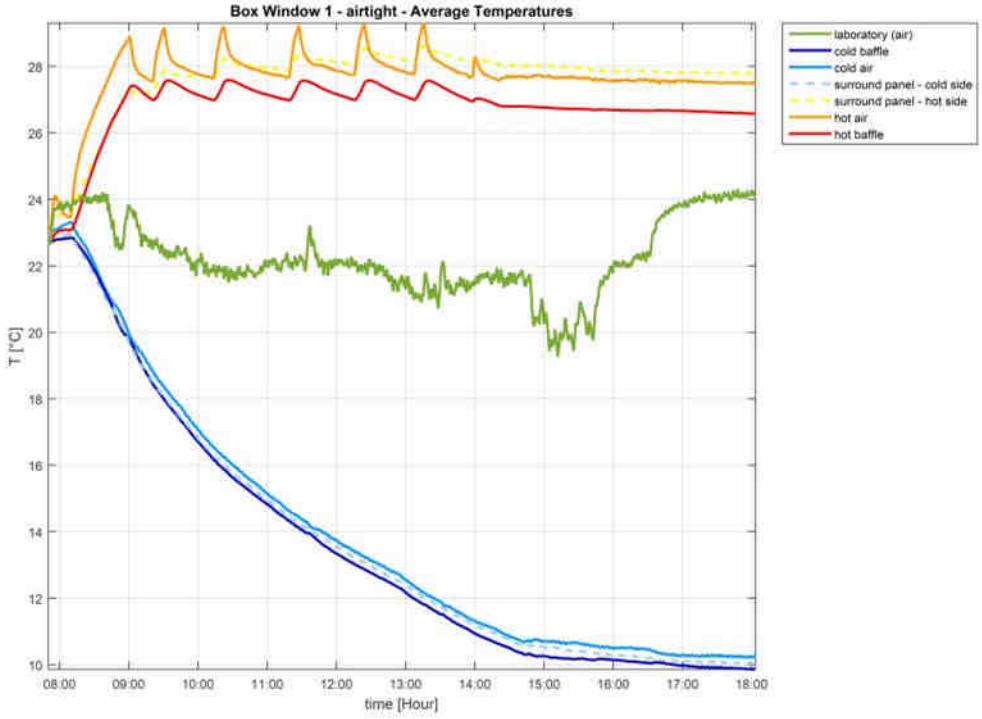

Fig. 35. – Window 1 – average temperatures in the hot box during the measurement

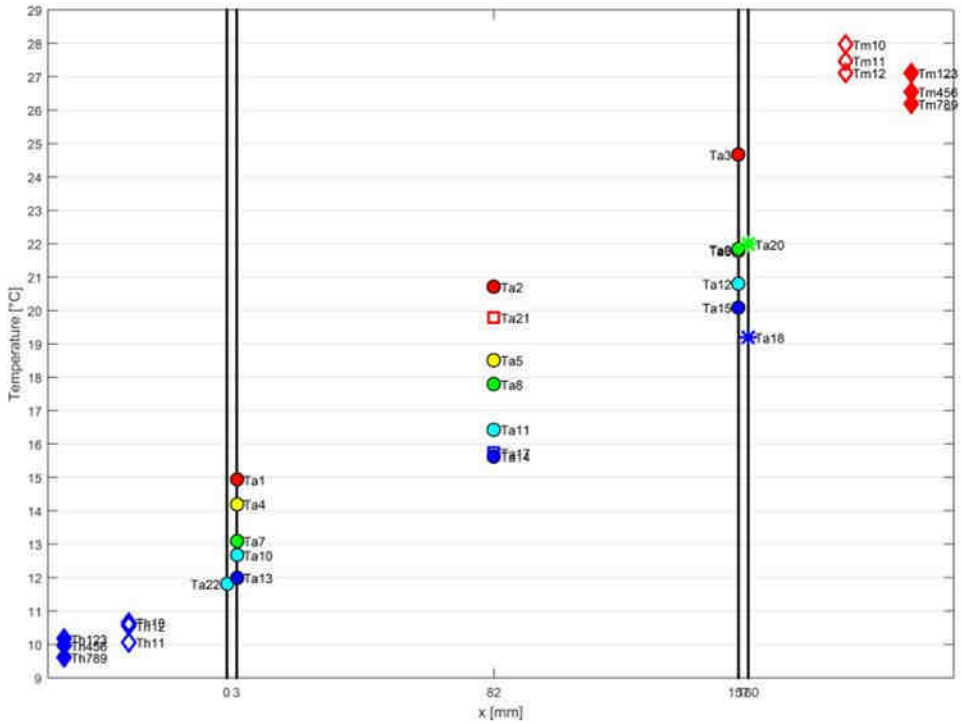

Fig. 36. – Window 1 – temperatures in the representative vertical 2D section of the window – averaged for the final stationary period of the measurement

A.4.2 Window 2

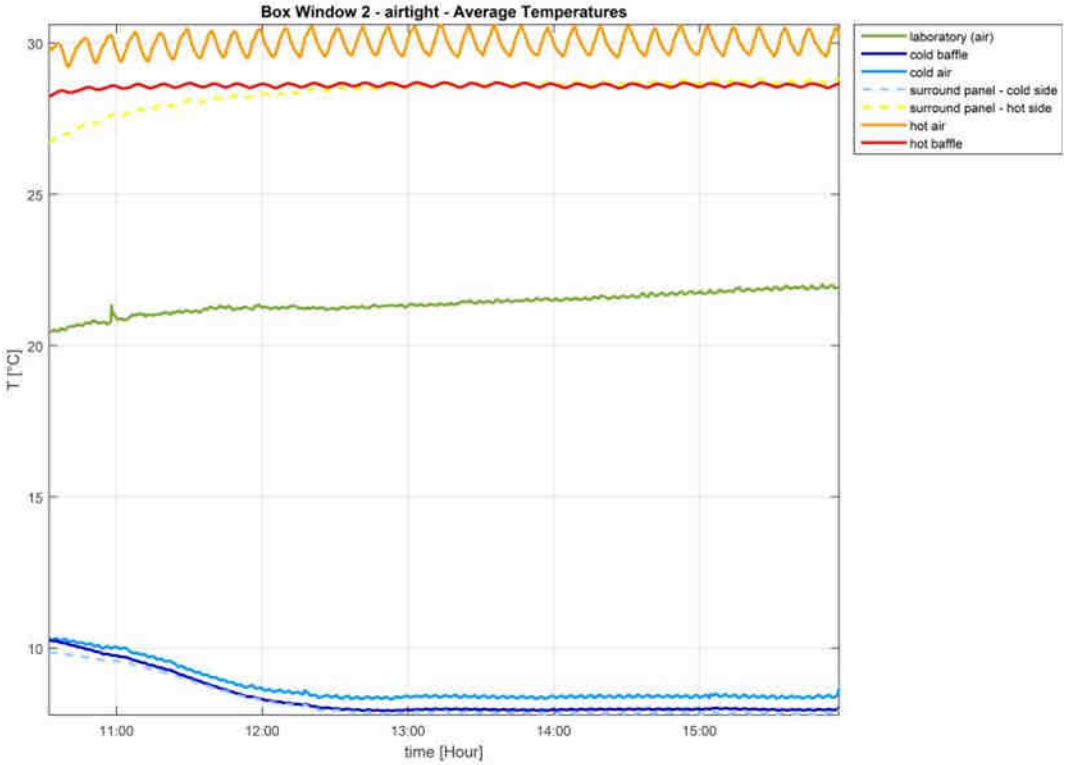

Fig. 37. – Window 2 – average temperatures in the hot box during the measurement

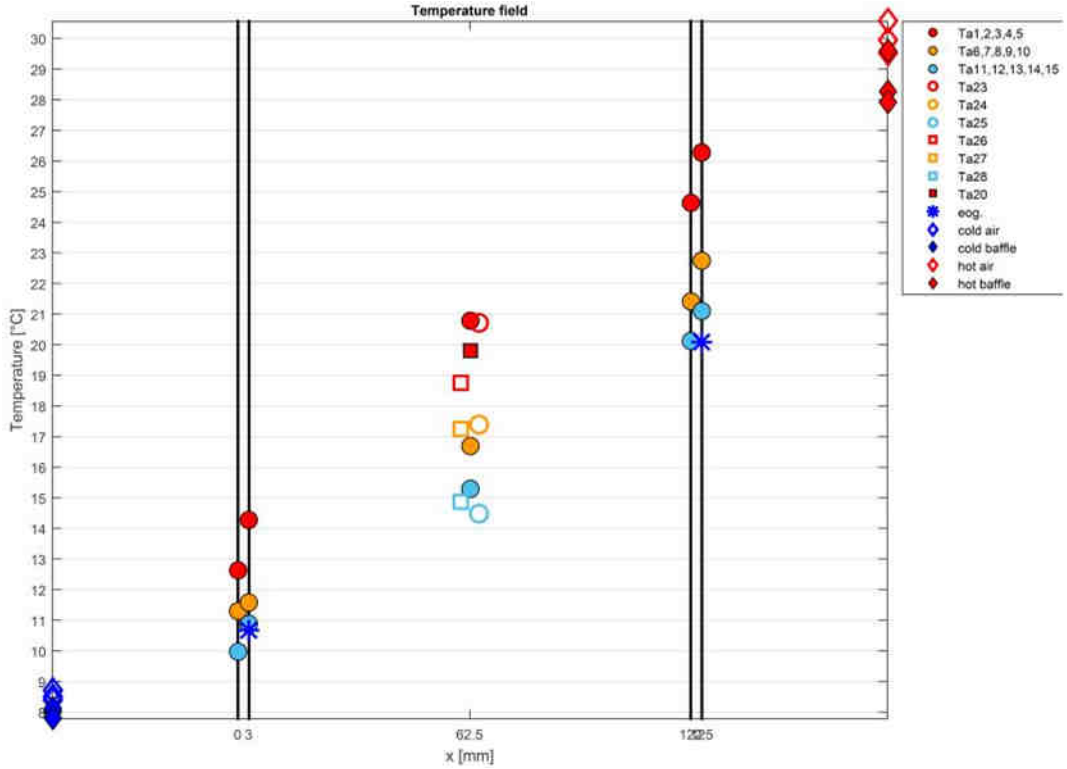

Fig. 38. – Window 2 – temperatures in the representative vertical 2D section of the window – averaged for the final stationary period of the measurement

A.4.3 Window 2b

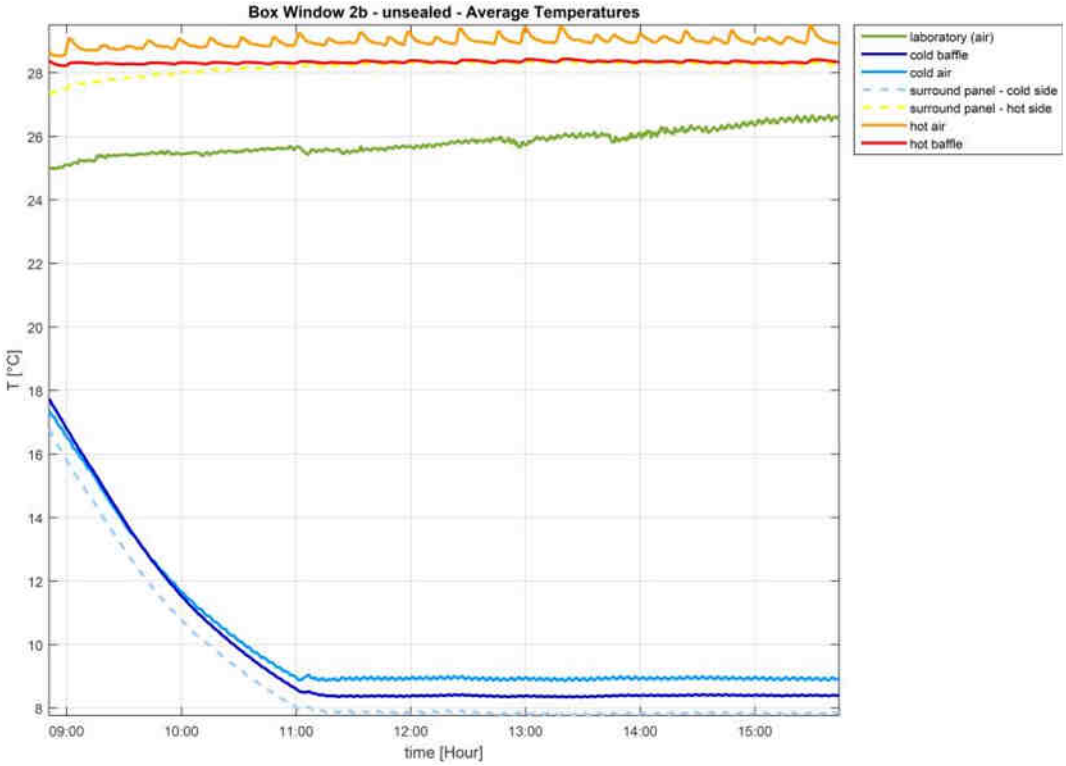

Fig. 39. – Window 2b – average temperatures in the hot box during the measurement

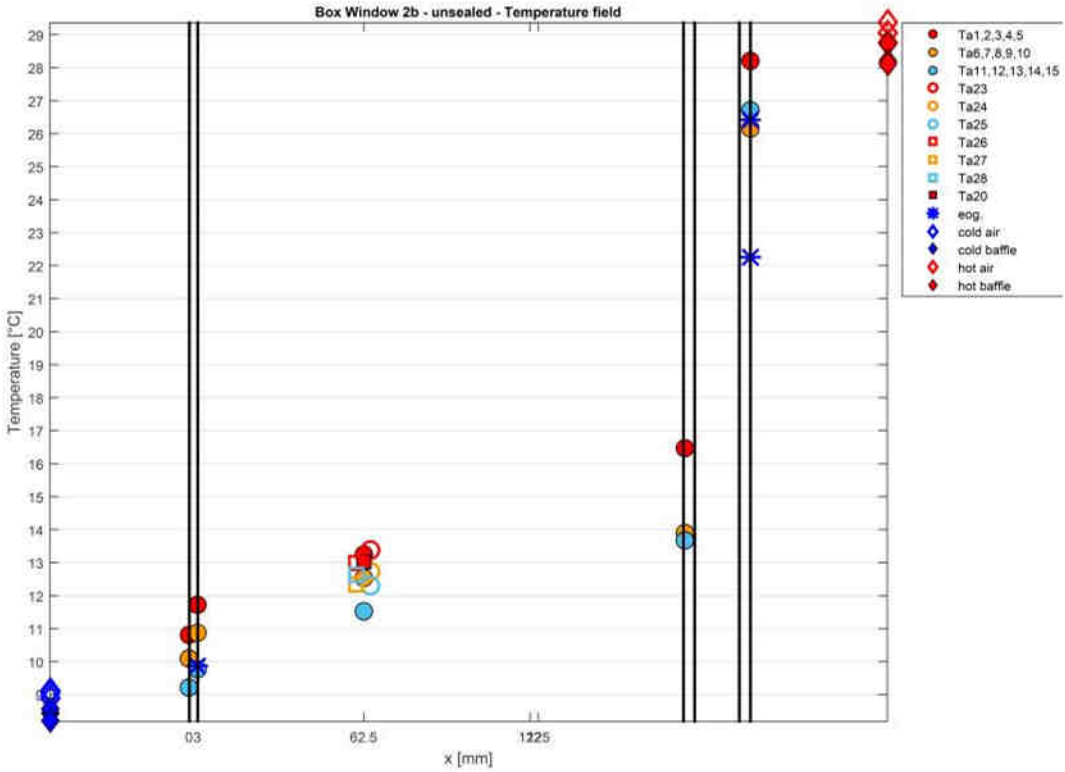

Fig. 40. – Window 2b – temperatures in the representative vertical 2D section of the window – averaged for the final stationary period of the measurement

A.4.4 Window 2c

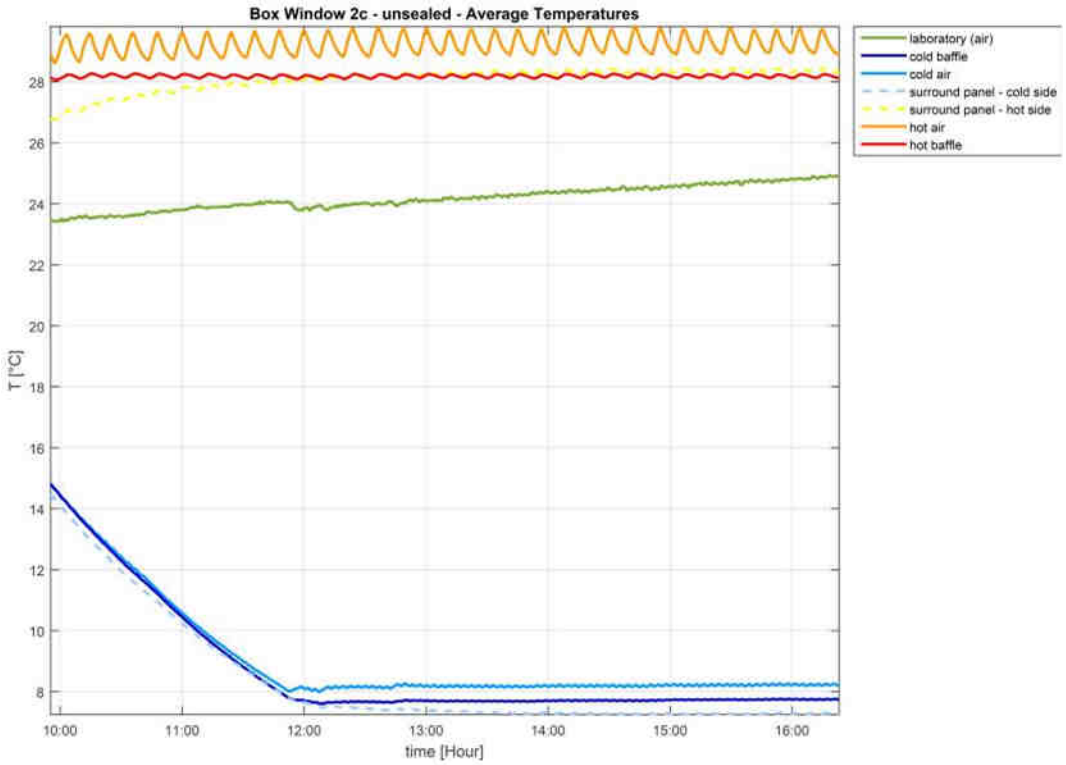

Fig. 41. – Window 2c – average temperatures in the hot box during the measurement

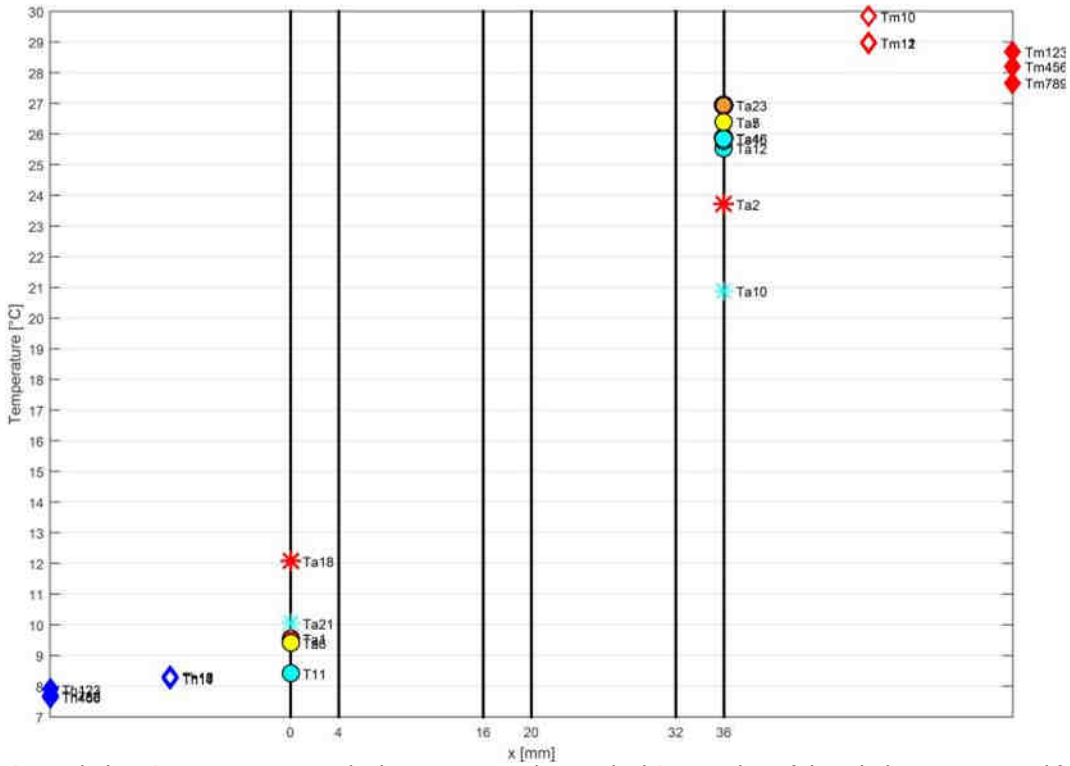

Fig. 42. – Window 2c – temperatures in the representative vertical 2D section of the window – averaged for the final stationary period of the measurement

A.4.5 Window 3a

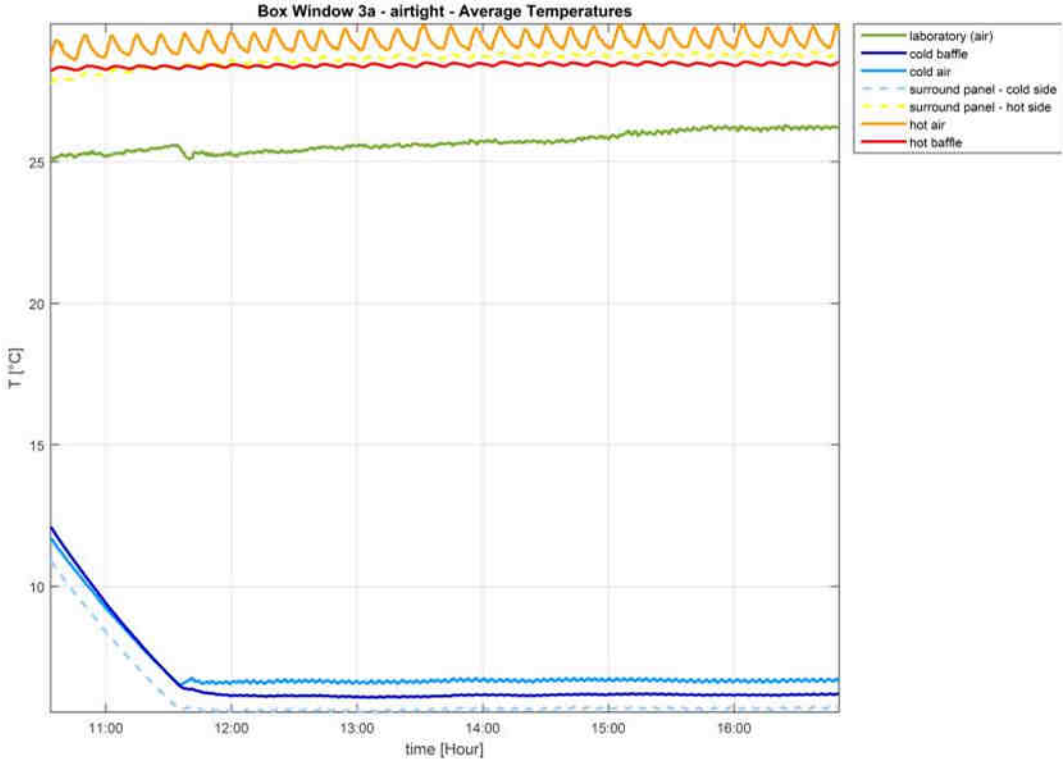

Fig. 43. – Window 3a – average temperatures in the hot box during the measurement

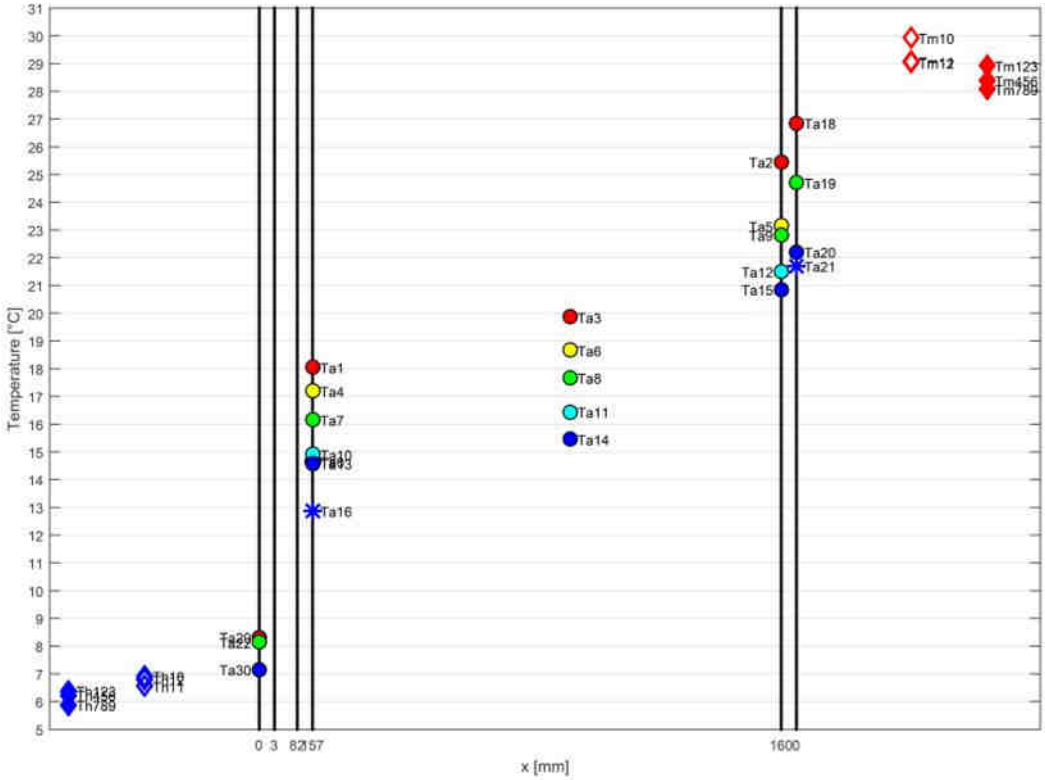

Fig. 44. – Window 3a – temperatures in the representative vertical 2D section of the window – averaged for the final stationary period of the measurement

A.4.6 Window 3b

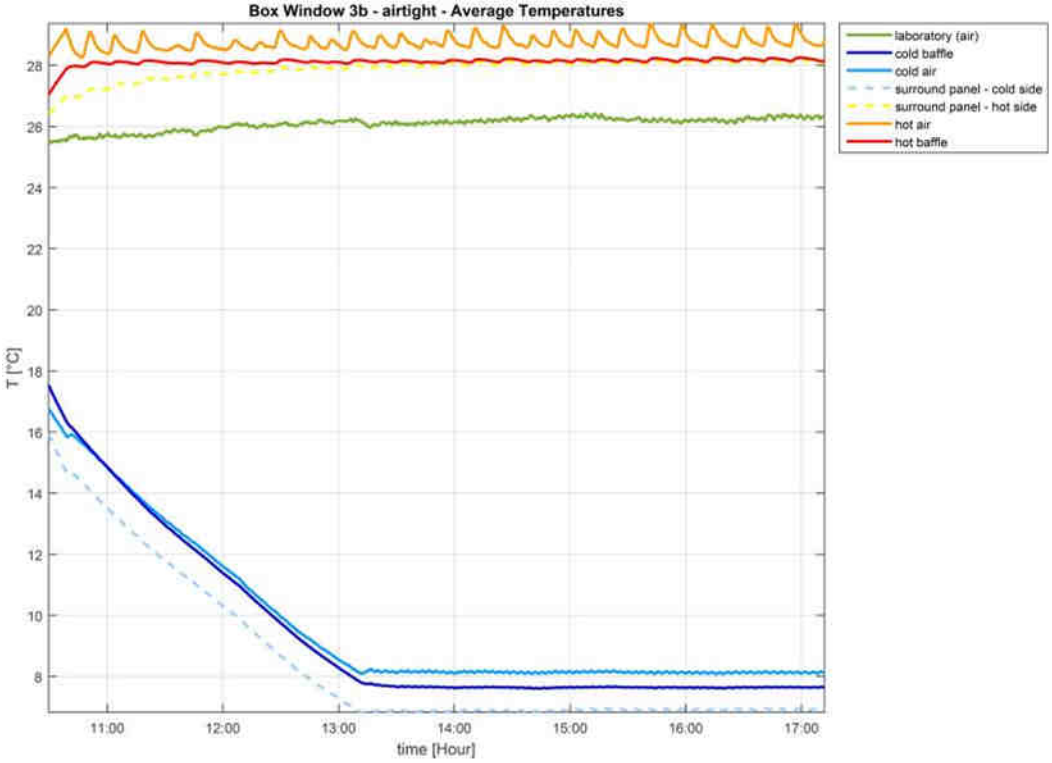

Fig. 45. – Window 3b – average temperatures in the hot box during the measurement

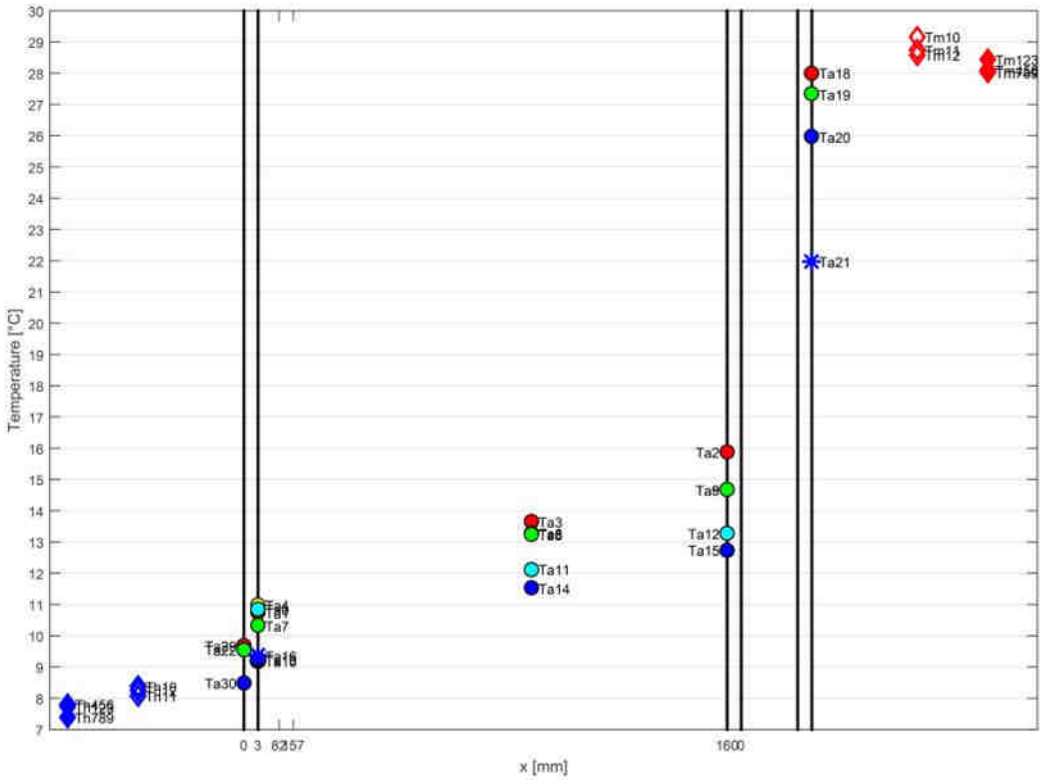

Fig. 46. – Window 3b – temperatures in the representative vertical 2D section of the window – averaged for the final stationary period of the measurement

B (Appendix B) – CFD simulations

B.1 k-ω SST turbulence model

The k-ω SST turbulence model of Menter[1] used in the CFD simulations in FLUENT is summarized below according to the ANSYS FLUENT theory guide[2]. The model is a hybrid of the standard k-ω and k-ε models and an attempt at combining their strengths and eliminating some of their weaknesses. It acts as the k-ω model in the near-wall region where the k-ε is not valid and as the k-ε model in the free-stream region as it provides a free-stream independence on the turbulence boundary conditions lacking in the k-ω model. This is achieved by rewriting the k-ε model in a k-ω formulation and combining the two with the help of blending functions.

The transport equation of the turbulent kinetic energy (in Cartesian vector notation) is:

$$\frac{\partial}{\partial t}(\rho k)+\frac{\partial}{\partial x_i}(\rho k u_i)=\frac{\partial}{\partial x_j}\left(\Gamma_k \frac{\partial k}{\partial x_j}\right)+\tilde{G}_k-Y_k+S_k \qquad (1)$$

where:

	t	the time
	ρ	the density
	k	the turbulent kinetic energy
	u_i	the i^{th} component of the mean velocity vector
	Γ_k	the transport coefficient for the turbulent kinetic energy (diffusivity)
	$\tilde{G}_k$	the generation of turbulent kinetic energy due to mean velocity gradient
	Y_k	the dissipation of turbulent kinetic energy due to turbulence
	S_k	the user-defined source term

The transport equation of the specific dissipation rate (in Cartesian vector notation) is:

$$\frac{\partial}{\partial t}(\rho \omega)+\frac{\partial}{\partial x_i}(\rho \omega u_i)=\frac{\partial}{\partial x_j}\left(\Gamma_\omega \frac{\partial \omega}{\partial x_j}\right)+\tilde{G}_\omega-Y_\omega+D_\omega+S_\omega \qquad (2)$$

where:

	ω	the specific turbulence dissipation rate
	Γ_ω	the transport coefficient for the specific dissipation rate (diffusivity)
	$\tilde{G}_\omega$	the generation of the specific dissipation rate due to mean velocity gradient
	Y_ω	the dissipation of the specific dissipation rate due to turbulence
	D_ω	the cross-diffusion term
	S_ω	the user-defined source term

[1] Menter, F. R. (1994) Two-Equation Eddy-Viscosity Turbulence Models for Engineering Applications, *AIAA Journal*, Vol. 32(8), pp. 1598-1605, DOI: http://dx.doi.org/10.2514/3.12149

[2] ANSYS FLUENT Theory Guide, Release 13.0, ANSYS, inc. Southpointe, 275 Technology Drive Canonsburg, PA 15317, ansysinfo@ansys.com, http://www.ansys.com, USA, 2010

The transport coefficients for k and ω are given as:

$$\Gamma_k = \mu + \frac{\mu_t}{\partial_k} \tag{3}$$

$$\Gamma_\omega = \mu + \frac{\mu_t}{\partial_\omega} \tag{4}$$

where:

Γ_k	the transport coefficient for the turbulent kinetic energy (diffusivity)
Γ_ω	the transport coefficient for the specific dissipation rate (diffusivity)
μ	the dynamic viscosity
μ_t	the turbulent eddy viscosity
σ_k	the turbulent Prandtl number for k
σ_ω	the turbulent Prandtl number for ω

The turbulent eddy viscosity is calculated as:

$$\mu_t = \frac{\rho k}{\omega} \frac{1}{\max\left[\frac{1}{\alpha^*}, \frac{SF_2}{\alpha_1 \omega}\right]} \tag{5}$$

The turbulent Prandtl numbers for k and ω are given with the help of the blending functions F_1:

$$\partial_k = \frac{1}{F_1 / \partial_{k,1} + (1 - F_1) / \partial_{k,2}} \tag{6}$$

$$\partial_\omega = \frac{1}{F_1 / \partial_{\omega,1} + (1 - F_1) / \partial_{\omega,2}} \tag{7}$$

The blending function F_1 is defined as:

$$F_1 = \tanh\left(\Phi_1^4\right) \tag{8}$$

$$\Phi_1 = \min\left[\max\left(\frac{\sqrt{k}}{0.09\omega y}, \frac{500\mu}{\rho y^2 \omega}\right), \frac{4\rho k}{\partial_{\omega,2} D_\omega^+ y^2}\right] \tag{9}$$

$$D_\omega^+ = \max\left[2\rho \frac{1}{\partial_{\omega,2}} \frac{1}{\omega} \frac{\partial k}{\partial x_j} \frac{\partial \omega}{\partial x_j}, 10^{-10}\right] \tag{10}$$

The blending function F_2 is defined as:

$$F_2 = \tanh\left(\Phi_2^2\right) \tag{11}$$

$$\Phi_2 = \max\left[2\frac{\sqrt{k}}{0.09\omega y}, \frac{500\mu}{\rho y^2 \omega}\right] \tag{12}$$

The production of k due to the mean velocity gradient is calculated as:

$$\tilde{G}_k = \min\left(G_k, 10\rho\beta^* k\omega\right) \tag{13}$$

The production of ω due to the mean velocity gradient is calculated as:

$$G_\omega = \frac{\alpha_\infty}{\nu_t}\tilde{G}_\omega \tag{14}$$

$$\alpha_\infty = F_1\alpha_{\infty,1} + \left(1-F_1\right)\alpha_{\infty,2} \tag{15}$$

$$\alpha_{\infty,1} = \frac{\beta_{i,1}}{\beta_\infty^*} - \frac{k^2}{\sigma_{\omega,1}\sqrt{\beta_\infty^*}} \tag{16}$$

$$\alpha_{\infty,2} = \frac{\beta_{i,2}}{\beta_\infty^*} - \frac{k^2}{\sigma_{\omega,2}\sqrt{\beta_\infty^*}} \tag{17}$$

The dissipation of k is calculated as:

$$Y_k = \rho\beta^* k\omega \tag{18}$$

The dissipation of ω is calculated as:

$$Y_\omega = \rho\beta\omega^2 \tag{19}$$

$$\beta_i = F_1\beta_{i,1} + \left(1-F_1\right)\beta_{i,2} \tag{20}$$

The cross-diffusion modification in the ω equation is calculated as

$$D_\omega = 2\left(1-F_1\right)\rho\sigma_{\omega,2}\frac{1}{\omega}\frac{\partial k}{\partial x_j}\frac{\partial \omega}{\partial x_j} \tag{21}$$

The model constants are the following:

$\sigma_{k,1} = 1.176$, $\sigma_{\omega,1} = 2.0$, $\sigma_{k,2} = 1.0$, $\sigma_{\omega,1} = 1.168$, $\alpha_1 = 0.31$, $\beta_{i,1} = 0.075$, $\beta_{i,2} = 0.0828$

$\kappa = 0.41$, $\alpha_\infty^* = 1$, $\alpha_\infty = 0.52$, $\alpha_0 = \frac{1}{9}$, $\beta_\infty^* = 0.09$, $R_\beta = 8$, $R_k = 6$, $R_\omega = 2.95$, $\zeta^* = 1.5$, $M_{t0} = 0.25$

B.2 Turbulence model validation

B.2.1 Temperature predictions

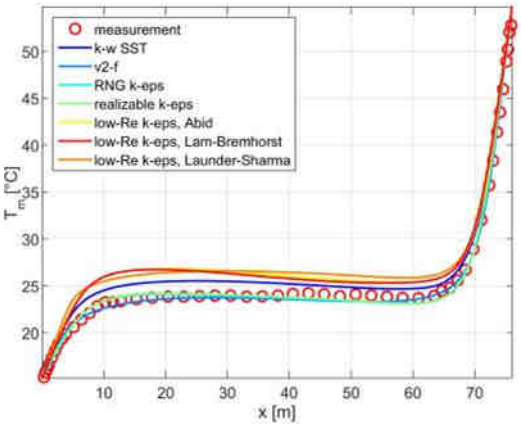

Fig. 47. – comparison of measurement an simulation – horizontal temperature profile at y/H = 0.05 [-]

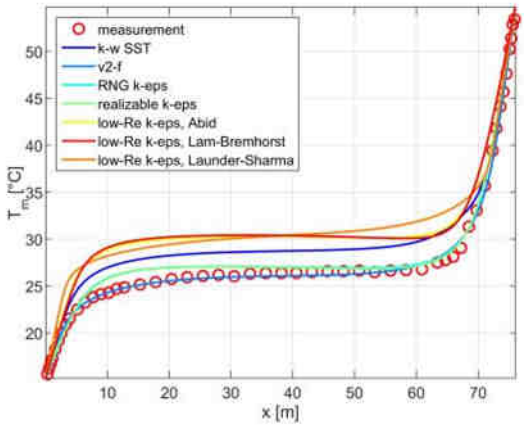

Fig. 48. – comparison of measurement an simulation – horizontal temperature profile at y/H = 0.10 [-]

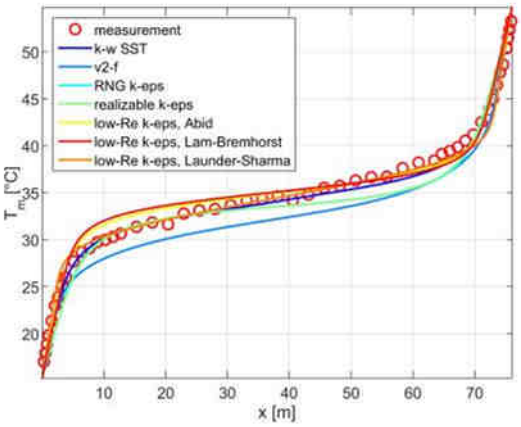

Fig. 49. – comparison of measurement an simulation – horizontal temperature profile at y/H = 0.30 [-]

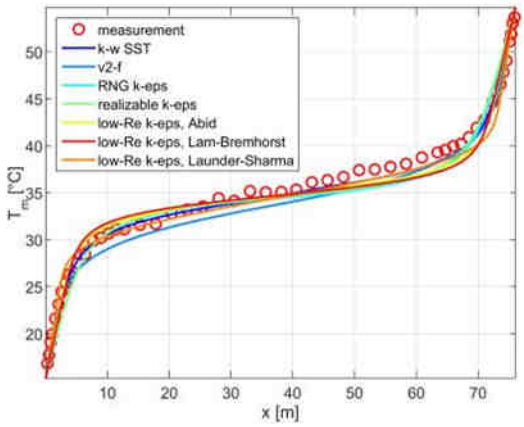

Fig. 50. – comparison of measurement an simulation – horizontal temperature profile at y/H = 0.40 [-]

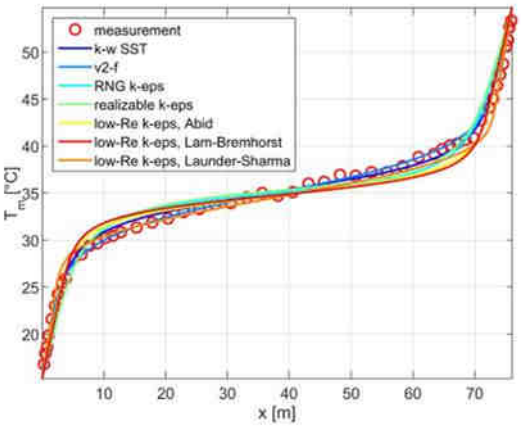

Fig. 51. – comparison of measurement an simulation – horizontal temperature profile at y/H = 0.50 [-]

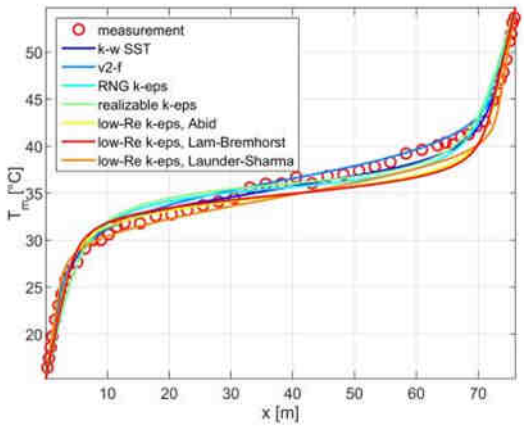

Fig. 52. – comparison of measurement an simulation – horizontal temperature profile at y/H = 0.60 [-]

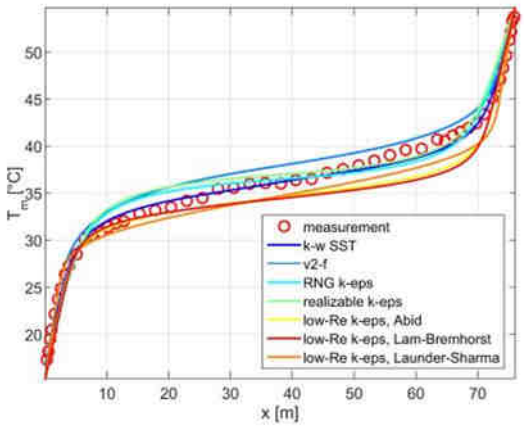

Fig. 53. – comparison of measurement an simulation – horizontal temperature profile at y/H = 0.70 [-]

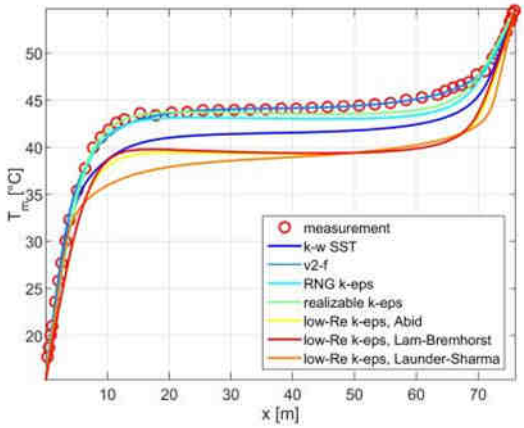

Fig. 54. – comparison of measurement an simulation – horizontal temperature profile at y/H = 0.90 [-]

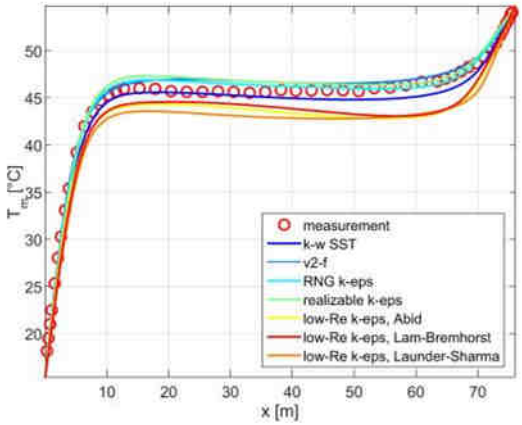

Fig. 55. – comparison of measurement an simulation – horizontal temperature profile at y/H = 0.95 [-]

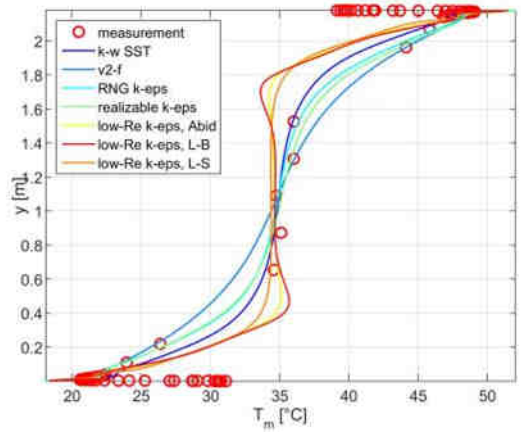

Fig. 56. – comparison of measurement an simulation – vertical temperature profile at the central axis

B.2.2 Velocity predictions

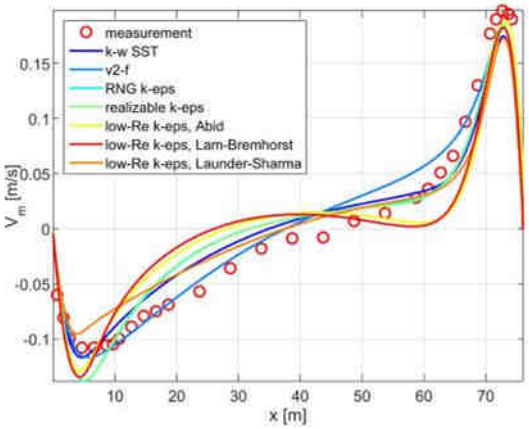

Fig. 57. – comparison of measurement an simulation – horizontal profile of vertical velocity at y/H = 0.05 [-]

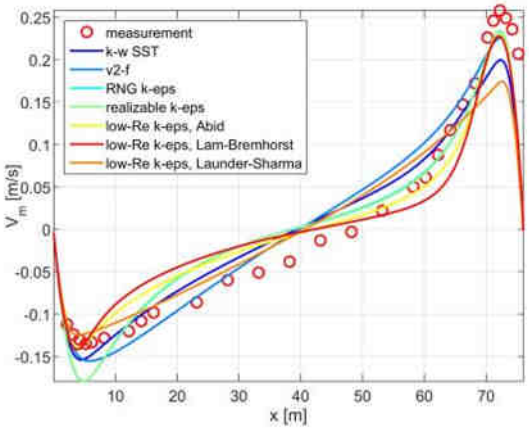

Fig. 58. – comparison of measurement an simulation – horizontal profile of vertical velocity at y/H = 0.10 [-]

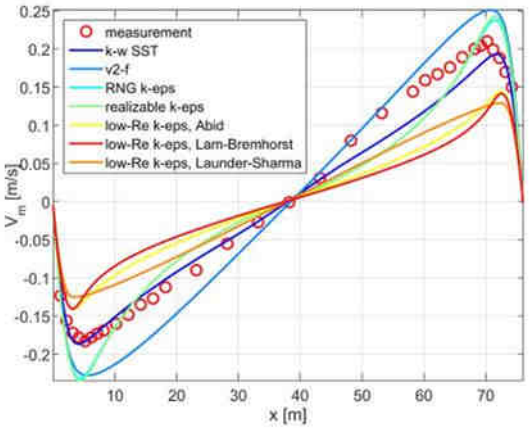

Fig. 59. – comparison of measurement an simulation – horizontal profile of vertical velocity at y/H = 0.30 [-]

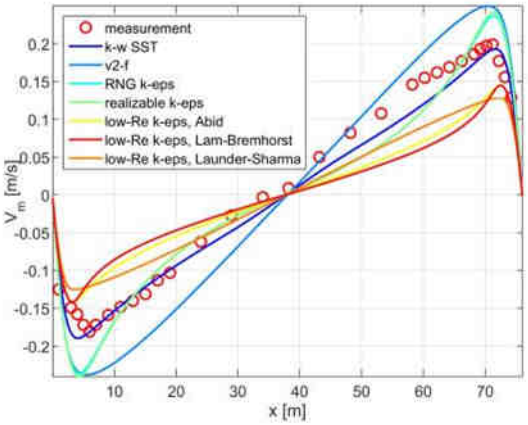

Fig. 60. – comparison of measurement an simulation – horizontal profile of vertical velocity at y/H = 0.40 [-]

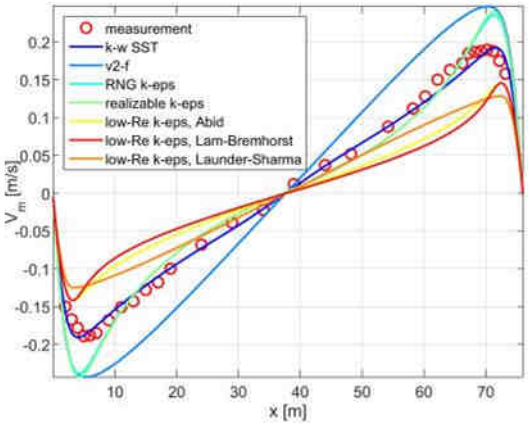

Fig. 61. – comparison of measurement an simulation – horizontal profile of vertical velocity at y/H = 0.50 [-]

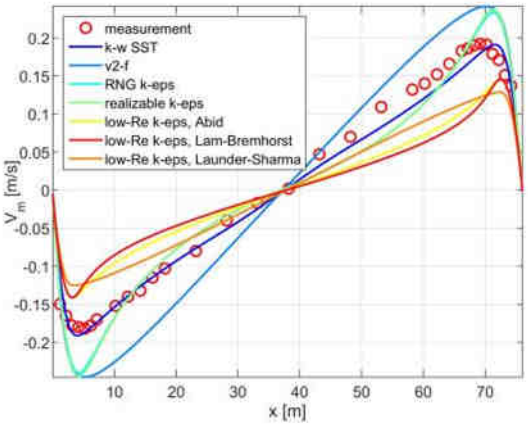

Fig. 62. – comparison of measurement an simulation – horizontal profile of vertical velocity at y/H = 0.60 [-]

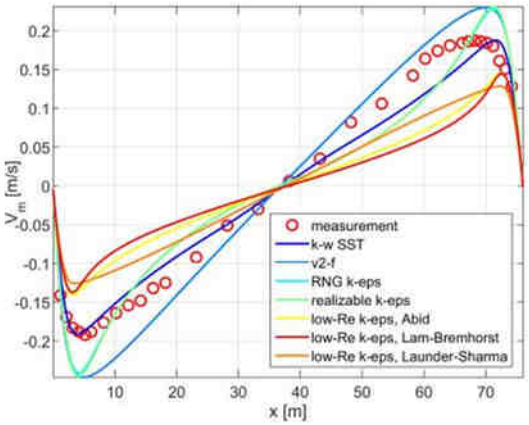

Fig. 63. – comparison of measurement an simulation – horizontal profile of vertical velocity at y/H = 0.70 [-]

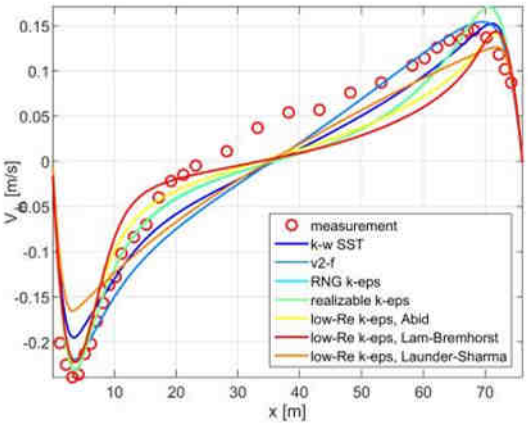

Fig. 64. – comparison of measurement an simulation – horizontal profile of vertical velocity at y/H = 0.90 [-]

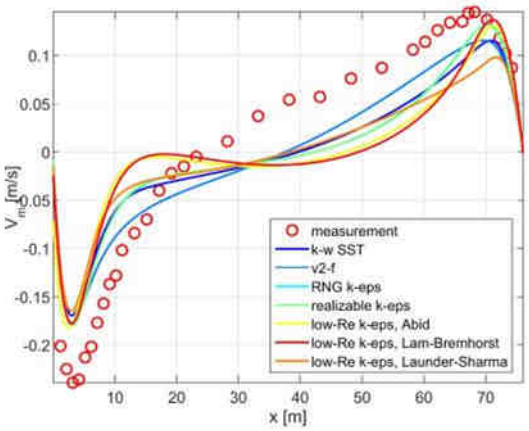

Fig. 65. – comparison of measurement an simulation – horizontal profile of vertical velocity at y/H = 0.95 [-]

B.3 Rectangular cavity parameter study

Fig. 66. – A=7, Ra=high, isotherms

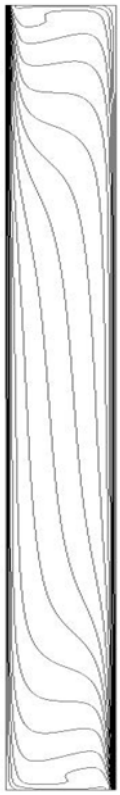

Fig. 67. – A=35, Ra=high, isotherms (vertically scaled)

B.4 2D simulations – comparison with measurements

B.4.1 window 1

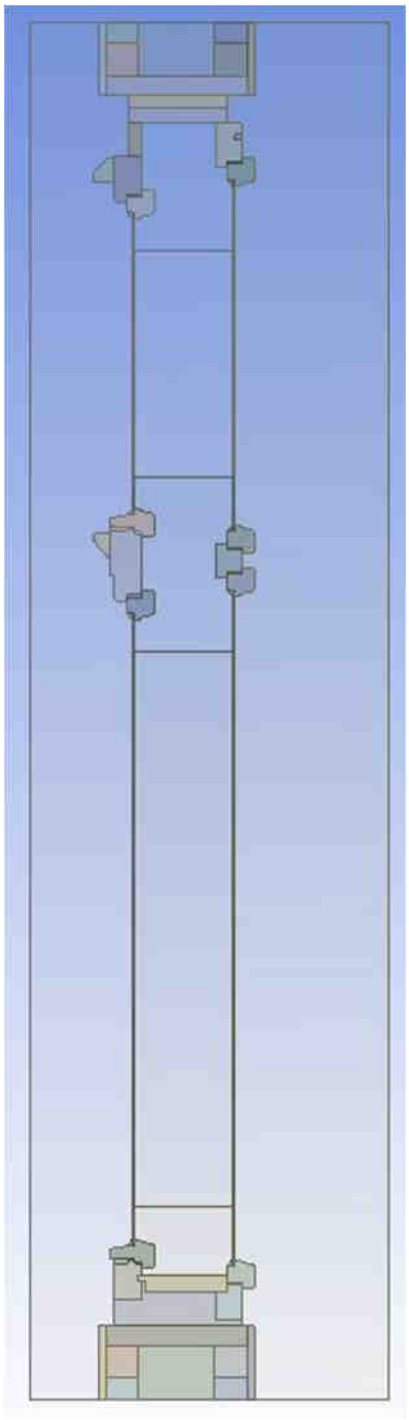

Fig. 68. – Window 1 - geometry

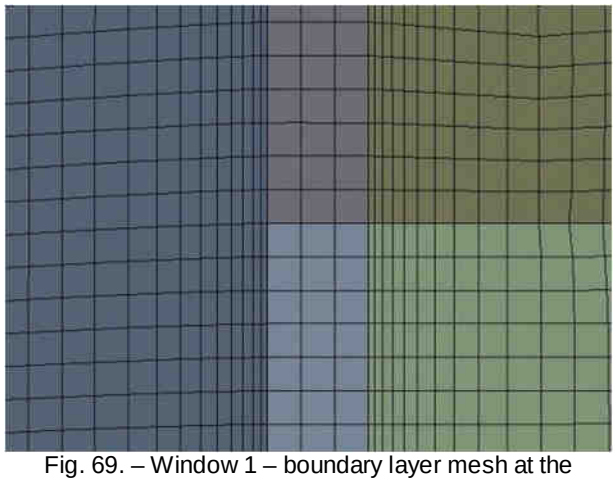

Fig. 69. – Window 1 – boundary layer mesh at the glazing

Fig. 70. – Window 1 – mesh (horizontal divider)

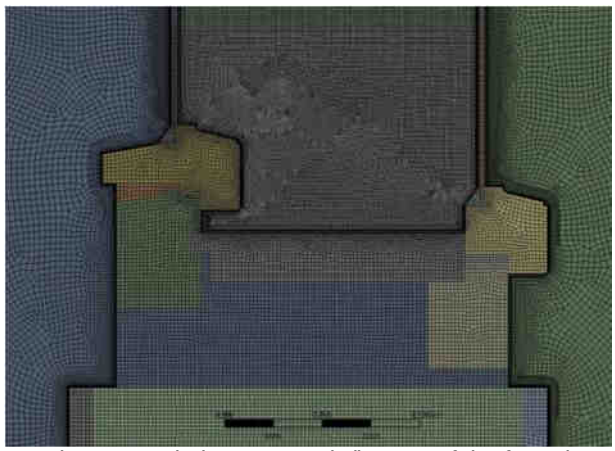

Fig. 71. – Window 1 – mesh (bottom of the frame)

Mesh: 501626 nodes and 500853 elements with 1 [mm] element length along every fluid/solid interface. 2 [mm] element size in the solid domains with the exception of the glazing layers where the element size is 1 [mm] to provide at least 3 elements for the thickness. Inflation mesh along every fluid wall with a first element thickness of 2e-4 [m], 10 layers and a growth rate of 1.2. The calculated dimensionless wall distance is y+<0.3 [-] everywhere.

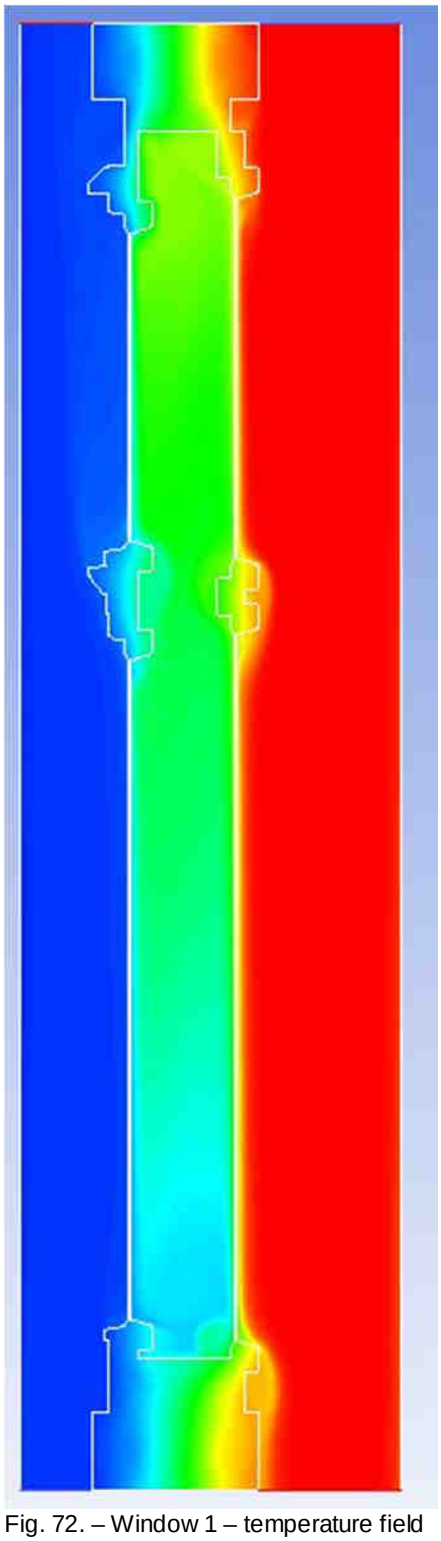

Fig. 72. – Window 1 – temperature field

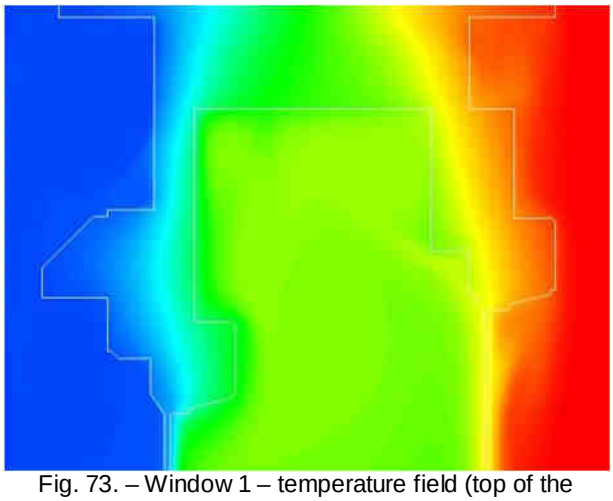

Fig. 73. – Window 1 – temperature field (top of the frame)

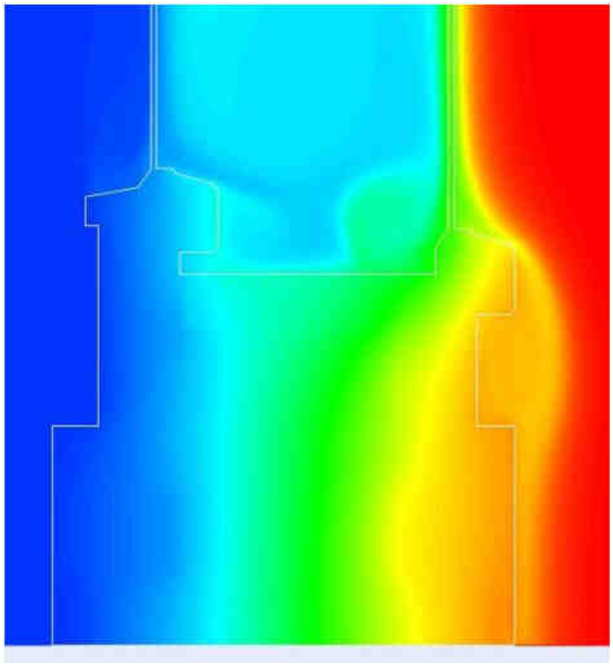

Fig. 74. – Window 1 – temperature frame – bottom of the frame

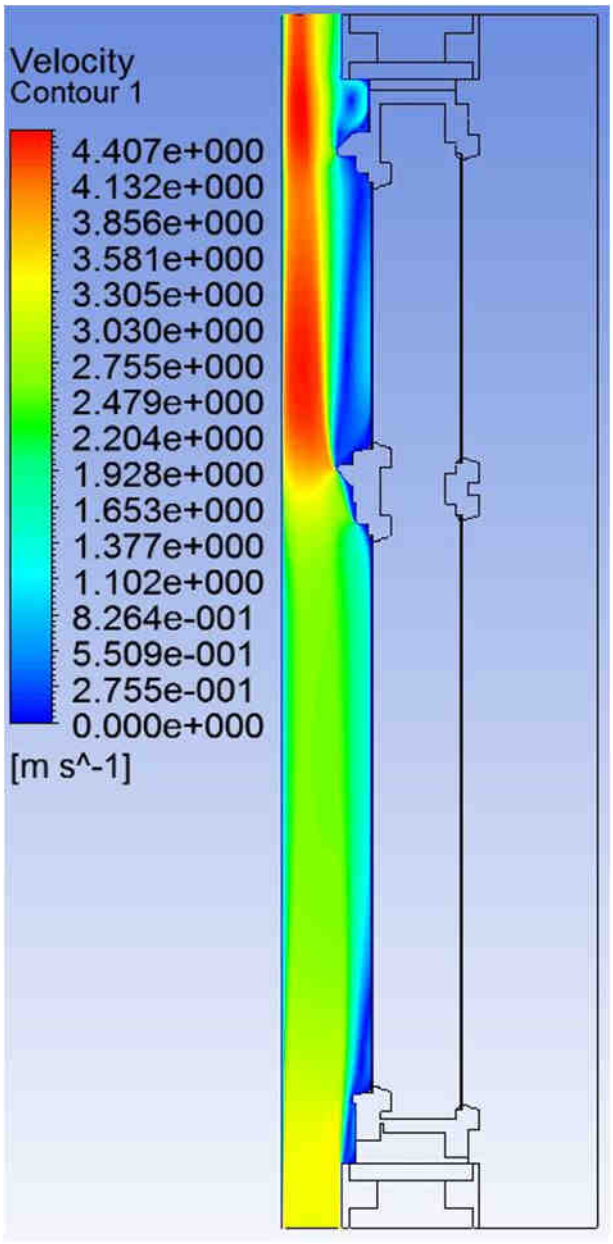

Fig. 75. – Window 1 – velocity magnitude in the external air channel

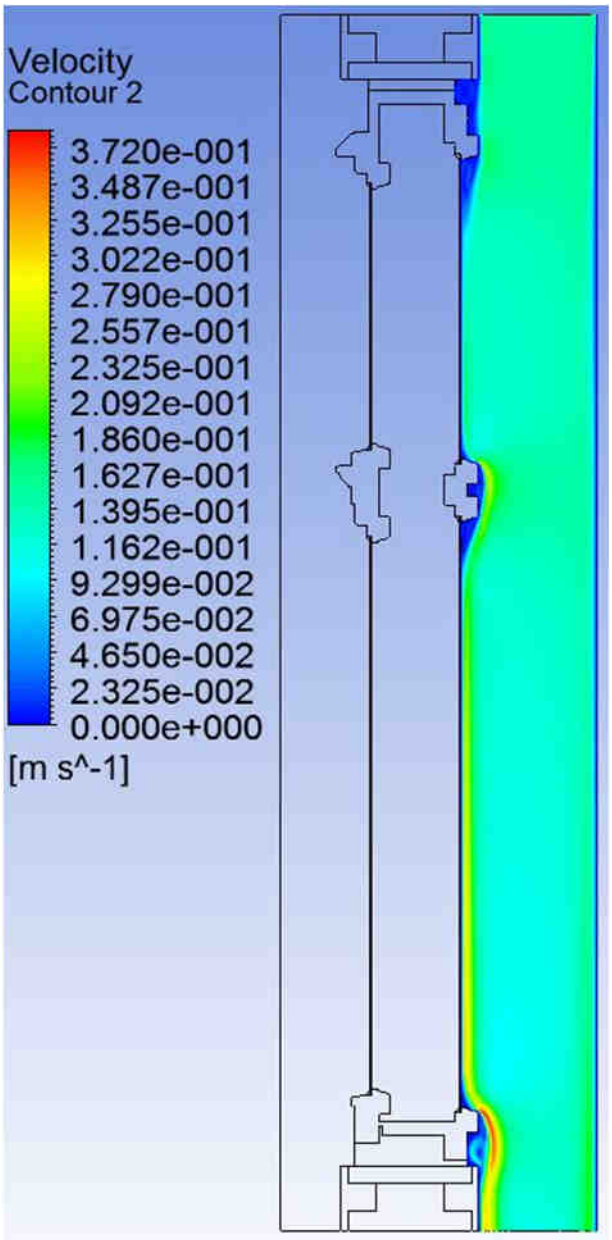

Fig. 76. – Window 1 – velocity magnitude in the internal air channel

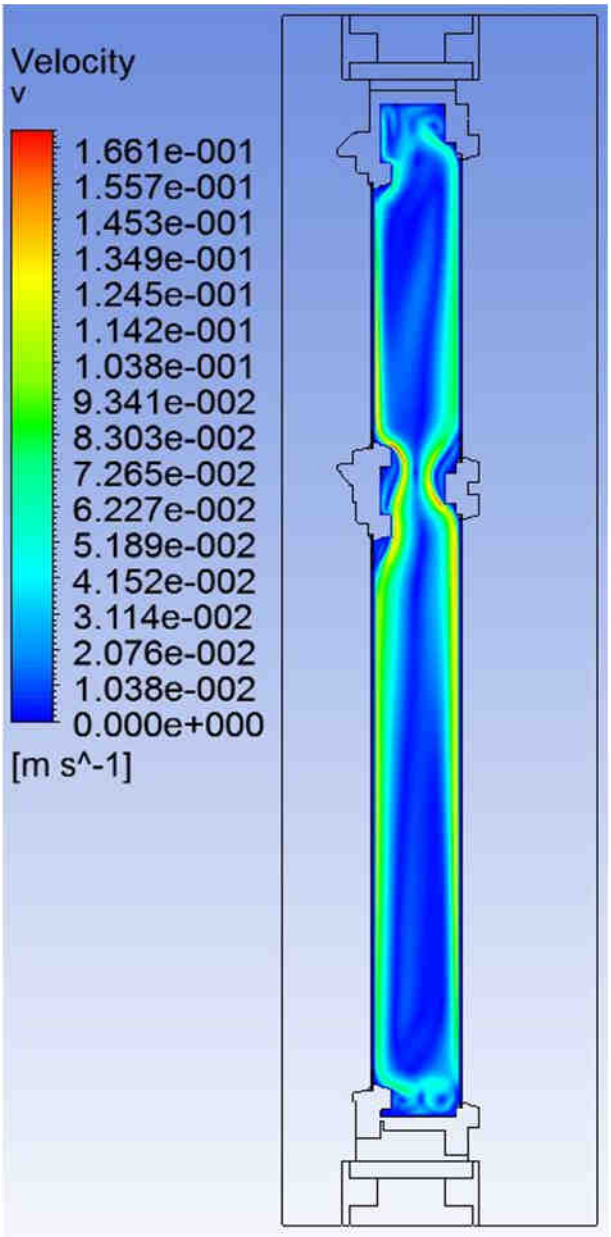

Fig. 77. – Window 1 – velocity magnitude in the window cavity

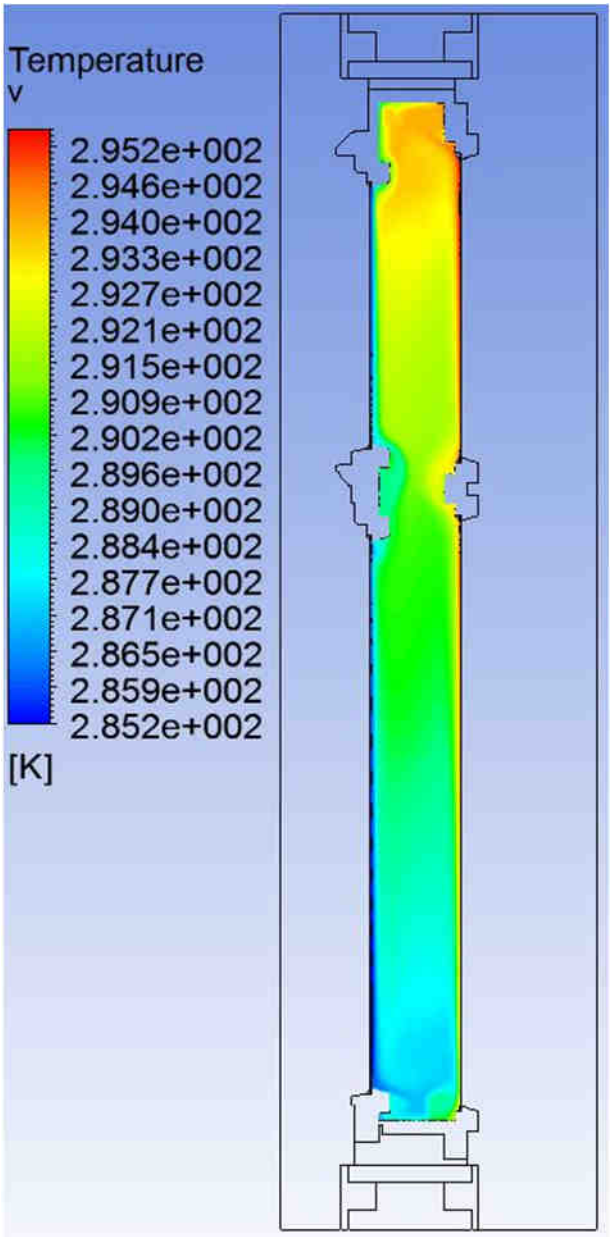

Fig. 78. – Window 1 – temperature field in the window cavity

Boundary conditions:

- External baffle: T_{surf}=f(y) from measurement, ε=0.95 [-] (painted matt black)
- External air channel inlet: 3.3 [m/s], turb. intensity=10% [-], I_{turb}=0.007 [m], T_{inlet}=283.7 [K]
- External air channel outlet: pressure outlet, Gauge pressure 0 [Pa], backflow: turb. intensitiy 5%, visc. ratio 10
- Internal baffle: T_{surf}=f(y) from measurement, ε=0.95 [-] (painted matt black)
- Internal air channel inlet: 15 [cm/s], turb intensity 2.5%, visc. ratio 3, T_{inlet}=301.12 [K]
- Internal air channel outlet: pressure outlet, gauge pressure 0 [Pa] backflow turb. in. 5%, visc. ratio 10

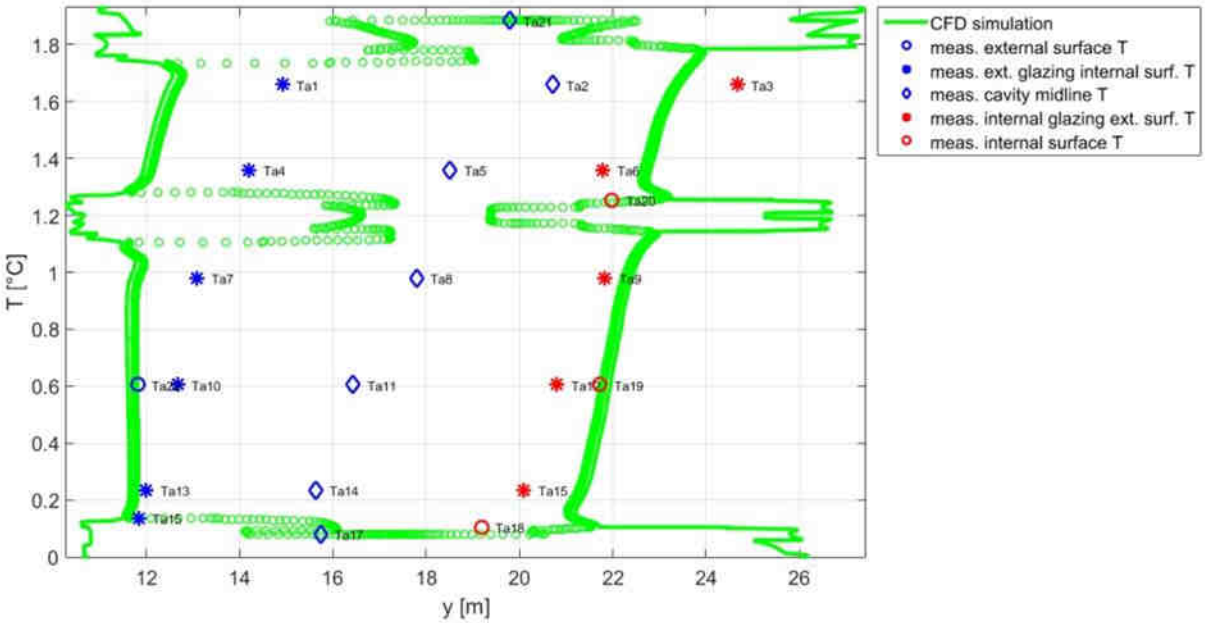

Fig. 79. – Window 1 – comparison of measurement and simulation – only the window is modelled

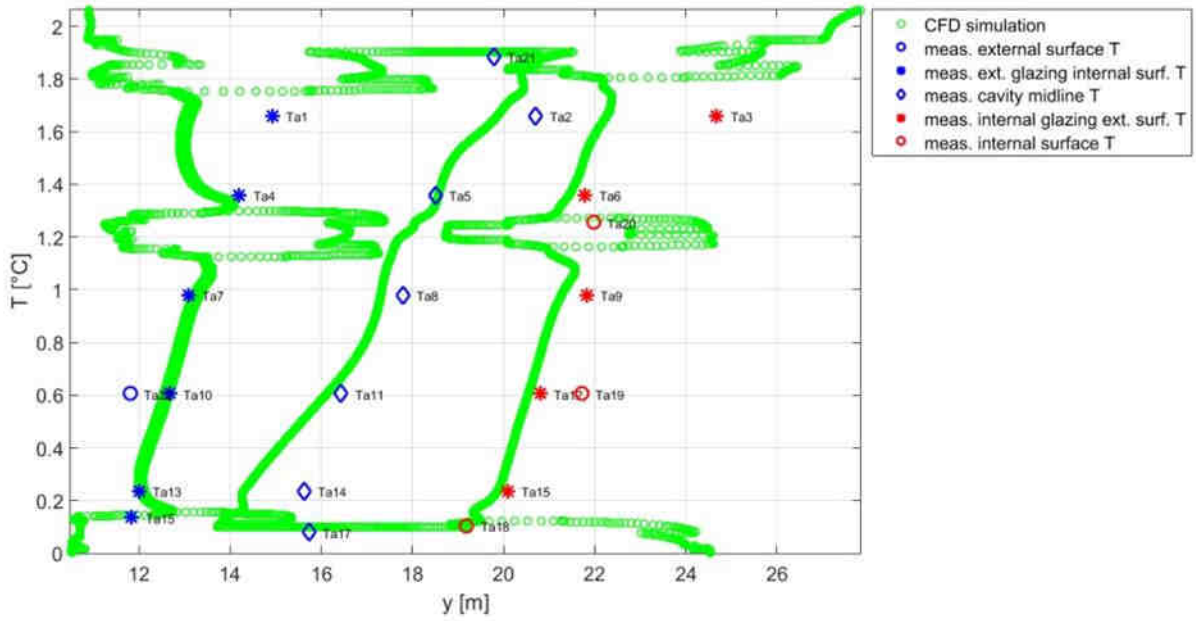

Fig. 80. – Window 1 – comparison of measurement and CFD simulation – external and internal baffle and air channels added to the simulation

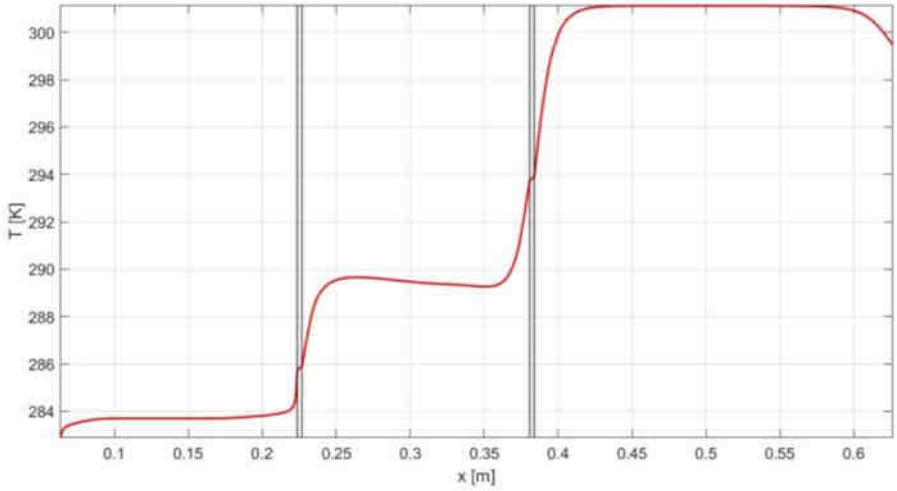

Fig. 81. – Window 1 – horizontal temperature section through the middle of the bottom glazing panes

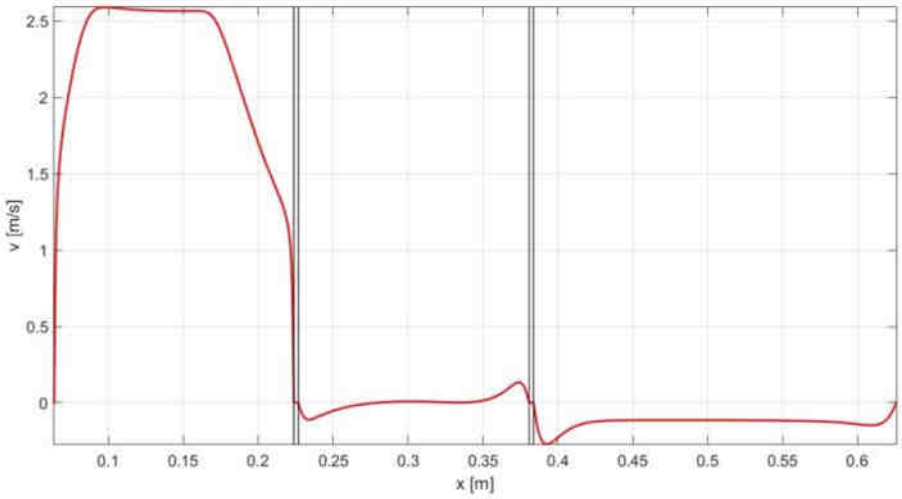

Fig. 82. – Window 1 – vertical velocity profile along the horizontal section through the middle of the bottom glazing panes

B.4.2 window 2

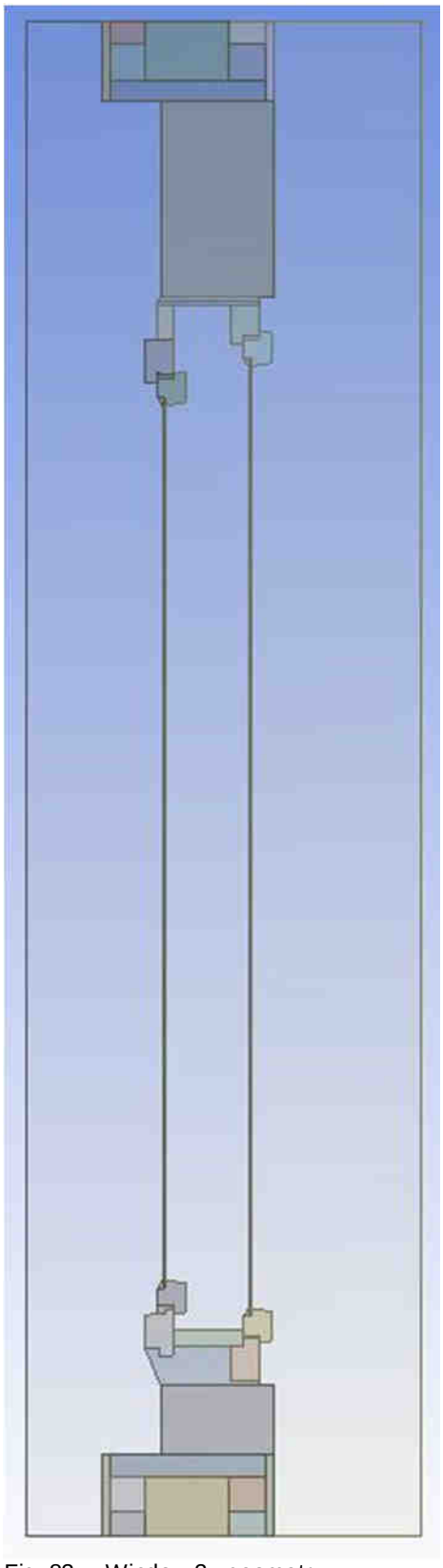

Fig. 83. – Window 2 - geometry

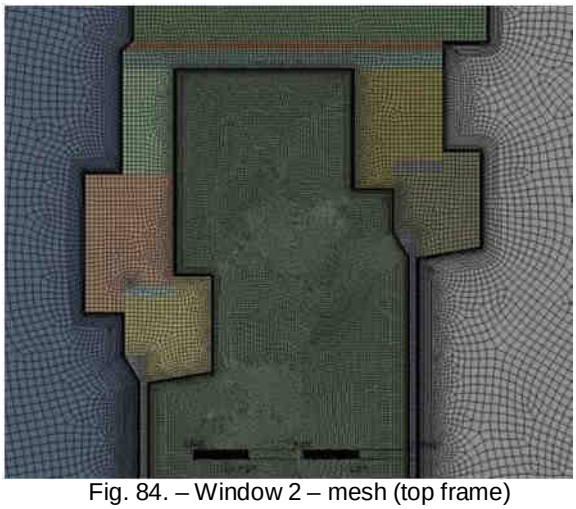

Fig. 84. – Window 2 – mesh (top frame)

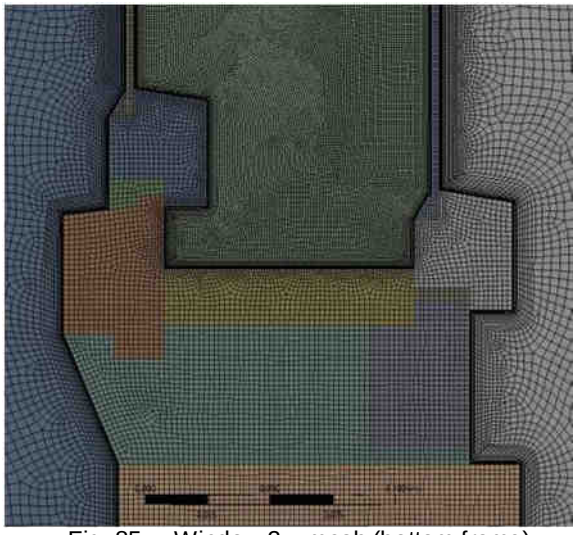

Fig. 85. – Window 2 – mesh (bottom frame)

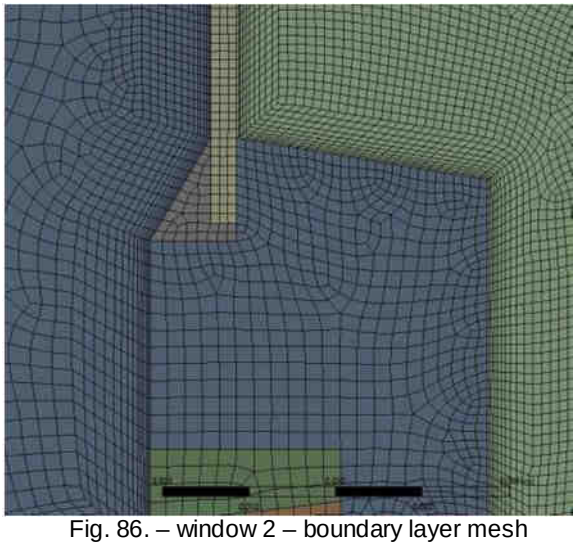

Fig. 86. – window 2 – boundary layer mesh

Mesh: 360459 nodes and 359832 elements with 1 [mm] element length along every fluid/solid interface. 2 [mm] element size in the solid domains with the exception of the glazing layers where the element size is 1 [mm] to provide at least 3 elements for the thickness. Inflation mesh along every fluid

wall with a first element thickness of 2e-4 [m], 10 layers and a growth rate of 1.2. The calculated dimensionless wall distance is y+<1 [-] everywhere.

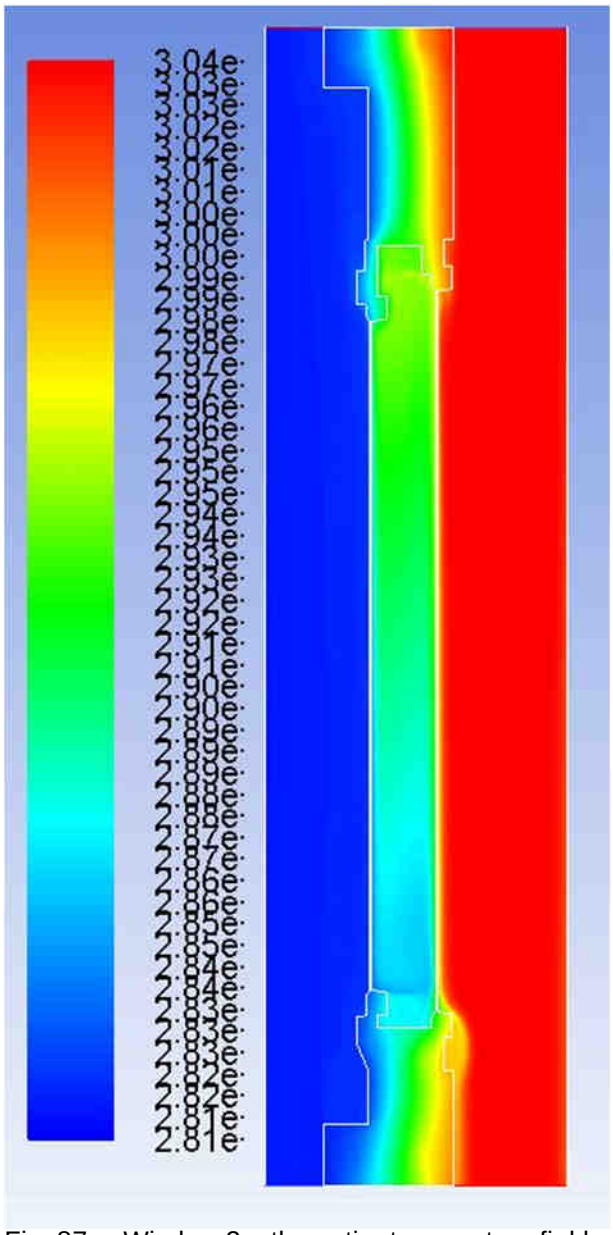

Fig. 87. – Window 2 – the entire temperature field

Fig. 88. – Window 2 – top frame temperature field

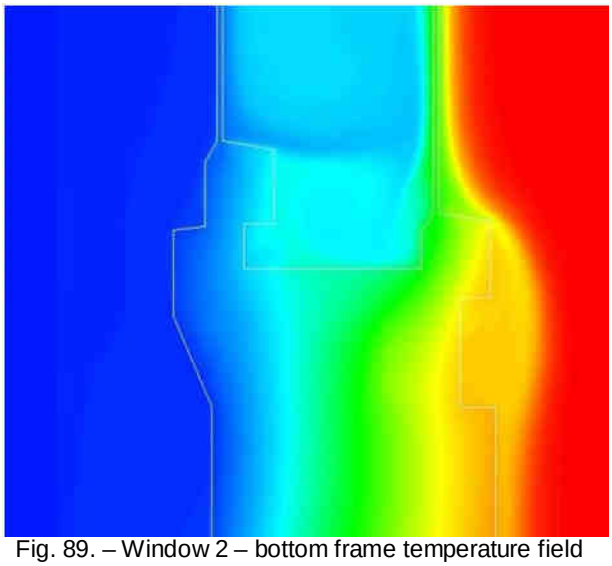

Fig. 89. – Window 2 – bottom frame temperature field

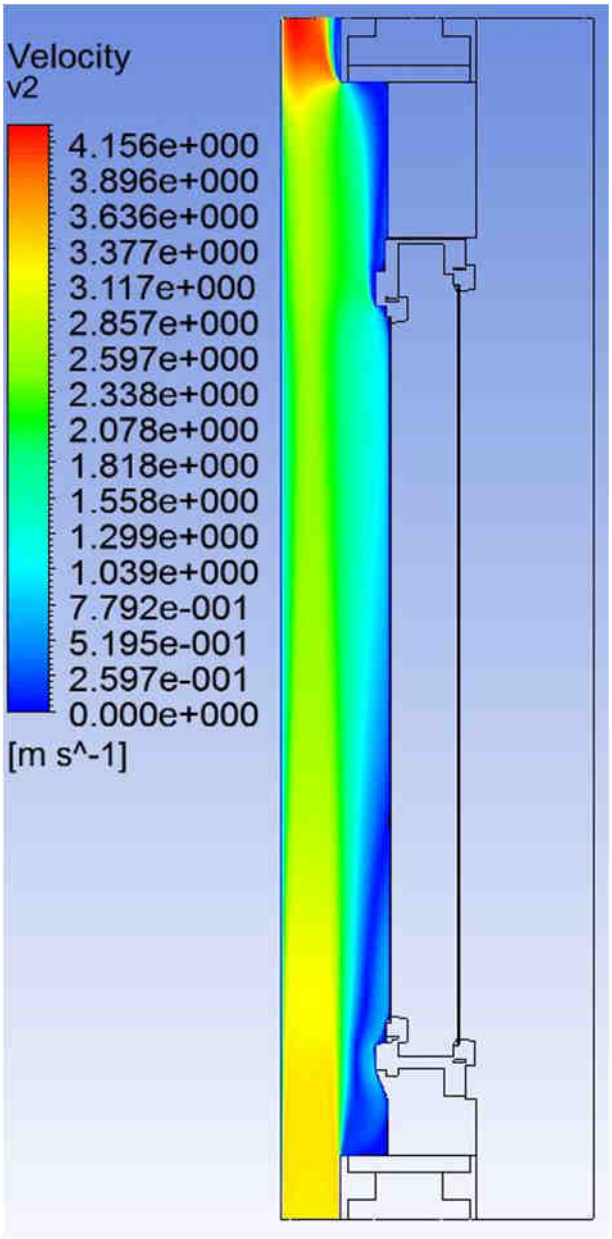

Fig. 90. – Window 2 – velocity magnitude in the external air channel

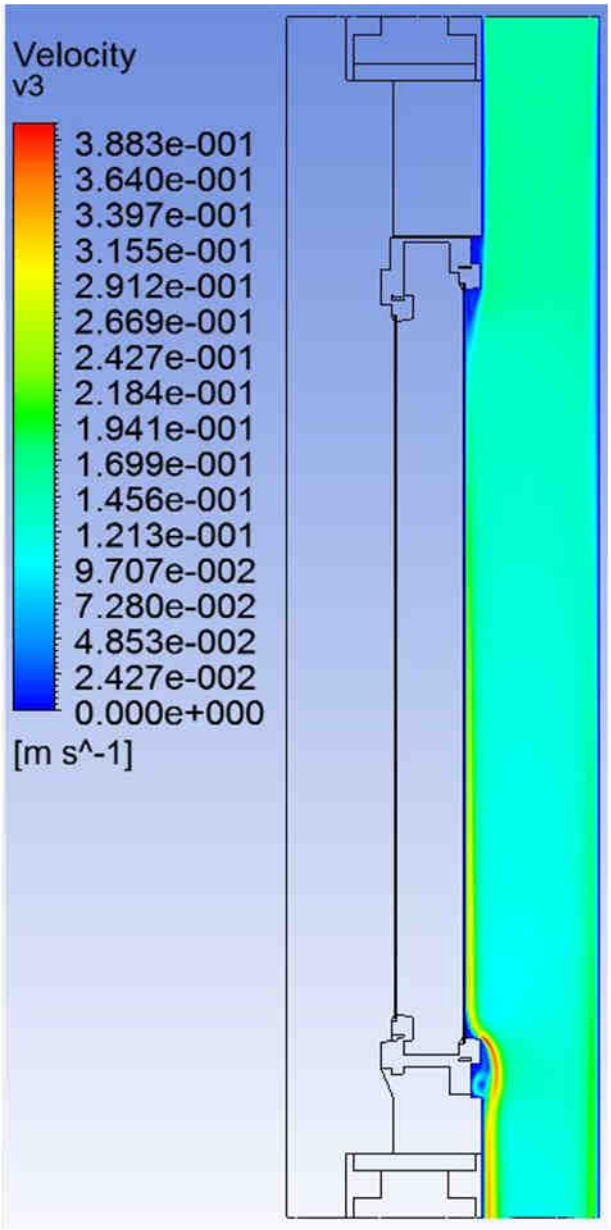

Fig. 91. – Window 2 – velocity magnitude in the internal air channel

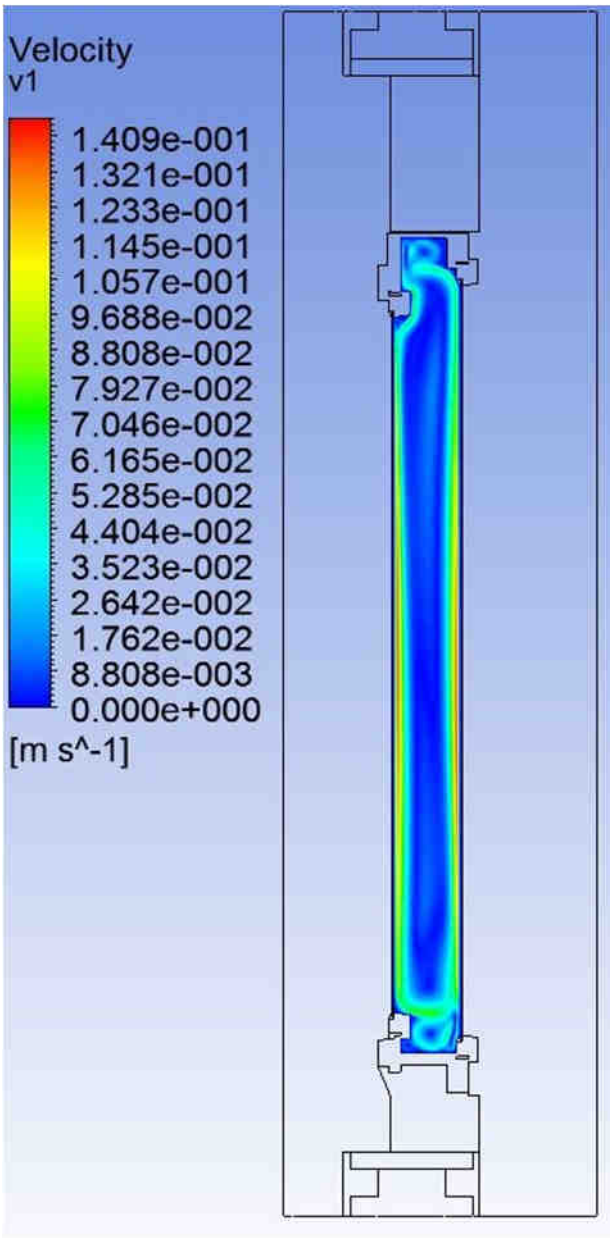

Fig. 92. – Window 2 – velocity magnitude in the main window cavity

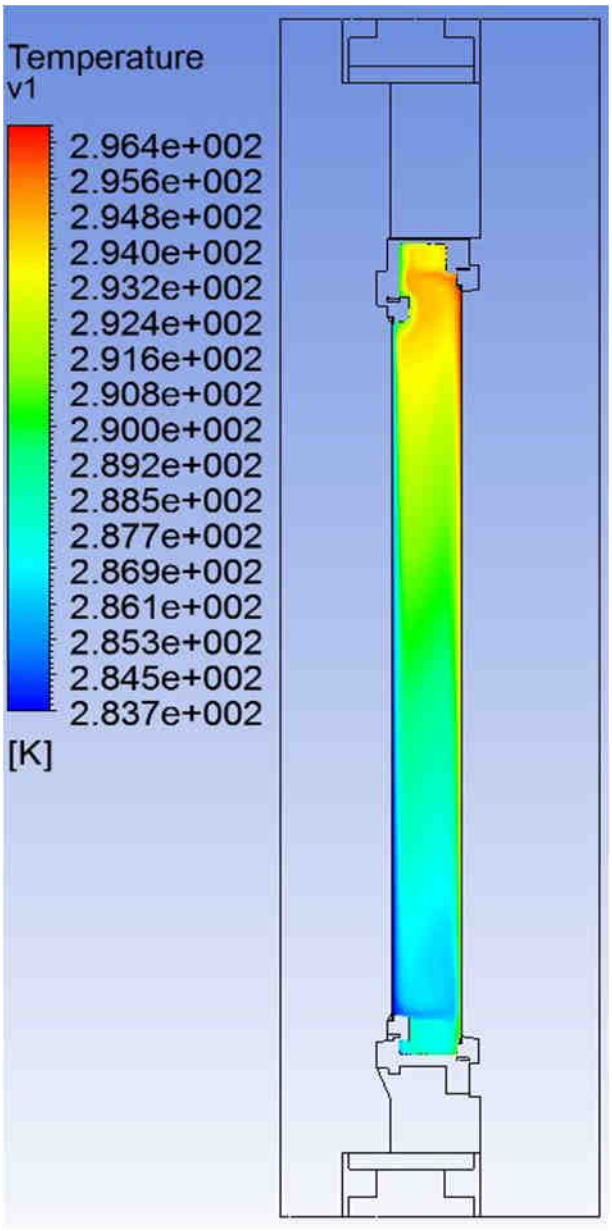

Fig. 93. – Window 2 – temperature field in the main glazing cavity

Boundary conditions:

- External baffle: T_{surf}=f(y) from measurement, ε=0.95 [-] (painted matt black)
- External air channel inlet: 3.3 [m/s], turb. intensity=10% [-], l_{turb}=0.007 [m], T_{inlet}=281.55 [K]
- External air channel outlet: pressure outlet, Gauge pressure 0 [Pa], backflow: turb. intensitiy 5%, visc. ratio 10
- Internal baffle: T_{surf}=f(y) from measurement, ε=0.95 [-] (painted matt black)
- Internal air channel inlet: 15 [cm/s], turb. intensity 2.5%, visc. ratio 3, T_{inlet}=303.71 [K]
- Internal air channel outlet: pressure outlet, gauge pressure 0 [Pa] backflow turb. in. 5%, visc. ratio 10

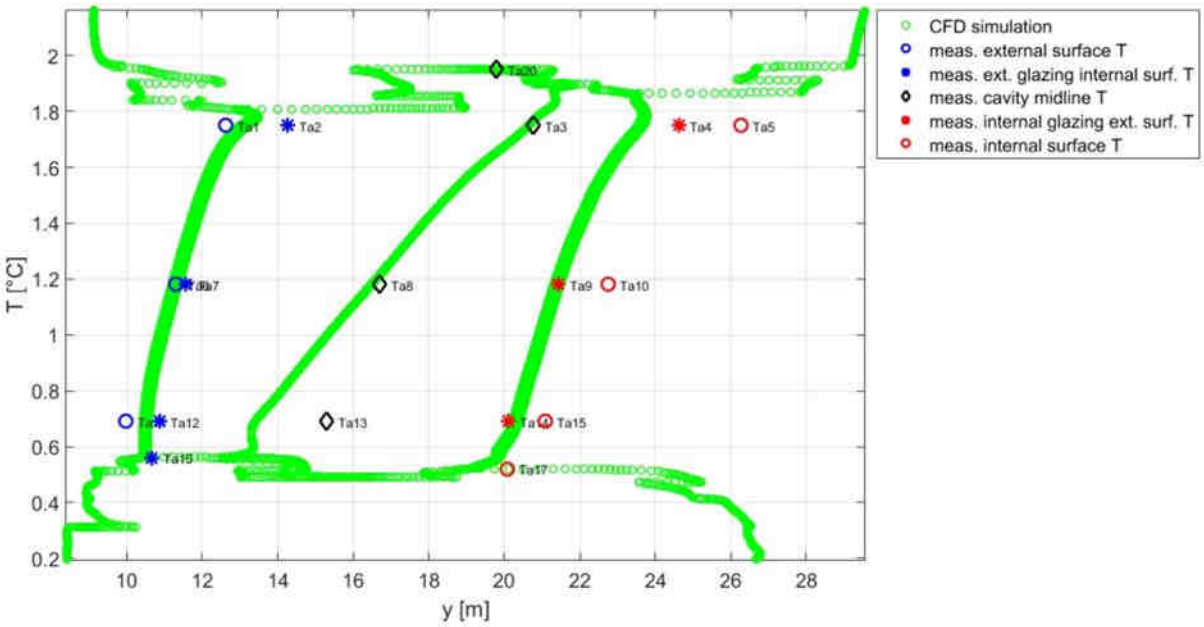

Fig. 94. – Window 2 – comparison of measurement and CFD simulation – external and internal baffle and air channels added to the simulation

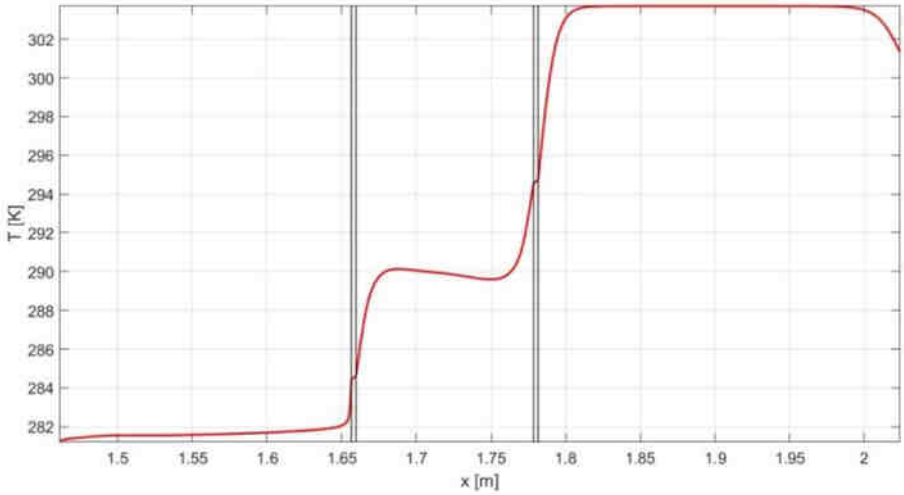

Fig. 95. – Window 2 – horizontal temperature section through the middle of the glazing

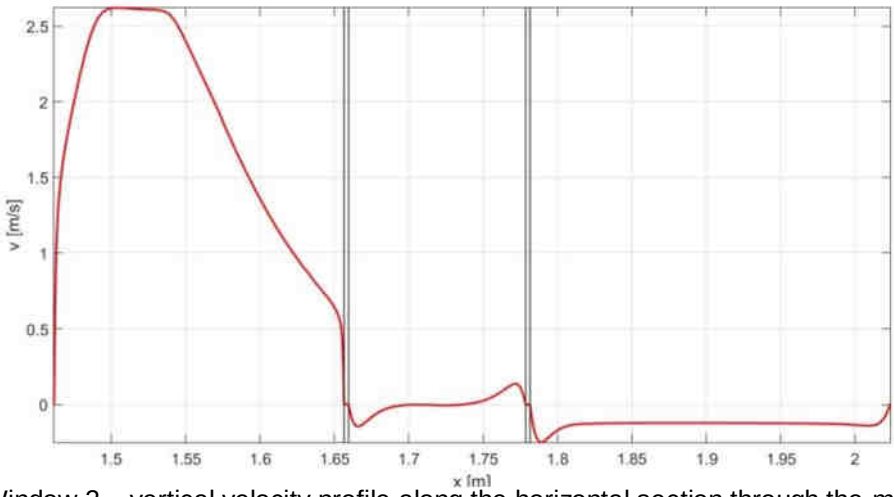

Fig. 96. – Window 2 – vertical velocity profile along the horizontal section through the middle of the glazing

B.4.3 window 2b

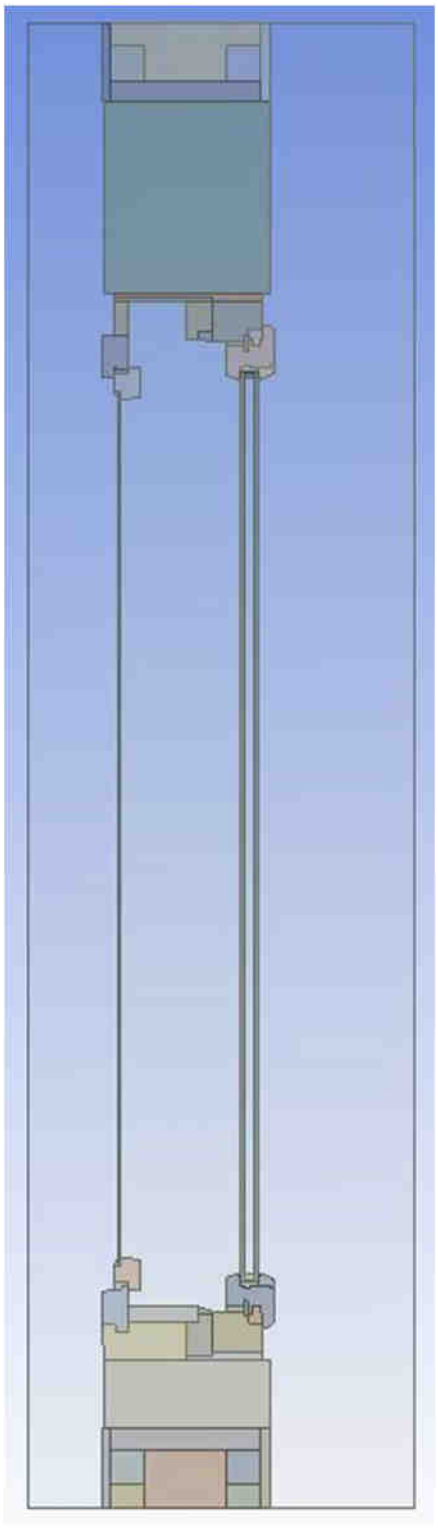

Fig. 97. – Window 2b - geometry

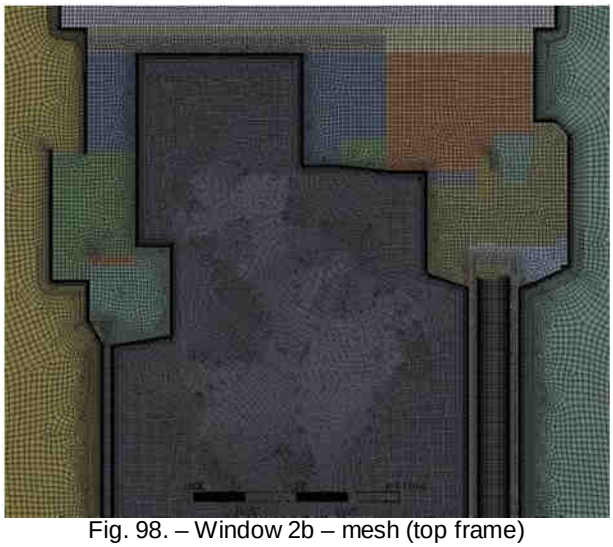

Fig. 98. – Window 2b – mesh (top frame)

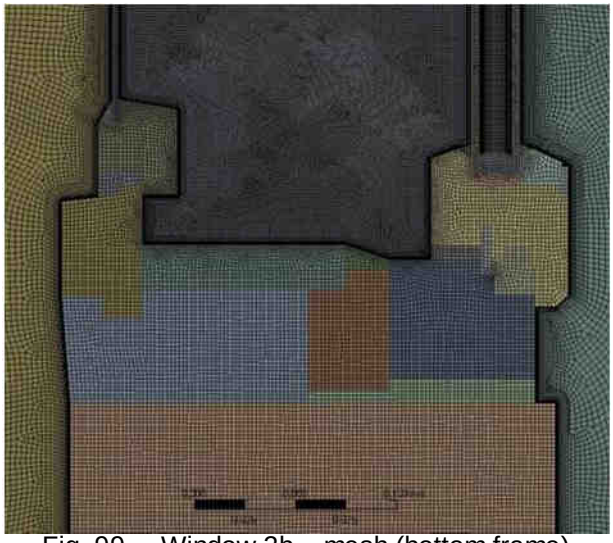

Fig. 99. – Window 2b – mesh (bottom frame)

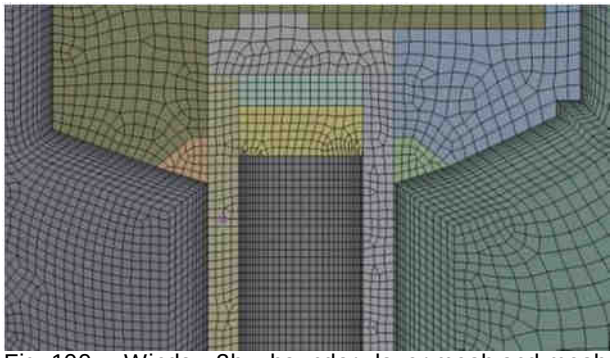

Fig. 100. – Window 2b – boundary layer mesh and mesh inside the insulating glass unit's cavity (laminar flow)

Mesh: 467880 nodes and 467195 elements with 1 [mm] element length along every fluid/solid interface. 2 [mm] element size in the solid domains with the exception of the glazing layers where the element size is 1 [mm] to provide at least 3 elements for the thickness. Inflation mesh along every fluid wall in the air filled internal and external cavities with a first element thickness of 2e-4 [m], 10 layers and a growth rate of 1.2. The mesh in the argon filled cavity of the IG unit has 30 element in x direction with a bias factor of 5. The calculated dimensionless wall distance is y+<1 [-] everywhere.

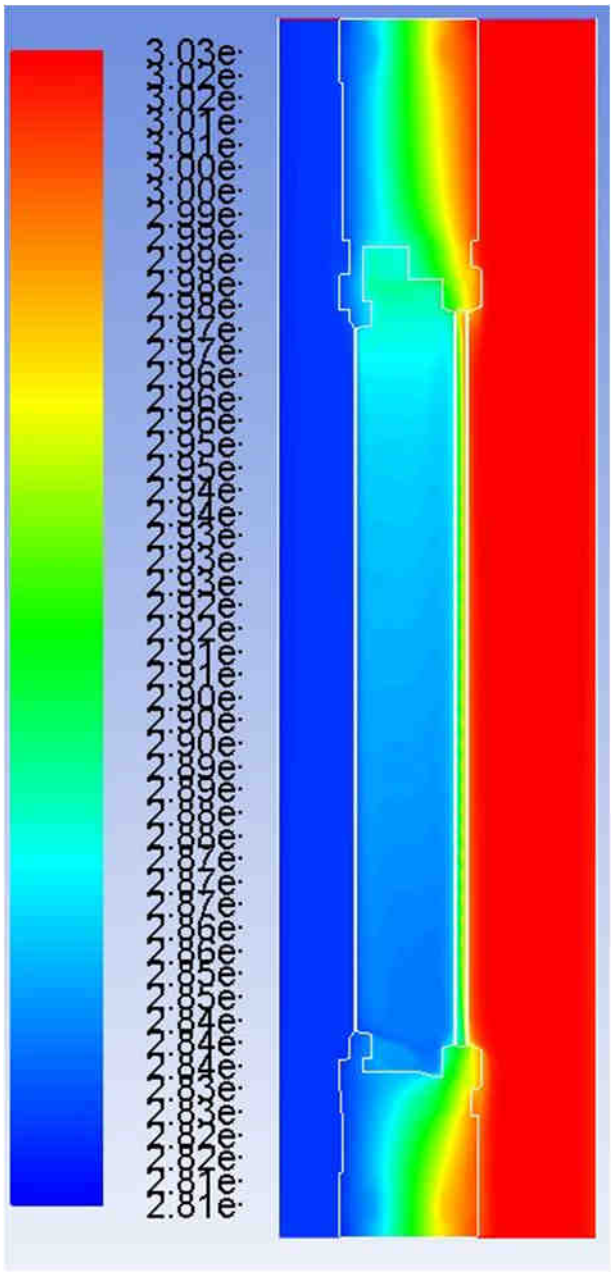

Fig. 101. – Window 2b – entire temperature field

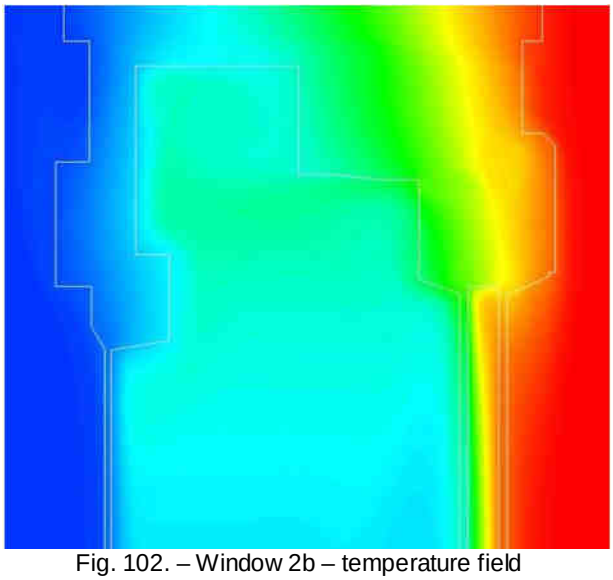

Fig. 102. – Window 2b – temperature field (top of the frame)

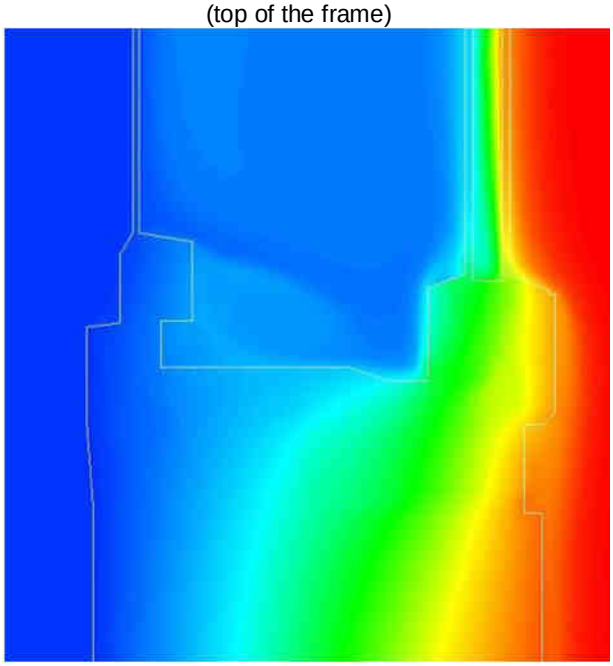

Fig. 103. – temperature field (bottom of the frame)

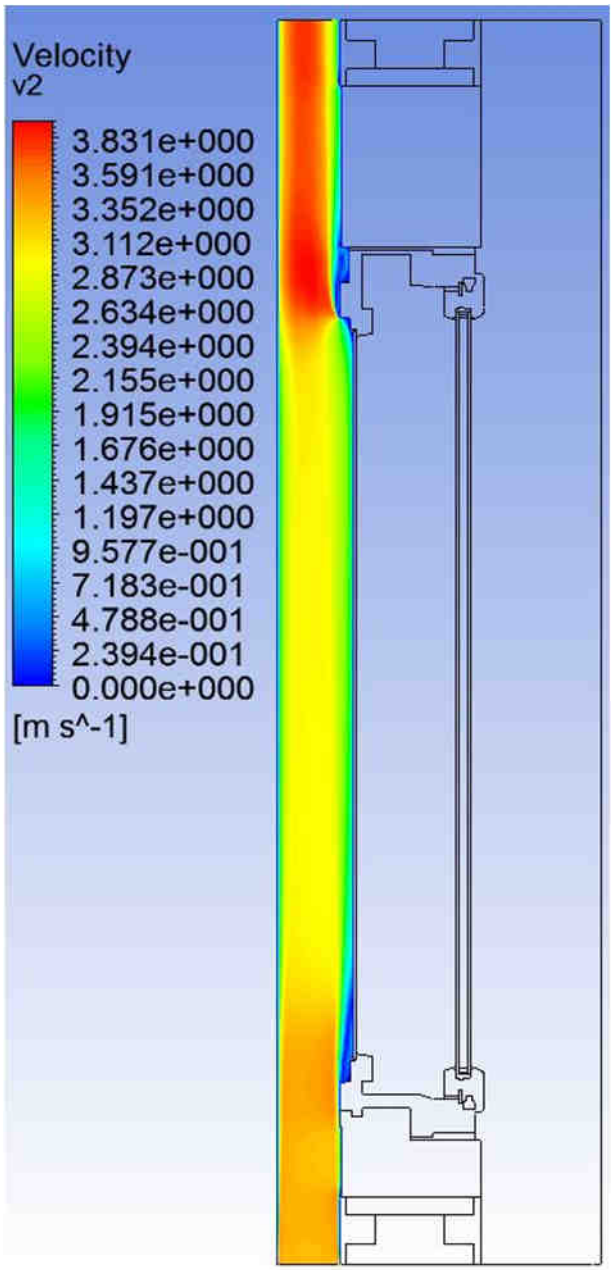

Fig. 104. – Window 2b – velocity magnitude in the external air channel

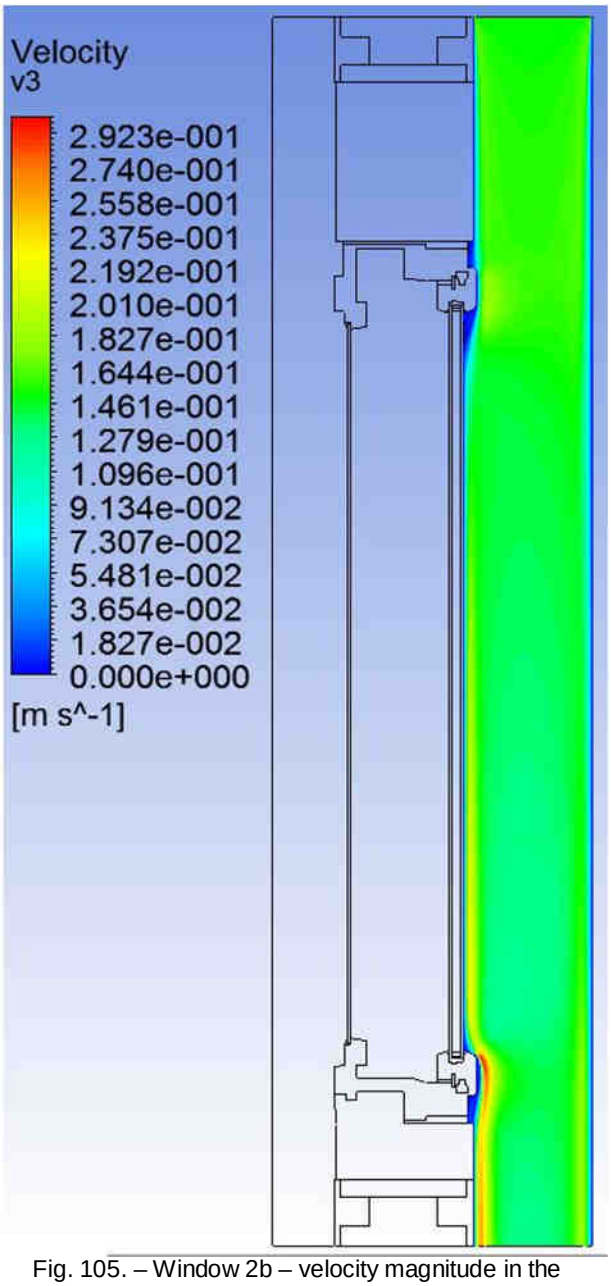

Fig. 105. – Window 2b – velocity magnitude in the internal air channel

Boundary conditions:

- External baffle: T_{surf}=f(y) from measurement, ε=0.95 [-] (painted matt black)
- External air channel inlet: 3.3 [m/s], turb. intensity=10% [-], I_{turb}=0.007 [m], T_{inlet}=282.2515 [K]
- External air channel outlet: pressure outlet, Gauge pressure 0 [Pa], backflow: turb. intensitiy 5%, visc. ratio 10
- Internal baffle: T_{surf}=f(y) from measurement, ε=0.95 [-] (painted matt black)
- Internal air channel inlet: 15 [cm/s], turb. intensity 2.5%, visc. ratio 3, T_{inlet}=302.5135 [K]
- Internal air channel outlet: pressure outlet, gauge pressure 0 [Pa] backflow turb. in. 5%, visc. ratio 10

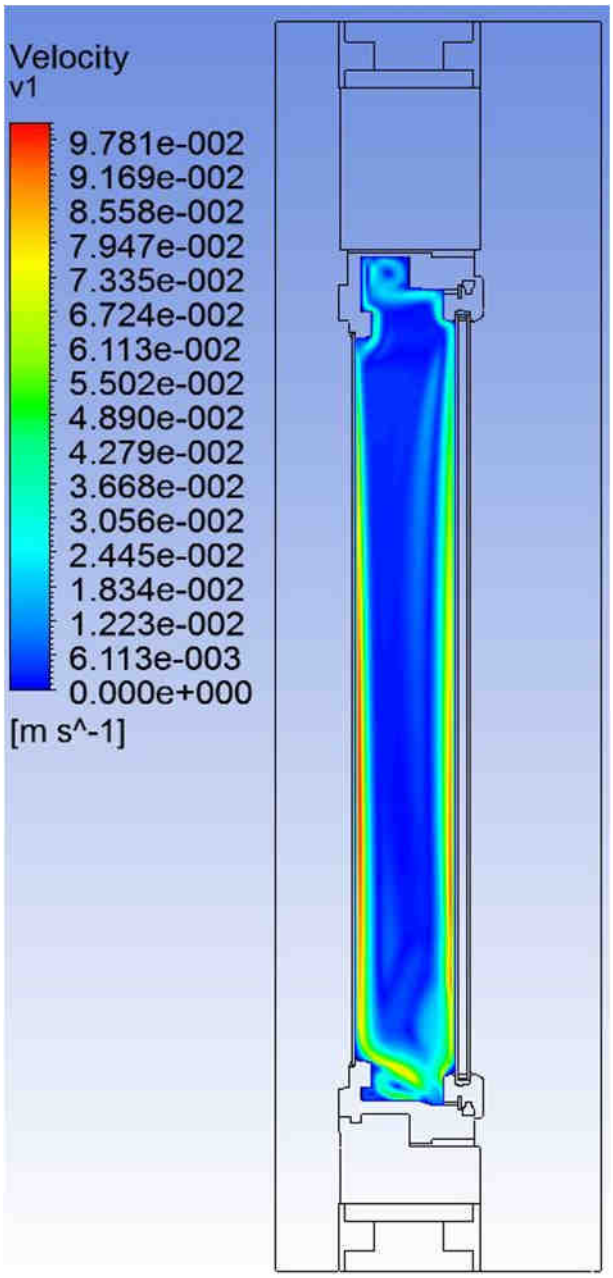

Fig. 106. – Window 2b – velocity magnitude in the main window cavity

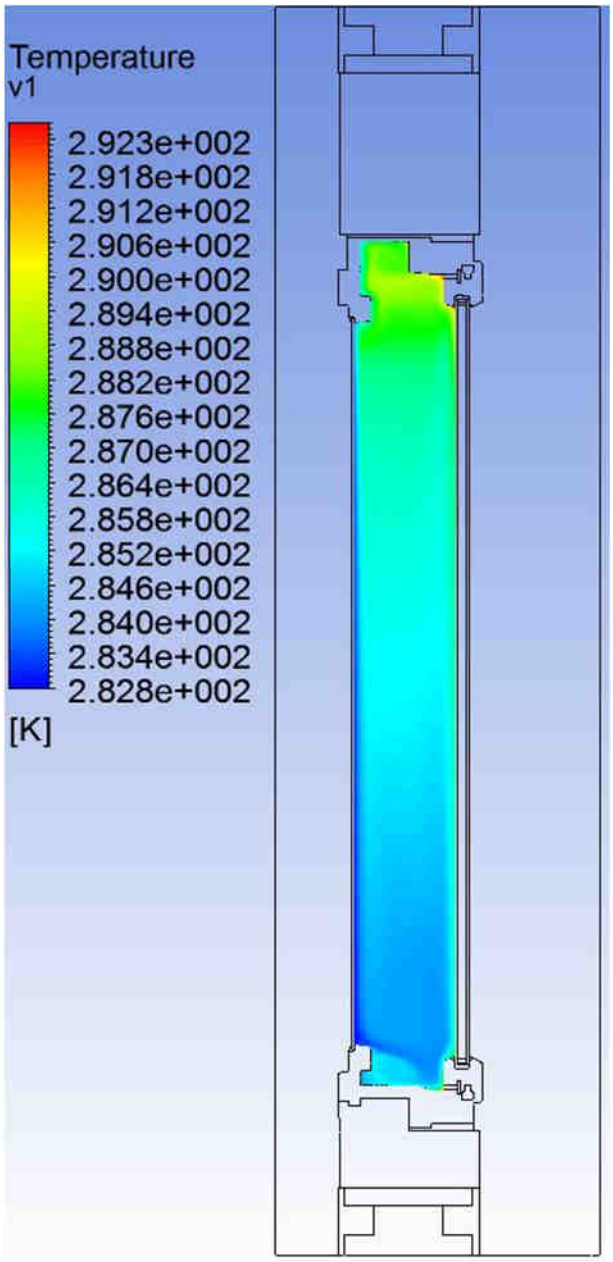

Fig. 107. – Window 2b – temperature field in the main window cavity

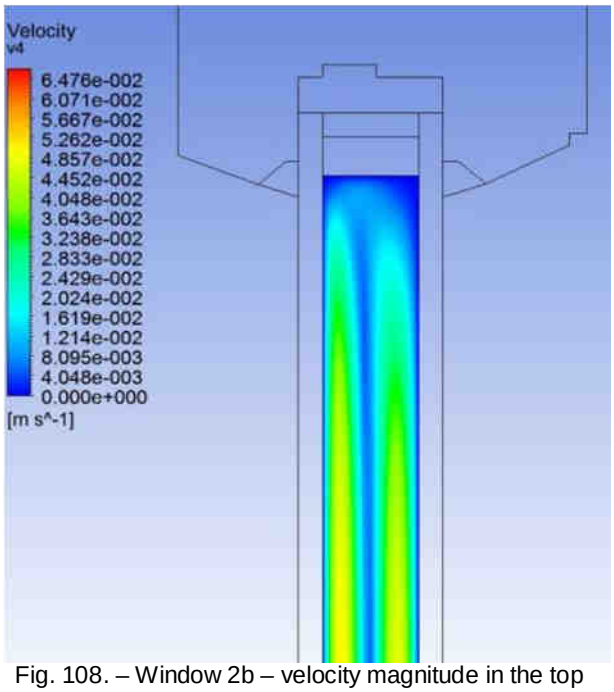

Fig. 108. – Window 2b – velocity magnitude in the top of the insulating glass unit's cavity

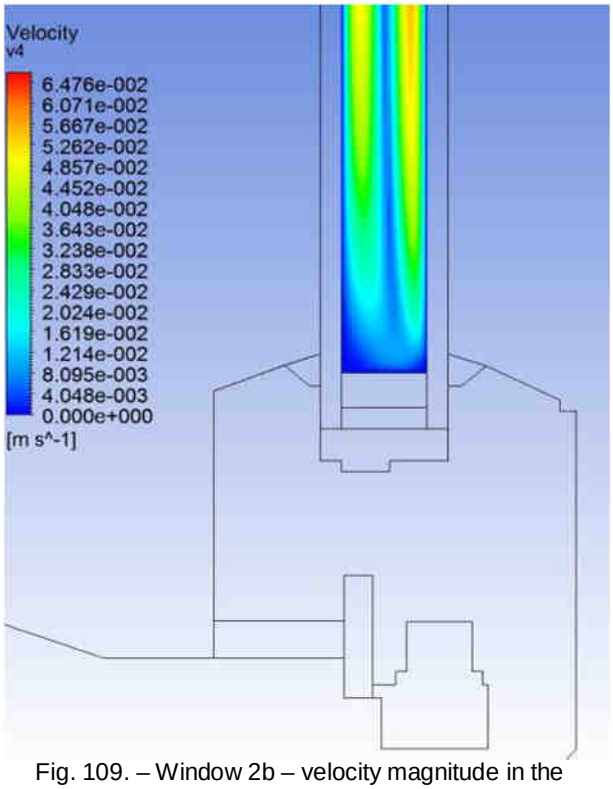

Fig. 109. – Window 2b – velocity magnitude in the bottom of the insulating glass unit's cavity

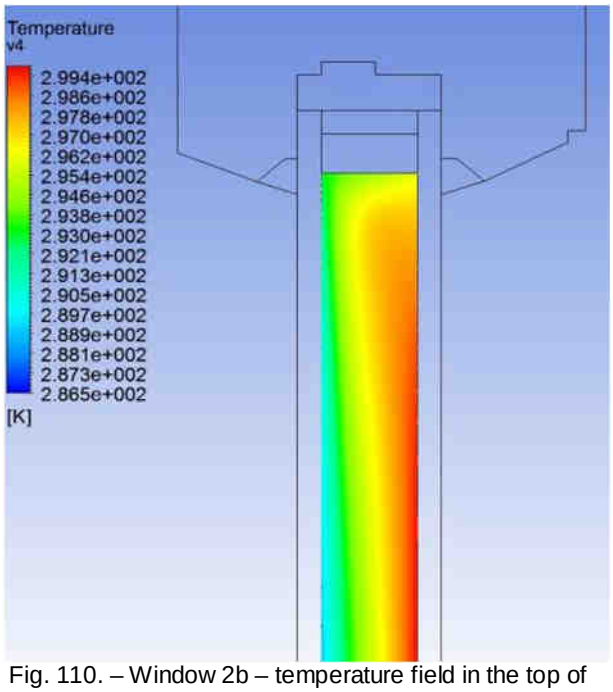

Fig. 110. – Window 2b – temperature field in the top of the insulating glass unit's cavity

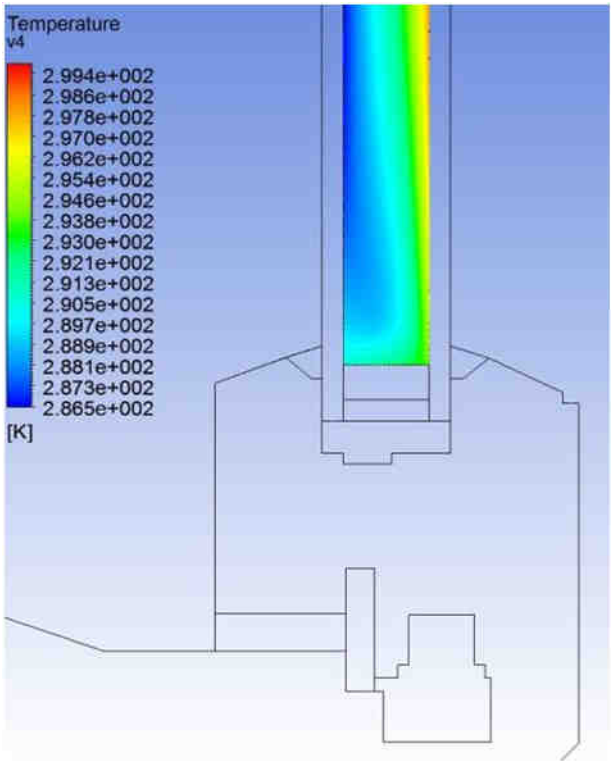

Fig. 111. – Window 2b – temperature field in the bottom of the insulating glass unit's cavity

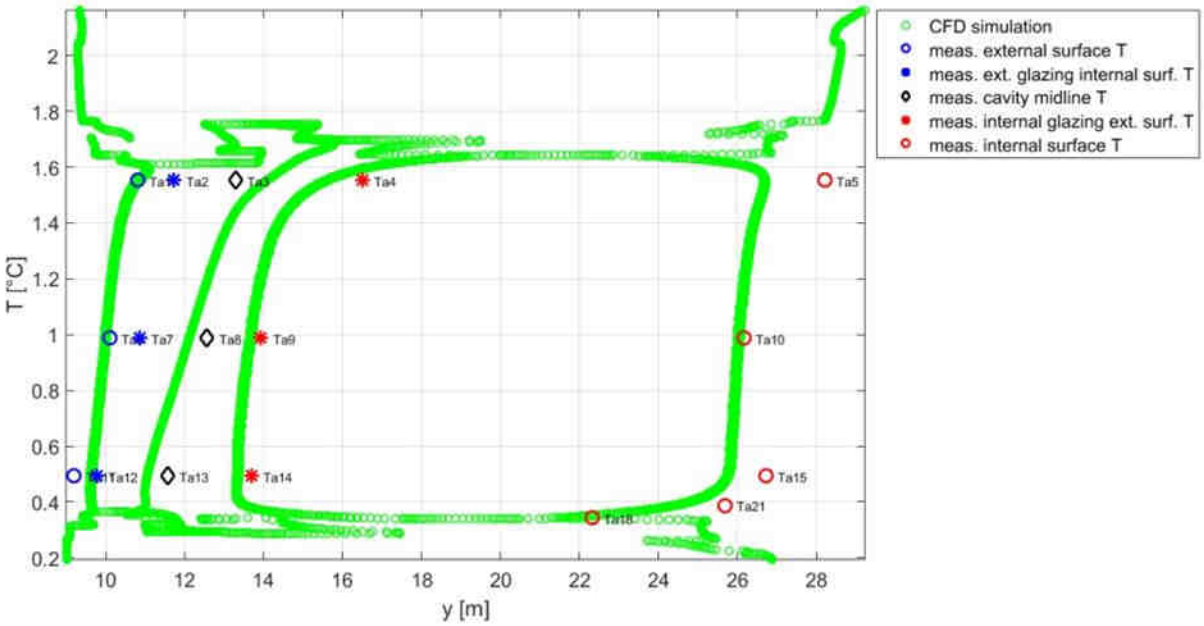

Fig. 112. – Window 2 – comparison of measurement and CFD simulation – external and internal baffle and air channels added to the simulation

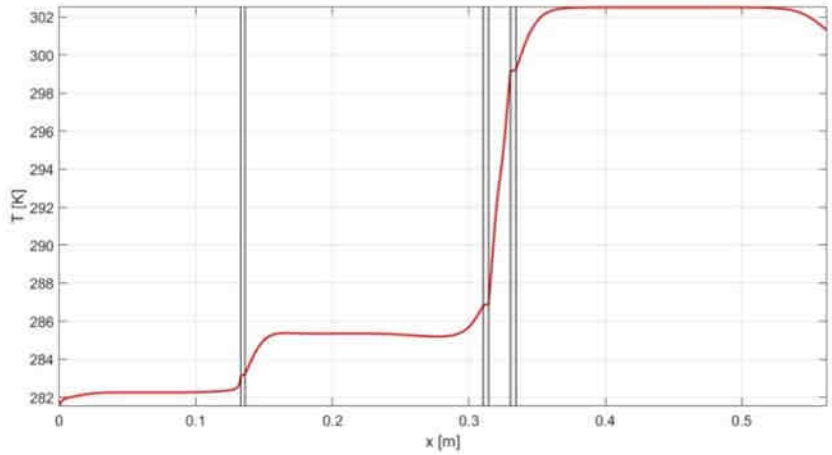

Fig. 113. – Window 2b – horizontal temperature section through the middle of the glazing

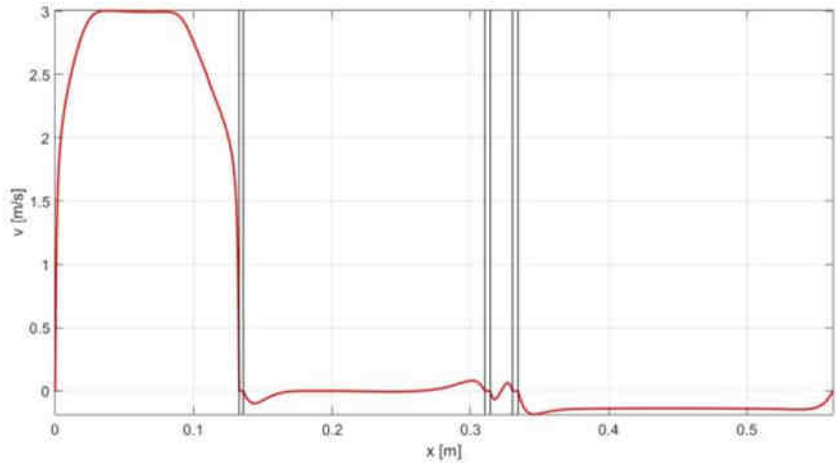

Fig. 114. – Window 2b – vertical velocity profile along the horizontal section through the middle of the glazing

B.4.4 window 3a

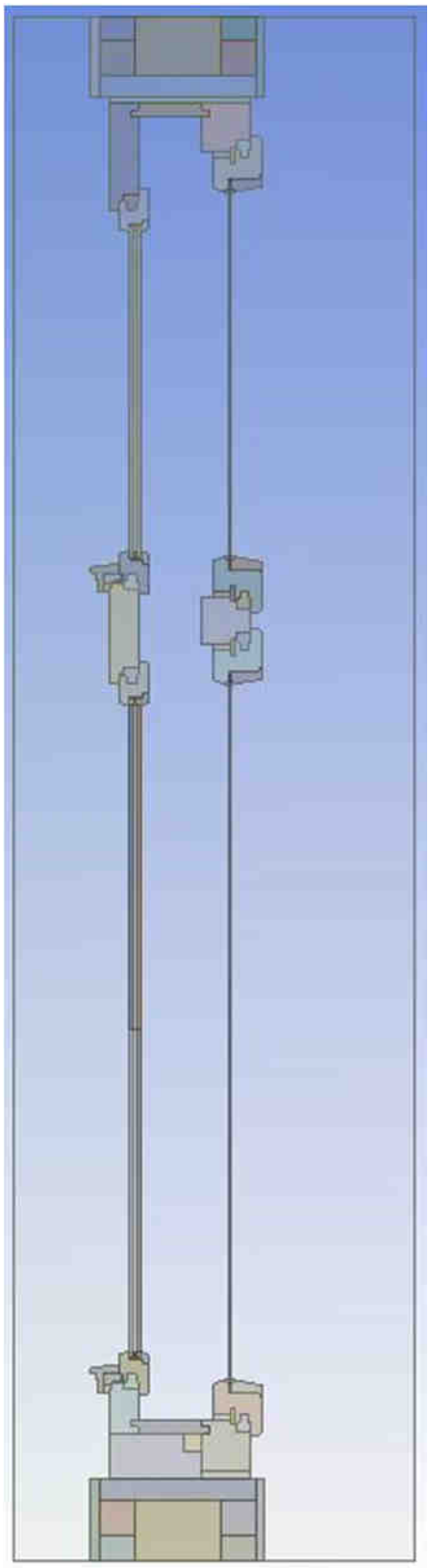

Fig. 115. – window 3a - geometry

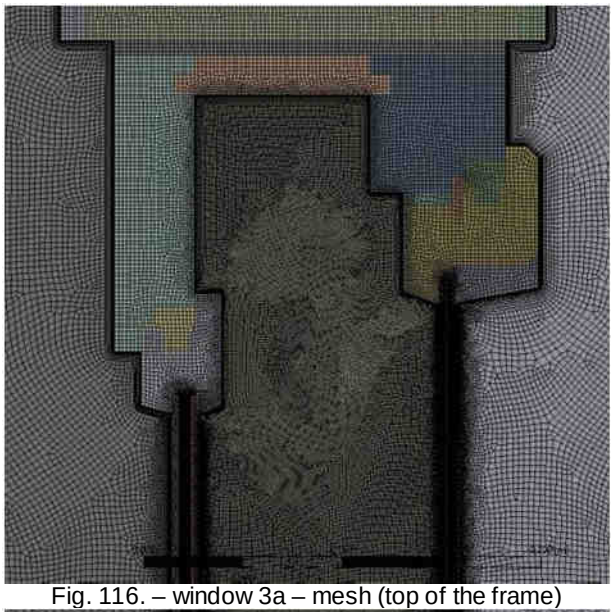

Fig. 116. – window 3a – mesh (top of the frame)

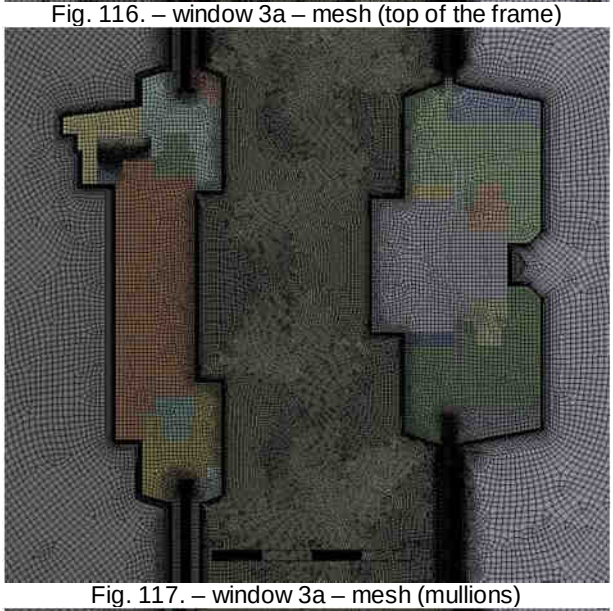

Fig. 117. – window 3a – mesh (mullions)

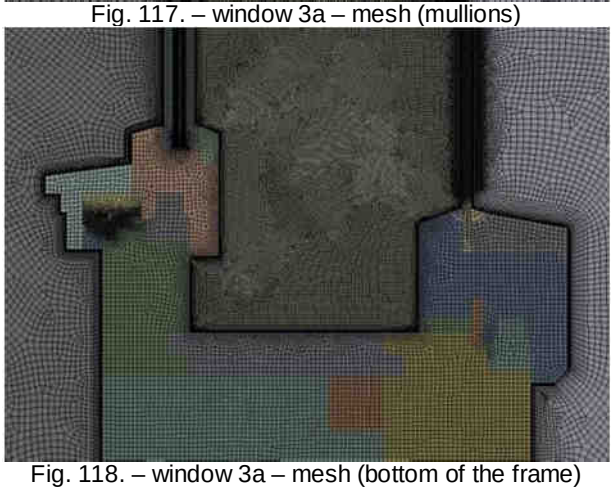

Fig. 118. – window 3a – mesh (bottom of the frame)

Mesh: 585768 nodes and 585308 elements with 1 [mm] element length along every fluid/solid interface. 2 [mm] element size in the solid domains with the exception of the glazing layers where the

element size is 1 [mm] to provide at least 3 elements for the thickness. Inflation mesh along every fluid wall in the air filled internal and external cavities with a first element thickness of 2e-4 [m], 10 layers and a growth rate of 1.2. The mesh in the argon filled cavity of the IG unit has 30 element in x direction with a bias factor of 5. The calculated dimensionless wall distance is y+<0.1 [-] everywhere.

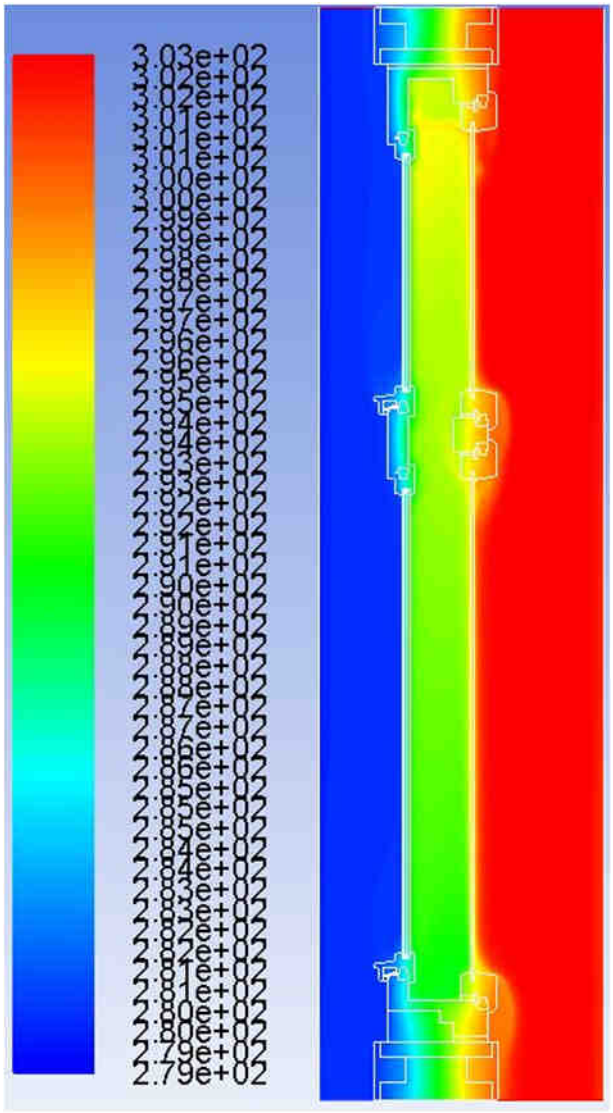

Fig. 119. – window 3a - entire temperature field

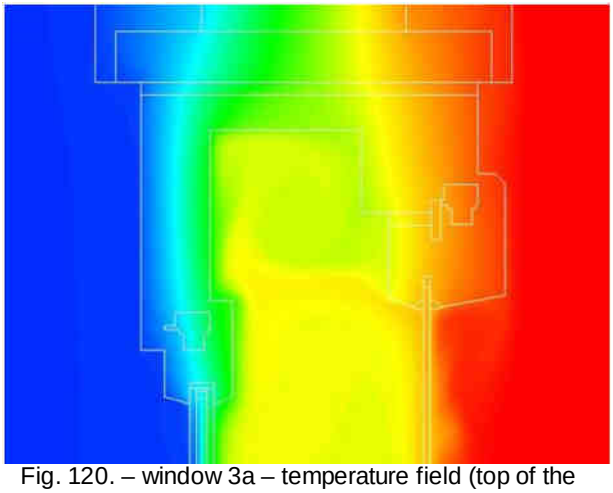

Fig. 120. – window 3a – temperature field (top of the frame)

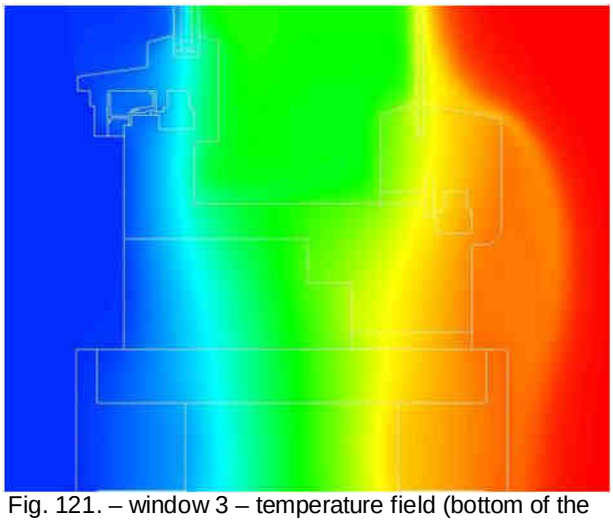

Fig. 121. – window 3 – temperature field (bottom of the frame)

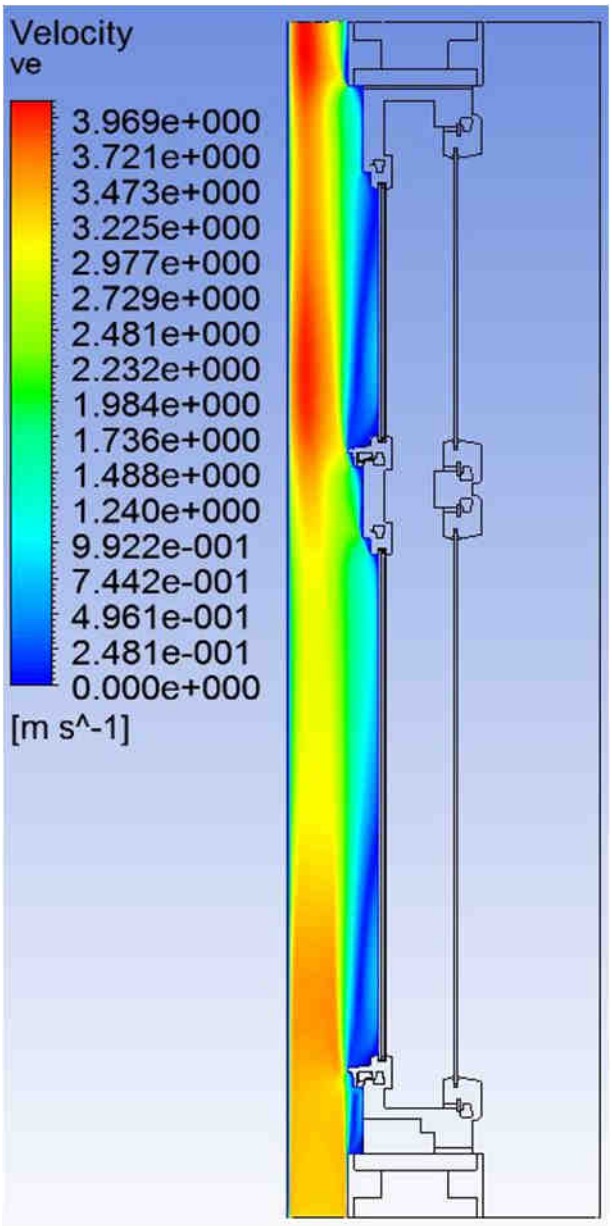

Fig. 122. – window 3a – velocity magnitude in the cold side air channel

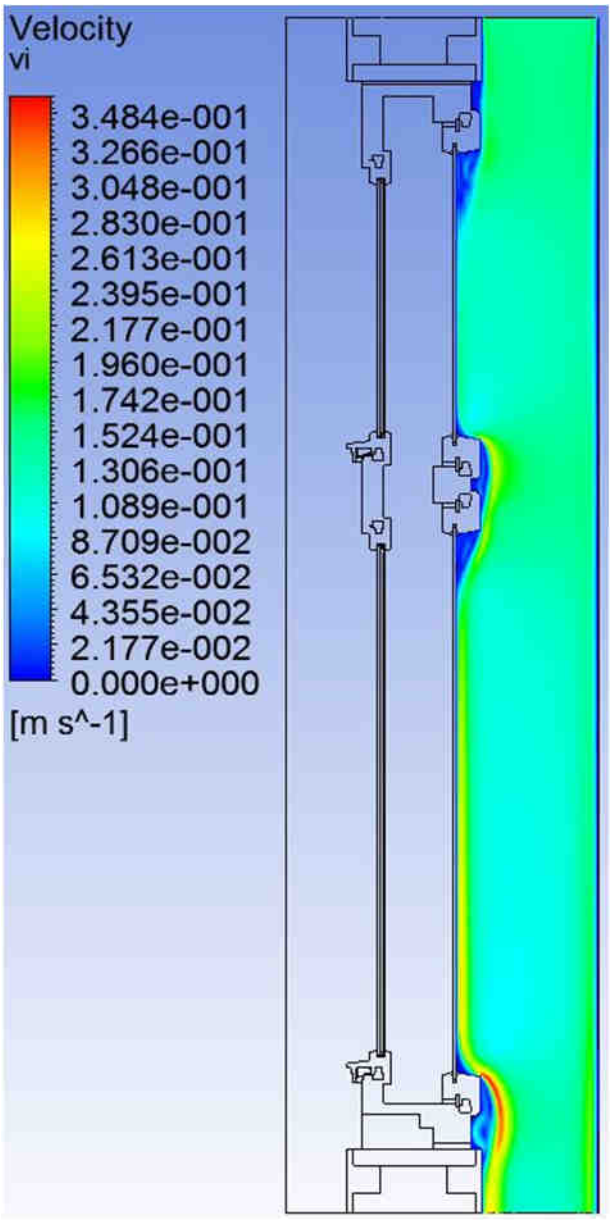

Fig. 123. – window 3a – velocity magnitude in the hot side air channel

Boundary conditions:

- External baffle: T_{surf}=f(y) from measurement, ε=0.95 [-] (painted matt black)
- External air channel inlet: 3.3 [m/s], turb. intensity=10% [-], I_{turb}=0.007 [m], T_{inlet}=279.94 [K]
- External air channel outlet: pressure outlet, Gauge pressure 0 [Pa],
  backflow: turb. intensitiy 5%, visc. ratio 10
- Internal baffle: T_{surf}=f(y) from measurement, ε=0.95 [-] (painted matt black)
- Internal air channel inlet: 15 [cm/s], turb. intensity 2.5%, visc. ratio 3, T_{inlet}=302.956 [K]
- Internal air channel outlet: pressure outlet, gauge pressure 0 [Pa]
  backflow turb. in. 5%, visc. ratio 10

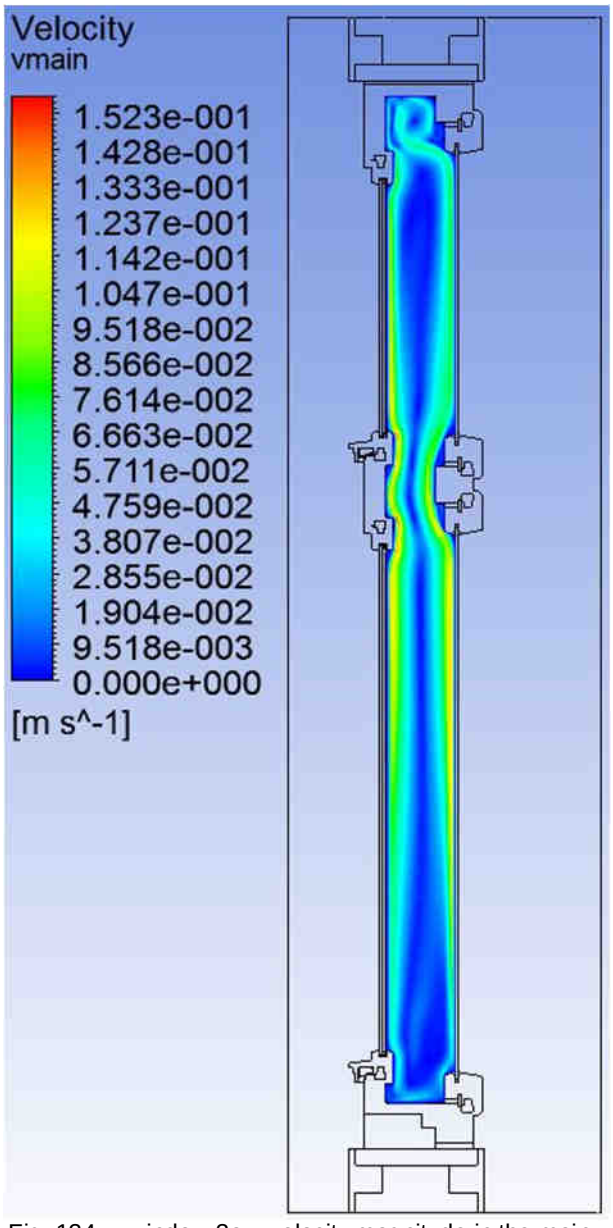

Fig. 124. – window 3a – velocity magnitude in the main window cavity

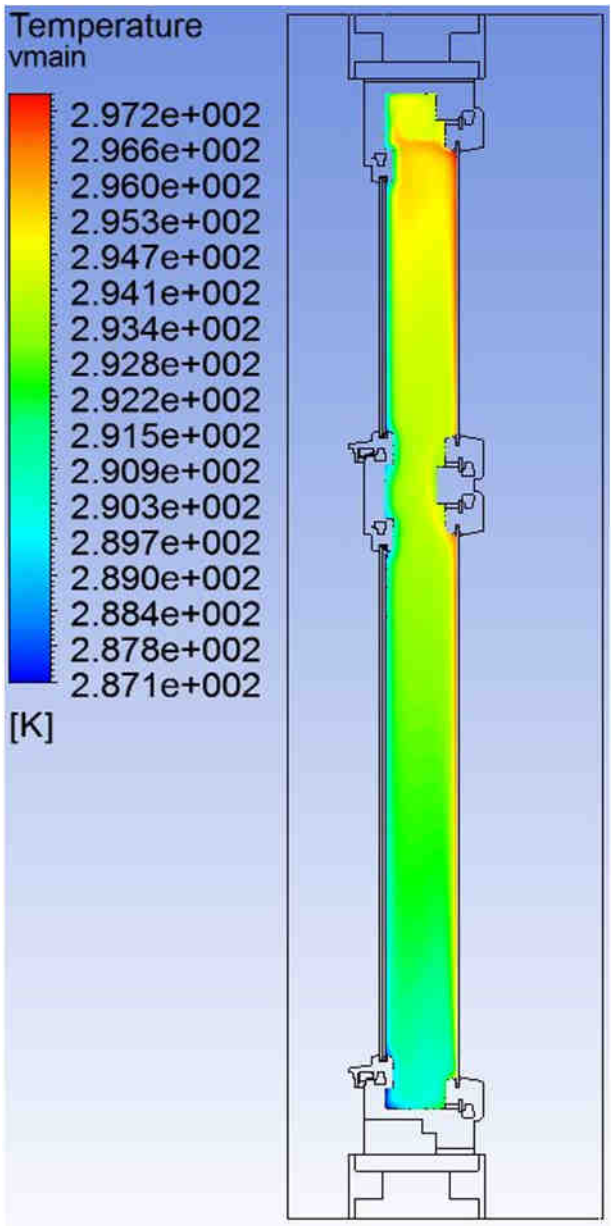

Fig. 125. – window 3a – temperature field in the main window cavity

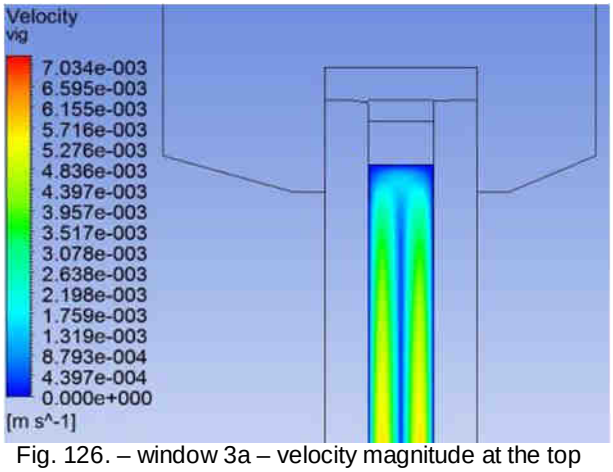

Fig. 126. – window 3a – velocity magnitude at the top of the thin insulating glass unit

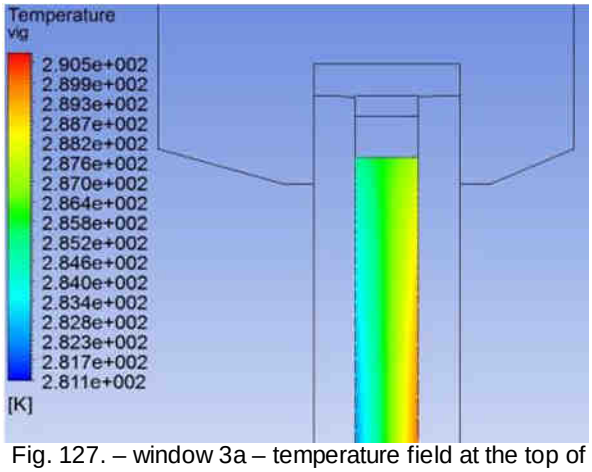

Fig. 127. – window 3a – temperature field at the top of the thin insulating glass unit

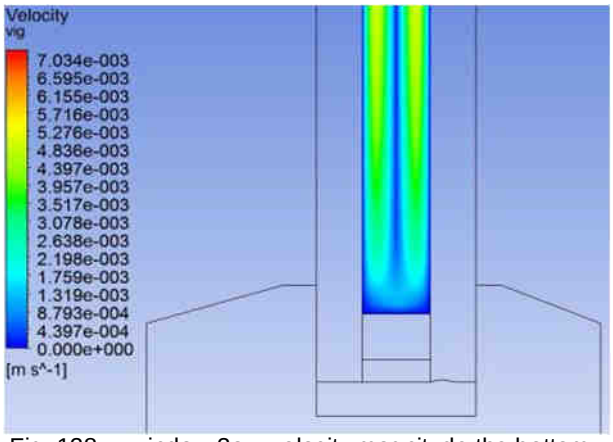

Fig. 128. – window 3a – velocity magnitude the bottom of the thin insulating glass unit's cavity

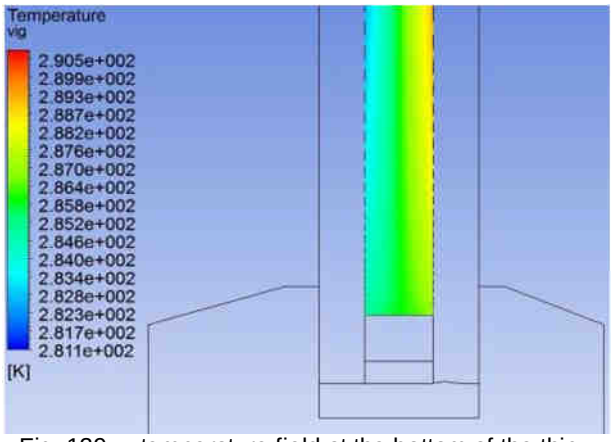

Fig. 129. – temperature field at the bottom of the thin insulating glass unit's cavity

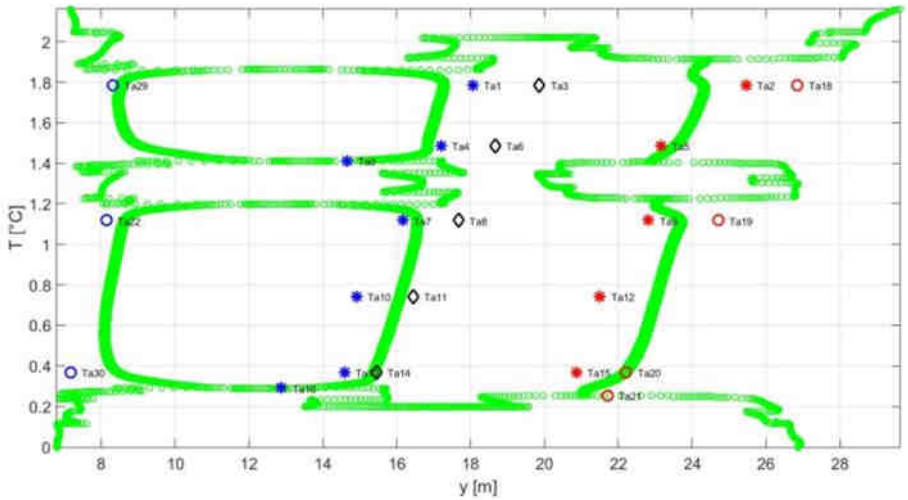

Fig. 130. – Window 3a – comparison of measurement and CFD simulation – external and internal baffle and air channels added to the simulation

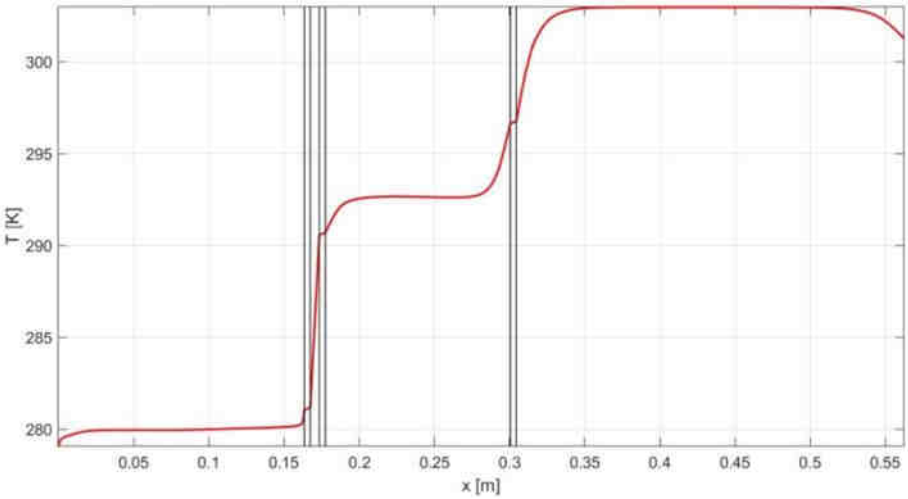

Fig. 131. – Window 3a – horizontal temperature section through the middle of the glazing

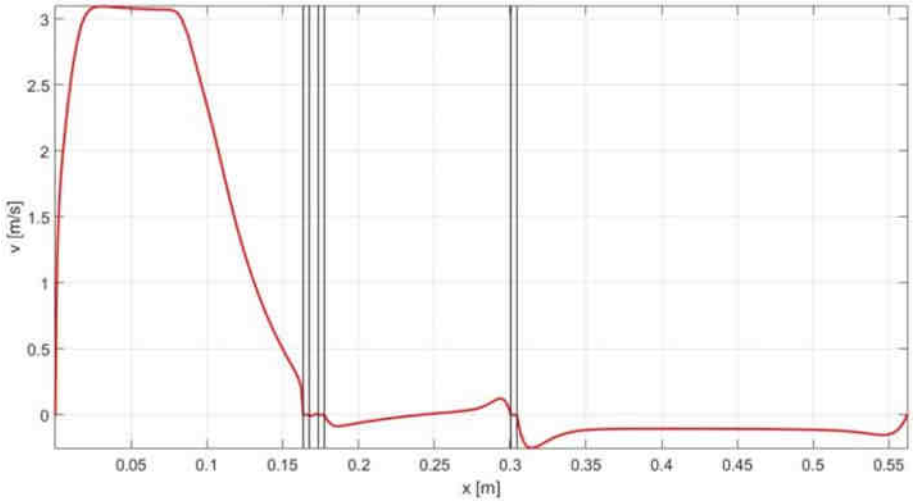

Fig. 132. – Window 3a – vertical velocity profile along the horizontal section through the middle of the glazing

B.5 Simulation of 3D heat transfer

B.5.1 Generic 3D box window

glazing system: • 3 [mm] float glass (IGDB: 11100), ε_f = 0.837 [-],ε_b = 0.837 [-] • 137 [mm] air gap • 3 [mm] float glass (IGDB: 11100), ε_f = 0.837 [-],ε_b = 0.837 [-]						Ug = 2.805 [W/m^{2}K] (ISO) 2.697 [W/m^{2}K] (new)	
cavity	L [mm]	H [mm]	A [-]	model	Ra [-]	Nu [-]	λ_{eff} [W/mK]
1	137	1392	10.16	ISO		10.1279	0.7531
				new		7.9204	0.6913

Table 1 – simple (original) glazing system – the calculated center-of-glazing heat transfer coefficient and glazing cavity properties for 20/0 [°C] simple boundary conditions

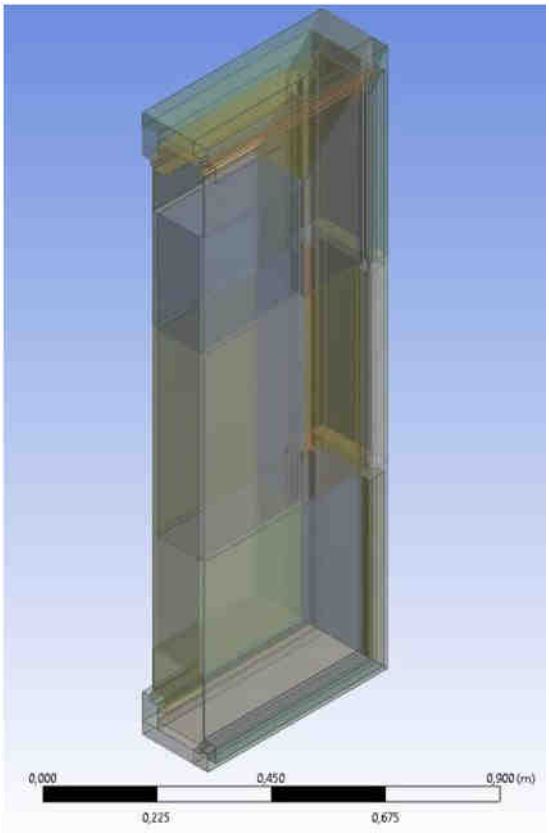

Fig. 133. – generic 3D box window – geometry

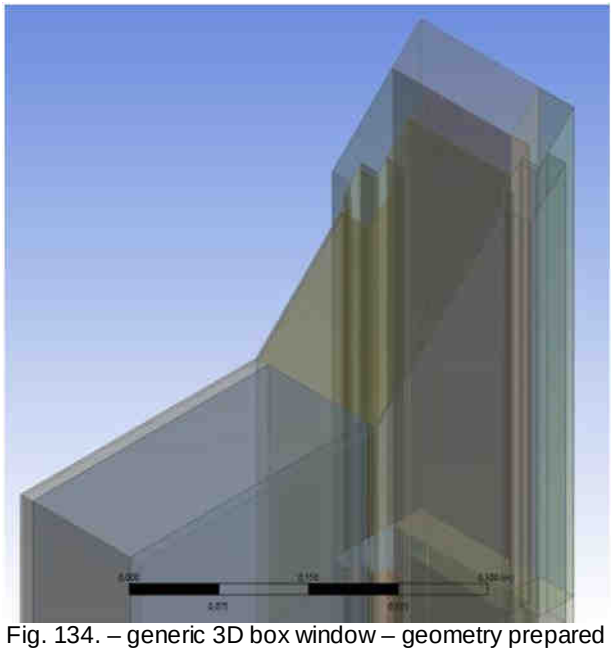

Fig. 134. – generic 3D box window – geometry prepared for swept meshing

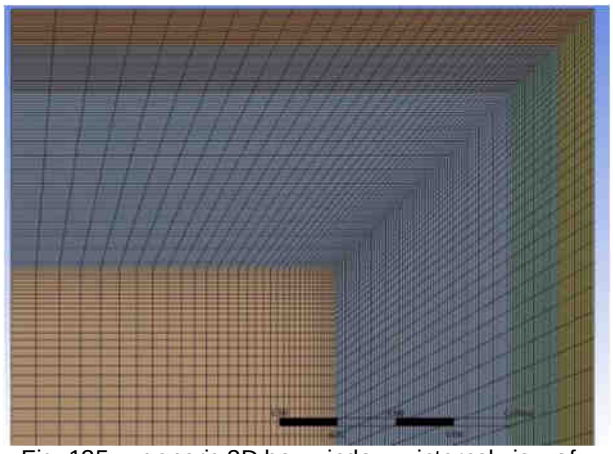

Fig. 135. – generic 3D box window – internal view of mesh in top right corner

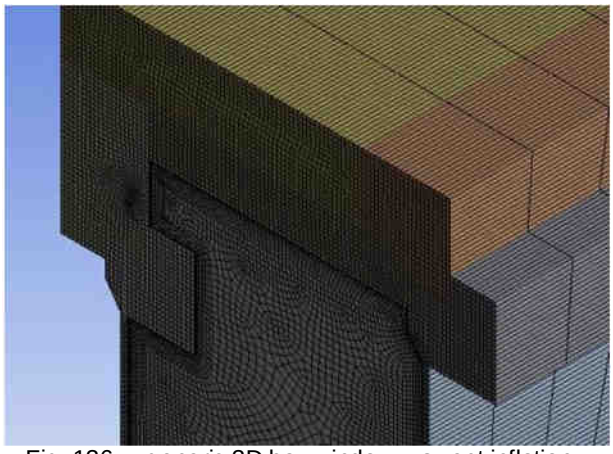

Fig. 136. – generic 3D box window – swept inflation mesh for the fame adjacent portion of the cavity

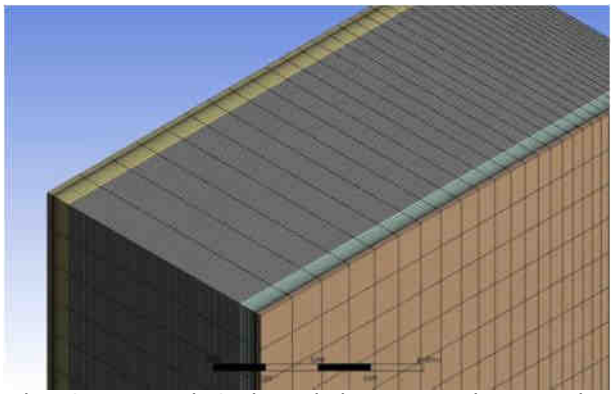

Fig. 137. – generic 3D box window – swept hexa mesh in the core of thecavity

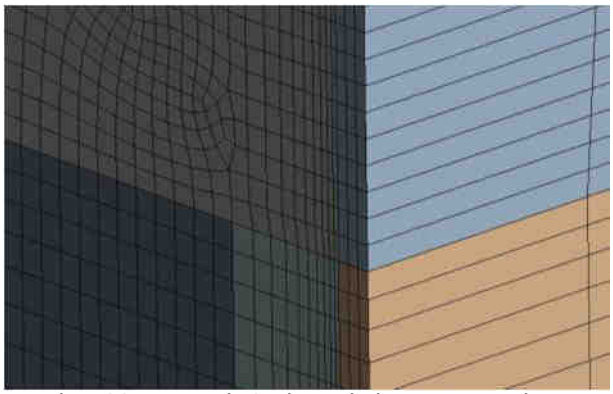

Fig. 138. – generic 3D box window – connection between hexa and inflation mesh

Mesh: 1822180 nodes and 177135 elements. The core of the flow cavity has a rectangular structured swept hexa mesh with bias toward the edged and boundary layers at the glazing surfaces. The sides of the geometry have a swept mixed hex / tetra + inflation mesh. the inflation layers have a first element height of 4.5e-4 [m], 10 layers and a growth rate of 1.2. The dimensionless wall distance is y+<0.5 [-] everywhere.

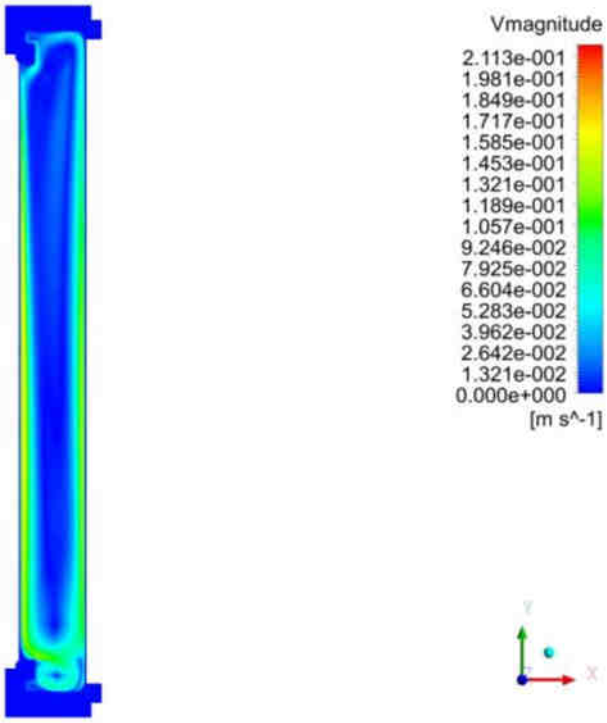

Fig. 139. – generic 3D box window – velocity magnitude in the vertical symmetry plane

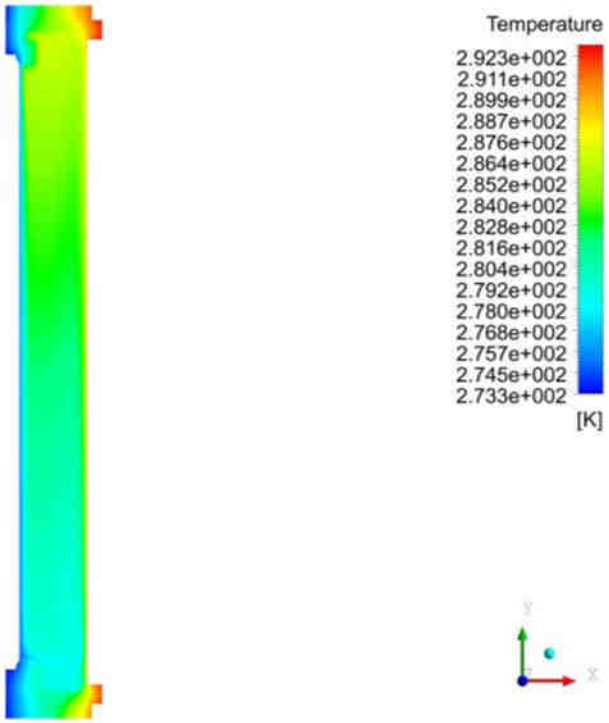

Fig. 140. – generic 3D box window – temperature field in the vertical symmetry plane

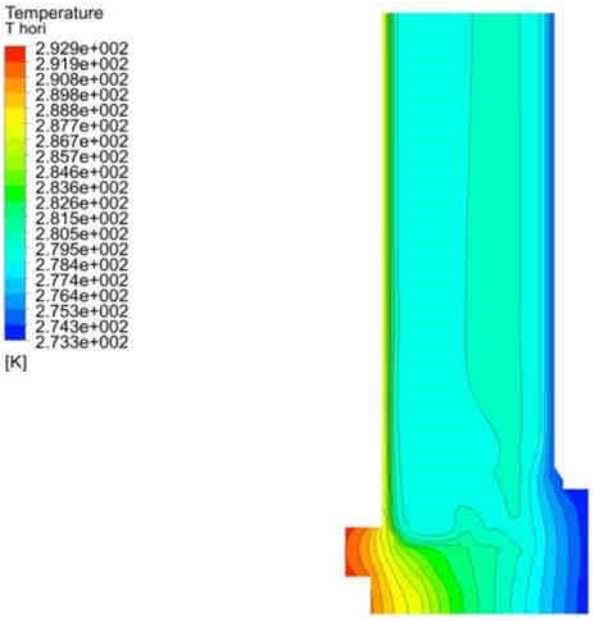

Fig. 141. – generic 3D box window – temperature field in the horizontal section, at y/H=0.1 [-] of the cavity

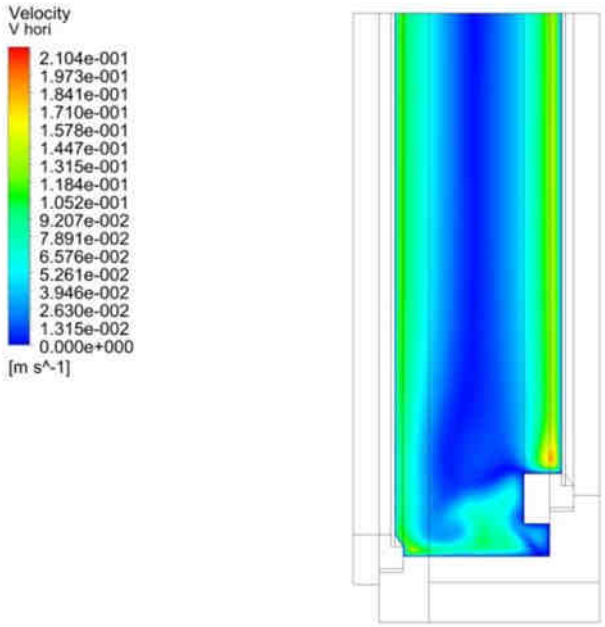

Fig. 142. – generic 3D box window – velocity magnitude in the horizontal section, at y/H=0.1 [-] of the cavity

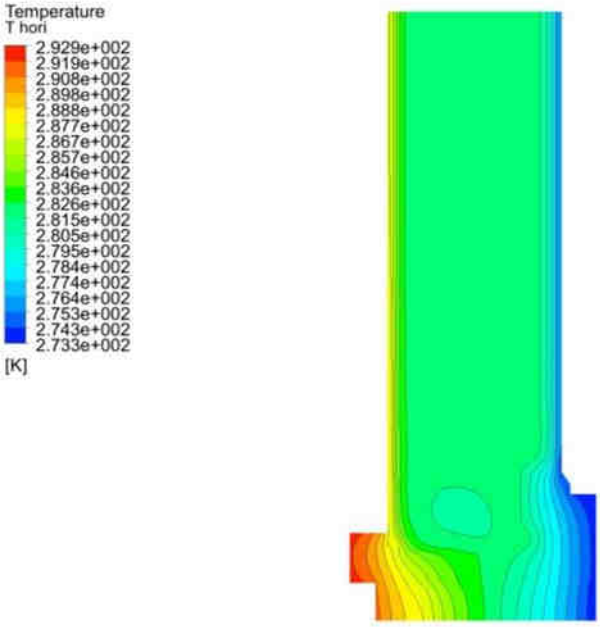

Fig. 143. – generic 3D box window – temperature field in the horizontal section, at y/H=0.5 [-] of the cavity

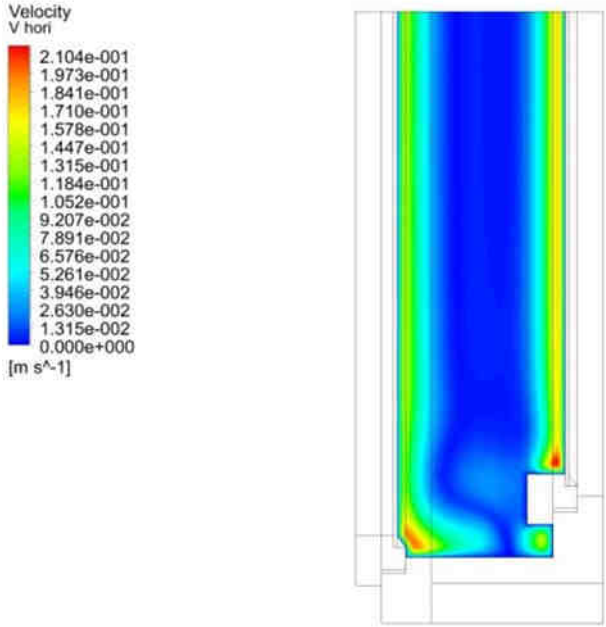

Fig. 144. – generic 3D box window – velocity magnitude in the horizontal section, at y/H=0.1 [-] of the cavity

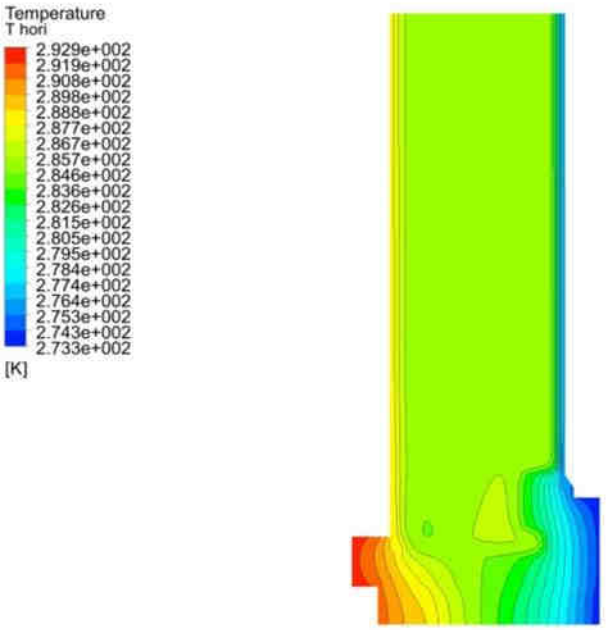

Fig. 145. – generic 3D box window – temperature field in the horizontal section, at y/H=0.9 [-] of the cavity

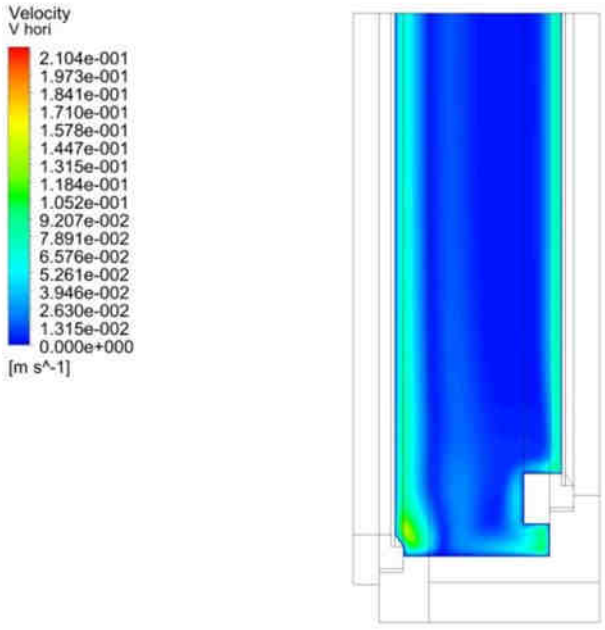

Fig. 146. – generic 3D box window – velocity magnitude in the horizontal section, at y/H=0.1 [-] of the cavity

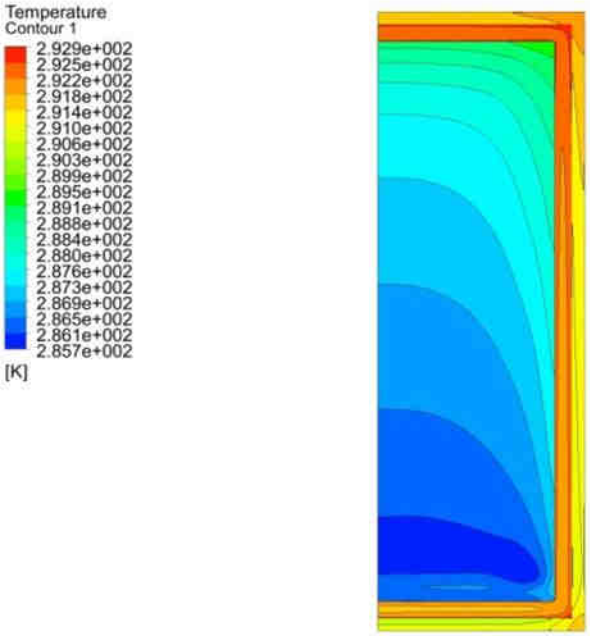

Fig. 147. – generic 3D box window – internal surface temperature field

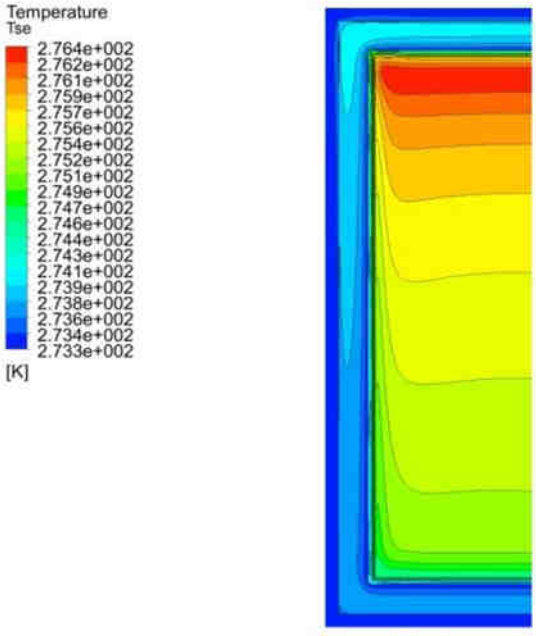

Fig. 148. – generic 3D box window – external surface temperature field

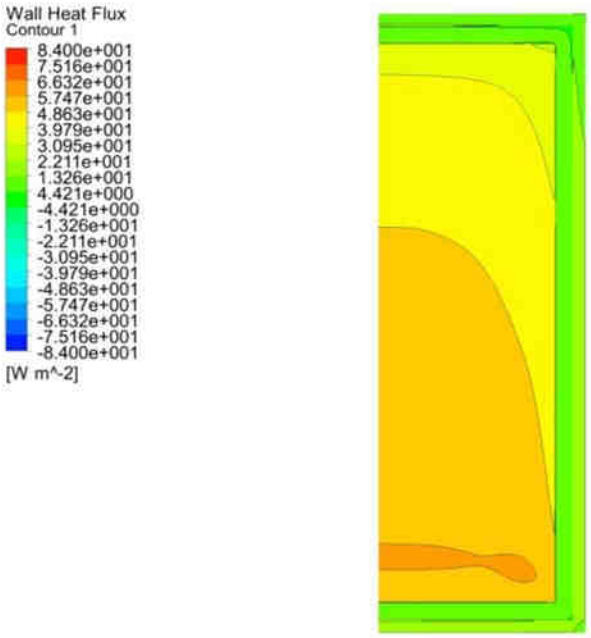

Fig. 149. – Window – generic 3D box window – total heat flux density at the internal surface

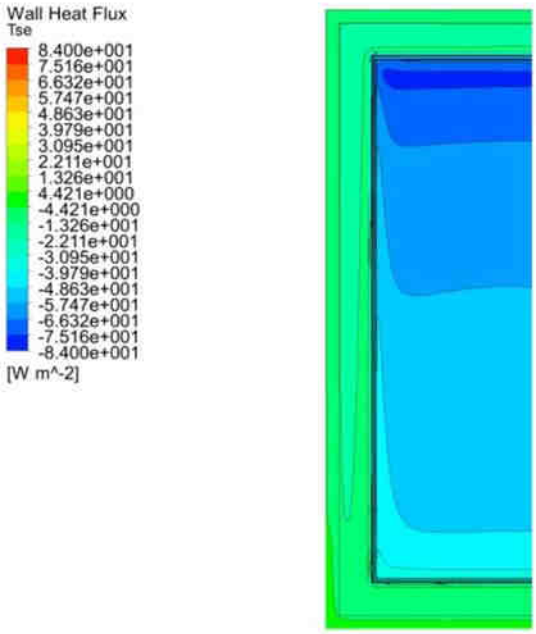

Fig. 150. – Window – generic 3D box window – total surface heat flux density at the external surface

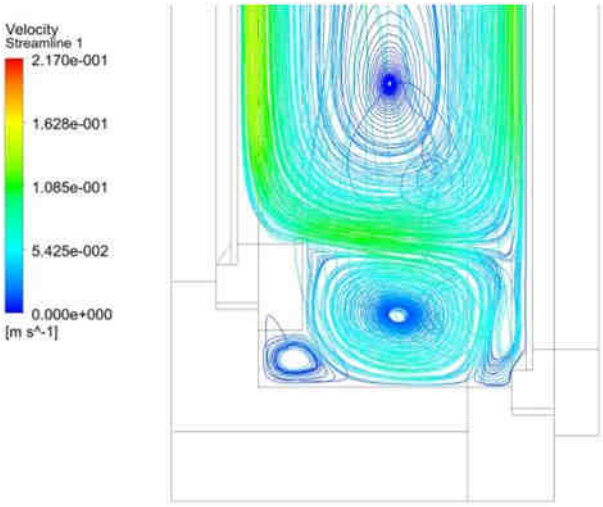

Fig. 151. – generic 3D box window – streamlines in the bottom of the cavity

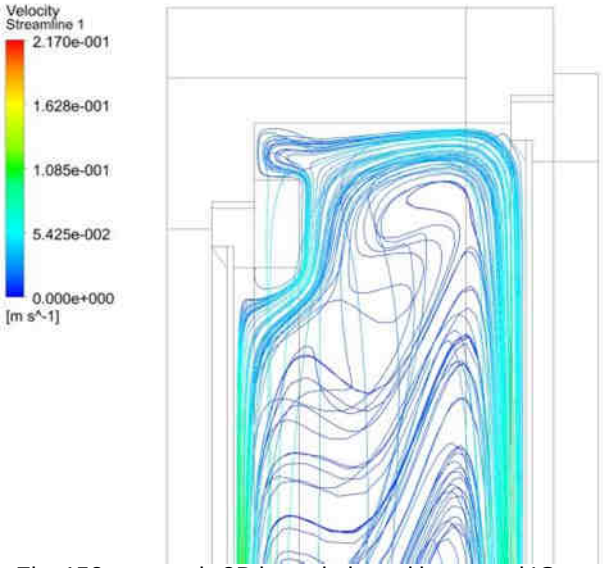

Fig. 152. – generic 3D box window with external IG – streamlines in the top of the cavity

B.5.2 Generic 3D box window with low-e coated glazing

glazing system: • 3 [mm] float glass (IGDB: 11100), ε_f = 0.837 [-], ε_b = 0.837 [-] • 137 [mm] air gap • 3 [mm] hard coated low-e glass (IGDB: 7200), ε_f = 0.18 [-], ε_b = 0.837 [-]						Ug = 1.917 [W/m^{2}K] (ISO) 1.708 [W/m^{2}K] (new)	
cavity	L [mm]	H [mm]	A [-]	model	Ra [-]	Nu [-]	λ_{eff} [W/mK]
1	137	1392	10.16	ISO	4.35e6	11.0	0.393
				new	4.57e6	8.833	0.332

Table 2 – glazing system with hard coated low-e glass – the calculated center-of-glazing heat transfer coefficient and glazing cavity properties for 20/0 [°C] simple boundary conditions

The geometry and mesh is the same as seen in B.5.1.

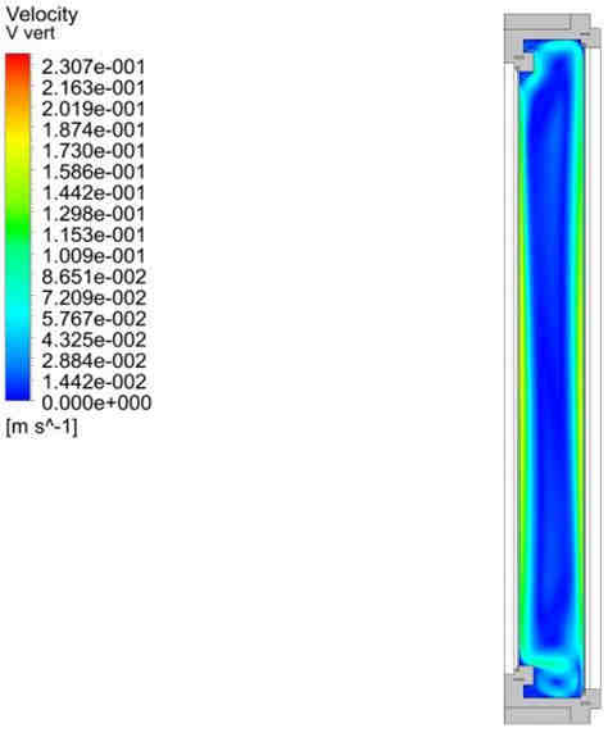

Fig. 153. – generic 3D box window with low-e – velocity magnitude in the vertical symmetry plane

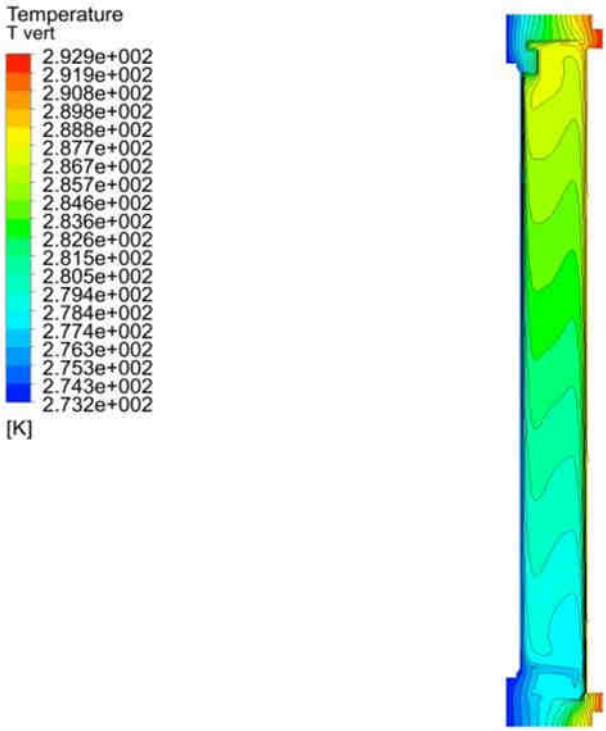

Fig. 154. – generic 3D box window with low-e – temperature field in the vertical symmetry plane

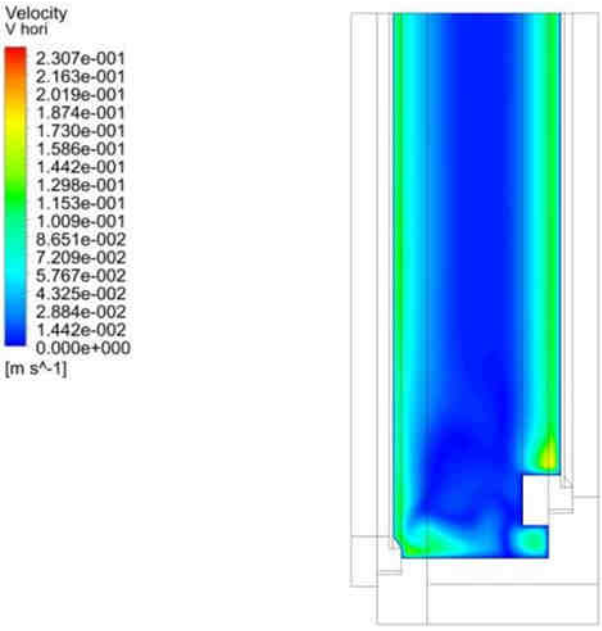

Fig. 155. – generic 3D box window with low-e – velocity magnitude in the horizontal section, at y/H=0.1 [-] of the cavity

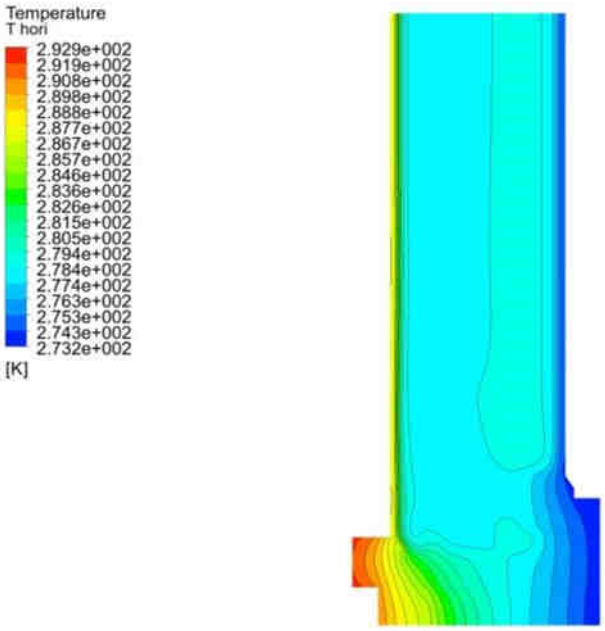

Fig. 156. – generic 3D box window with low-e – temperature field in the horizontal section, at y/H=0.1 [-] of the cavity

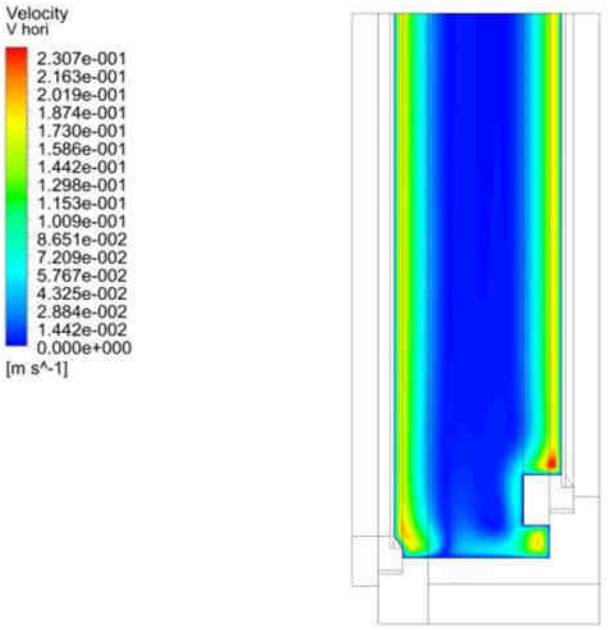

Fig. 157. – generic 3D box window with low-e – velocity magnitude in the horizontal section, at y/H=0.5 [-] of the cavity

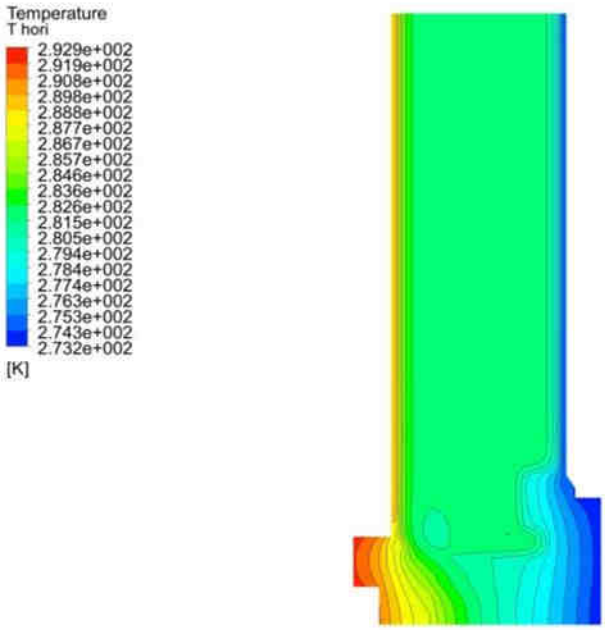

Fig. 158. – generic 3D box window with low-e – temperature field in the horizontal section, at y/H=0.5 [-] of the cavity

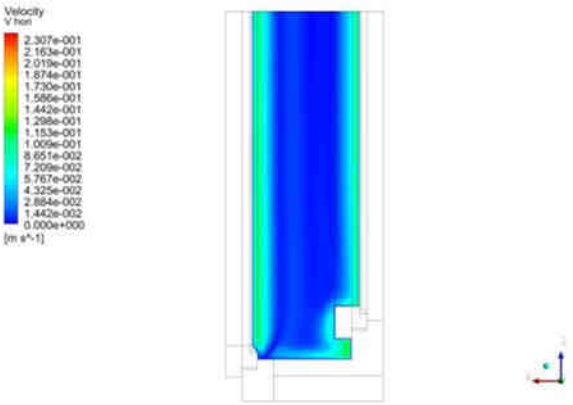

Fig. 159. – generic 3D box window with low-e – velocity magnitude in the horizontal section, at y/H=0.9 [-] of the cavity

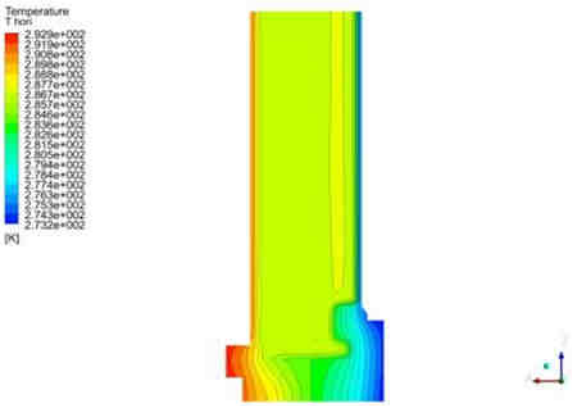

Fig. 160. – generic 3D box window with low-e – temperature field in the horizontal section, at y/H=0.9 [-] of the cavity

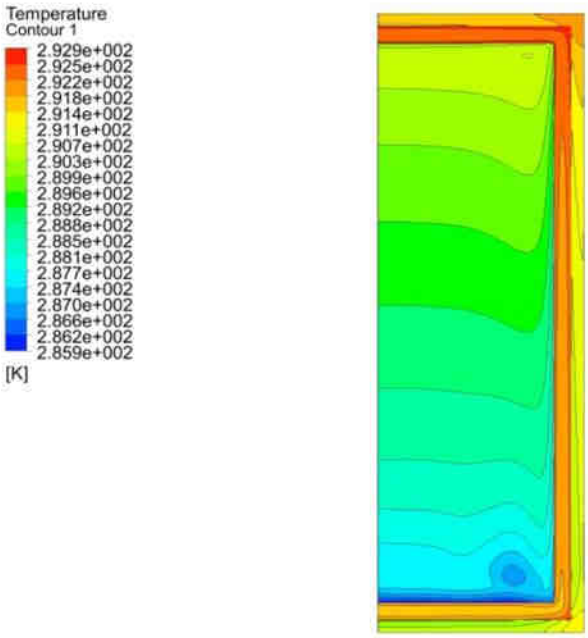

Fig. 161. – generic 3D box window with low-e – internal surface temperature field

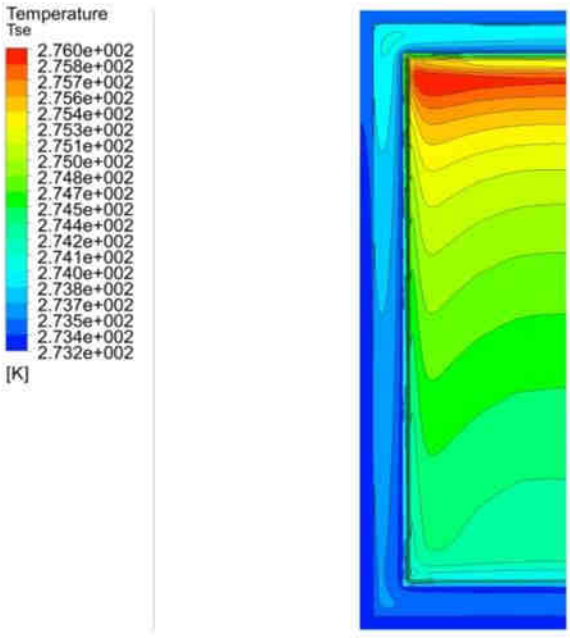

Fig. 162. – generic 3D box window with low-e – external surface temperature field

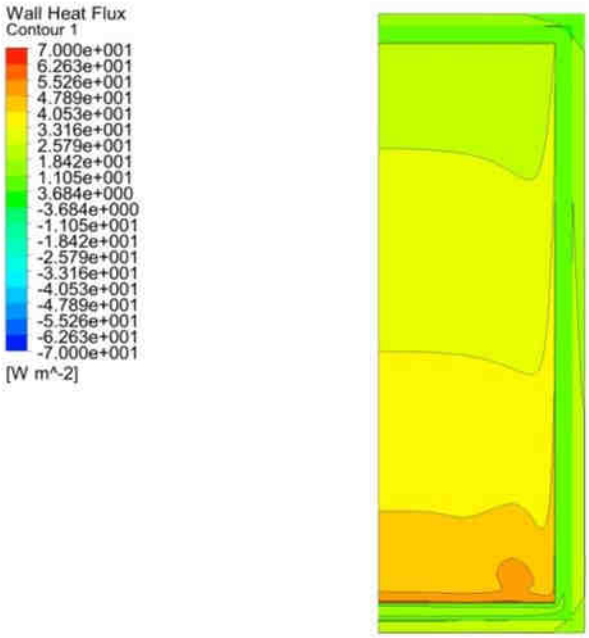

Fig. 163. – generic 3D box window with low-e – total heat flux density at the internal surface

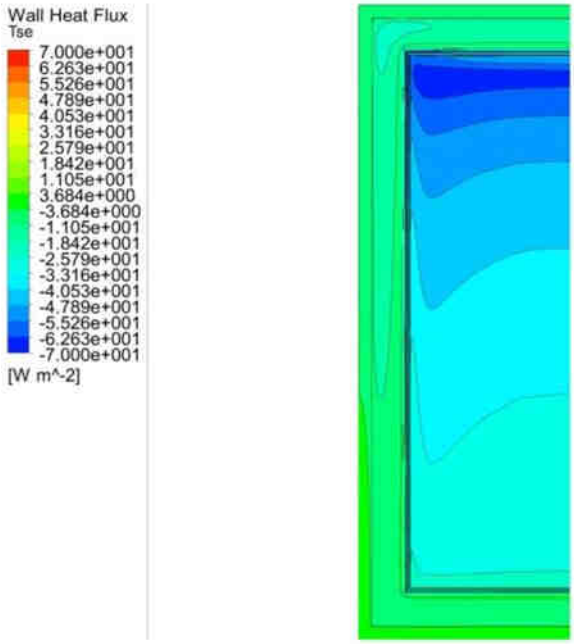

Fig. 164. – generic 3D box window with low-e – total surface heat flux density at the external surface

Fig. 165. – generic 3D box window with low-e –

Fig. 166. – generic 3D box window with low-e –

B.5.3 Generic 3D box window with internal glazing

glazing system: • 3 [mm] hard coated low-e glass (IGDB: 7200), ε_f = 0.837 [-], ε_b = 0.18 [-] • 137 [mm] air gap • 3 [mm] float glass (IGDB: 11100), ε_f = 0.837 [-], ε_b = 0.837 [-] • 6 [mm] Krypton • 3 [mm] soft coated low-e glass (IGDB: 11463), ε_f = 0.037 [-], ε_b = 0.837 [-]						Ug = 0.854[W/m^{2}K] (ISO) 0.814 [W/m^{2}K] (new)	
cavity	L [mm]	H [mm]	A [-]	model	Ra [-]	Nu [-]	λ_{eff} [W/mK]
1	137	1392	10.16	ISO	2.51e6	11.0	0.393
				new	2.76e6	8.833	0.332
2	6			ISO	1.1e3	1.002	0.0102

Table 3 – glazing system with internal thin IG unit and hard coated low-e glass in the main cavity – the calculated center-of-glazing heat transfer coefficient and glazing cavity properties for 20/0 [°C] simple boundary conditions

glazing system: • 3 [mm] float glass (IGDB: 11100), ε_f = 0.837 [-], ε_b = 0.837 [-] • 137 [mm] air gap • 3 [mm] float glass (IGDB: 11100), ε_f = 0.837 [-], ε_b = 0.837 [-] • 6 [mm] Krypton • 3 [mm] soft coated low-e glass (IGDB: 11463), ε_f = 0.037 [-], ε_b = 0.837 [-]						Ug = 1.027 [W/m^{2}K] (ISO) 1.015 [W/m^{2}K] (new)	
cavity	L [mm]	H [mm]	A [-]	model	Ra [-]	Nu [-]	λ_{eff} [W/mK]
1	137	1392	10.16	ISO	1.58e6	7.853	0.6623
				new	1.65e6	6.395	0.6274
2	6			ISO	1.4e3	1.003	0.0102

Table 4 – glazing system with internal thin IG unit – the calculated center-of-glazing heat transfer coefficient and glazing cavity properties for 20/0 [°C] simple boundary conditions

Mesh: 2160038 nodes and 2114418 elements. The core of the flow cavity has a rectangular structured swept hexa mesh with bias toward the edged and boundary layers at the glazing surfaces. The sides of the geometry have a swept mixed hex / tetra + inflation mesh. the inflation layers have a first element height of 4.5e-4 [m], 10 layers and a growth rate of 1.2. The dimensionless wall distance is y+<0.5 [-] everywhere. The internal cavity if the thin insulating glass units (laminar zone) has 20 elements in the crosswise direction with a bias factor of 3.

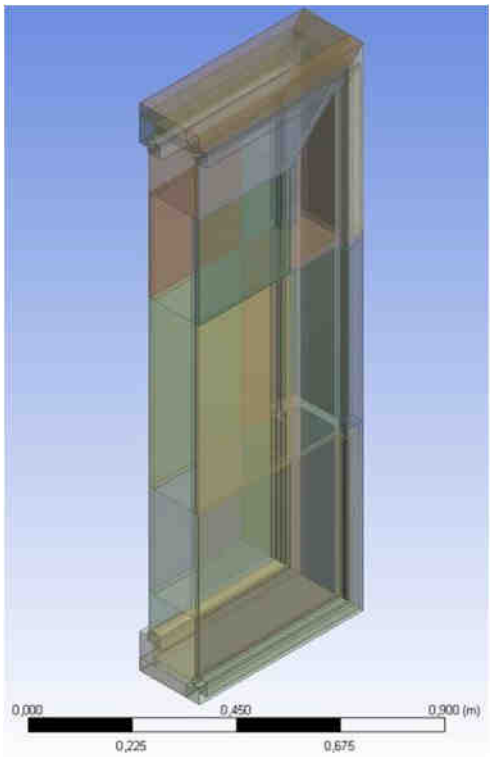

Fig. 167. – generic 3D box window with internal IG – geometry

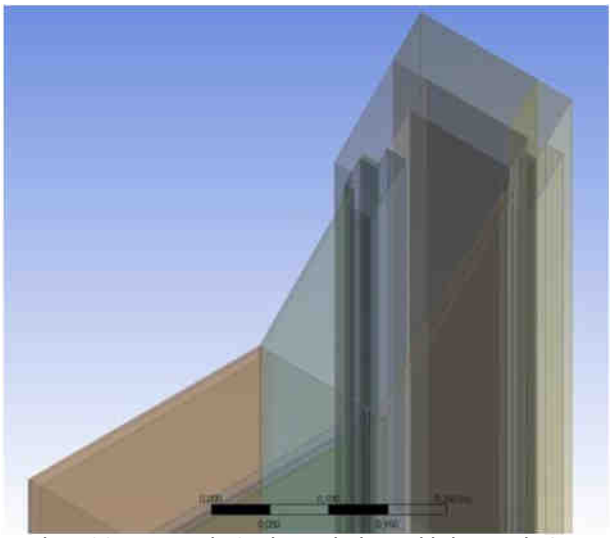

Fig. 168. – generic 3D box window with internal IG – geometry prepared for swept meshing

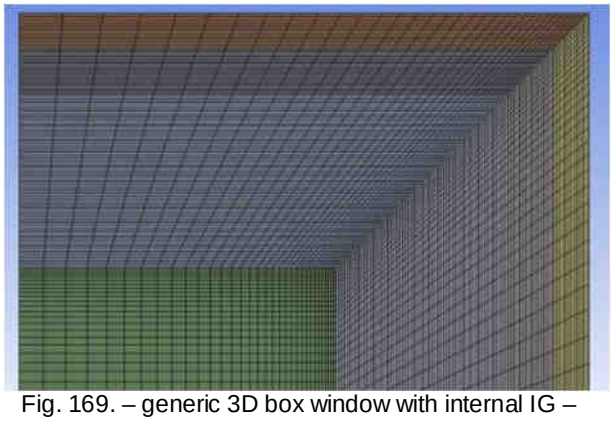

Fig. 169. – generic 3D box window with internal IG – internal view of the generated mesh in the top right corner

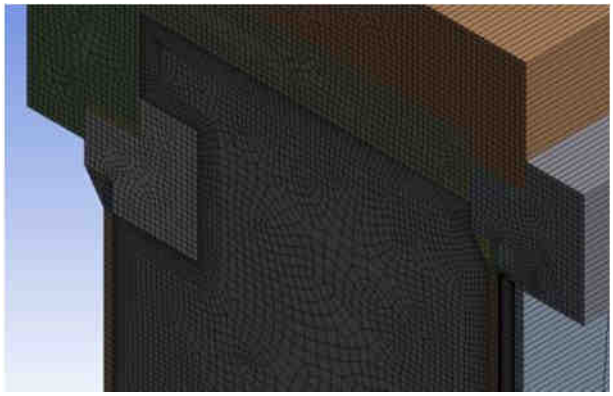

Fig. 170. – generic 3D box window with internal IG – swept inflation mesh for the frame adjacent portion of the cavity

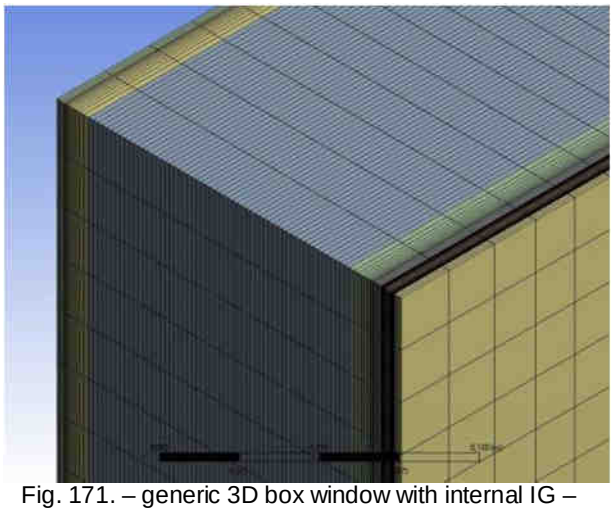

Fig. 171. – generic 3D box window with internal IG – swept hexa mesh in the core of the cavity

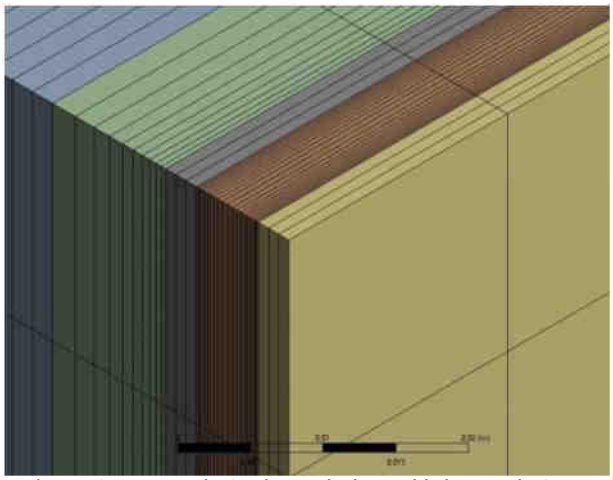

Fig. 172. – generic 3D box window with internal IG – mesh for the insulating glass units cavity

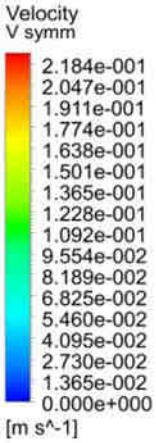

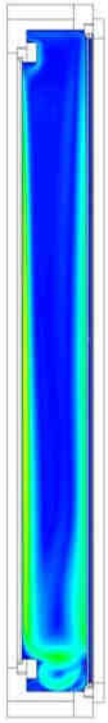

Fig. 173. – generic 3D box window with internal IG – velocity magnitude in the vertical symmetry plane

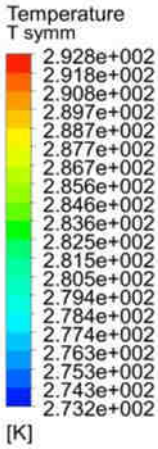

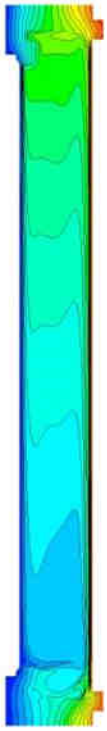

Fig. 174. – generic 3D box window with internal IG – temperature field in the vertical symmetry plane

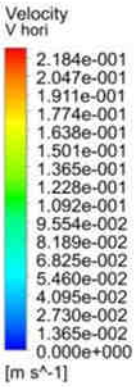

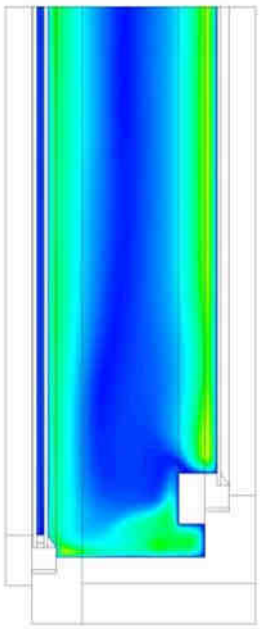

Fig. 175. – generic 3D box window with internal IG – velocity agnitude in the horizontal section, at y/H=0.1 [-] of the cavity

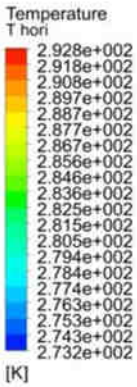

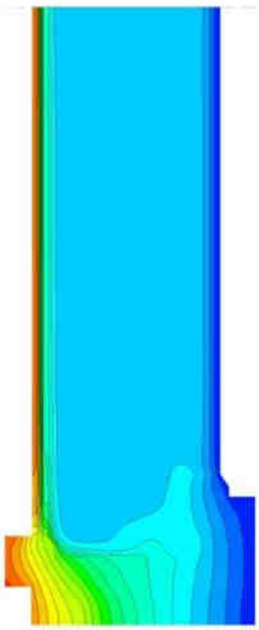

Fig. 176. – generic 3D box window with internal IG – temperature field in the horizontal section, at y/H=0.1 [-] of the cavity

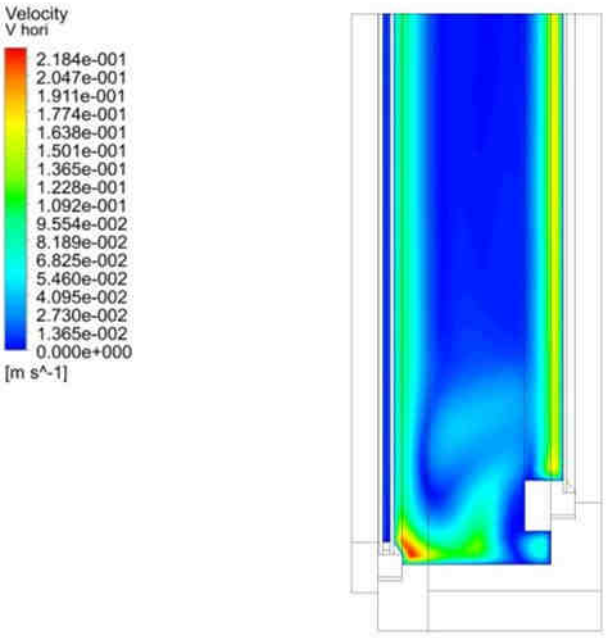

Fig. 177. – generic 3D box window with internal IG – velocity agnitude in the horizontal section, at y/H=0.5 [-] of the cavity

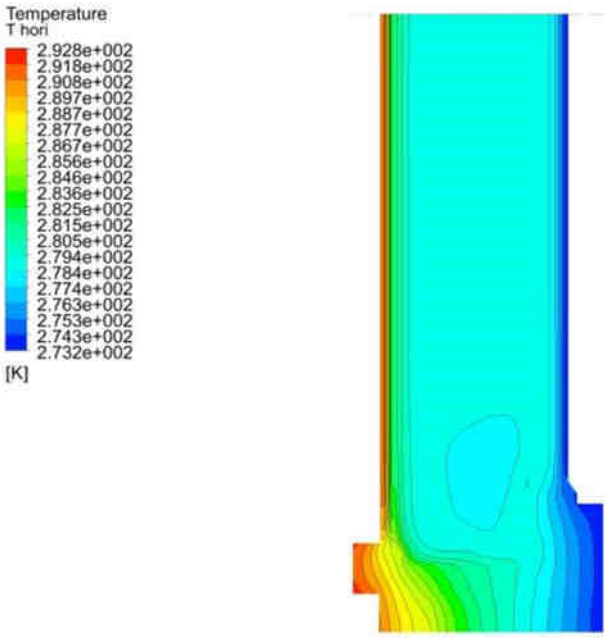

Fig. 178. – generic 3D box window with internal IG – temperature field in the horizontal section, at y/H=0.1 [-] of the cavity

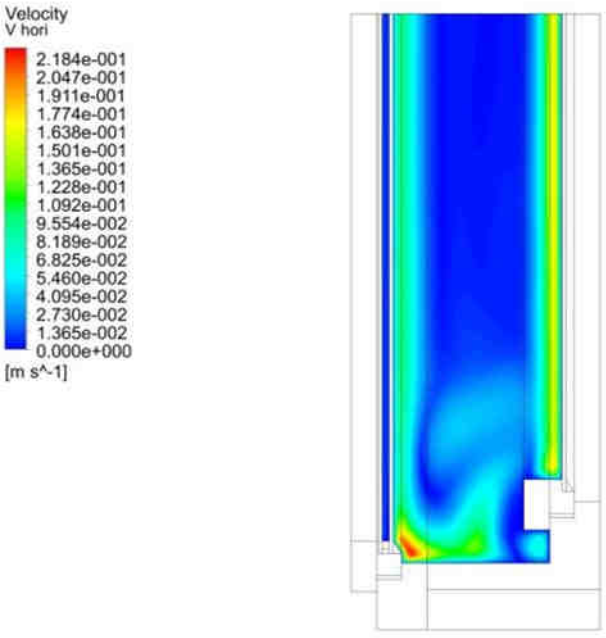

Fig. 179. – generic 3D box window with internal IG – velocity agnitude in the horizontal section, at y/H=0.9 [-] of the cavity

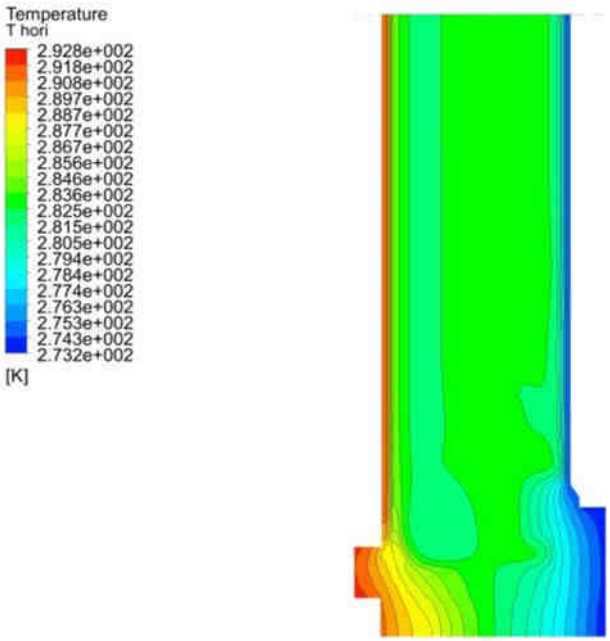

Fig. 180. – generic 3D box window with internal IG – temperature field in the horizontal section, at y/H=0.1 [-] of the cavity

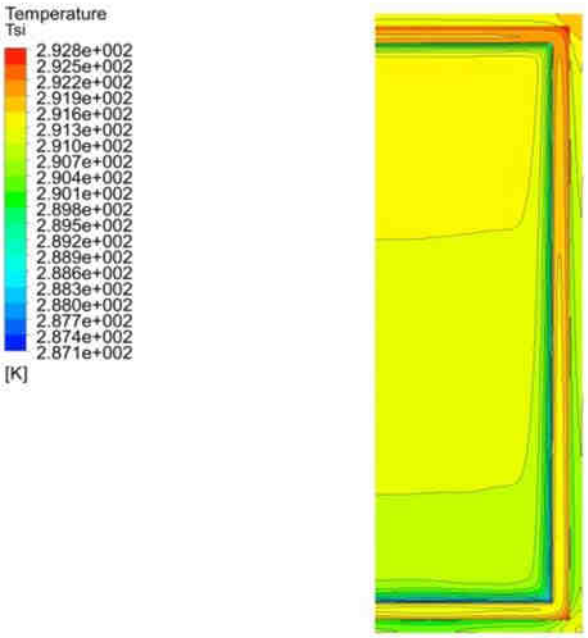

Fig. 181. – generic 3D box window with internal IG – internal surface temperature field

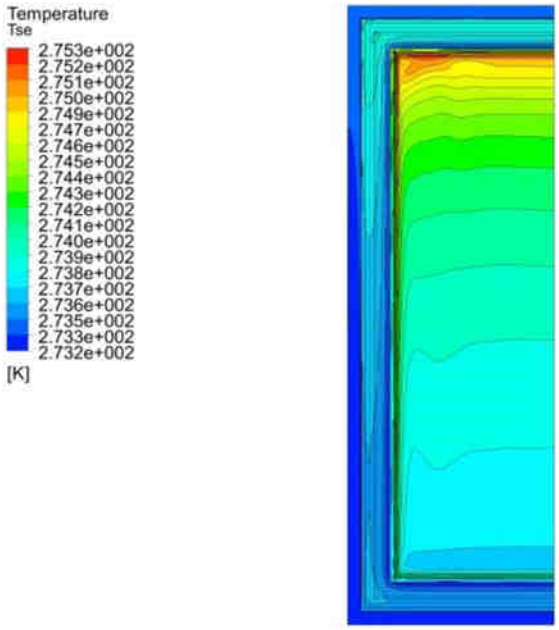

Fig. 182. – generic 3D box window with internal IG – external surface temperature field

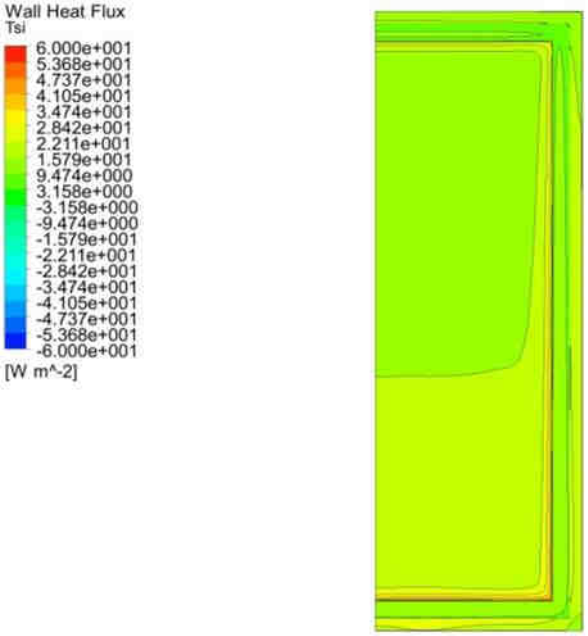

Fig. 183. – generic 3D box window with internal IG – total heat flux density at the internal surface

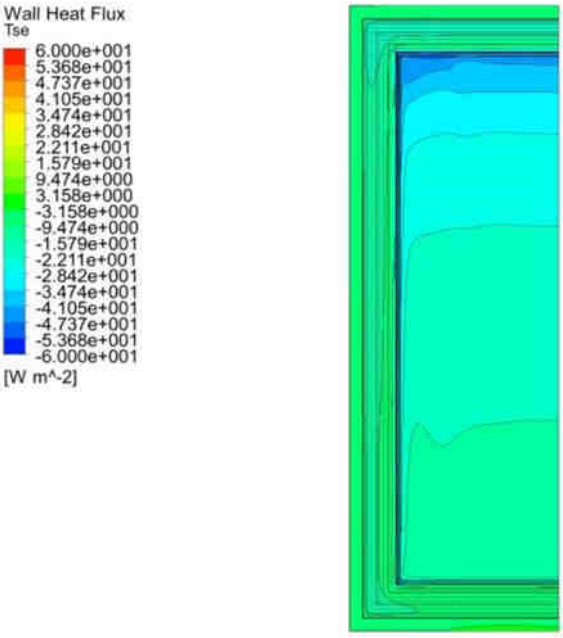

Fig. 184. – generic 3D box window with internal IG – total surface heat flux density at the external surface

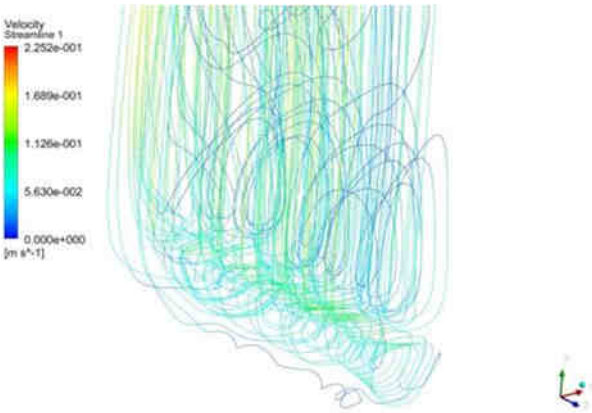

Fig. 185. – generic 3D box window with internal IG –

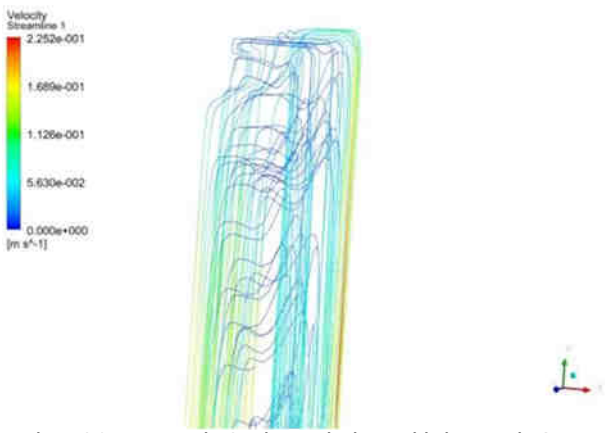

Fig. 186. – generic 3D box window with internal IG –

B.5.4 Generic 3D box window with external glazing

glazing system: • 3 [mm] float glass (IGDB: 11100), ε_f = 0.837 [-], ε_b = 0.837 [-] • 6 [mm] Krypton • 3 [mm] soft coated low-e glass (IGDB: 11463), ε_f = 0.037 [-], ε_b = 0.837 [-] • 128 [mm] air gap • 3 [mm] float glass (IGDB: 11100), ε_f = 0.837 [-], ε_b = 0.837 [-]						Ug = 0.848[W/m^{2}K] (ISO) 0.812 [W/m^{2}K] (new)	
cavity	L [mm]	H [mm]	A [-]	model	Ra [-]	Nu [-]	λ_{eff} [W/mK]
1	6			ISO	1.51e3	1.004	0.01
2	128	1392	10.875	ISO	9.65e5	0.6737	6.659
				new	9.99e5	0.645	5.5378

Table 5 – glazing system with external thin IG unit – the calculated center-of-glazing heat transfer coefficient and glazing cavity properties for 20/0 [°C] simple boundary conditions

glazing system: • 3 [mm] float glass (IGDB: 11100), ε_f = 0.837 [-], ε_b = 0.837 [-] • 6 [mm] Krypton • 3 [mm] soft coated low-e glass (IGDB: 11463), ε_f = 0.037 [-], ε_b = 0.837 [-] • 128 [mm] air gap • 3 [mm] hard coated low-e glass (IGDB: 7200), ε_f = 0.18 [-], ε_b = 0.837 [-]						Ug = 0.848[W/m^{2}K] (ISO) 0.812 [W/m^{2}K] (new)	
cavity	L [mm]	H [mm]	A [-]	model	Ra [-]	Nu [-]	λ_{eff} [W/mK]
1	6			ISO	1.3e3	1.002	0.0099
2	128	1392	10.875	ISO	1.67e6	7.995	0.3224
				new	1.81e6	6.5494	0.2856

Table 6 – glazing system with external thin IG unit and hard coated low-e glass in the main cavity – the calculated center-of-glazing heat transfer coefficient and glazing cavity properties for 20/0 [°C] simple boundary conditions

Mesh: 1942728 nodes and 1897935 elements. The core of the flow cavity has a rectangular structured swept hexa mesh with bias toward the edged and boundary layers at the glazing surfaces. The sides of the geometry have a swept mixed hex / tetra + inflation mesh. the inflation layers have a first element height of 4.5e-4 [m], 10 layers and a growth rate of 1.2. The dimensionless wall distance is y+<0.5 [-] everywhere. The internal cavity if the thin insulating glass units (laminar zone) has 20 elements in the crosswise direction with a bias factor of 3.

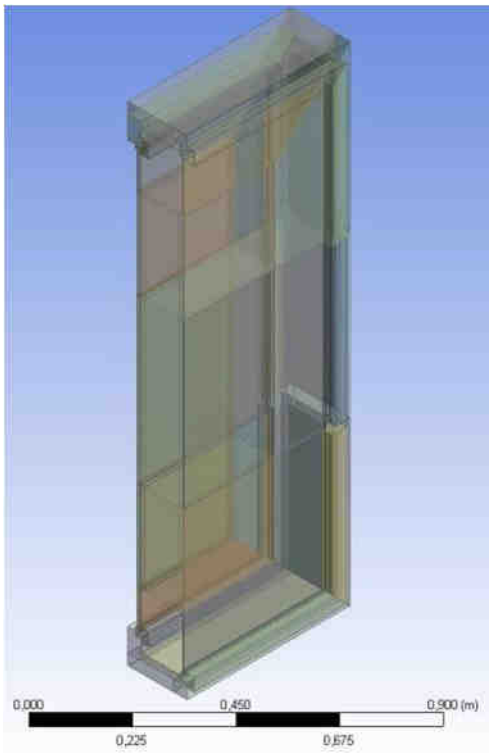

Fig. 187. – generic 3D box window with external IG – geometry

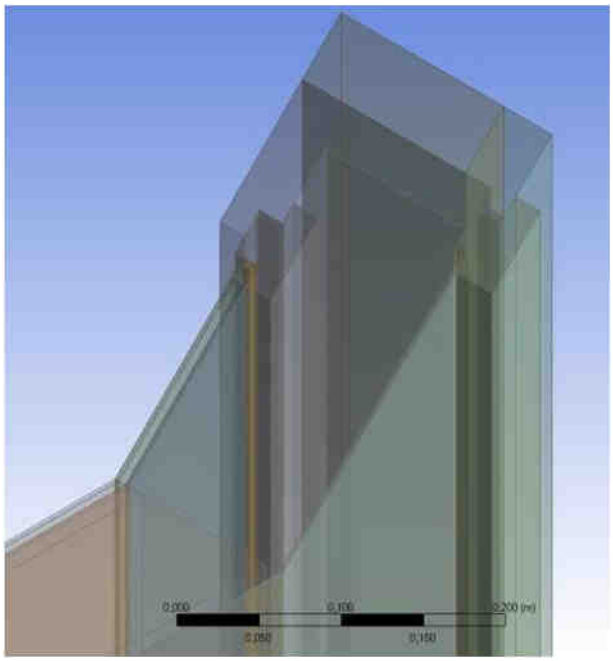

Fig. 188. – generic 3D box window with external IG – geometry prepared for swept meshing

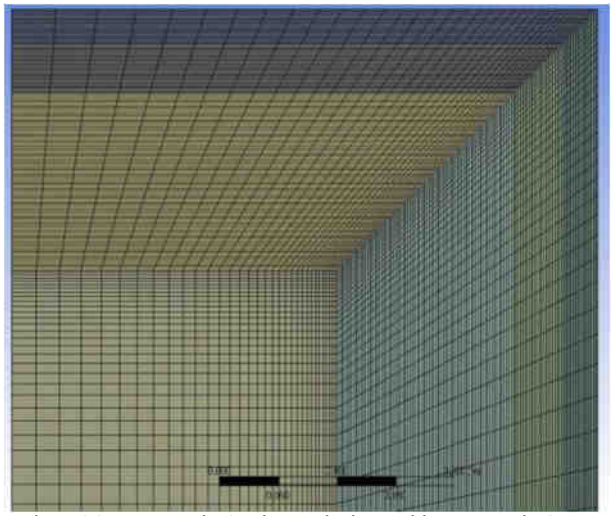

Fig. 189. – generic 3D box window with external IG – internal view of the generated mesh in the top right corner

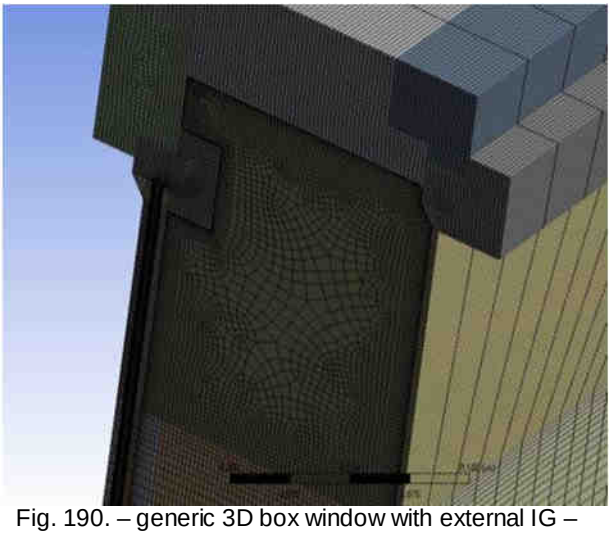

Fig. 190. – generic 3D box window with external IG – swept inflation mesh in the frame adjacent portion of the cavity

Fig. 191. – generic 3D box window with external IG – swept hexa mesh in the cavity's core

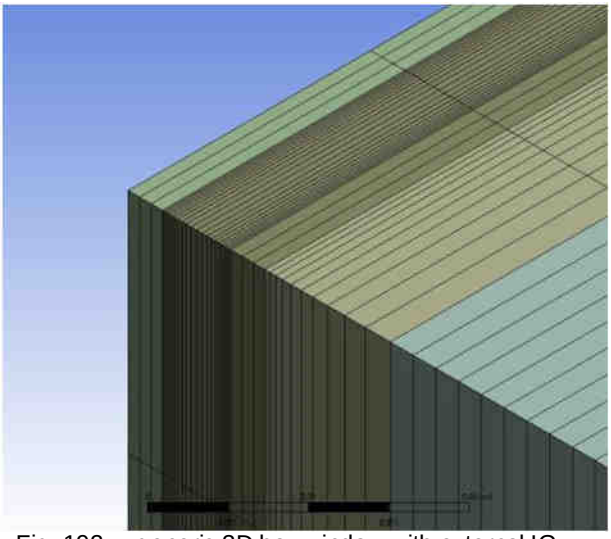

Fig. 192. – generic 3D box window with external IG – mesh for the IG unit's cavity

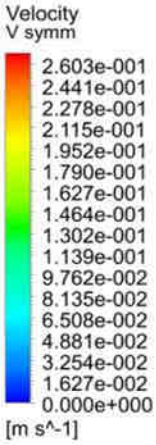

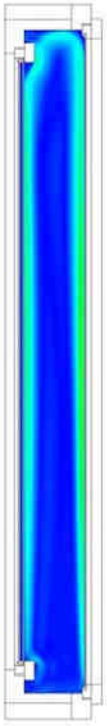

Fig. 193. – generic 3D box window with external IG – velocity magnitude in the vertical symmetry plane

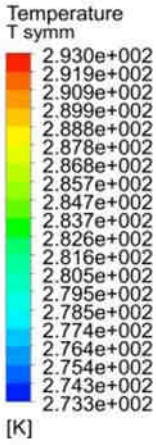

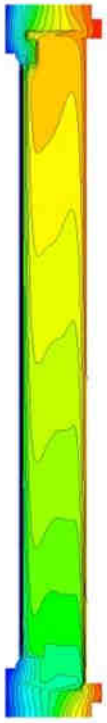

Fig. 194. – generic 3D box window with external IG – temperature field in the vertical symmetry plane

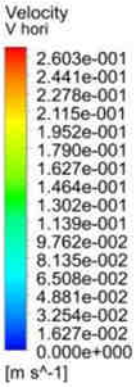

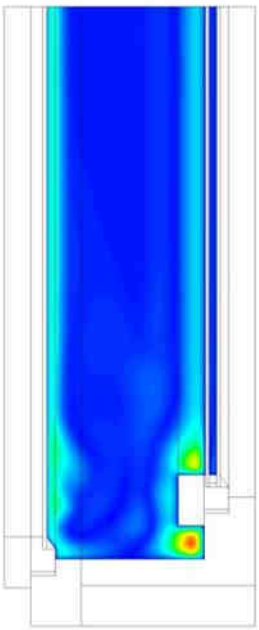

Fig. 195. – generic 3D box window with external IG – velocity magnitude in the horizontal section, at y/H=0.1 [-] of the cavity

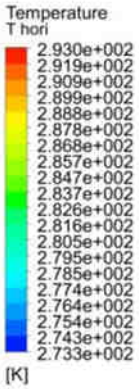

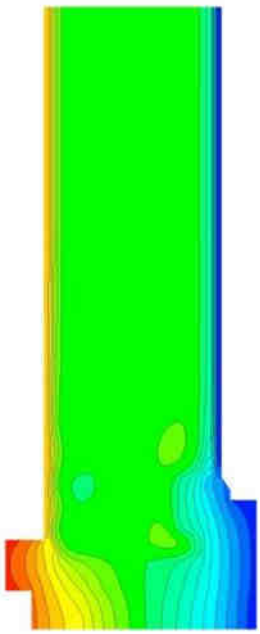

Fig. 196. – generic 3D box window with external IG – temperature field in the horizontal section, at y/H=0.1 [-] of the cavity

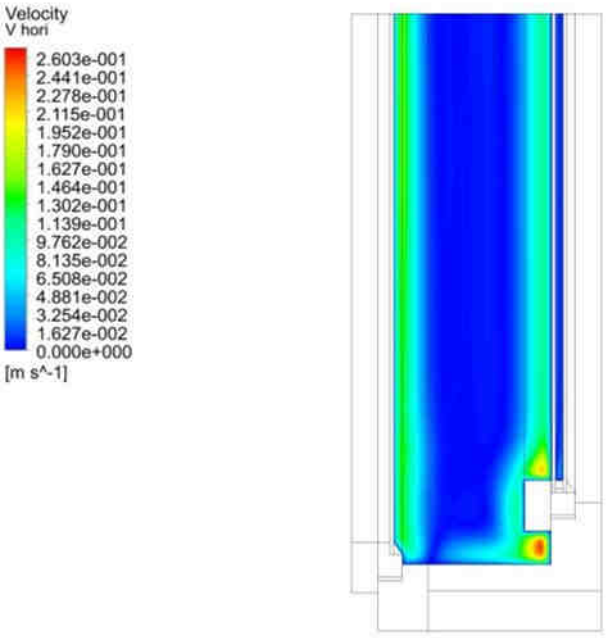

Fig. 197. – generic 3D box window with external IG – velocity magnitude in the horizontal section, at y/H=0.5 [-] of the cavity

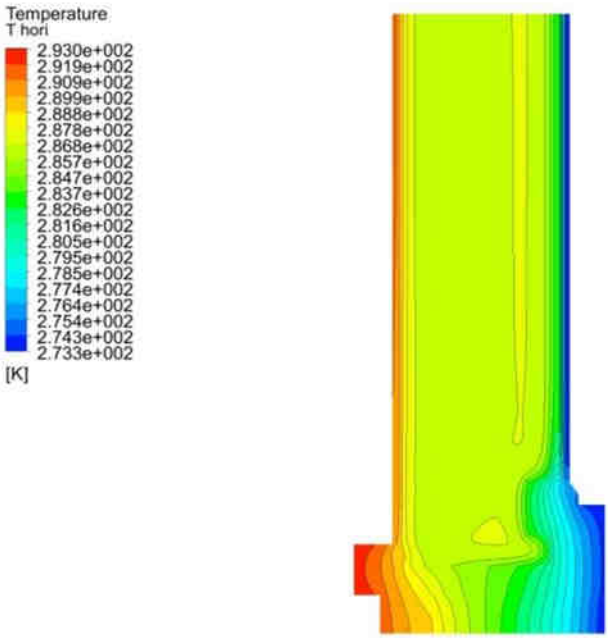

Fig. 198. – generic 3D box window with external IG – temperature field in the horizontal section, at y/H=0.5 [-] of the cavity

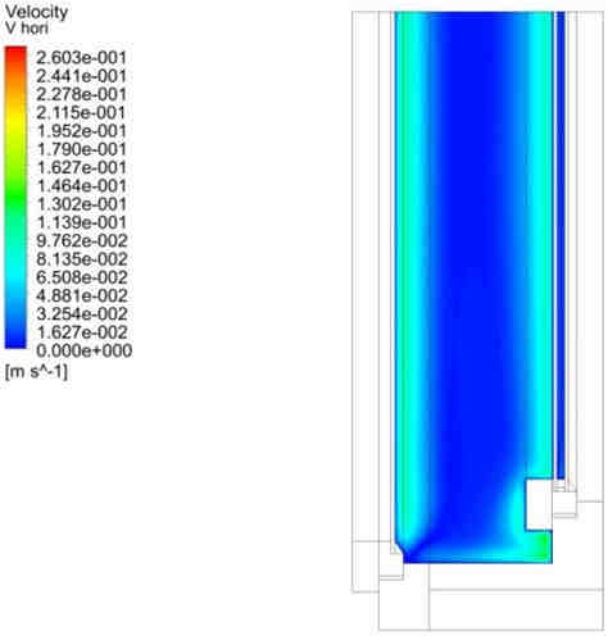

Fig. 199. – generic 3D box window with external IG – velocity magnitude in the horizontal section, at y/H=0.9 [-] of the cavity

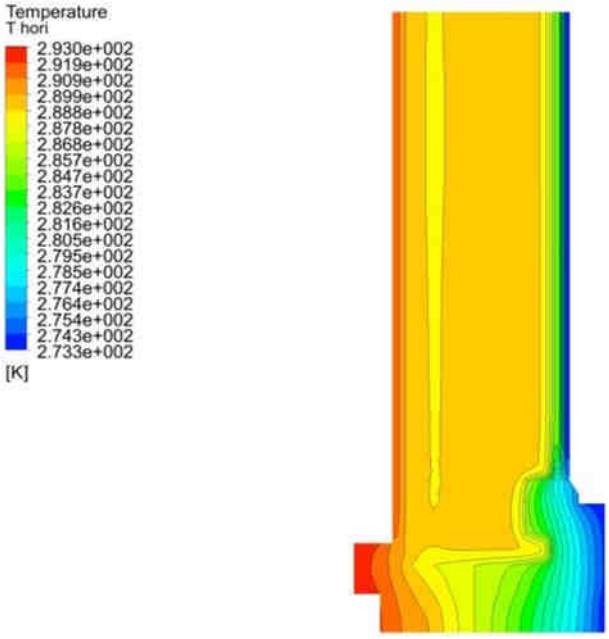

Fig. 200. – generic 3D box window with external IG – temperature field in the horizontal section, at y/H=0.9 [-] of the cavity

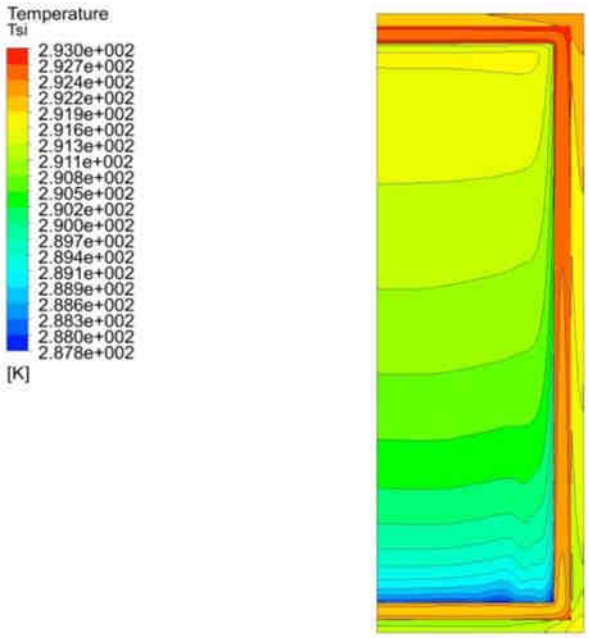

Fig. 201. – generic 3D box window with external IG – internal surface temperature field

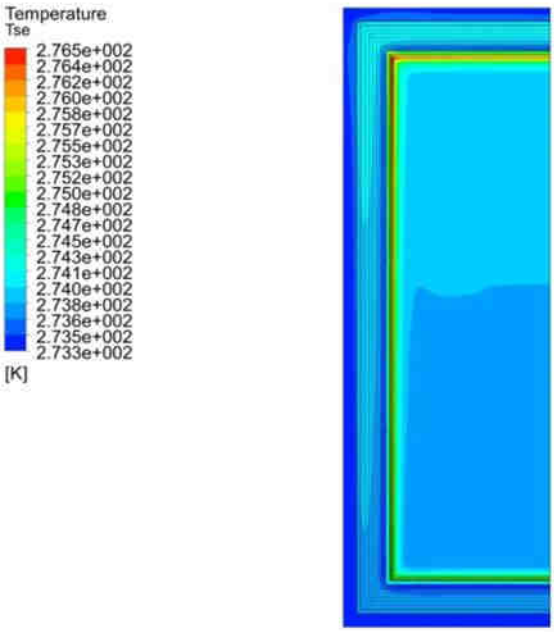

Fig. 202. – generic 3D box window with external IG – external surface temperature field

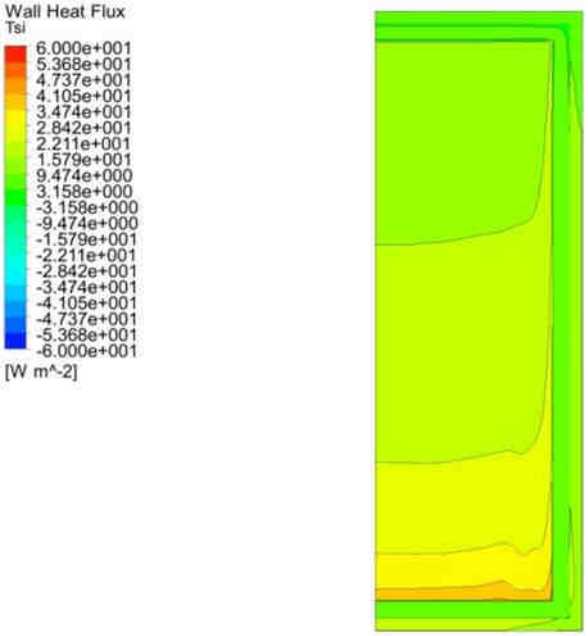

Fig. 203. – generic 3D box window with external IG – total heat flux density at the internal surface

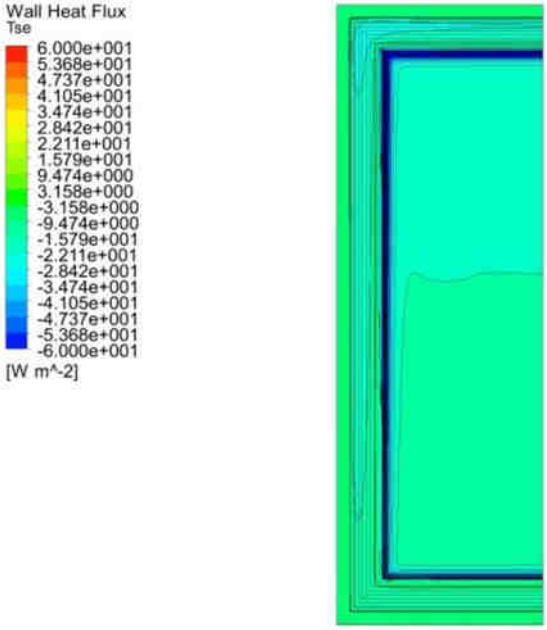

Fig. 204. – generic 3D box window with external IG – total surface heat flux density at the external surface

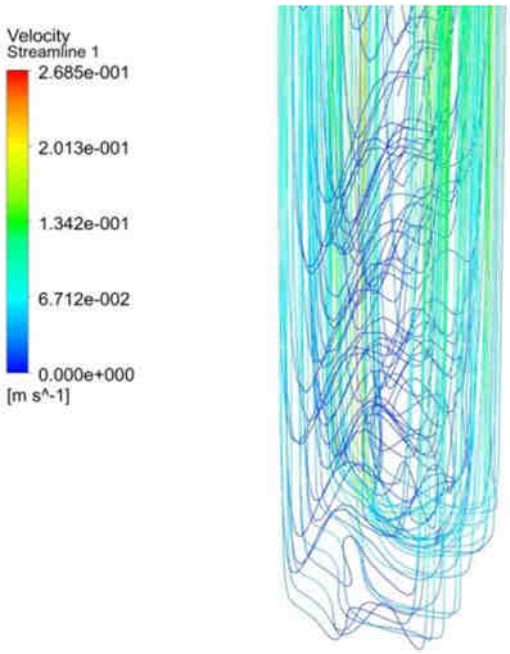

Fig. 205. – generic 3D box window with external IG – streamlines in the bottom of the cavity

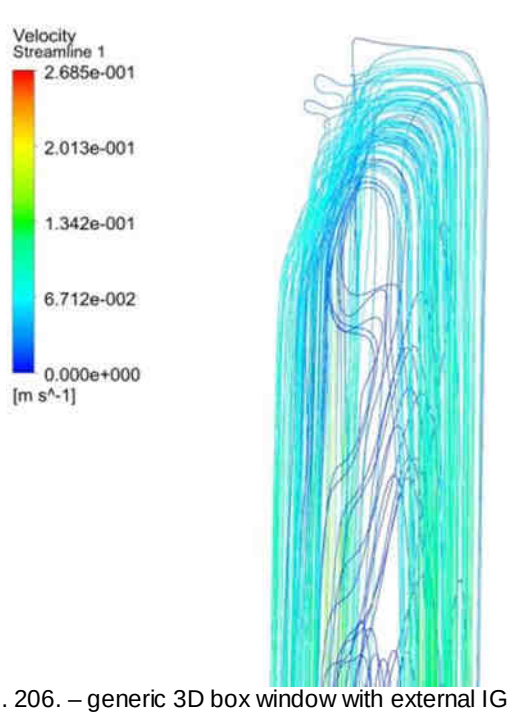

Fig. 206. – generic 3D box window with external IG – streamlines in the top of the cavity

B.5.5 Realistic 3D box window (test window No. 2)

glazing system: • 3 [mm] float glass (IGDB: 11100), ε_f = 0.837 [-],ε_b = 0.837 [-] • 119 [mm] air gap • 3 [mm] float glass (IGDB: 11100), ε_f = 0.837 [-],ε_b = 0.837 [-]						Ug = 2.805 [W/m^{2}K] (ISO) 2.698 [W/m^{2}K] (new)	
cavity	L [mm]	H [mm]	A [-]	model	Ra [-]	Nu [-]	λ_{eff} [W/mK]
1	119	14595	12.26	ISO	2.23e6	8.7972	0.6473
				new	2.3e6	6.9103	0.6012

Table 7 – glazing system of test window No. 2 – the calculated center-of-glazing heat transfer coefficient and glazing cavity properties for 20/0 [°C] simple boundary conditions

Mesh: 3347074 nodes and 7089787 elements. The core of the flow cavity has a rectangular structured swept hexa mesh with bias toward the edged and boundary layers at the glazing surfaces. The vertical and horizontal sides of the geometry have a swept mixed hex / tetra + inflation mesh. The corers could not be swept and have a free tetrahedral mesh with inflation layers. The inflation layers have a first element height of 4.5e-4 [m], 10 layers and a growth rate of 1.2. The dimensionless wall distance is y+<1 [-] everywhere.

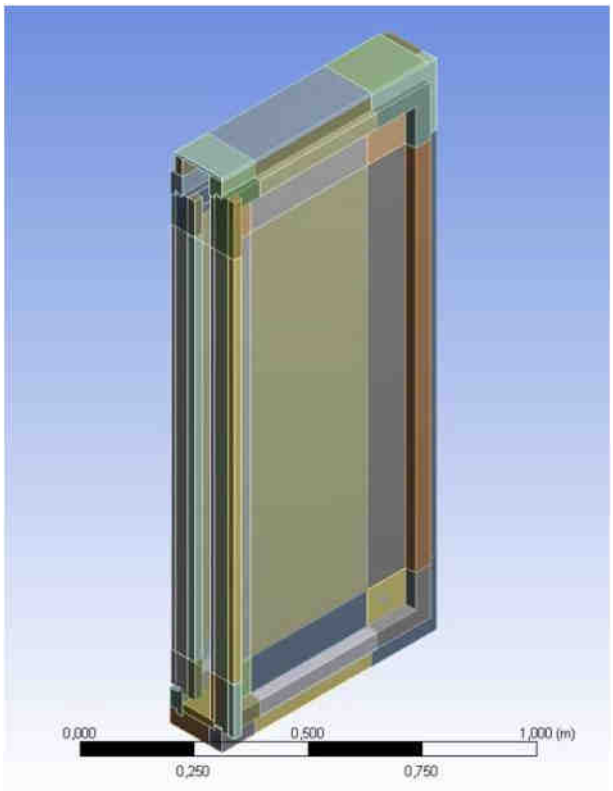

Fig. 207. – realistic 3D box window (window 2) – geometry

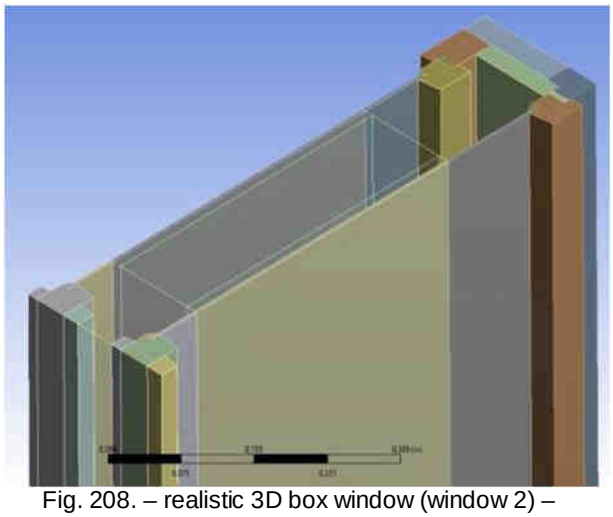

Fig. 208. – realistic 3D box window (window 2) – preparing the geometry for swept meshing

Fig. 209. – realistic 3D box window (window 2) – swept hexa mesh on the core of the cavity

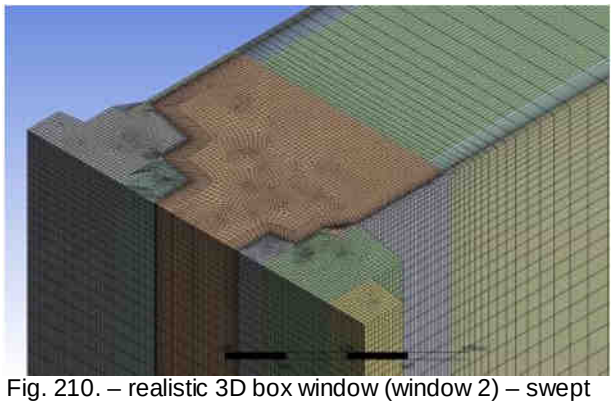

Fig. 210. – realistic 3D box window (window 2) – swept inflation mesh along the vertical and horizontal frame profiles

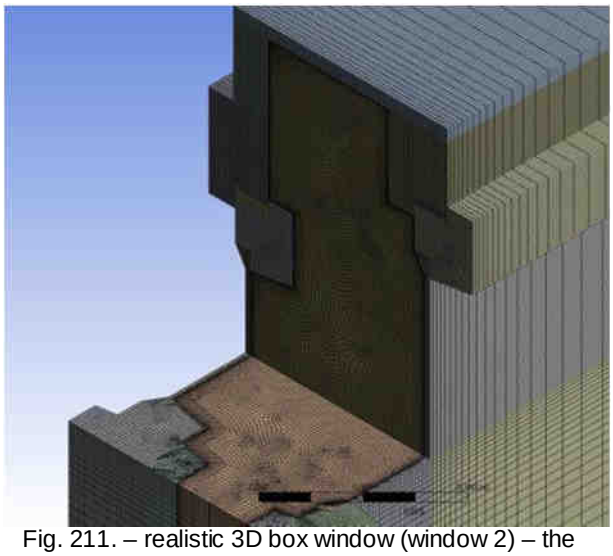

Fig. 211. – realistic 3D box window (window 2) – the top left corner of the mesh that can't be swept

Fig. 212. – realistic 3D box window (window 2) – free tetrahedral mesh (with inflation in the cavity) in the corner regions

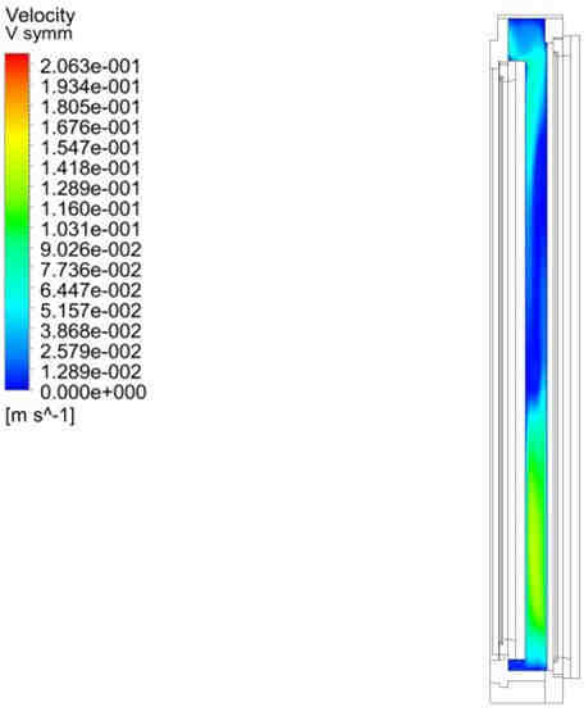

Fig. 213. – realistic 3D box window (window 2) – velocity magnitude in the vertical symmetry plane

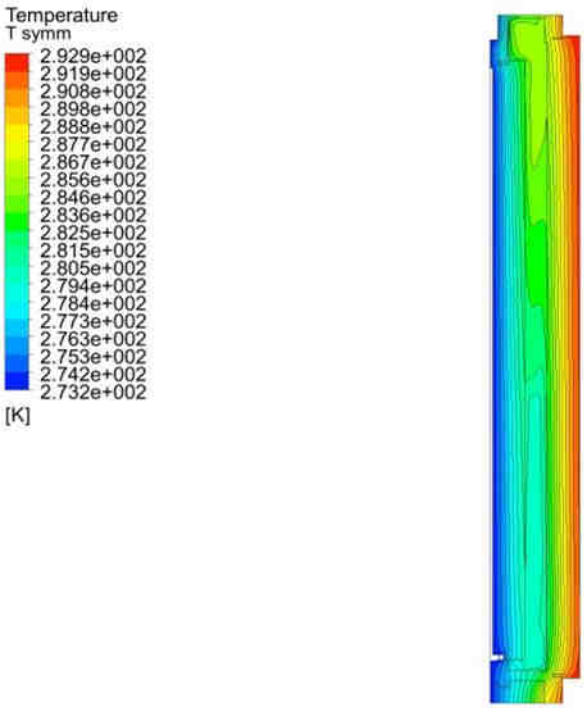

Fig. 214. – realistic 3D box window (window 2) – temperature field in the vertical symmetry plane

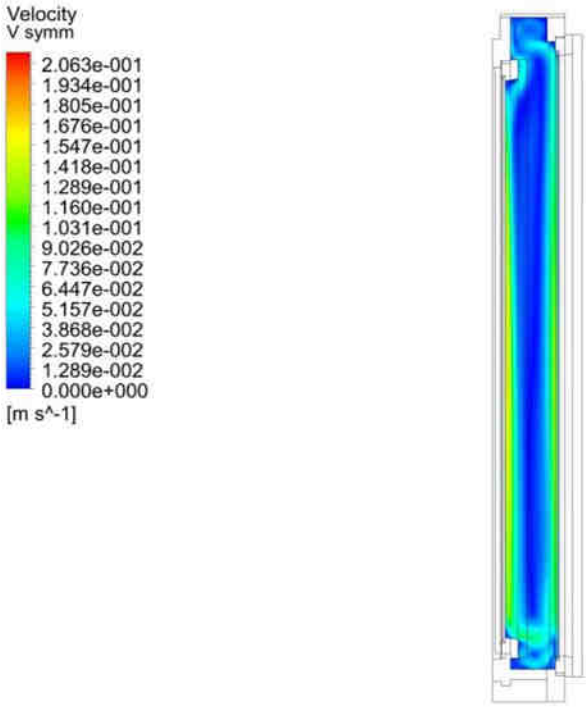

Fig. 215. – realistic 3D box window (window 2) – velocity magnitude in the vertical symmetry plane of the internal glazing

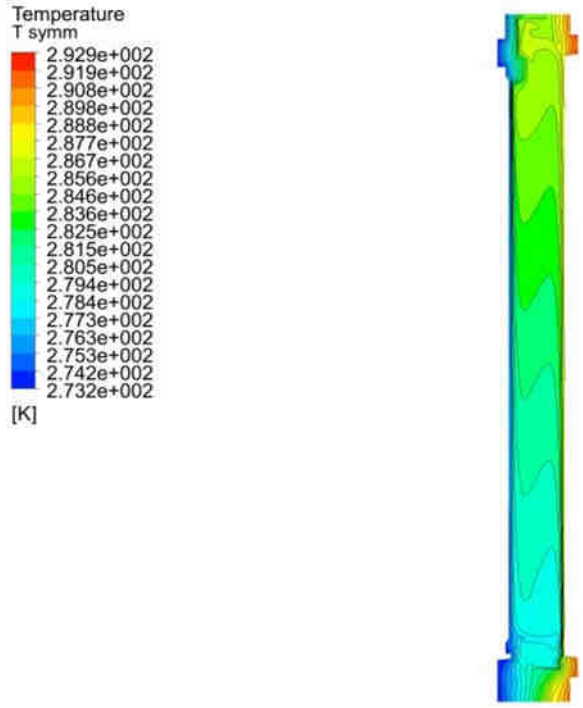

Fig. 216. – realistic 3D box window (window 2) – temperature field in the vertical symmetry plane of the internal glazing

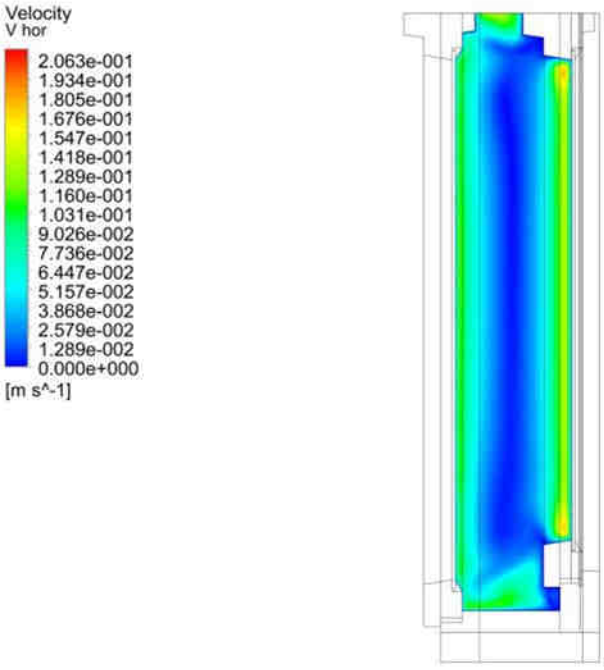

Fig. 217. – realistic 3D box window (window 2) – velocity magnitude in the horizontal section, at y/H=0.1 [-] of the cavity

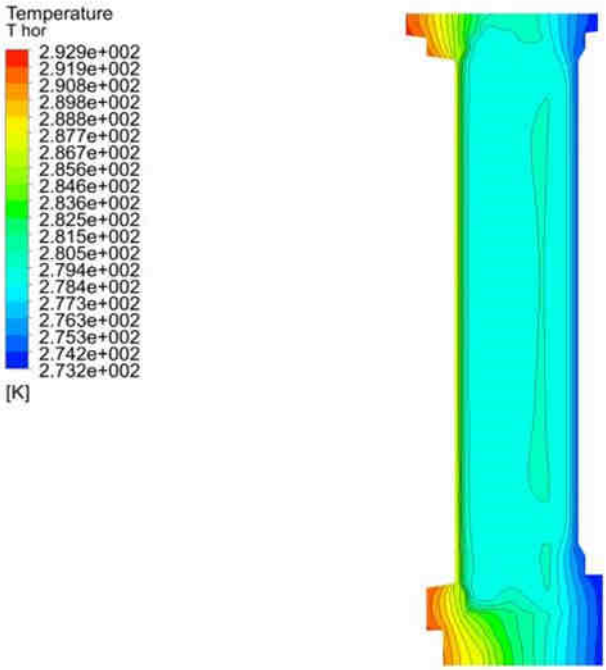

Fig. 218. – realistic 3D box window (window 2) – temperature field in the horizontal section, at y/H=0.1 [-] of the cavity

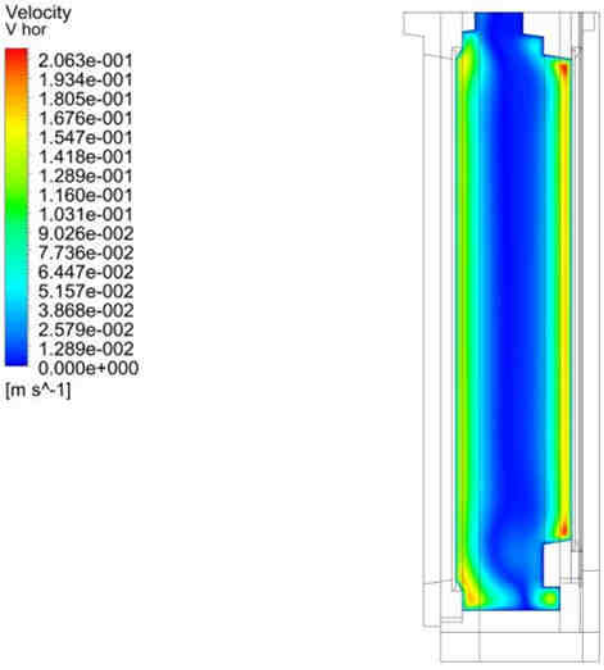

Fig. 219. – realistic 3D box window (window 2) – velocity magnitude in the horizontal section, at y/H=0.1 [-] of the cavity

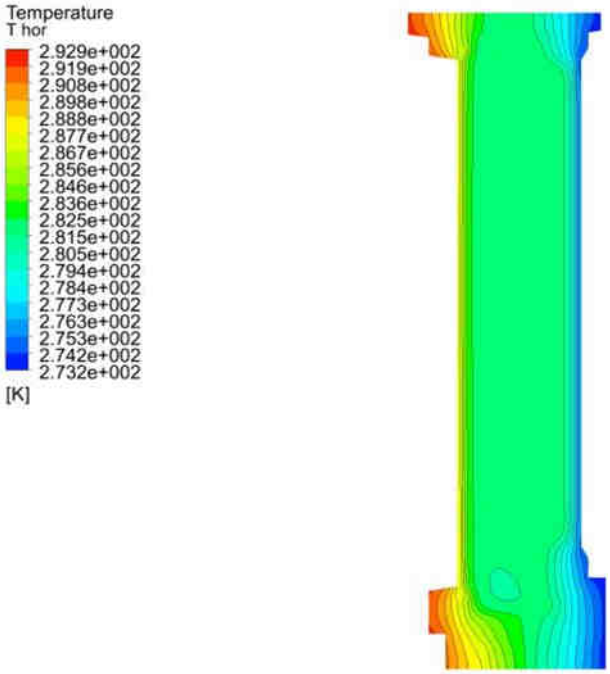

Fig. 220. – realistic 3D box window (window 2) – temperature field in the horizontal section, at y/H=0.1 [-] of the cavity

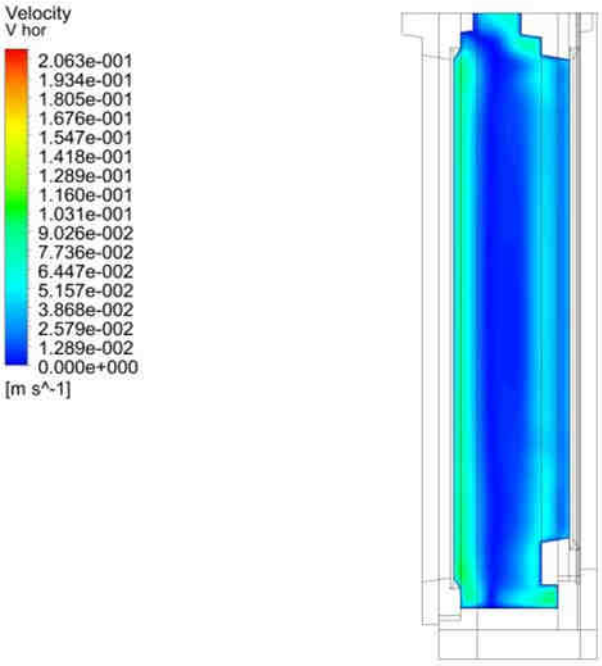

Fig. 221. – realistic 3D box window (window 2) – velocity magnitude in the horizontal section, at y/H=0.1 [-] of the cavity

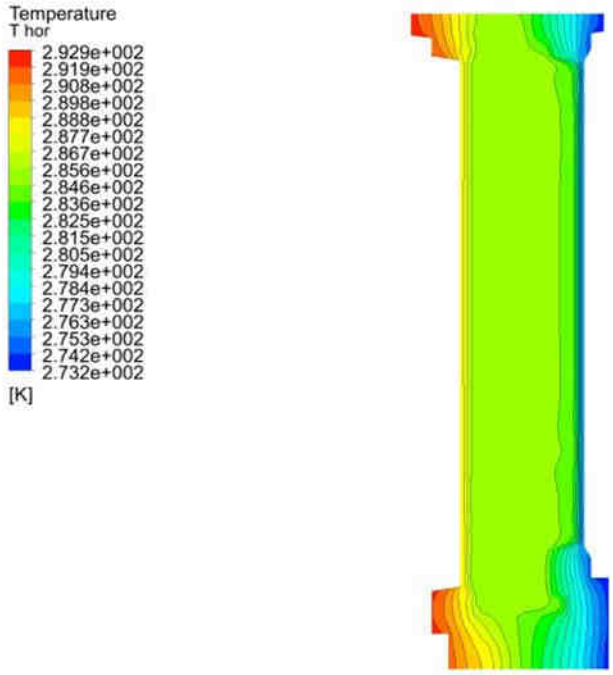

Fig. 222. – realistic 3D box window (window 2) – temperature field in the horizontal section, at y/H=0.1 [-] of the cavity

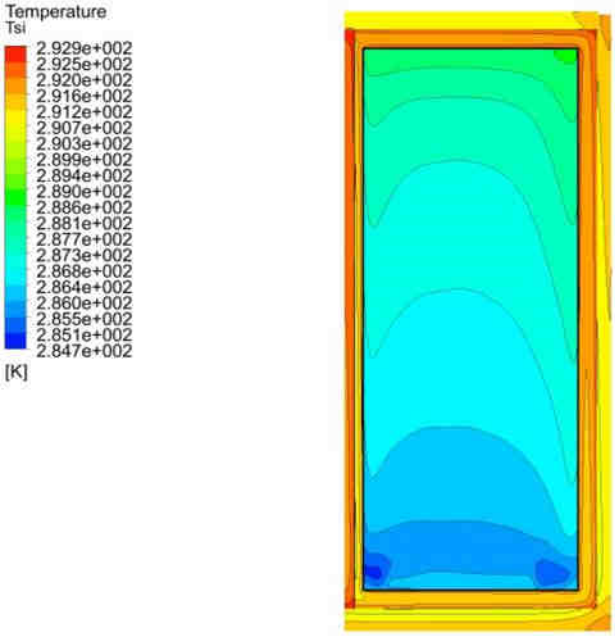

Fig. 223. – realistic 3D box window (window 2) – internal surface temperature field

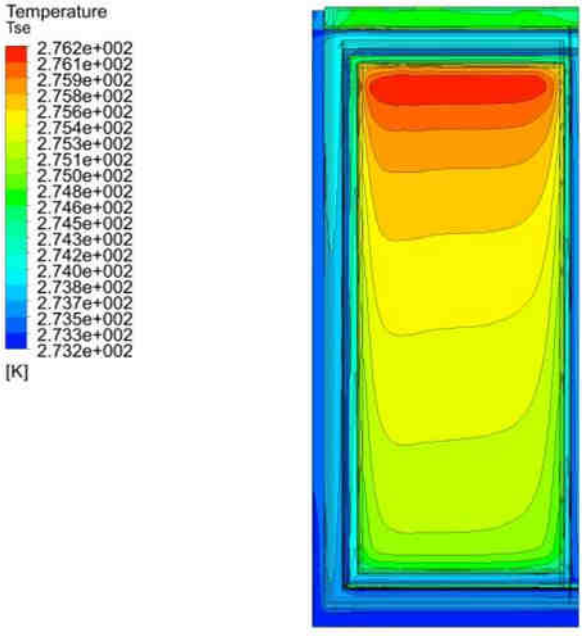

Fig. 224. – realistic 3D box window (window 2) – external surface temperature field

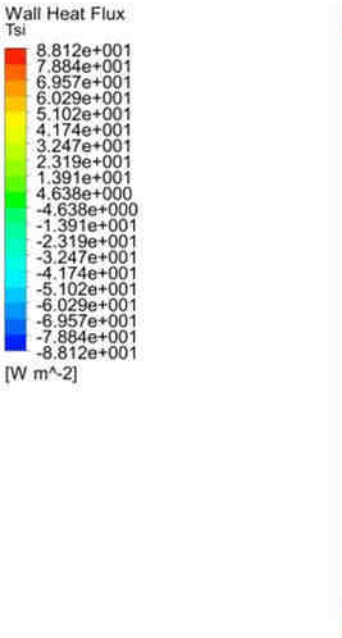

Fig. 225. – realistic 3D box window (window 2) – total heat flux density at the internal surface

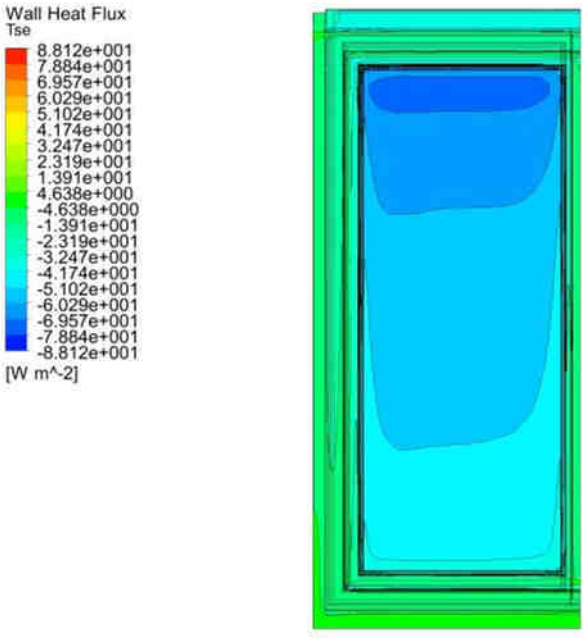

Fig. 226. – realistic 3D box window (window 2) – total heat flux density at the external surface

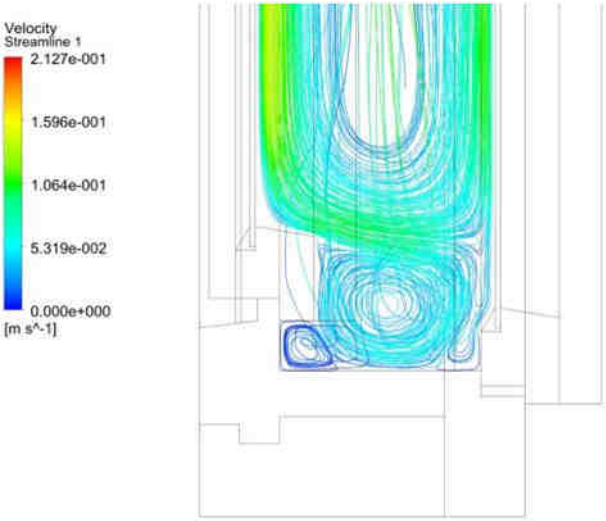

Fig. 227. – realistic 3D box window (window 2) – streamlines at the top of the cavity

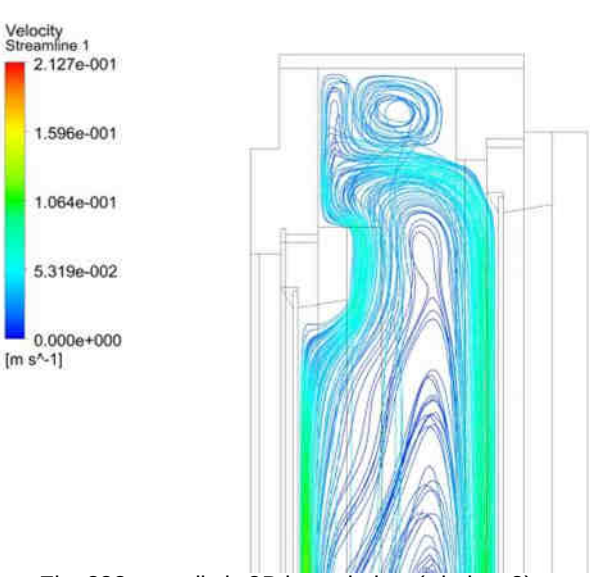

Fig. 228. – realistic 3D box window (window 2) – streamlines at the bottom of the cavity

C (Appendix C) – Thermal Bridge Calculations

C.1 Detailed description of the investigated building types and parameter sets

C.1.1 19th century Central-European urban apartment buildings

Multi-story apartment buildings from the second half of the 19th and the first decade of the 20th century represent a significant portion of the Hungarian building stock and the building stock of many other Central-European countries. These buildings are very similar in their construction and basic floor plan, and although the architecture of the period used many different historic styles underneath the adornments their facades are very much defined by their function and structure and exhibit a reasonably small variance. Furthermore, since their facades are geometrically very repetitive we can faithfully represent them with a small, well-chosen representative surface patch (e.g. a façade element belonging to a single small flat).

We can differentiate between street facing (external) façade and internal or courtyard façades. The latter differ in that they are characterized by cantilever stone, steel beam supported brick vault or in later times concrete corridors. The expected limits for the geometrical parameters were determined and in absence of a better guess a uniform random distribution was assumed. For a summary of the investigated façade type and the geometrical parameters see Fig. 229.

In terms of different constructional solutions three distinct cases were set up: external solid brick masonry wall in the original state (no thermal insulation), external wall with interior (discontinuous) insulation and external wall with external (continuous) insulation. The possible thickness of the masonry is known from the building regulations of the period (1.5 brick thick walls for top floors, 2 and 2.5 brick walls below acc. to the loads), while the thickness of the thermal insulation was taken as between 2 and 8 [cm] in 2 [cm] increments. A thicker internal insulation is rarely possible due to hygrothermal reasons, while the thickness of an external insulation in this case is limited by current building regulations and simple geometry to 10 cm including plaster as these buildings were usually built right at the property line and there is rarely enough room for more. For the internal insulation both standard and thermally optimized details were investigated. For a summary of the examined constructional parameters and their assumed values see Fig. 230. and for the constructional details from which the thermal bridge heat transfer coefficients were calculated Fig. 231, Fig. 232 and Fig. 233.

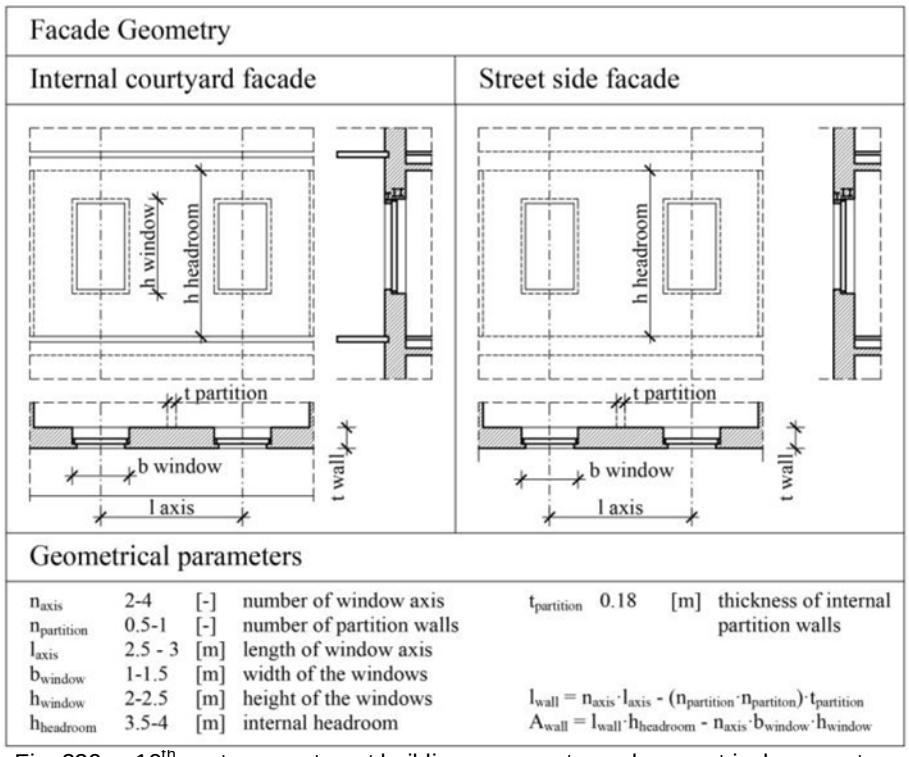

Fig. 229. – 19th century apartment building – geometry and geometrical parameters

Constructional parameters			
	No insulation	Internal insulation	External insulation
t_{wall} [m]	0.44 - 0.59 - 0.74	0.44 - 0.59 - 0.74	0.44 - 0.59 - 0.74
R_{wall} [m²K/W]	0.6076 - 0,8 - 0.9922	0.6076 - 0,8 - 0.9922	0.6076 - 0,8 - 0.9922
$\lambda_{ins.}$ [W/mK]	0	0.045	0.04
$t_{ins.}$ [m]	0	0.02 - 0.04 - 0.06 - 0.08	0.02 - 0.04 - 0.06 - 0.08
$R_{ins.}$ [m²K/W]	0	0.44 - 0.88 - 1.33 - 1.77	0.5 - 1 - 1.5 - 2

Fig. 230. – 19th century apartment building – constructional parameters

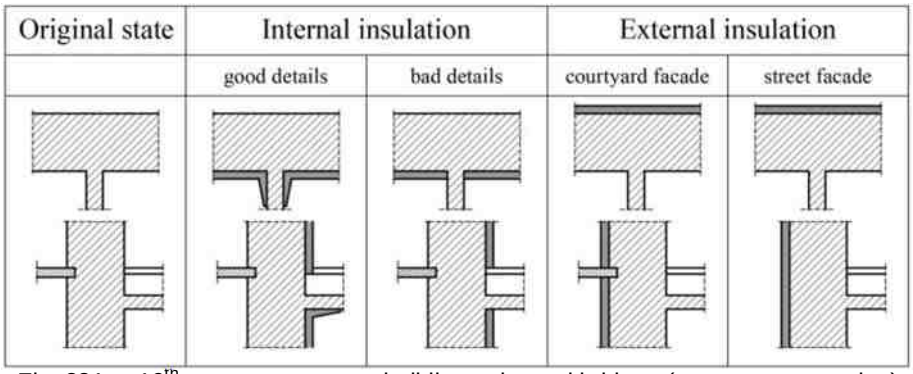

Fig. 231. – 19th century apartment building – thermal bridges (opaque construction)

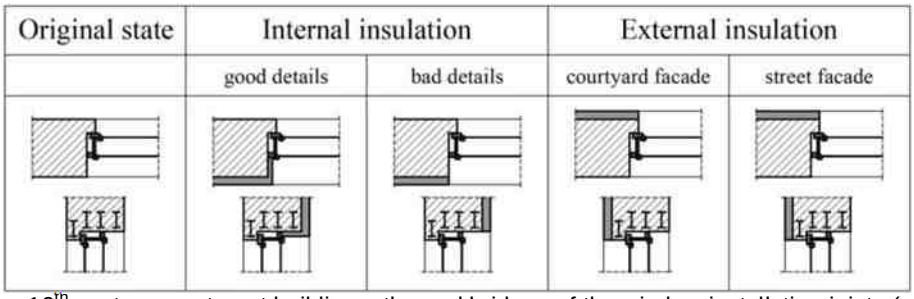

Fig. 232. – 19th century apartment building – thermal bridges of the window installation joints (window 1)

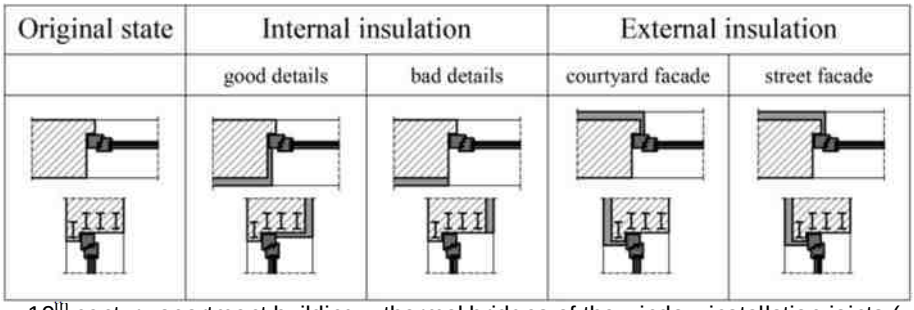

Fig. 233. – 19th century apartment building – thermal bridges of the window installation joints (window 2)

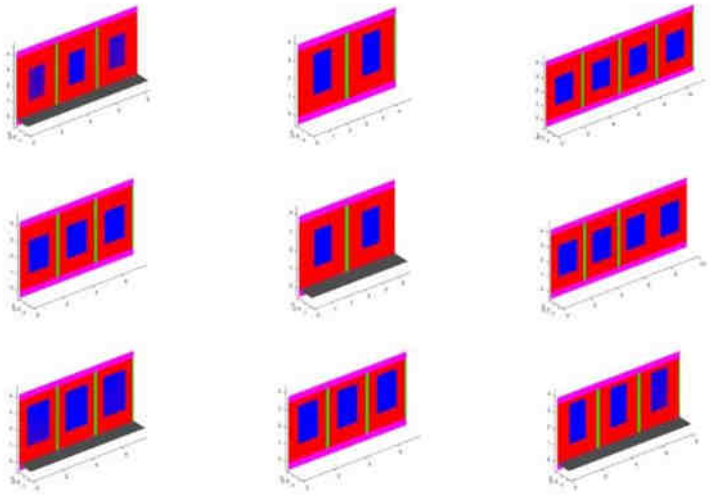

Fig. 234. – a large sample of the generated virtual façade geometries

C.1.2 Small suburban or rural detached houses based on typical Central-European type plans

This type of small detached houses, colloquially known in Hungary as ‘cube houses’, were built in large numbers after the second world war in Central- and Eastern-European countries, based on very similar type plans, in an effort to replace more traditional buildings that were deemed outdated by the political thinking of the time. These buildings are by no means completely identical in their floorplan or structures, as construction techniques varied according to what materials were at hand at the time. However, there is still a significant commonality between them. The vast majority share a single storey, approximately square floor plan with two external and one internal loadbearing walls and are topped by an unheated and unused attic with a hip roof which is usually close to a pyramid shape. The floor level is elevated from the ground with a large plaster, cast- or quarry-stone covered footing. The bedrooms, living rooms and kitchens have large, horizontally aligned windows, most commonly with two large symmetric windows oriented towards the street. The main entrance door is either connected to a terrace or is in a small lobby protruding from the main body of the building.

Due to the small size of the buildings we can generate complete façade geometries for the calculations, the algorithm for which is summarized in Fig. 236. and the main geometrical parameters in Fig. 235. Each virtual building has four facades numbered 1-4 assigned sequentially as either loadbearing or not, starting with the main street facing façade with the characteristic double windows. Then a secondary façade (hiding the kitchen and possible other bedrooms), a rear façade with the small openings usually oriented towards the neighbor and finally the entrance with either a terrace or a lobby is generated. Two of the façades have loadbearing walls, parallel to each other and perpendicular to the rest. Additional connecting internal loadbearing and partition walls are assigned to each façade element according to its type. The number of openings on the rear and secondary facades can vary. The generated façade geometries were not intended to correspond to real viable floor plans, our only goal was to capture the characteristic distribution of thermal bridges on the external walls.

As already mentioned these type of buildings were built using whatever constructional materials were available at the time and place. For the current investigation two common variants were chosen: a 38 [cm] thick fired solid clay brick masonry and a 25 [cm] thick fired aerated clay brick masonry. These have roughly the same U value which is a good way to investigate the dependence of thermal bridging on wall thickness. The floor is always 50 [cm] above ground, uninsulated and has a concrete plinth. The slab between the main floor and the attic is a prefabricated RC beam construction with prefab. slag filled concrete trays. The slab and walls are connected wit a reinforced concrete ringbeam without perimeter thermal insulation, as was the common practice at the rime. The lintel beams are prefabricated reinforced concrete elements. The walls and the attic slab are either uninsulated, or have an external insulation of 8-20 [cm] in 2 [cm] increments. The thermal conductivity of the insulation is λ=0.04 [W/mK]. These constructional parameters are summed up in Fig. 237.

The main constructional details / thermal bridges of the masonry are shown in Fig. 238. The wall-to-slab and plinth details have both a good and a bad quality variant. This is a necessary parameter to investigate as the thermal insulation of the wall-to-slab details is often not continuous because people try to avoid disturbing the existing roof and eaves construction, while in the case of the plinth the thermal insulation often ends at the bottom of the actual masonry as people try to preserve an existing stone footing or the existing pavement around the building.

The openings are either traditional double-skinned Central-European box type windows (most commonly known as Kastenfenster in German) or single skin contemporary constructions (wood or plastic), either with or without an inbuilt roller shutter. The window types are numbered 1-4 and their installation joints / thermal bridges are summed up in Fig. 239. All window details have original (no insulation) and insulated good and bad quality variants. The position of the window frames in the masonry was taken as a representative example, actual geometries can differ.

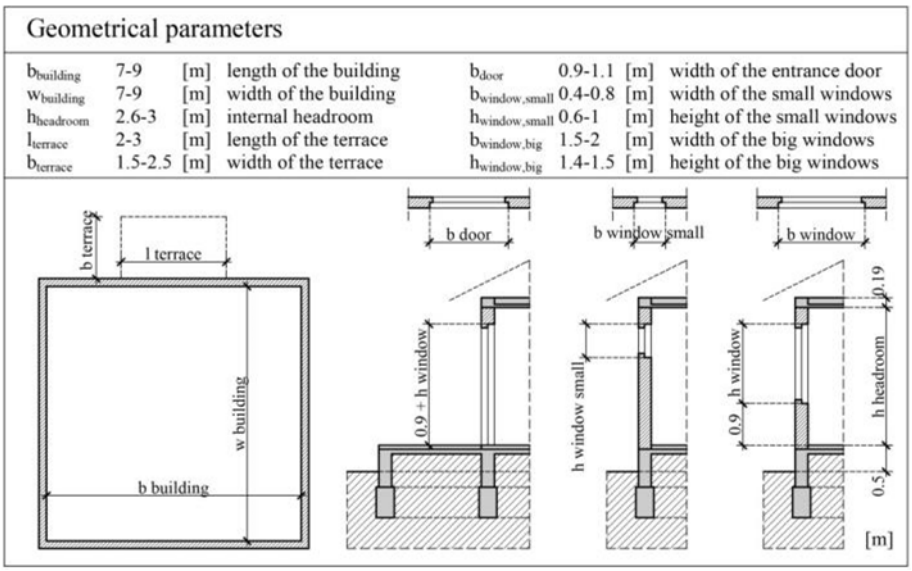

Fig. 235. – ‘cube house’ building type – geometrical parameters

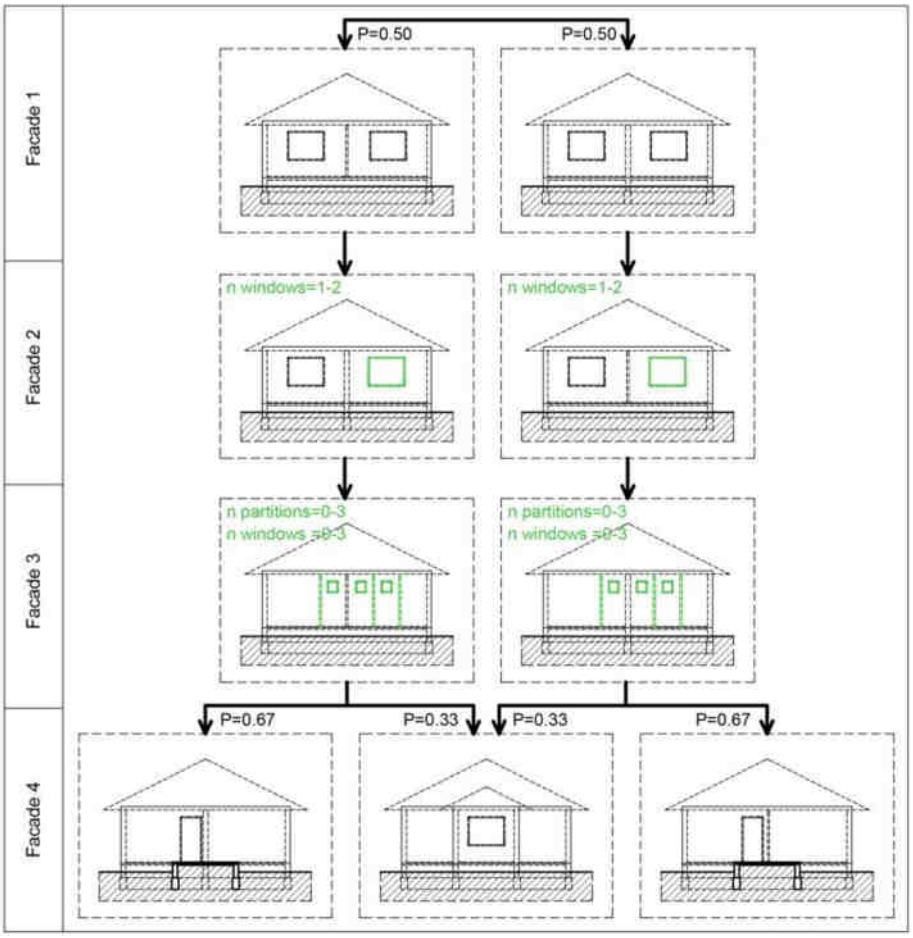

Fig. 236. – 'cube house' building type – geometry generation

Constructional parameters		
	Fired solid clay brick masonry	Fired aerated clay brick masonry
t_{wall} [m] λ_{wall} [W/mK] R_{wall} [m²K/W] $\lambda_{ins.}$ [W/mK] $t_{ins.}$ [m] $R_{ins.}$ [m²K/W]	0.38 0.78 0.487 0.04 0-0.08-0.10-0.12-0.14-0.16-0.18-0.20 0-2-2.5-3-3.5-4-4.5-5	0.25 0.50 0.50 0.04 0-0.08-0.10-0.12-0.14-0.16-0.18-0.20 0-2-2.5-3-3.5-4-4.5-5
window	window 1 - traditional window window 2 - contemporary window	window 1 - traditional window window 2 - contemporary window window 3 - traditional window + roller sh. window 4 - contemporary win. + rollet sh.

Fig. 237. – 'cube house' building type – constructional parameters

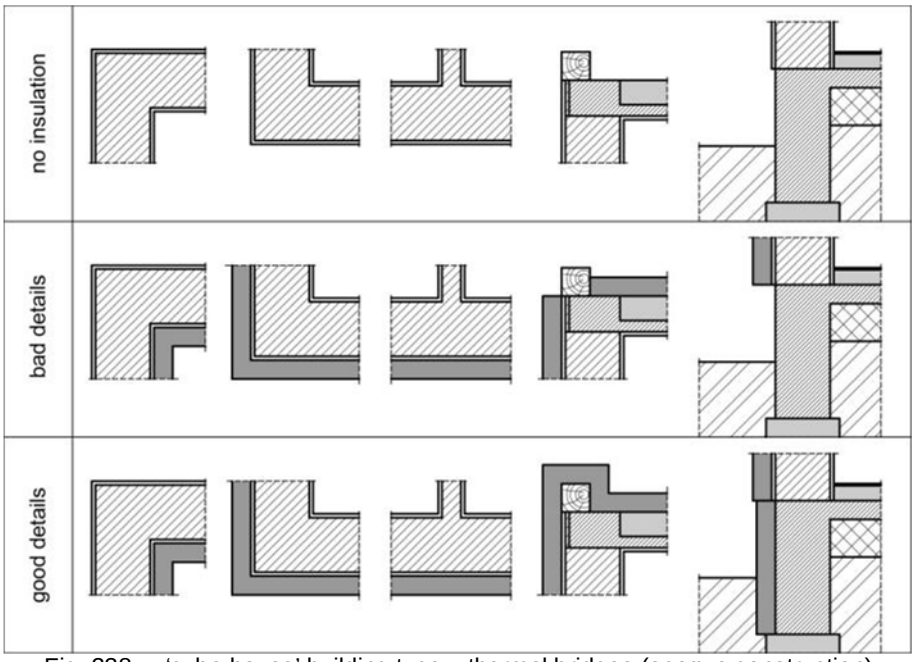

Fig. 238. – 'cube house' building type – thermal bridges (opaque construction)

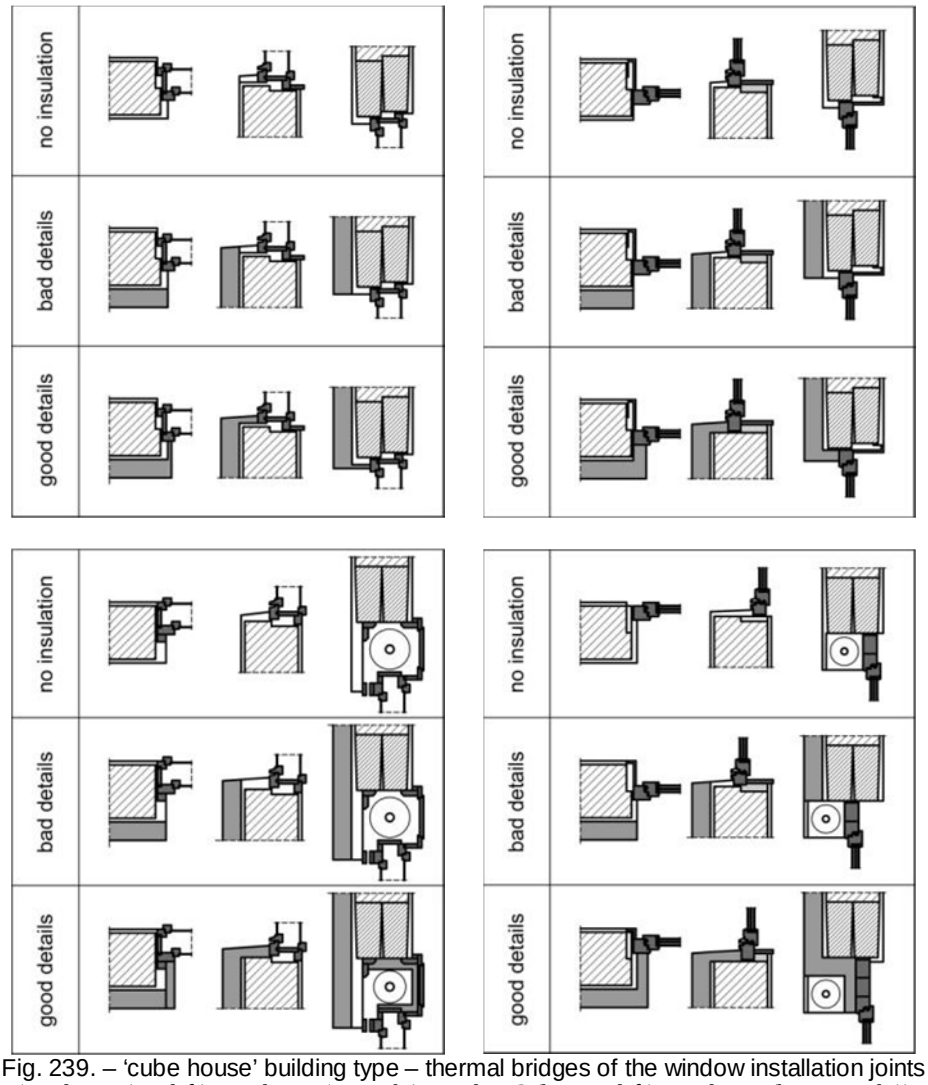

Fig. 239. – 'cube house' building type – thermal bridges of the window installation joints (window 1 (top left), window 2 (top right), window 3 (bottom left), window 4 (bottom right))

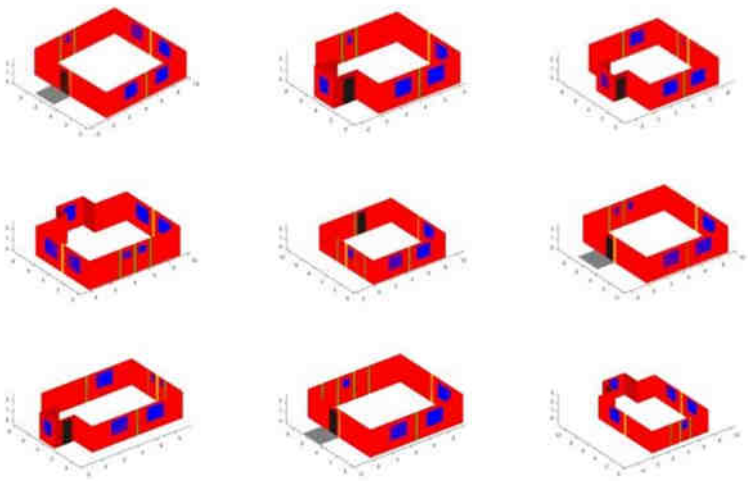

Fig. 240. – a large sample of the generated virtual façade geometries

C.1.3 Ca. 1960' type plan of urban apartment buildings built with prefabricated wall blocks

This type of building (henceforth 'block house') stems from type plans in the 1960' utilizing a constructional technique that used prefabricated slag-concrete blocks that were either half or full storey high (ca. 279 [cm] slab-to-slab) and 60-90 [cm] long. The blocks were placed next to each other to form the walls with only simple mortar filled joints in between. The buildings were built with a perpendicular shearing wall type loadbearing system and longitudinal prefabricated RC slab panels. Most such type plans (e.g. MOT I.58-40/63, I.58-39/63, MOT I.58-41/63[3]) had 5 storeys with a flat roof and a long and narrow or tower shaped plan with 3-4 flats per floor clustered around each staircase. Most buildings have loggias that were made with the same kind of prefabricated panels as the internal slabs, without any thermal insulation or thermal brake.

Like the 19th century urban apartment building type these buildings' façade is quite repetitive so for each virtual building geometry only generated 3 random façade elements were calculated according to the algorithm summed up in Fig. 242. to make up the façade of an imaginary flat. For the geometrical parameters see Fig. 241. The façade elements were either 3 to 4 panel wide and made out of panels either 60 or 90 [cm] long. As almost all such building are 5 storey high so each generated façade element has a 4/5 chance of being an intermediate storey and a 1/5 chance of being the top floor. Each wall is either loadbearing or not (P=0.23 vs. 0.77 acc. to a survey of the type plans), where loadbearing walls have much fewer openings and an additional lintel beam above the windows). Each façade element is set to be either normal or a loggia element, with the neighboring parts being loggias, regular façade sections or a perpendicular façade (building corner). The likelihood of a virtual façade element being either type was determined by analyzing the type plans. Finally the window type, width and connecting partition wall types were also assigned based on their frequency in the available type plans.

All such buildings used virtually the same constructions. The wall panels are 29 [cm] thick with 2 [cm] plaster on either side. The calculations are made for the original case (no insulation) or a 8-20 [cm] thick external insulation in 2 [cm] increments (see Fig. 243). When applicable the details are calculated as either good or bad according to the continuity of the thermal insulation. The horizontal details / thermal bridges are summed up in Fig. 244. and the vertical details / thermal bridges in Fig. 245. The openings have either traditional double-skinned Central-European box type windows or single skin contemporary constructions (wooden or plastic). No built-in shading is considered for this building type. The window types are numbered 1 and 2 and their installation joints / thermal bridges are summed up in Fig. 246 and Fig. 247. All window installation details have original (no insulation) and insulated good and bad quality variants. The position of the window frames in the masonry was taken as a representative example, actual geometries can differ.

---

[1] [3] Type plans found in: D. Szabó L. (1966) Magyar Országos Typustervek Katalógusa I. – Lakóépületek, ÉM Építésügyi Tájékoztatási Központ, Budapest

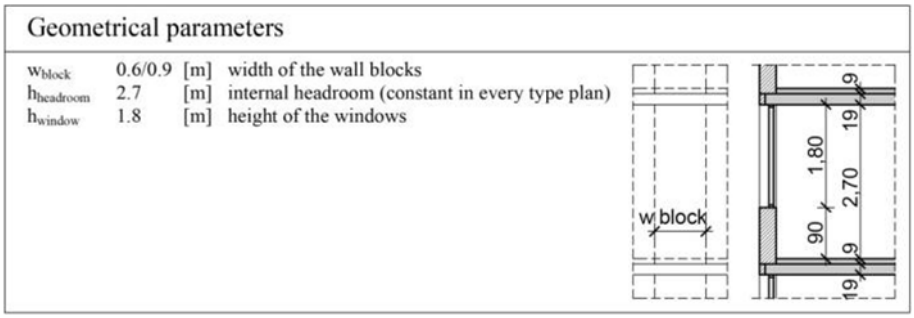

Fig. 241. – 'block house' building type – geometrical parameters

Fig. 242. – 'block house' building type – geometry generation

Constructional parameters	
t_{wall} [m]	0.29
λ_{wall} [W/mK]	0.62
R_{wall} [m²K/W]	0.468
$\lambda_{ins.}$ [W/mK]	0.04
$t_{ins.}$ [m]	0-0.08-0.10-0.12-0.14-0.16-0.18-0.20
$R_{ins.}$ [m²K/W]	0-2-2.5-3-3.5-4-4.5-5
window	window 1 - traditional window window 2 - contemporary window

Fig. 243. – 'block house' building type – constructional parameters

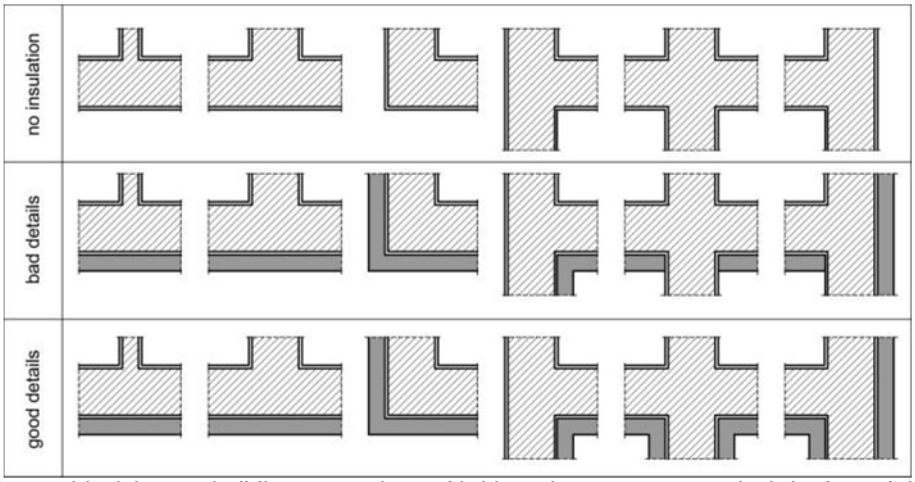

Fig. 244. – 'block house' building type – thermal bridges (opaque construction), horizontal details

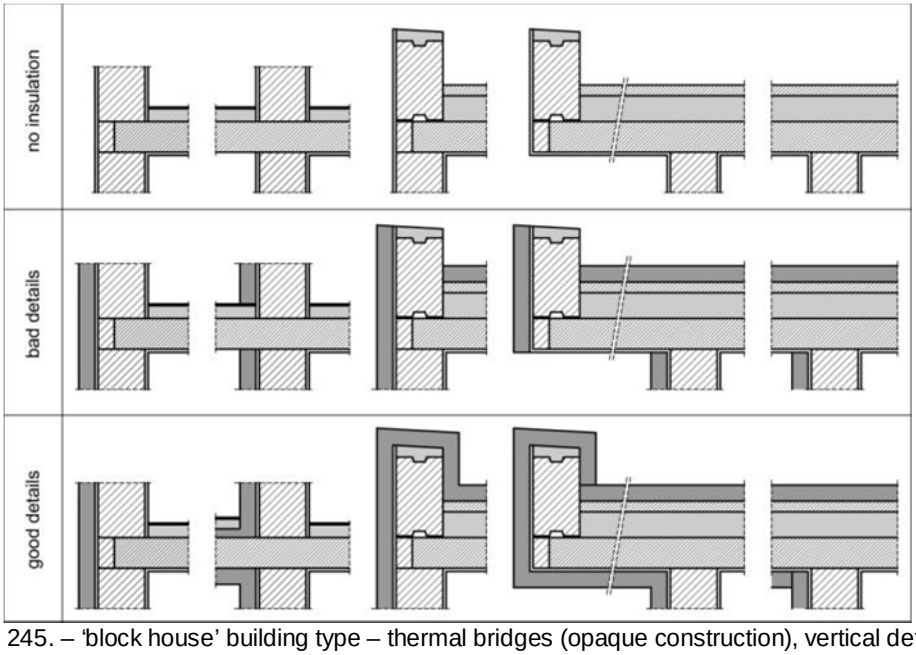

Fig. 245. – 'block house' building type – thermal bridges (opaque construction), vertical details

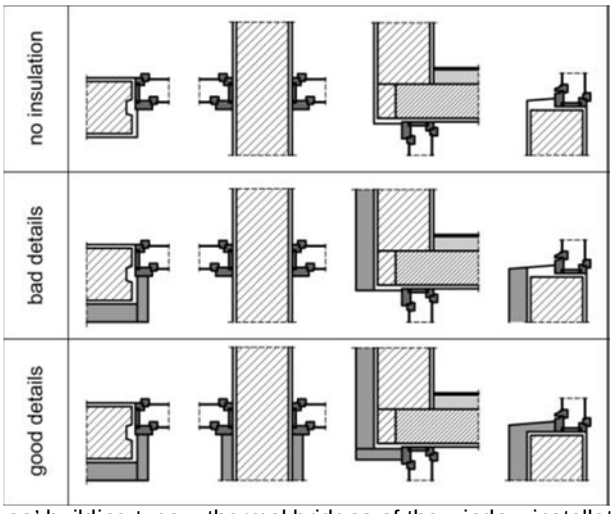

Fig. 246. – 'block house' building type – thermal bridges of the window installation joints (window 1)

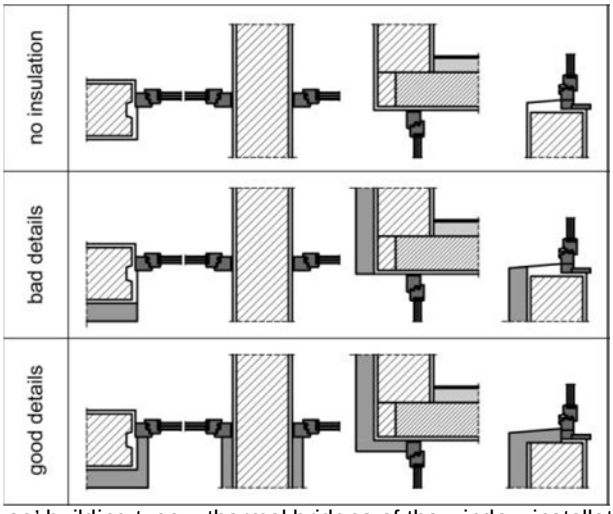

Fig. 247. – 'block house' building type – thermal bridges of the window installation joints (window 2)

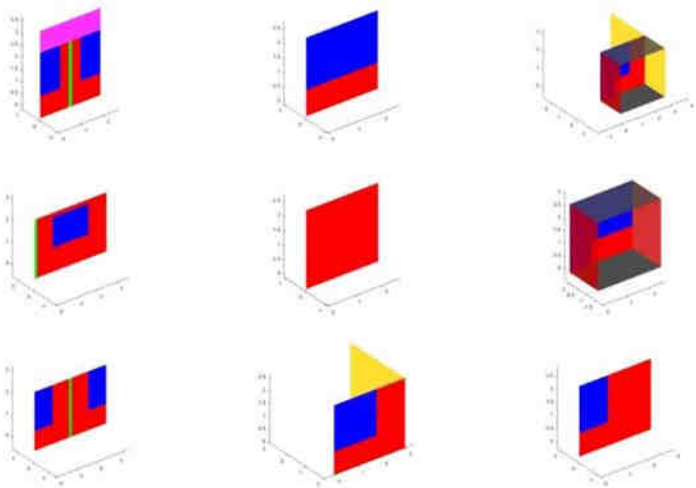

Fig. 248. – a large sample of the generated virtual façade element geometries

C.2 Detailed Monte Carlo simulation results

C.2.1 19th century urban residential building

C.2.1.1 Internal insulation – bad details

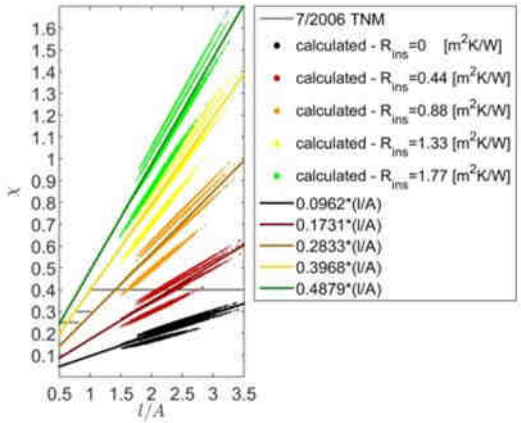

Fig. 249. – 44 [cm] thick wall, internal insulation, bad details, window 1

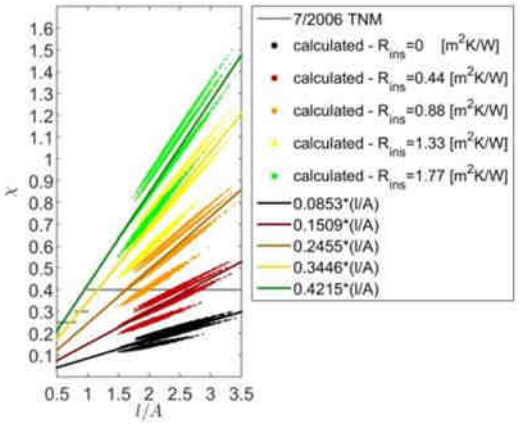

Fig. 250. – 44 [cm] thick wall, internal insulation, bad details, window 1b

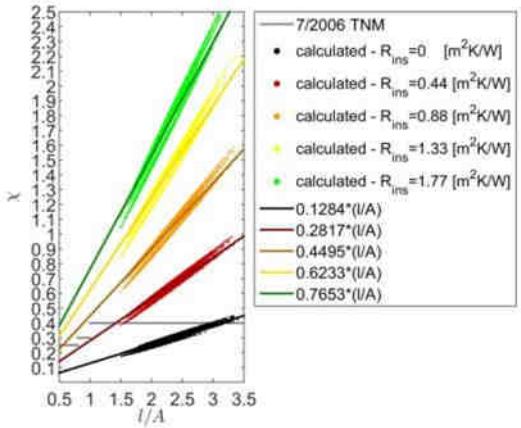

Fig. 251. – 44 [cm] thick wall, internal insulation, bad details, window 2

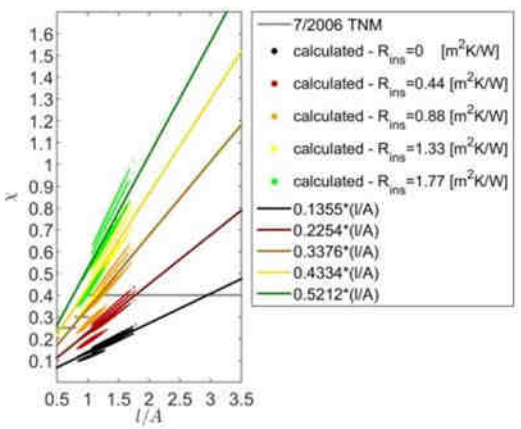

Fig. 252. – 44 [cm] thick wall, internal insulation, bad details, no window installation thermal bridges

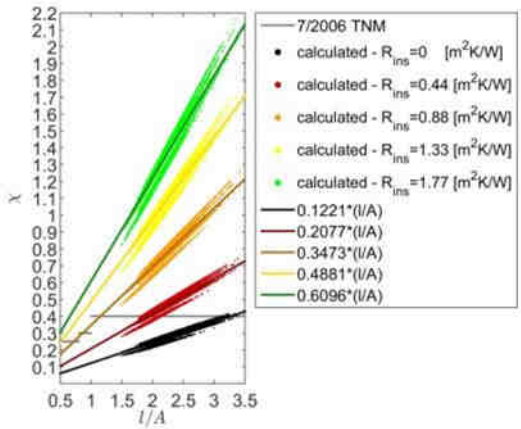

Fig. 253. – 59 [cm] thick wall, internal insulation, bad details, window 1

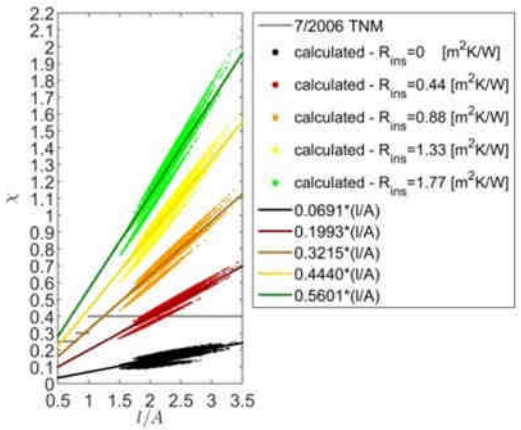

Fig. 254. – 59 [cm] thick wall, internal insulation, bad details, window 1b

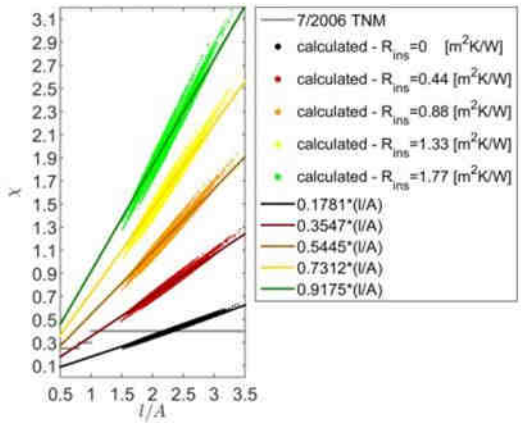

Fig. 255. – 59 [cm] thick wall, internal insulation, bad details, window 2

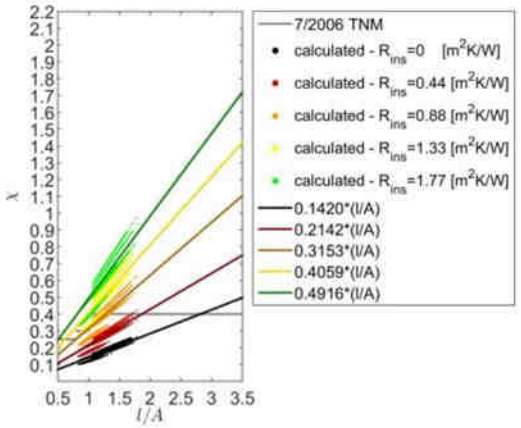

Fig. 256. – 59 [cm] thick wall, internal insulation, bad details, no window installation thermal bridges

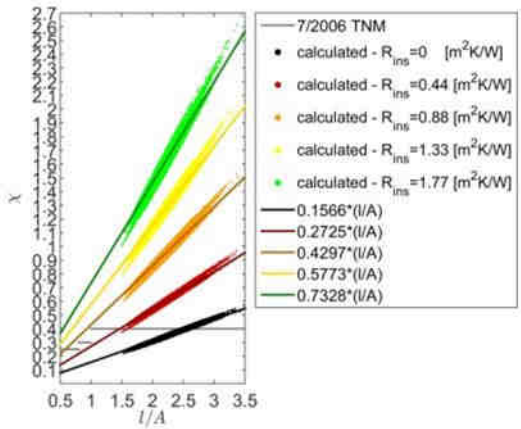

Fig. 257. – 74 [cm] thick wall, internal insulation, bad details, window 1

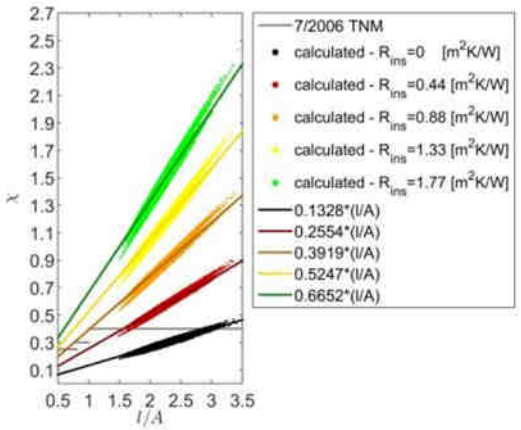

Fig. 258. – 74 [cm] thick wall, internal insulation, bad details, window 1b

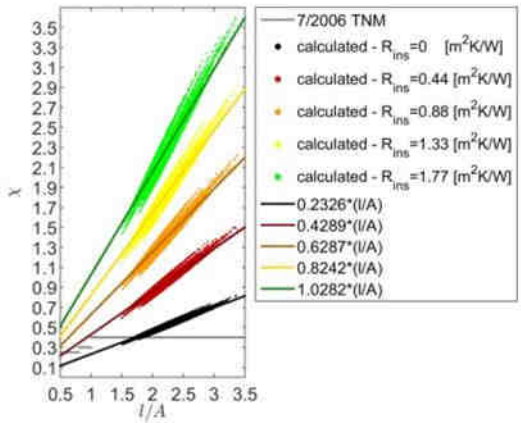

Fig. 259. – 74 [cm] thick wall, internal insulation, bad details, window 2

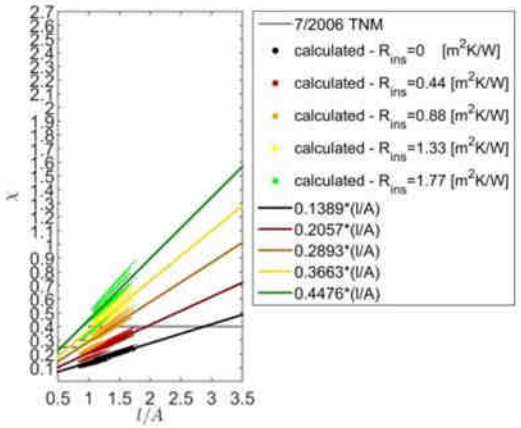

Fig. 260. – 74 [cm] thick wall, internal insulation, bad details, no window installation thermal bridges

C.2.1.2 Internal insulation – good details

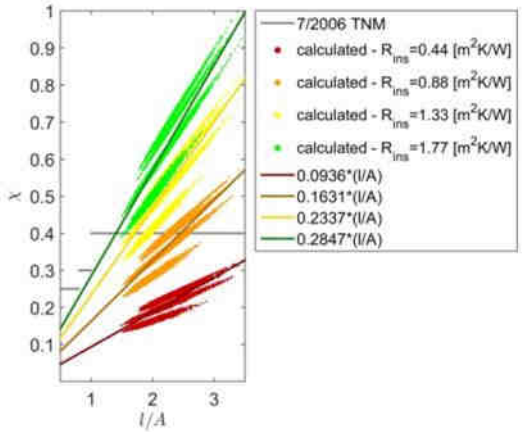

Fig. 261. – 44 [cm] thick wall, internal insulation, good details, window 1

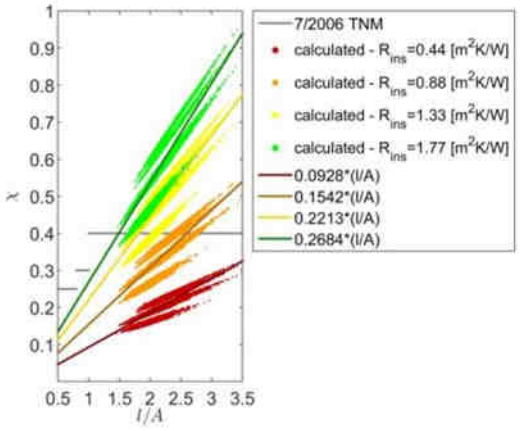

Fig. 262. – 44 [cm] thick wall, internal insulation, good details, window 1b

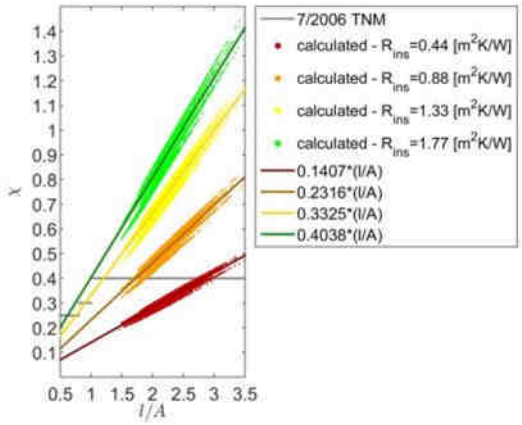

Fig. 263. – 44 [cm] thick wall, internal insulation, good details, window 2

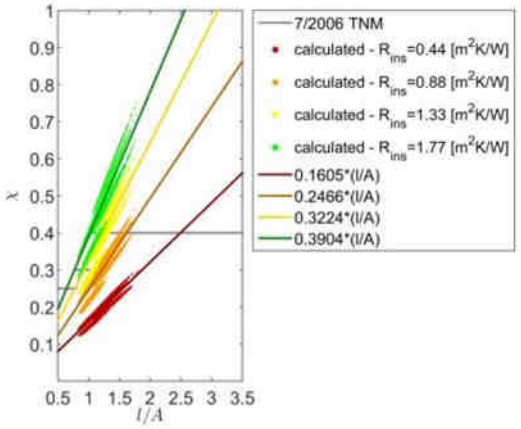

Fig. 264. – 44 [cm] thick wall, internal insulation, good details, no window installation thermal bridges

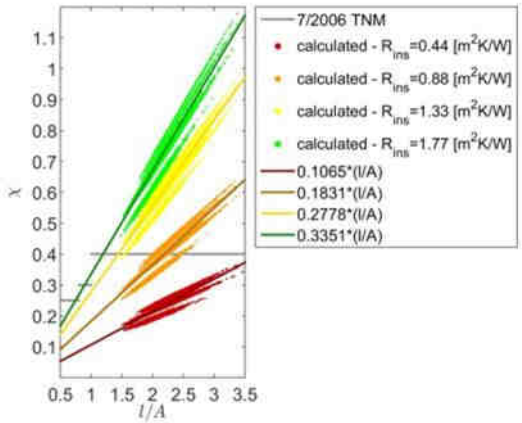

Fig. 265. – 59 [cm] thick wall, internal insulation, good details, window 1

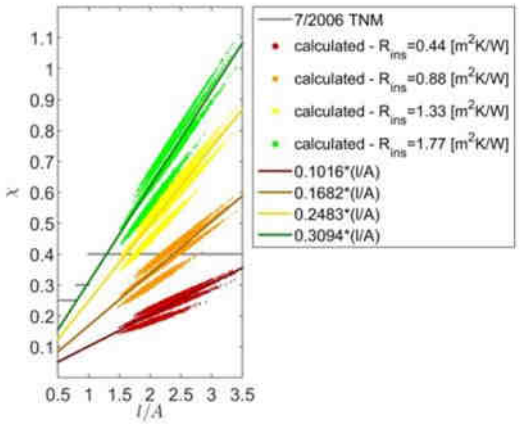

Fig. 266. – 59 [cm] thick wall, internal insulation, good details, window 1b

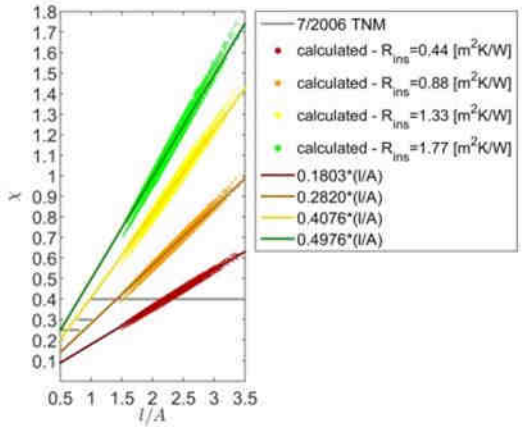

Fig. 267. – 59 [cm] thick wall, internal insulation, good details, window 2

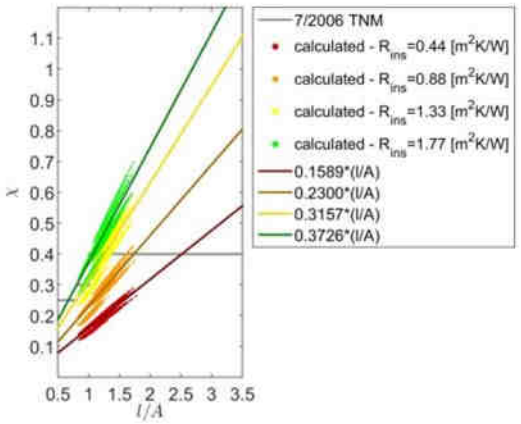

Fig. 268. – 59 [cm] thick wall, internal insulation, good details, no window installation thermal bridges

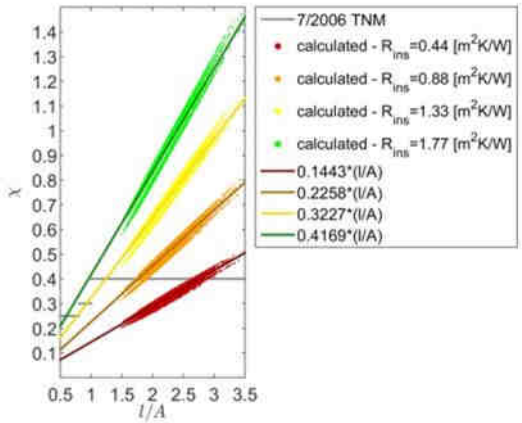

Fig. 269. – 74 [cm] thick wall, internal insulation, good details, window 1

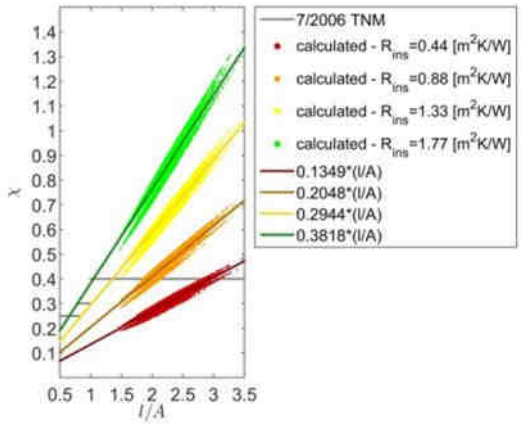

Fig. 270. – 74 [cm] thick wall, internal insulation, good details, window 1b

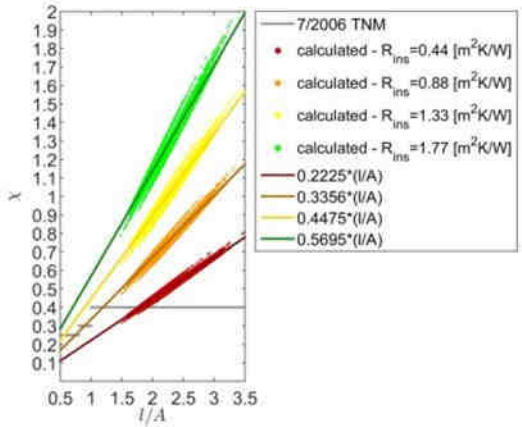

Fig. 271. – 74 [cm] thick wall, internal insulation, good details, window 2

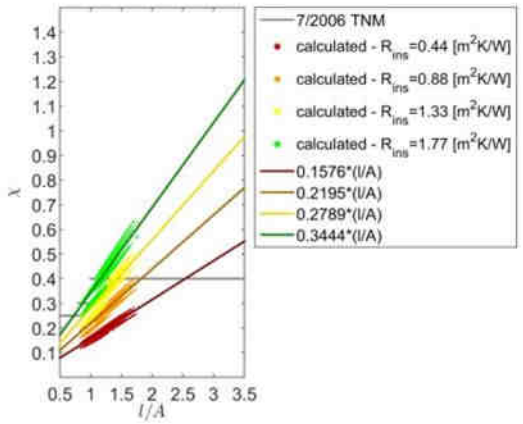

Fig. 272. – 74 [cm] thick wall, internal insulation, good details, no window installation thermal bridges

C.2.1.3 External insulation – external (street) façade

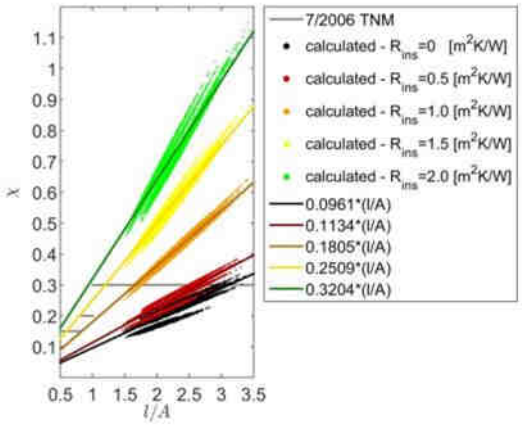

Fig. 273. – 44 [cm] thick wall, external insulation, external (street) façade, window 1

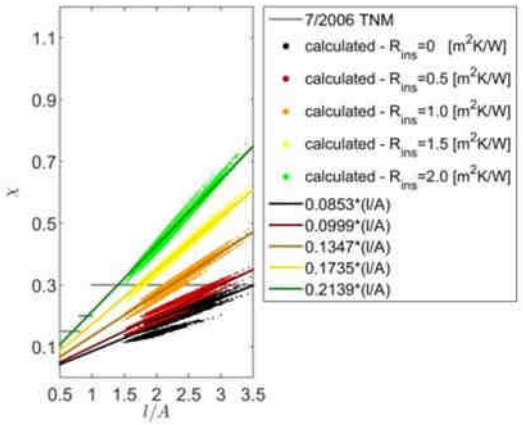

Fig. 274. – 44 [cm] thick wall, external insulation, external (street) façade, window 1b

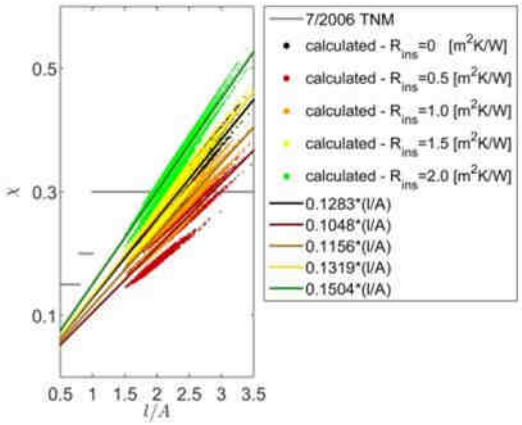

Fig. 275. – 44 [cm] thick wall, external insulation, external (street) façade, window 2

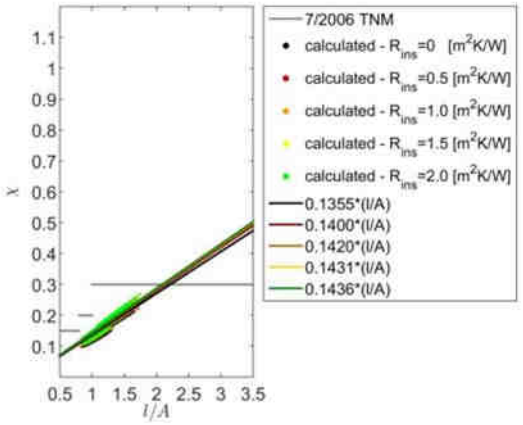

Fig. 276. – 44 [cm] thick wall, external insulation, external (street) façade, no window installation thermal bridges

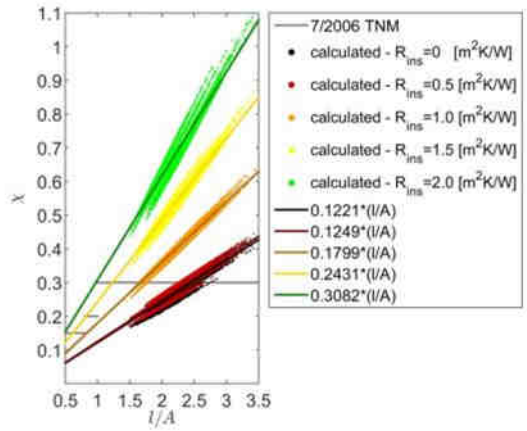

Fig. 277. – 59 [cm] thick wall, external insulation, external (street) façade, window 1

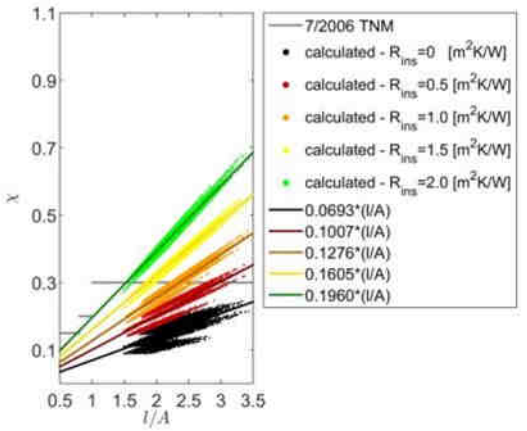

Fig. 278. – 59 [cm] thick wall, external insulation, external (street) façade, window 1b

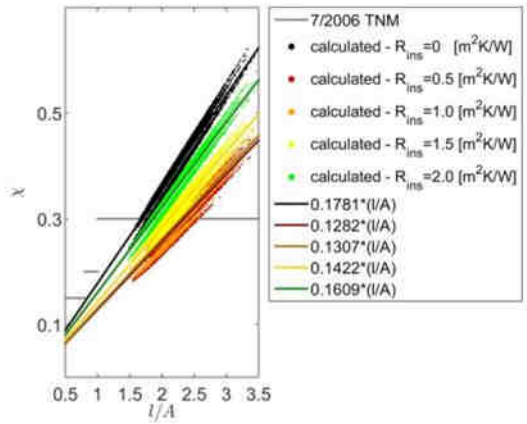

Fig. 279. – 59 [cm] thick wall, external insulation, external (street) façade, window 2

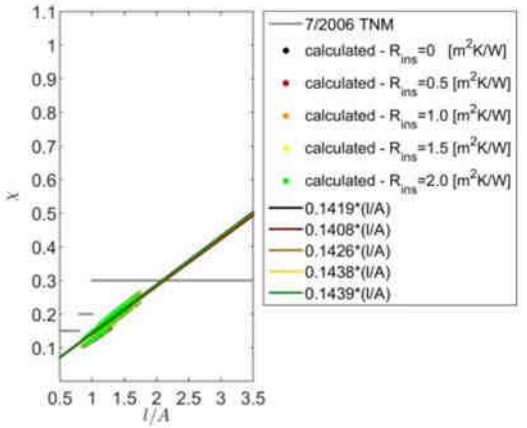

Fig. 280. – 59 [cm] thick wall, external insulation, external (street) façade, no window installation thermal bridges

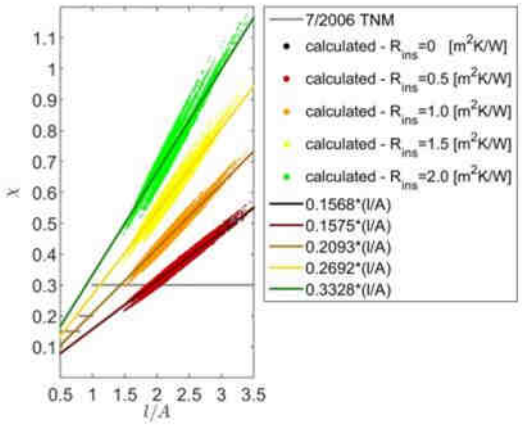

Fig. 281. – 74 [cm] thick wall, external insulation, external (street) façade, window 1

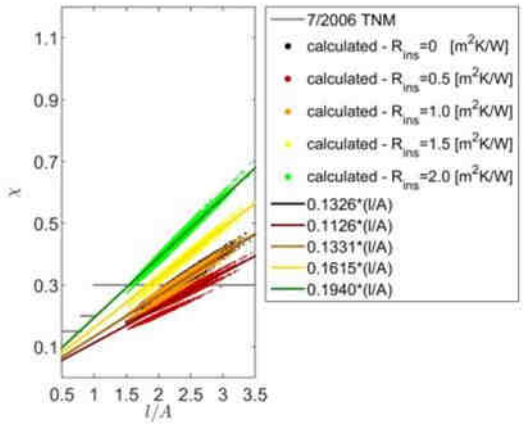

Fig. 282. – 74 [cm] thick wall, external insulation, external (street) façade, window 1b

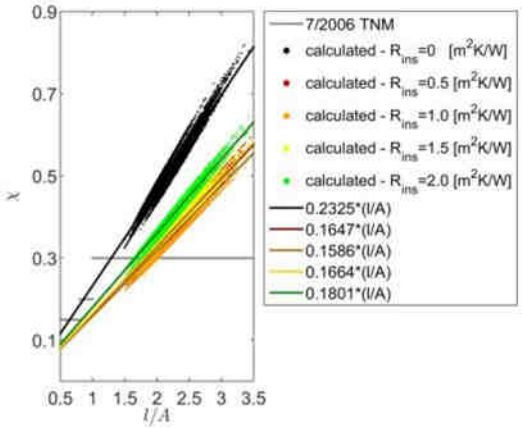

Fig. 283. – 74 [cm] thick wall, external insulation, external (street) façade, window 2

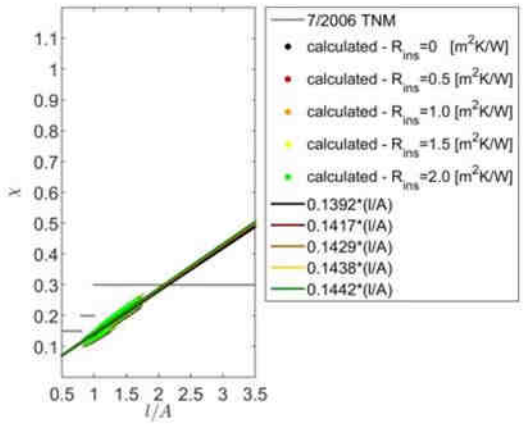

Fig. 284. – 74 [cm] thick wall, external insulation, external (street) façade, no window installation thermal bridges

C.2.1.4 External insulation – internal (courtyard) façade

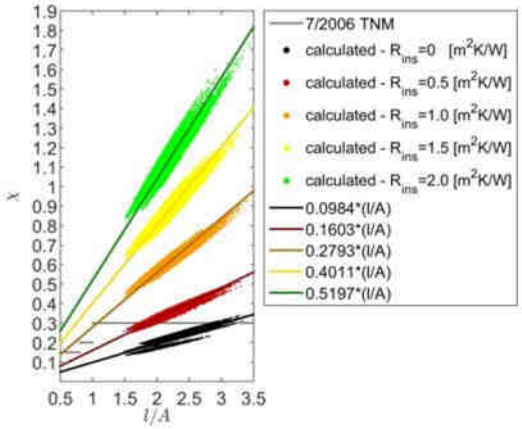

Fig. 285. – 44 [cm] thick wall, external insulation, internal (courtyard) façade, window 1

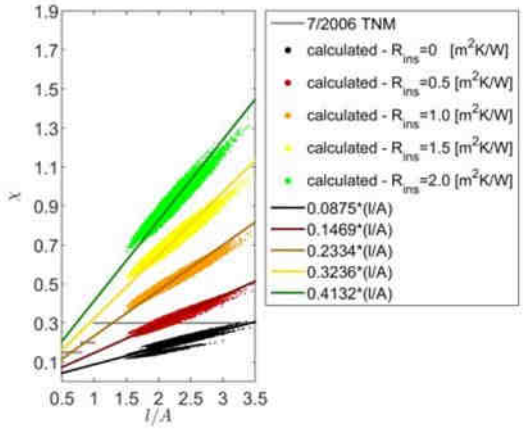

Fig. 286. – 44 [cm] thick wall, external insulation, internal (courtyard) façade, window 1b

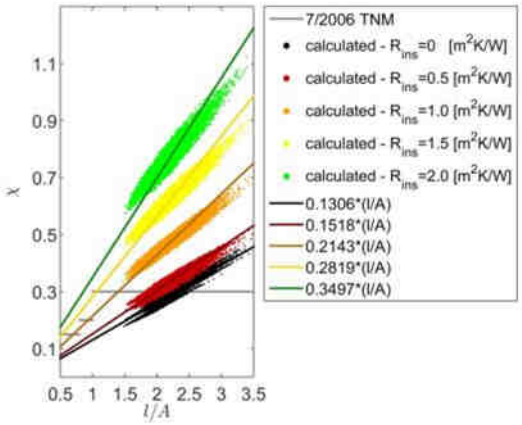

Fig. 287. – 44 [cm] thick wall, external insulation, internal (courtyard) façade, window 2

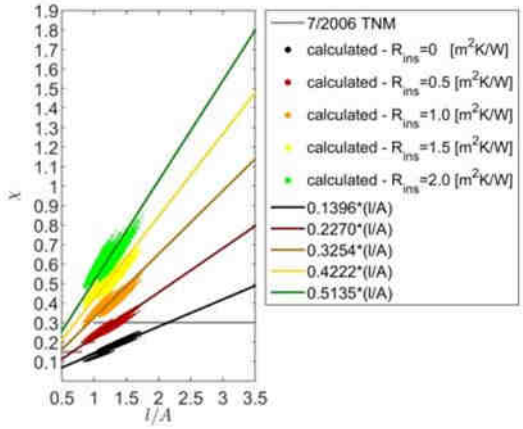

Fig. 288. – 44 [cm] thick wall, external insulation, internal (courtyard) façade, no window installation thermal bridges

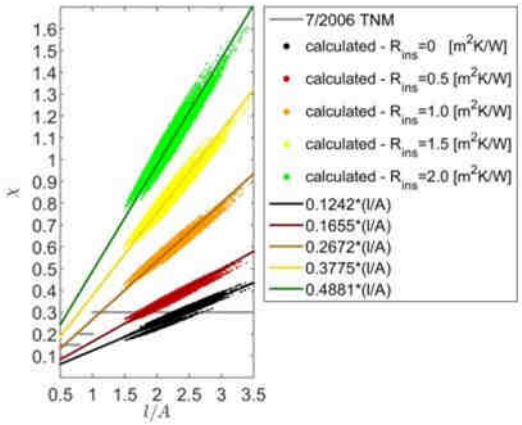

Fig. 289. – 59 [cm] thick wall, external insulation, internal (courtyard) façade, window 1

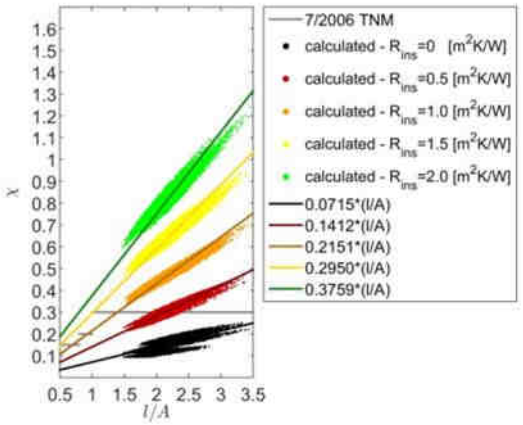

Fig. 290. – 59 [cm] thick wall, external insulation, internal (courtyard) façade, window 1b

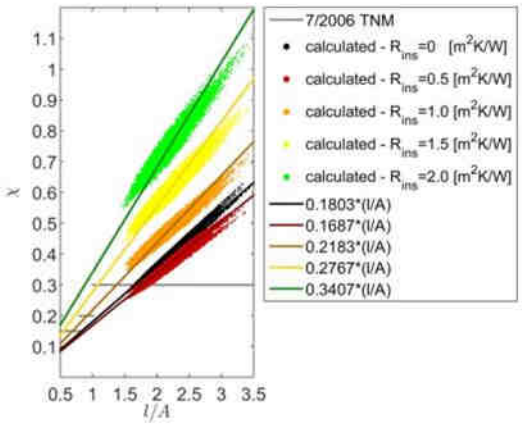

Fig. 291. – 59 [cm] thick wall, external insulation, internal (courtyard) façade, window 2

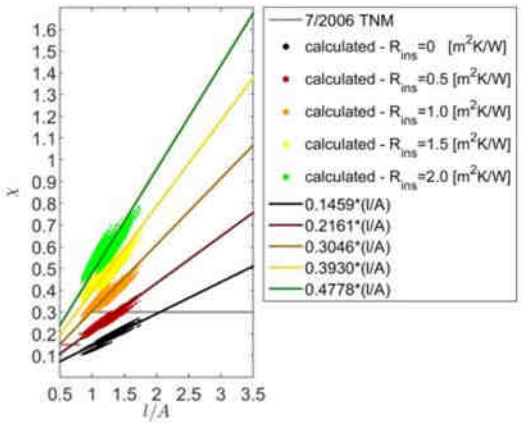

Fig. 292. – 59 [cm] thick wall, external insulation, internal (courtyard) façade, no window installation thermal bridges

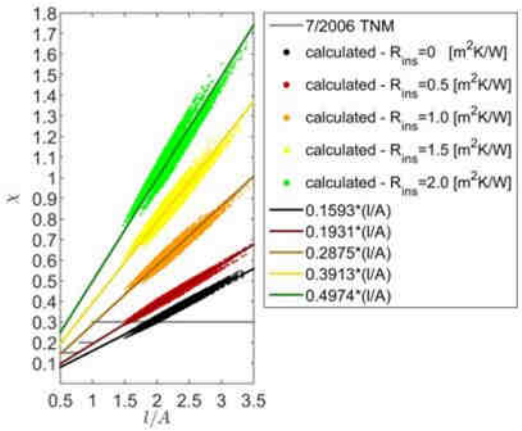

Fig. 293. – 74 [cm] thick wall, external insulation, internal (courtyard) façade, window 1

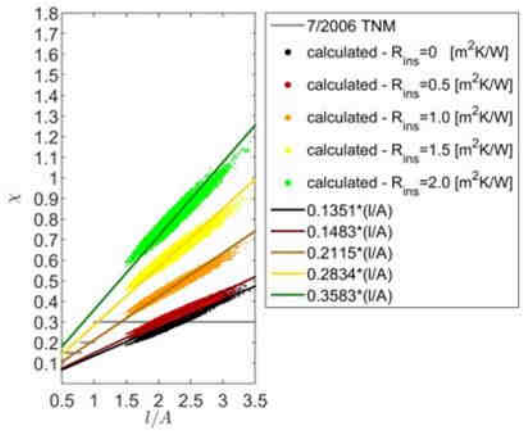

Fig. 294. – 74 [cm] thick wall, external insulation, internal (courtyard) façade, window 1b

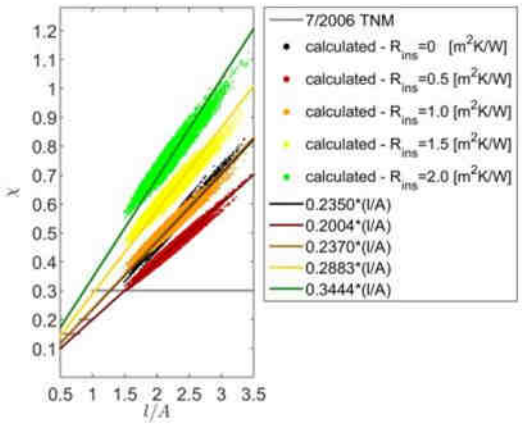

Fig. 295. – 74 [cm] thick wall, external insulation, internal (courtyard) façade, window 2

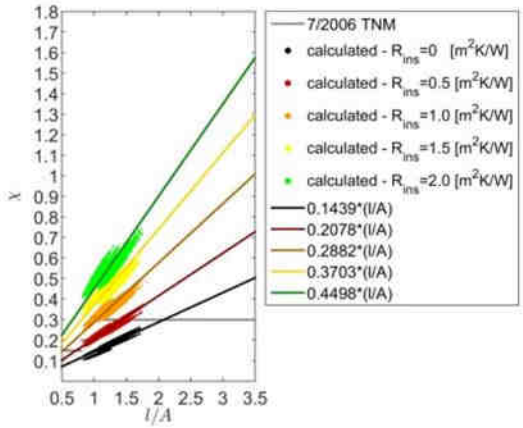

Fig. 296. – 74 [cm] thick wall, external insulation, internal (courtyard) façade, no window installation thermal bridges

C.2.1.5 Summary of data

insulation	details	windows	R_{wall}	s [m]				
				R_{ins}=0	R_{ins} =0.44	R_{ins} =0.88	R_{ins} =1.33	R_{ins} =1.77
internal ins.	bad details	window 1	0.608 (44 cm)	0.0962	0.1731	0.2834	0.3973	0.4880
			0.800 (59 cm)	0.1220	0.2078	0.3476	0.4879	0.6092
			0.992 (74 cm)	0.1567	0.2726	0.4294	0.5775	0.7325
		window 1b	0.608 (44 cm)	0.0853	0.1509	0.2455	0.3446	0.4215
			0.800 (59 cm)	0.0691	0.1993	0.3215	0.4440	0.5601
			0.992 (74 cm)	0.1328	0.2554	0.3919	0.5247	0.6652
		window 2	0.608 (44 cm)	0.1284	0.2817	0.4495	0.6233	0.7653
			0.800 (59 cm)	0.1781	0.3547	0.5445	0.7312	0.9175
			0.992 (74 cm)	0.2326	0.4289	0.6287	0.8242	1.0282
	good details	window 1	0.608 (44 cm)	0.0962	0.0936	0.1633	0.2337	0.2843
			0.800 (59 cm)	0.1220	0.1067	0.1832	0.2777	0.3353
			0.992 (74 cm)	0.1567	0.1444	0.2259	0.3225	0.4166
		window 1b	0.608 (44 cm)	0.0853	0.0928	0.1542	0.2213	0.2684
			0.800 (59 cm)	0.0691	0.1016	0.1682	0.2483	0.3094
			0.992 (74 cm)	0.1328	0.1349	0.2048	0.2944	0.3818
		window 2	0.608 (44 cm)	0.1284	0.1407	0.2316	0.3325	0.4038
			0.800 (59 cm)	0.1781	0.1803	0.2820	0.4076	0.4976
			0.992 (74 cm)	0.2326	0.2225	0.3356	0.4475	0.5695
insulation	**details**	**windows**	R_{wall}	s [m]				
				R_{ins}=0	R_{ins} =0.5	R_{ins} =1	R_{ins} =1.5	R_{ins} =2
external ins.	ext. façade	window 1	0.608 (44 cm)	0.0963	0.1133	0.1805	0.2506	0.3203
			0.800 (59 cm)	0.1219	0.1250	0.1800	0.2340	0.3082
			0.992 (74 cm)	0.1567	0.1574	0.2092	0.2693	0.3325
		window 1b	0.608 (44 cm)	0.0853	0.0999	0.1347	0.1735	0.2139
			0.800 (59 cm)	0.0693	0.1007	0.1276	0.1605	0.1960
			0.992 (74 cm)	0.1326	0.1126	0.1331	0.1615	0.1940
		window 2	0.608 (44 cm)	0.1283	0.1048	0.1156	0.1319	0.1504
			0.800 (59 cm)	0.1781	0.1282	0.1307	0.1422	0.1609
			0.992 (74 cm)	0.2325	0.1647	0.1586	0.1664	0.1801
	int. façade	window 1	0.608 (44 cm)	0.0984	0.1603	0.2792	0.4009	0.5200
			0.800 (59 cm)	0.1242	0.1655	0.2673	0.3775	0.4881
			0.992 (74 cm)	0.1592	0.1931	0.2876	0.3912	0.4974
		window 1b	0.608 (44 cm)	0.0875	0.1469	0.2334	0.3236	0.4132
			0.800 (59 cm)	0.0715	0.1412	0.2151	0.2950	0.3759
			0.992 (74 cm)	0.1351	0.1483	0.2115	0.2834	0.3583
		window 2	0.608 (44 cm)	0.1306	0.1518	0.2143	0.2819	0.3497
			0.800 (59 cm)	0.1803	0.1687	0.2183	0.2767	0.3407
			0.992 (74 cm)	0.2350	0.2004	0.2370	0.2883	0.3444

Table 8 – Summary of s values for the 19th century urban residential building type

C.2.2 Small suburban or rural detached houses based on typical Central-European type plans

C.2.2.1 Aerated clay brick masonry – good details

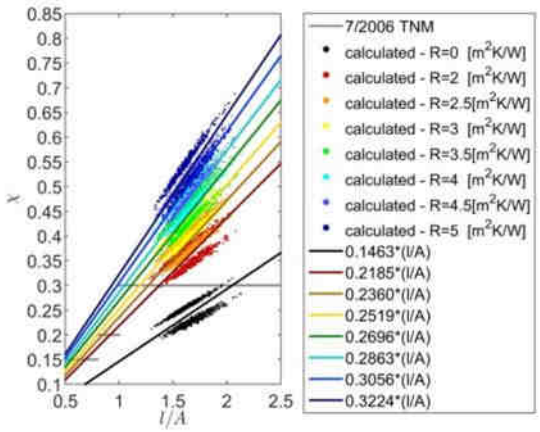

Fig. 297. – aerated clay brick masonry, good details, window 1

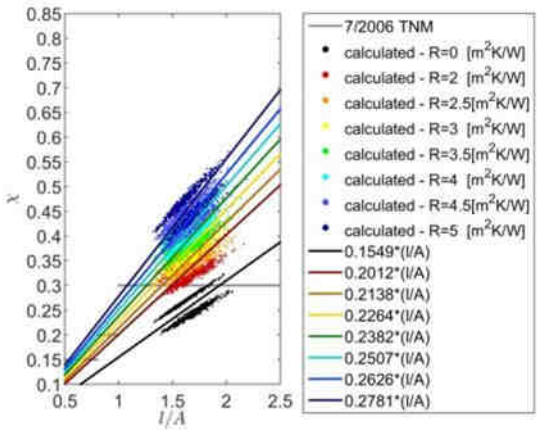

Fig. 298. – aerated clay brick masonry, good details, window 2

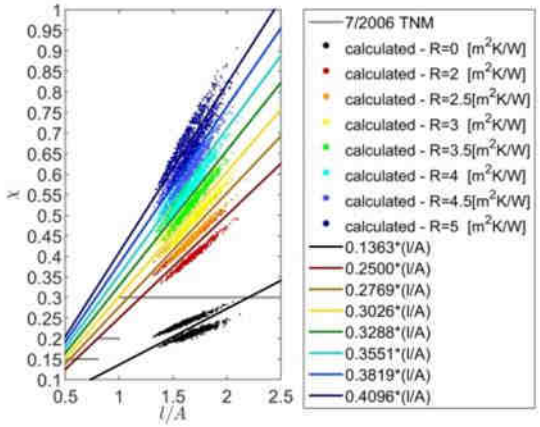

Fig. 299. – aerated clay brick masonry, good details, window 3

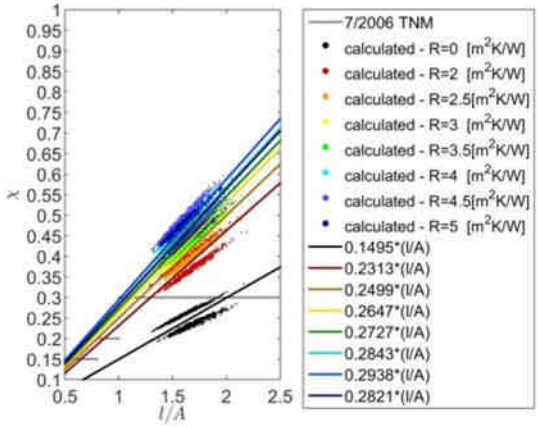

Fig. 300. – aerated clay brick masonry, good details, window 4

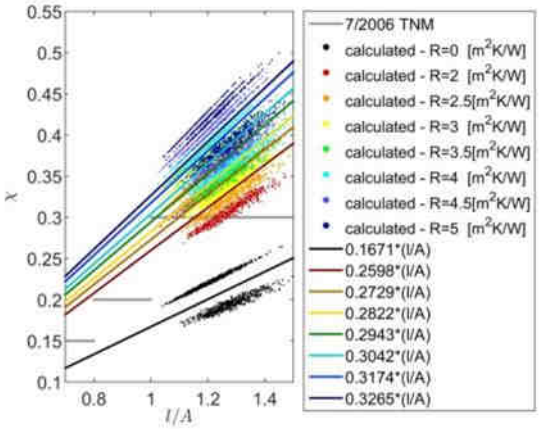

Fig. 301. – aerated clay brick masonry, good details, no windows

C.2.2.2 Aerated clay brick masonry – bad details

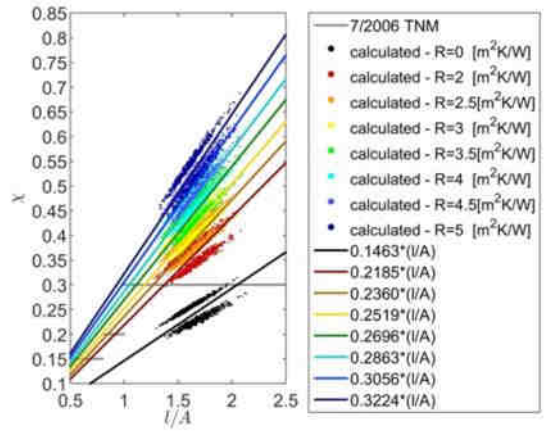

Fig. 302. – aerated clay brick masonry, bad details, window 1

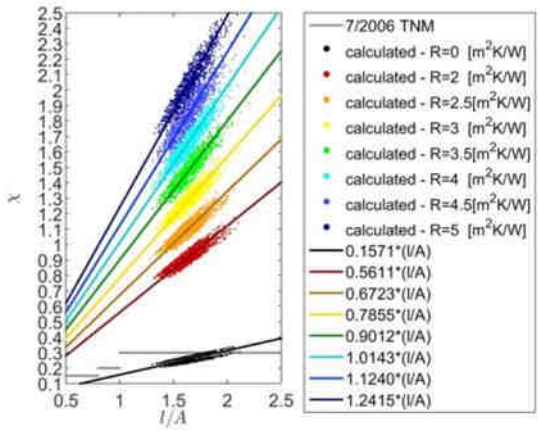

Fig. 303. – aerated clay brick masonry, bad details, window 2

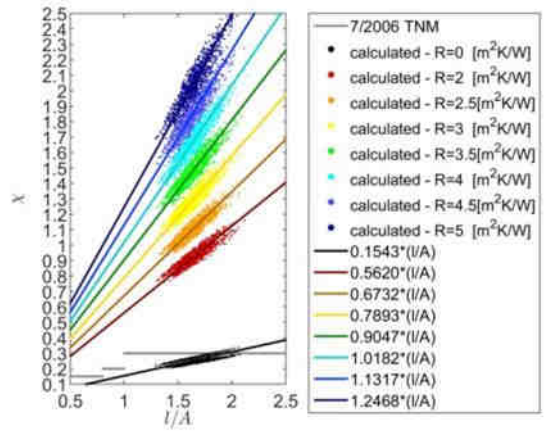

Fig. 304. – aerated clay brick masonry, bad details, window 3

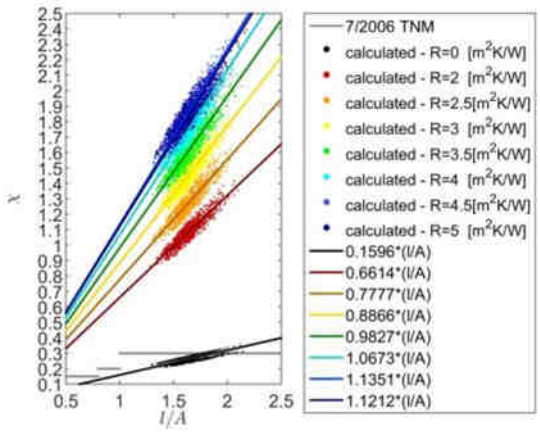

Fig. 305. – aerated clay brick masonry, bad details, window 4

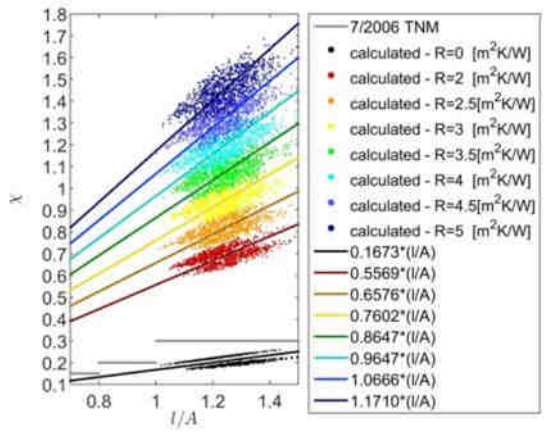

Fig. 306. – aerated clay brick masonry, bad details, no windows

C.2.2.3 Solid brick masonry – good details

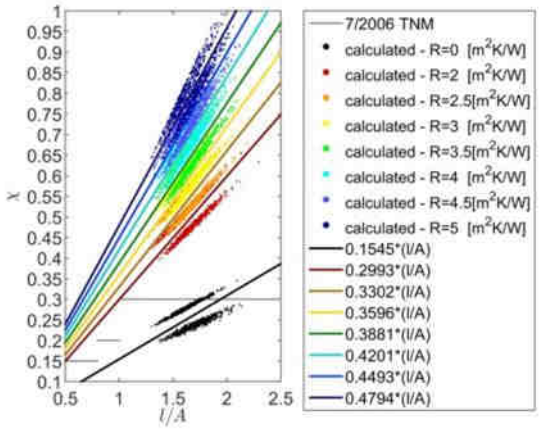

Fig. 307. – solid brick masonry, good details, window 1

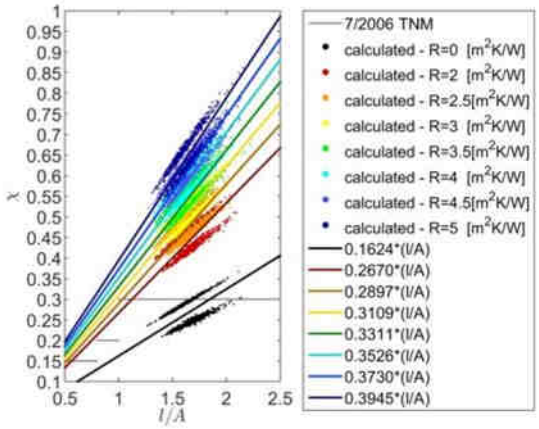

Fig. 308. – solid brick masonry, good details, window 2

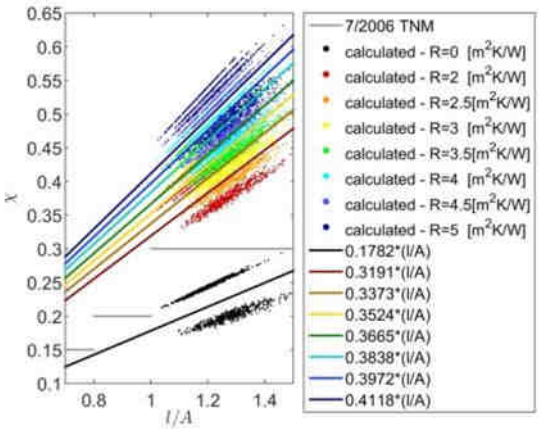

Fig. 309. – solid brick masonry, good details, no windows

C.2.2.4 Solid brick masonry – bad details

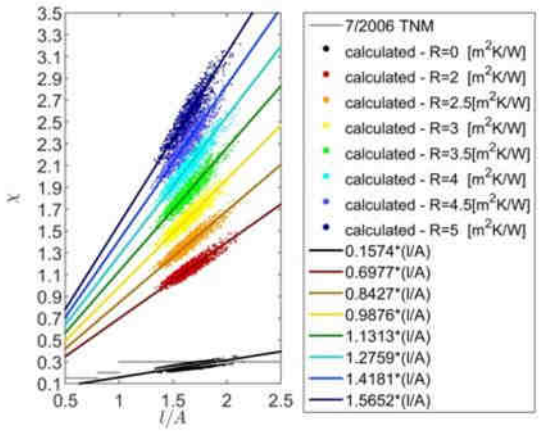

Fig. 310. – solid brick masonry, bad details, window 1

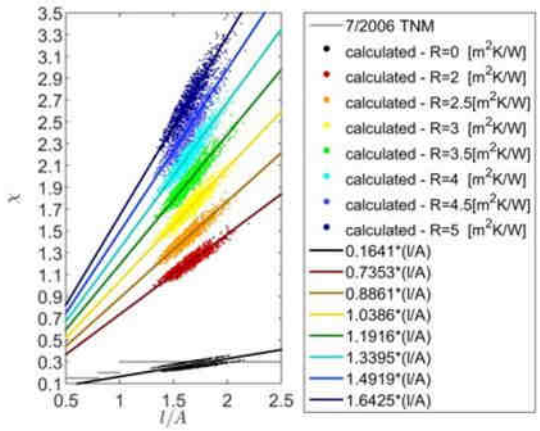

Fig. 311. – solid brick masonry, bad details, window 2

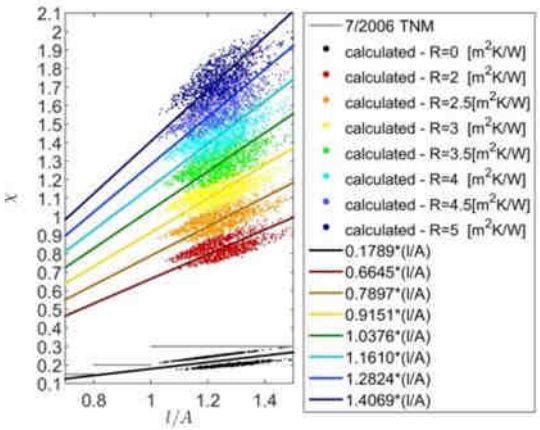

Fig. 312. – solid brick masonry, bad details, no windows

C.2.2.5 Summary of data

masonry	details	win.	s [m]							
			R_{ins}=0	R_{ins}=2	R_{ins}=2.5	R_{ins}=3	R_{ins}=3.5	R_{ins}=4	R_{ins}=4.5	R_{ins}=5
aerated c.b.	good	win. 1	0.1463	0.2185	0.2360	0.2519	0.2696	0.2863	0.3056	0.3224
		win. 2	0.1549	0.2012	0.2138	0.2264	0.2382	0.2507	0.2626	0.2781
		win. 3	0.1363	0.2500	0.2769	0.3026	0.3288	0.3551	0.3819	0.4096
		win. 4	0.1495	0.2313	0.2499	0.2647	0.2727	0.2843	0.2938	0.2821
	bad	win. 1	0.1465	0.5196	0.6218	0.7261	0.8323	0.9353	1.0397	1.1463
		win. 2	0.1571	0.5611	0.6723	0.7855	0.9012	1.0143	1.1240	1.2415
		win. 3	0.1543	0.5620	0.6732	0.7893	0.9047	1.0182	1.1317	1.2468
		win. 4	0.1596	0.6614	0.7777	0.8866	0.9827	1.0673	1.1351	1.1212
solid brick	good	win. 1	0.1545	0.2993	0.3302	0.3596	0.3881	0.4201	0.4493	0.4794
		win. 2	0.1624	0.2670	0.2897	0.3109	0.3311	0.3526	0.3730	0.3945
	bad	win. 1	0.1574	0.6977	0.8427	0.9876	1.1313	1.2759	1.4181	1.5652
		win. 2	0.1641	0.7353	0.8861	1.0386	1.1916	1.3395	1.4919	1.6425

Table 9 – Summary of s values for the ‘cube house’ building type with the aerated fired clay brick masonry

C.2.3 Ca. 1960' type plan of urban apartment buildings built with prefabricated wall blocks

C.2.3.1 Good details

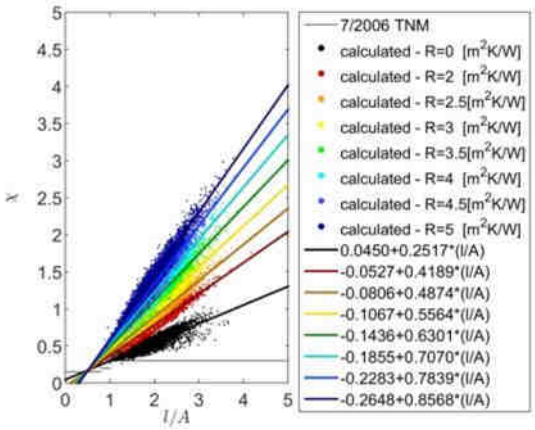

Fig. 313. – external insulation, good details, window 1

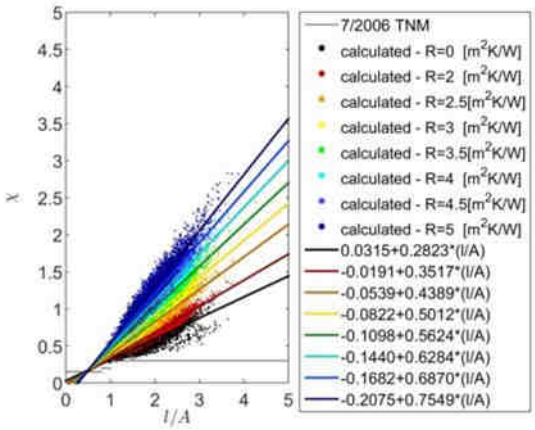

Fig. 314. – external insulation, good details, window 2

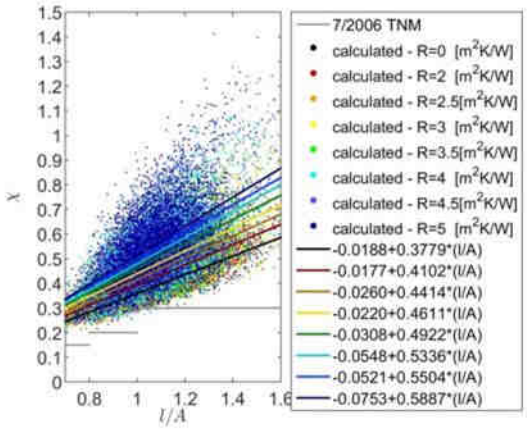

Fig. 315. – external insulation, good details, no windows

C.2.3.2 Bad details

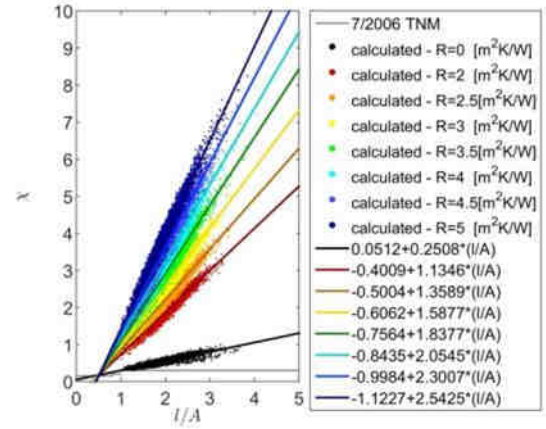

Fig. 316. – external insulation, bad details, window 1

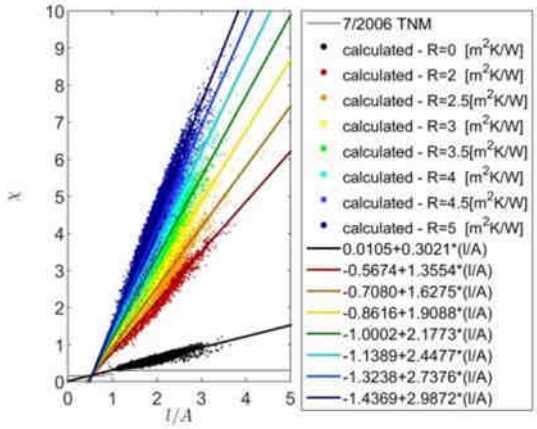

Fig. 317. – external insulation, bad details, window 2

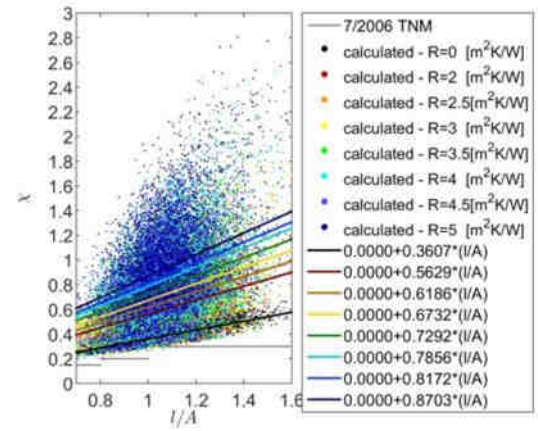

Fig. 318. – external insulation, bad details, no windows

C.2.3.3 Summary of data

details	window	s [m]							
		R_{ins}=0	**R_{ins}=2**	**R_{ins}=2.5**	**R_{ins}=3**	**R_{ins}=3.5**	**R_{ins}=4**	**R_{ins}=4.5**	**R_{ins}=5**
good	win. 1	s=0.2517 a=0.0450	s=0.4189 a= -0.053	s=0.4874 a=-0.081	s=0.5564 a=-0.107	s=0.6301 a=-0.144	s=0.7070 a=-0.186	s=0.7839 a=-0.228	s=0.8568 a=-0.264
	win. 2	s=0.2823 a=0.032	s=0.3517 a=-0.019	s=0.4389 a=-0.054	s=0.5012 a=-0.082	s=0.5624 a=-0.110	s=0.6284 a=-0.144	s=0.6870 a=-0.168	s=0.7549 a=-0.208
bad	win. 1	s=0.2508 a=0.0512	s=1.1346 a=-0.401	s=1.3589 a=-0.500	s=1.5877 a=-0.606	s=1.8377 a=-0.757	s=2.0545 a=-0.844	s=2.3007 a=-0.998	s=2.5425 a=-1.123
	win. 2	s=0.3021 a=0.0105	s=1.3554 a=-0.567	s=1.6275 a=-0.708	s=1.9088 a=-0.862	s=2.1773 a=-1.000	s=2.4477 a=-1.139	s=2.7376 a=-1.324	s=2.9872 a=-1.437

Table 10 – Summary of a and s values for the 'block house' building type

C.3 The Improved thermal bridge calculation method

C.3.1 19th century urban residential building

C.3.1.1 Percentage errors

C.3.1.1.1 No insulation

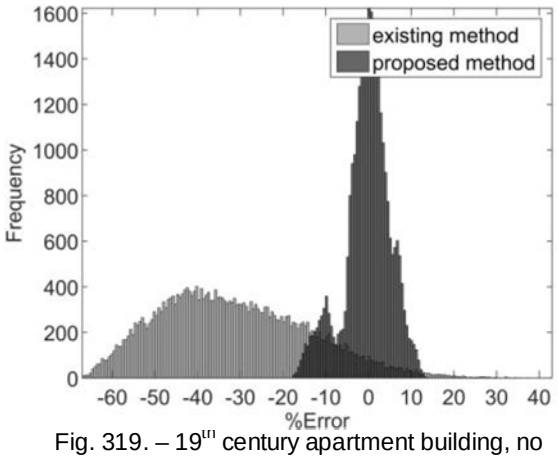

Fig. 319. – 19th century apartment building, no insulation, window 1, %Error in χ for the existing an proposed calculation method

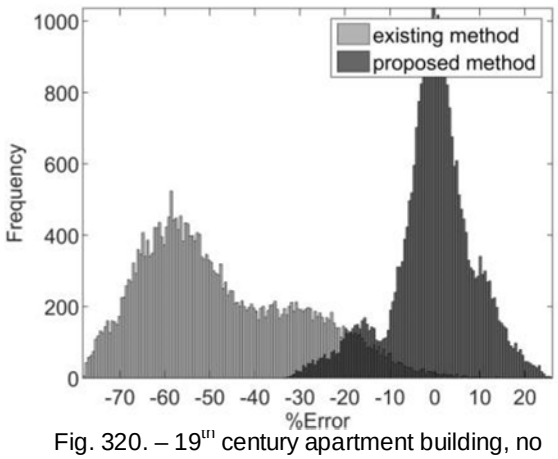

Fig. 320. – 19th century apartment building, no insulation, window 1b, %Error in χ for the existing an proposed calculation method

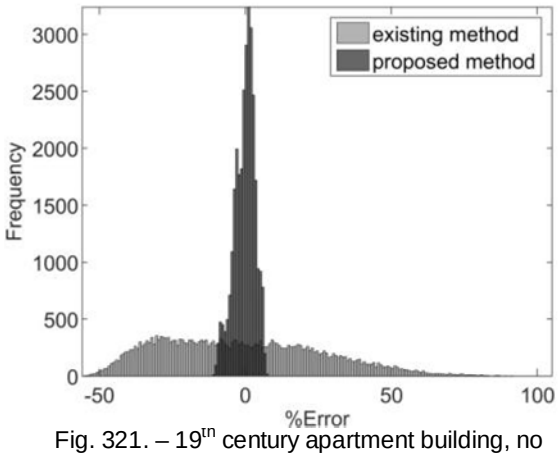

Fig. 321. – 19th century apartment building, no insulation, window 2, %Error in χ for the existing an proposed calculation method

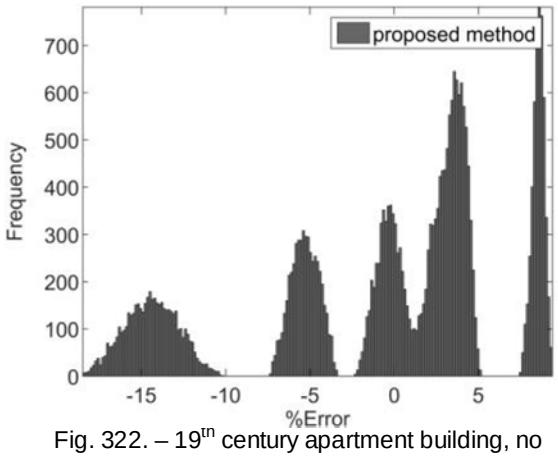

Fig. 322. – 19th century apartment building, no insulation, no windows, %Error in χ for the existing an proposed calculation method

C.3.1.1.2 Internal insulation – good details

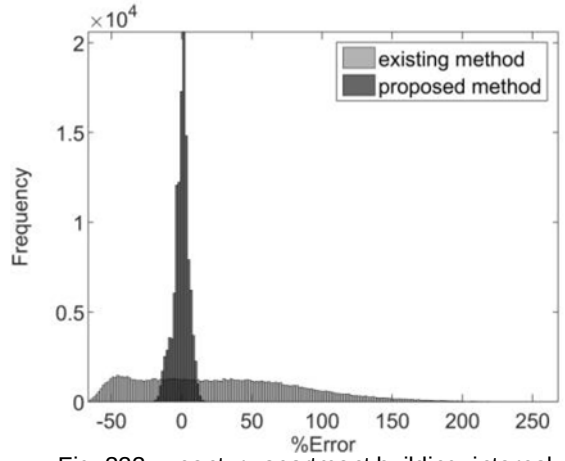

Fig. 323. – century apartment building, internal insulation, good details, window 1, %Error in χ for the existing an proposed calculation method

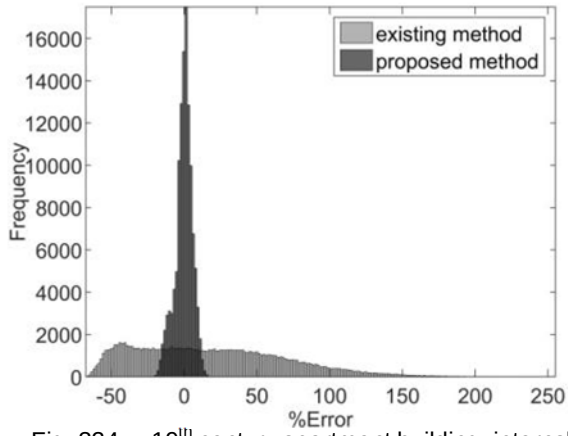

Fig. 324. – 19th century apartment building, internal insulation, good details, window 1b, %Error in χ for the existing an proposed calculation method

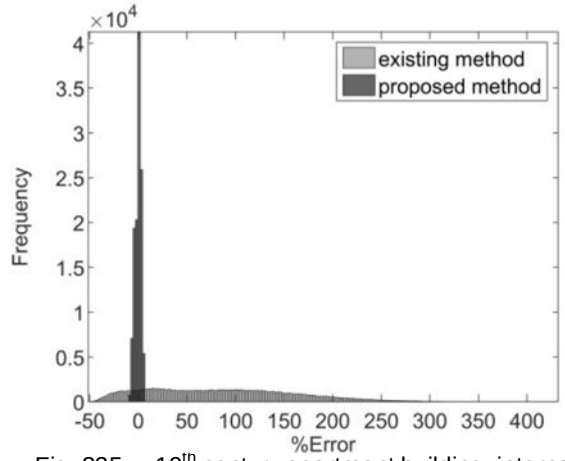

Fig. 325. – 19th century apartment building, internal insulation, good details, window 2, %Error in χ for the existing an proposed calculation method

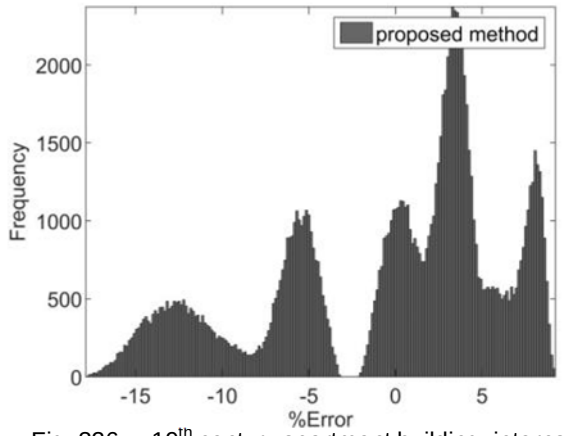

Fig. 326. – 19th century apartment building, internal insulation, good details, no windows, %Error in χ for the existing an proposed calculation method

C.3.1.1.3 Internal insulation – bad details

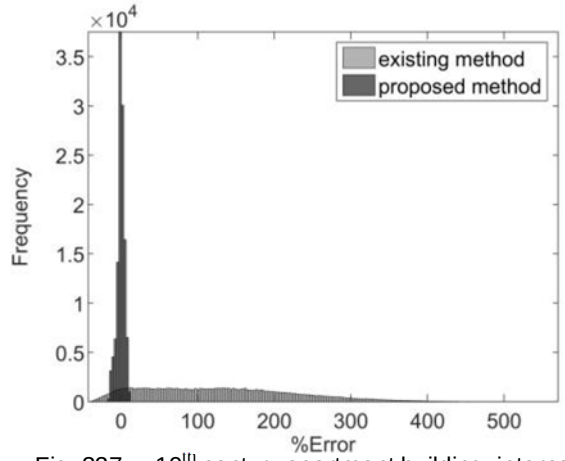

Fig. 327. – 19th century apartment building, internal insulation, bad details, window 1, %Error in χ for the existing an proposed calculation method

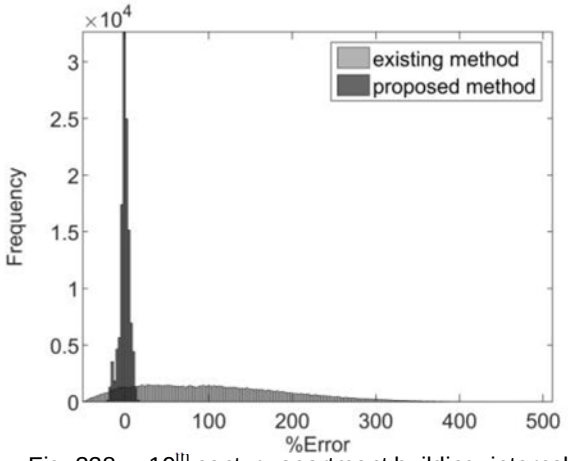

Fig. 328. – 19th century apartment building, internal insulation, bad details, window 1b, %Error in χ for the existing an proposed calculation method

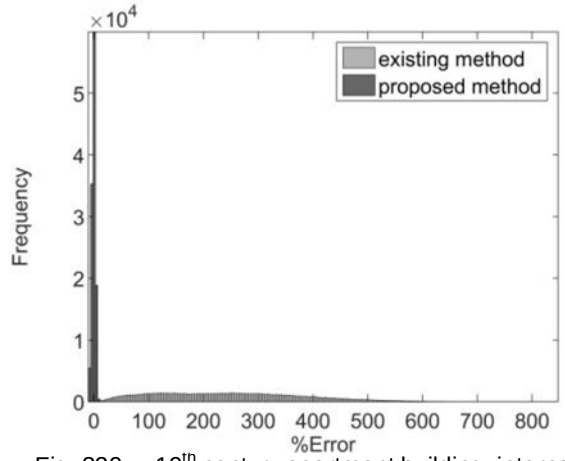

Fig. 329. – 19th century apartment building, internal insulation, bad details, window 2, %Error in χ for the existing an proposed calculation method

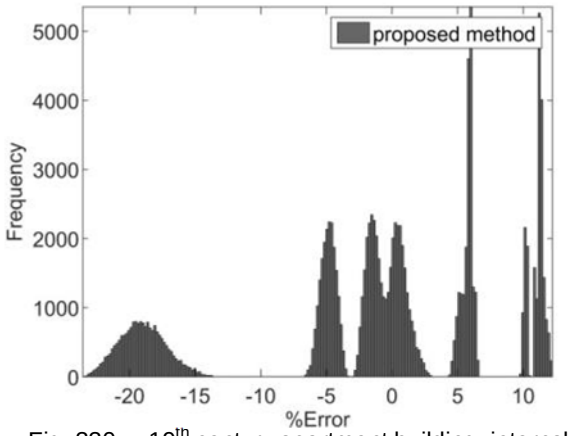

Fig. 330. – 19th century apartment building, internal insulation, bad details, no windows, %Error in χ for the existing an proposed calculation method

C.3.1.1.4 External insulation – external (street) façade

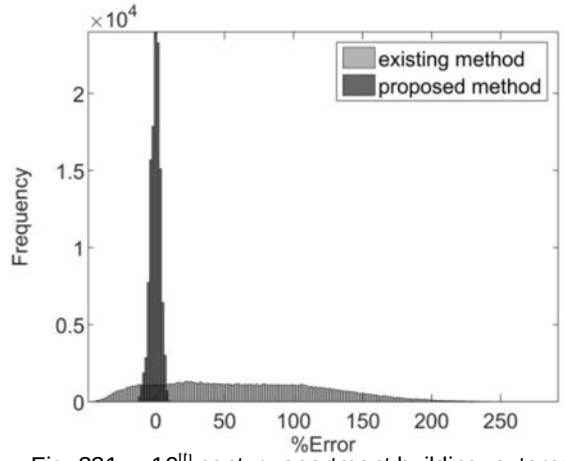

Fig. 331. – 19th century apartment building, external insulation, external (street) facade, window 1, %Error in χ for the existing an proposed calculation method

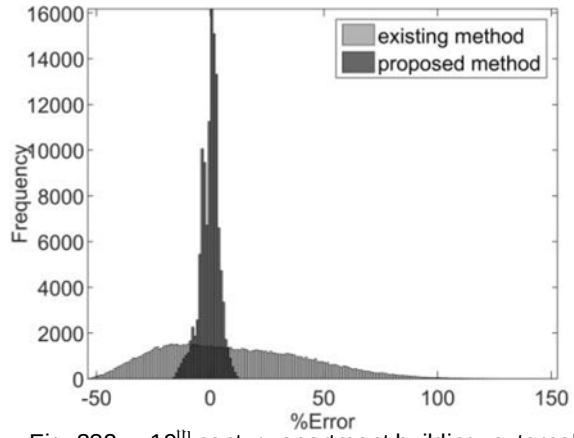

Fig. 332. – 19th century apartment building, external insulation, external (street) facade, window 1b, %Error in χ for the existing an proposed calculation method

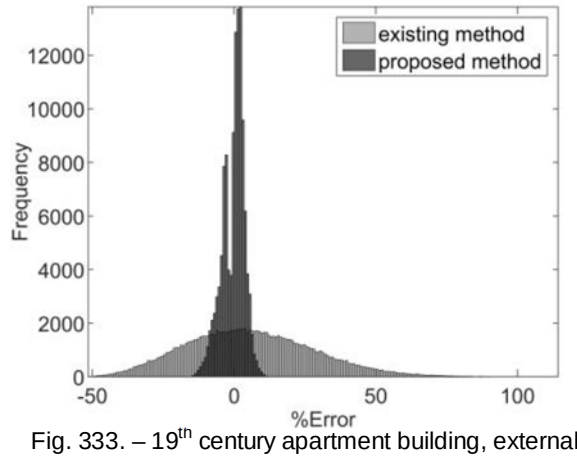

Fig. 333. – 19th century apartment building, external insulation, external (street) facade, window 2, %Error in χ for the existing an proposed calculation method

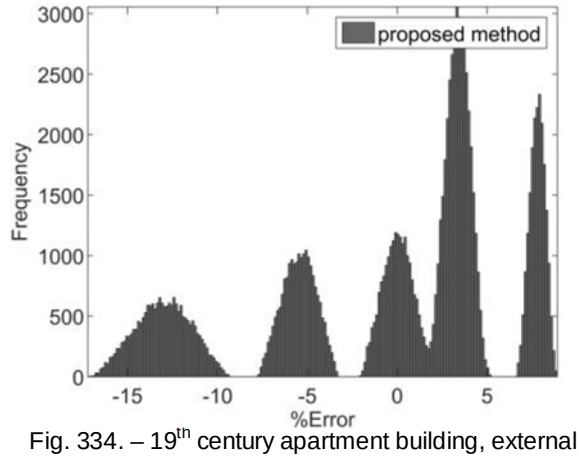

Fig. 334. – 19th century apartment building, external insulation, external (street) facade, no windows, %Error in χ for the existing an proposed calculation method

C.3.1.1.5 *External insulation – internal (courtyard) façade*

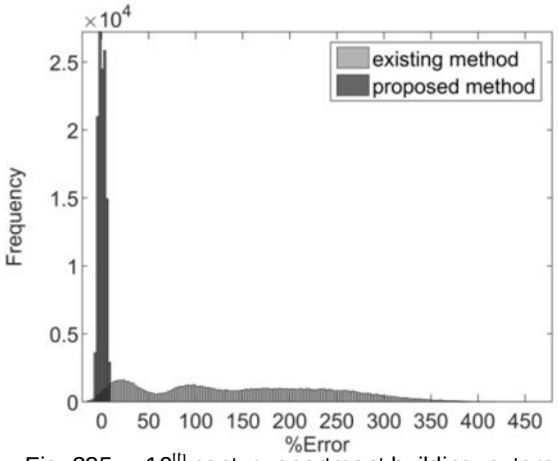

Fig. 335. – 19th century apartment building, external insulation, internal (courtyard) facade, window 1, %Error in χ for the existing an proposed calculation method

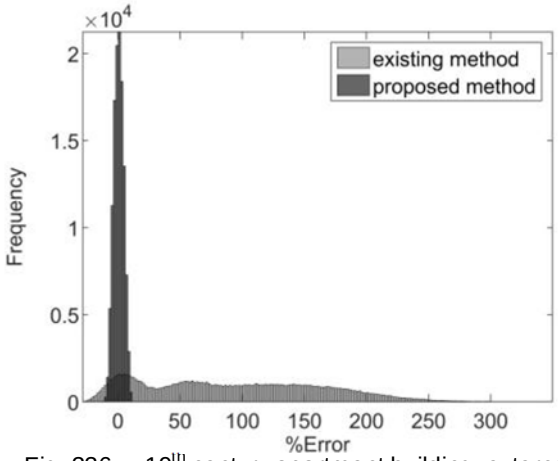

Fig. 336. – 19th century apartment building, external insulation, internal (courtyard) facade, window 1b, %Error in χ for the existing an proposed calculation method

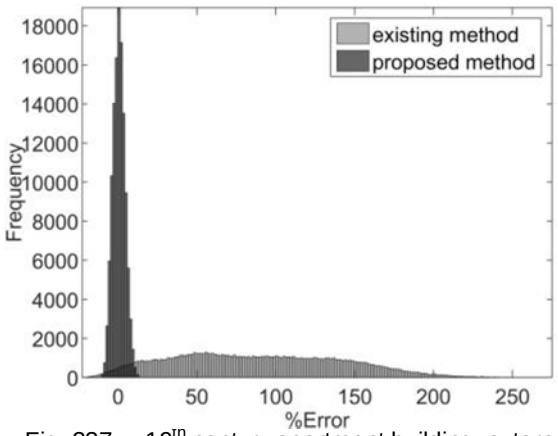

Fig. 337. – 19th century apartment building, external insulation, internal (courtyard) facade, window 2, %Error in χ for the existing an proposed calculation method

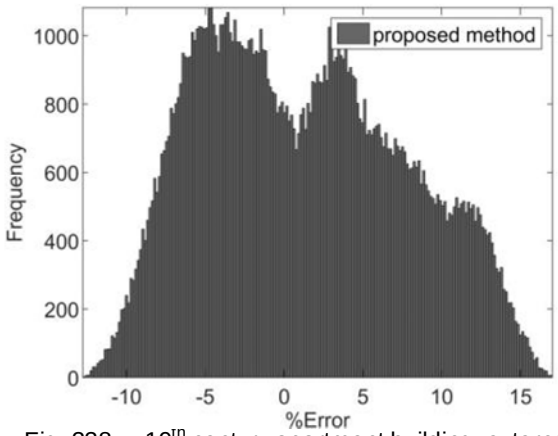

Fig. 338. – 19th century apartment building, external insulation, internal (courtyard) facade, no windows, %Error in χ for the existing an proposed calculation method

C.3.1.2 Thermal bridge corrected U values of the wall

C.3.1.2.1 Internal insulation

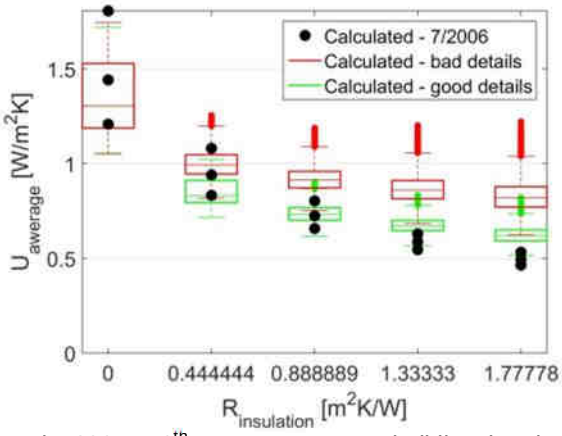

Fig. 339. – 19th century apartment building, interior insulation, window 1

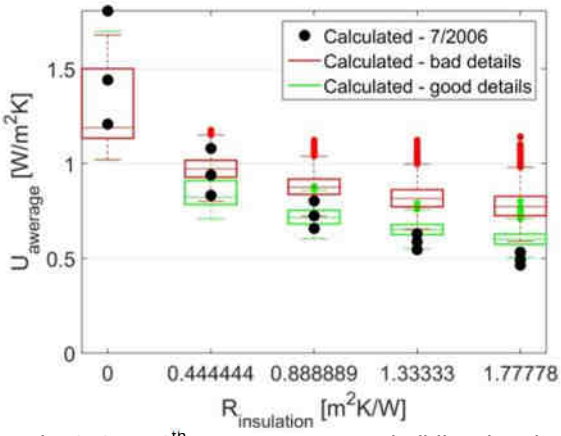

Fig. 340. – 19th century apartment building, interior insulation, window 1b

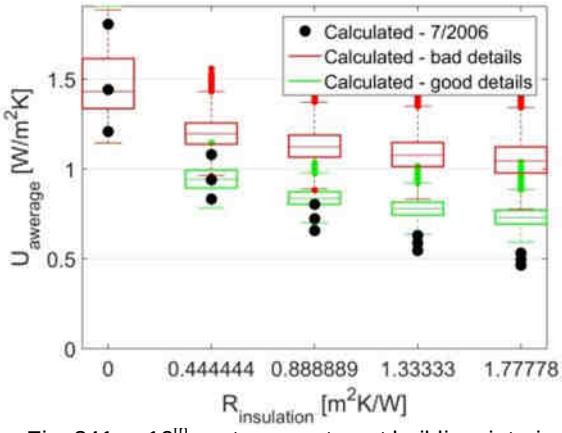

Fig. 341. – 19th century apartment building, interior insulation, window 2

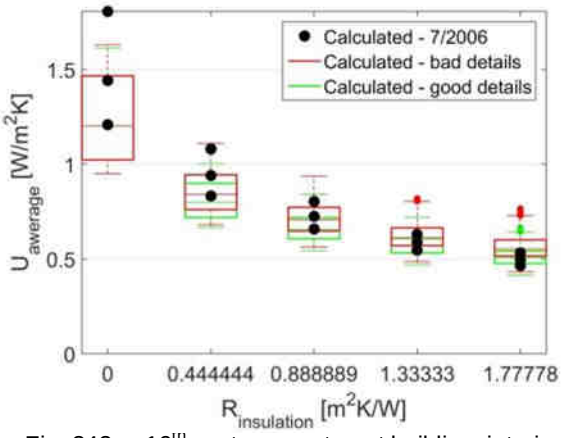

Fig. 342. – 19th century apartment building, interior insulation, no window

C.3.1.2.2 External insulation

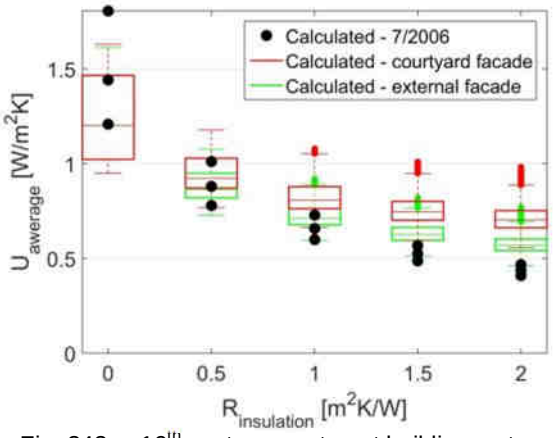

Fig. 343. – 19th century apartment building, external insulation, window 1

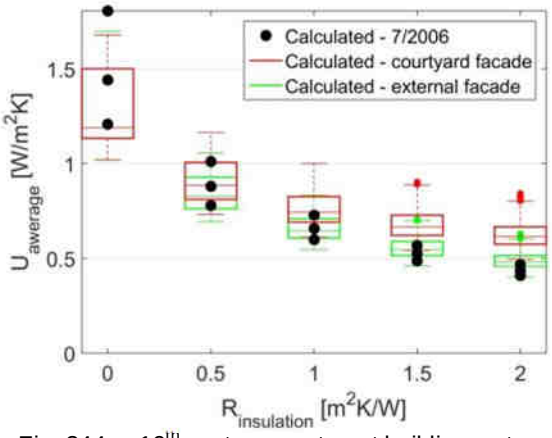

Fig. 344. – 19th century apartment building, external insulation, window 1b

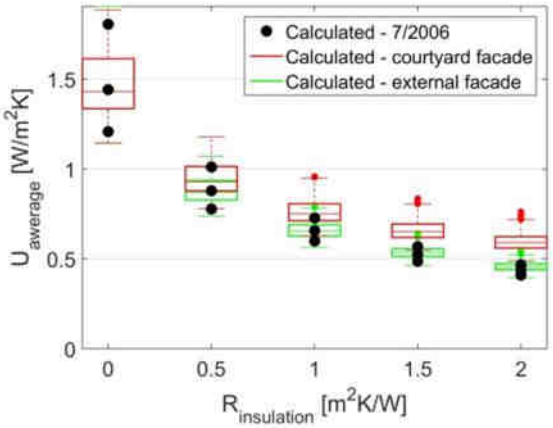

Fig. 345. – 19th century apartment building, external insulation, window 2

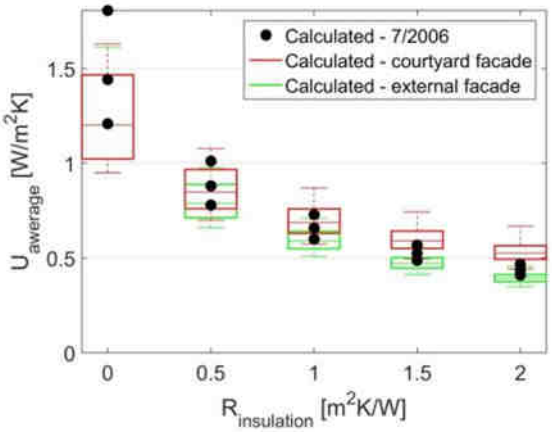

Fig. 346. – 19th century apartment building, external insulation, no windows

C.3.2 Small suburban or rural detached houses based on typical Central-European type plans

C.3.2.1 Percentage errors

C.3.2.1.1 Aerated clay brick masonry – no insulation

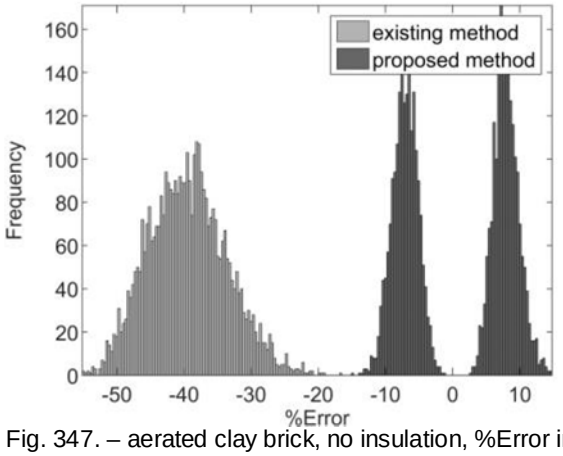

Fig. 347. – aerated clay brick, no insulation, %Error in χ for the existing an proposed calculation method

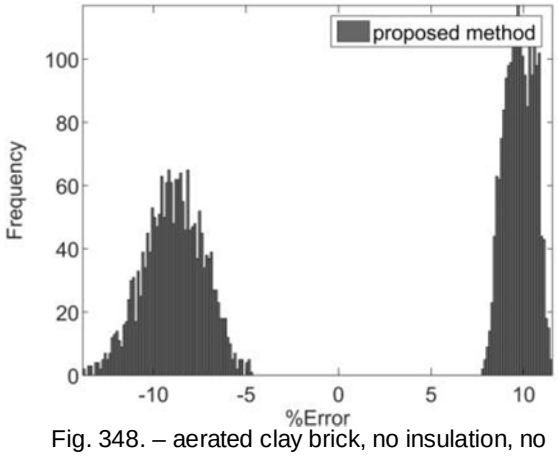

Fig. 348. – aerated clay brick, no insulation, no windows, %Error in χ for the proposed calculation method

C.3.2.1.2 Aerated clay brick masonry – external insulation, good details

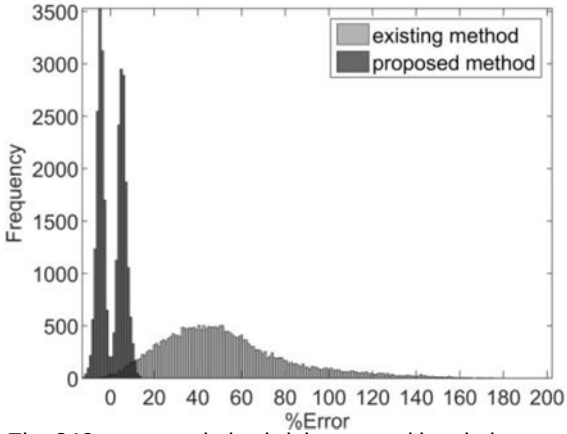

Fig. 349. – aerated clay brick, external insulation, good details, %Error in χ for the existing an proposed calculation method

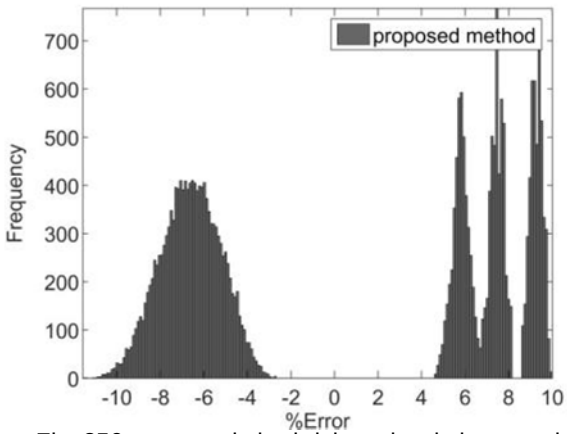

Fig. 350. – aerated clay brick, no insulation, good details, no windows, %Error in χ for the proposed calculation method

C.3.2.1.3 Aerated clay brick masonry – external insulation, bad details

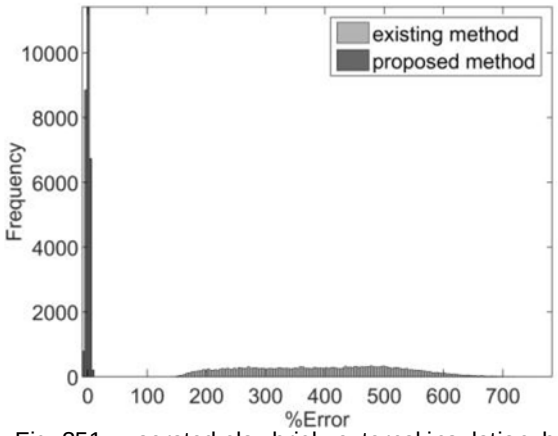

Fig. 351. – aerated clay brick, external insulation, bad details, %Error in χ for the existing an proposed calculation method

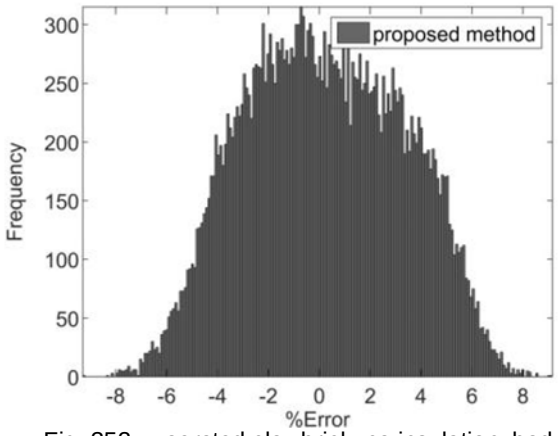

Fig. 352. – aerated clay brick, no insulation, bad details, no windows, %Error in χ for the proposed calculation method

C.3.2.1.4 Solid brick masonry – no insulation

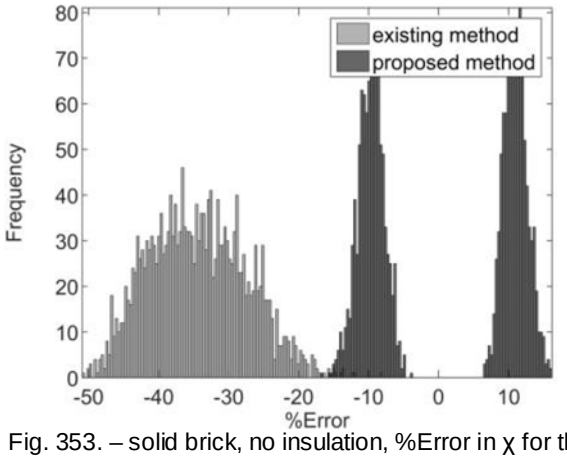

Fig. 353. – solid brick, no insulation, %Error in χ for the existing an proposed calculation method

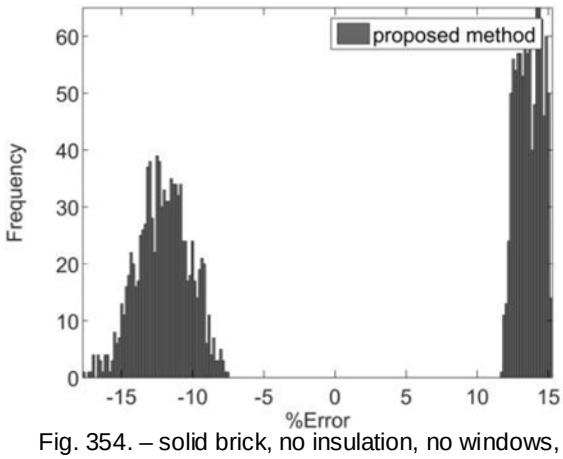

Fig. 354. – solid brick, no insulation, no windows, %Error in χ for the proposed calculation method

C.3.2.1.5 Solid brick masonry – external insulation, good details

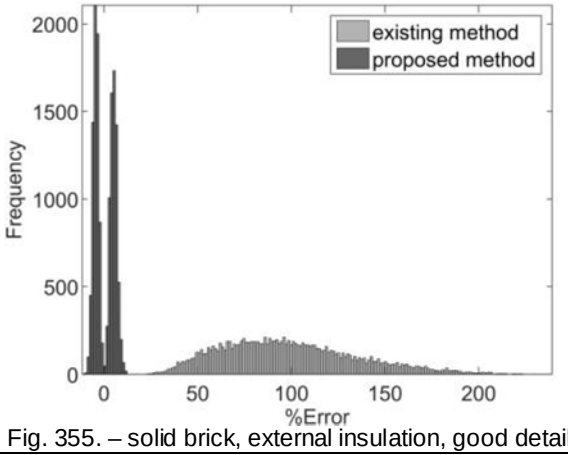

Fig. 355. – solid brick, external insulation, good details,

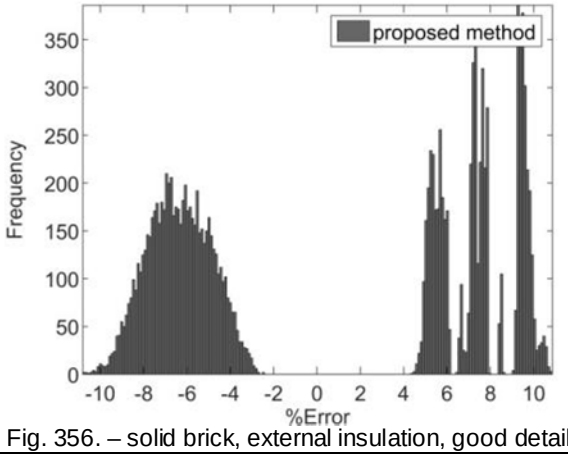

Fig. 356. – solid brick, external insulation, good details,

%Error in χ for the existing an proposed calculation method	no windows, %Error in χ for the proposed calculation method

C.3.2.1.6 Solid brick masonry – external insulation, bad details

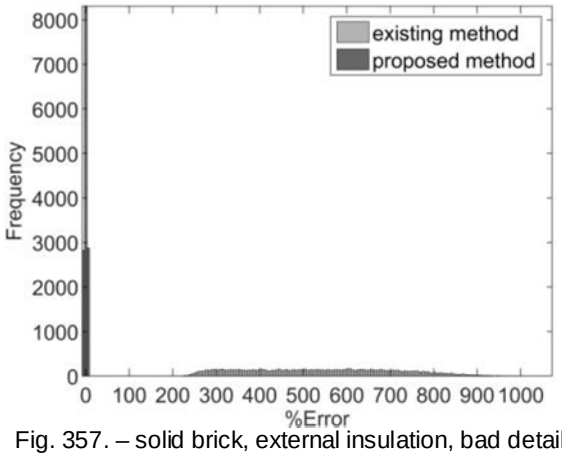

Fig. 357. – solid brick, external insulation, bad details, %Error in χ for the existing an proposed calculation method

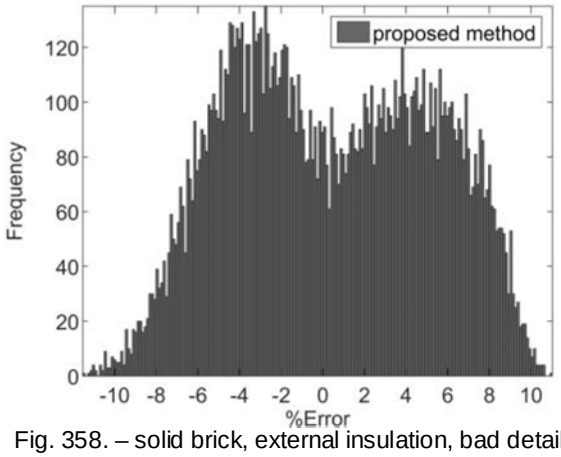

Fig. 358. – solid brick, external insulation, bad details, no windows, %Error in χ for the proposed calculation method

C.3.2.2 Thermal bridge corrected U values of the wall

C.3.2.2.1 Aerated clay brick masonry – External insulation

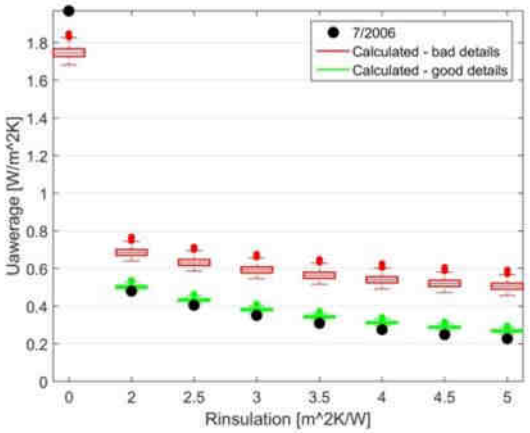

Fig. 359. – aerated clay brick, external insulation, window 1

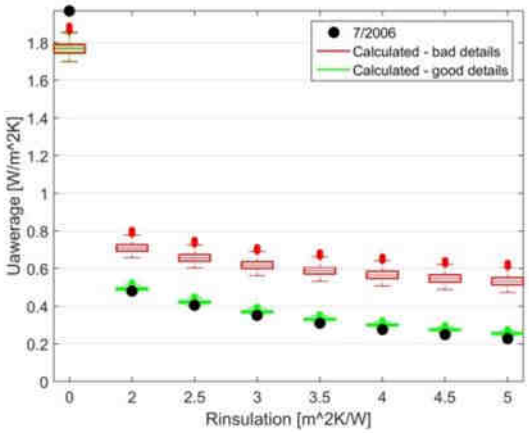

Fig. 360. – aerated clay brick, external insulation, window 2

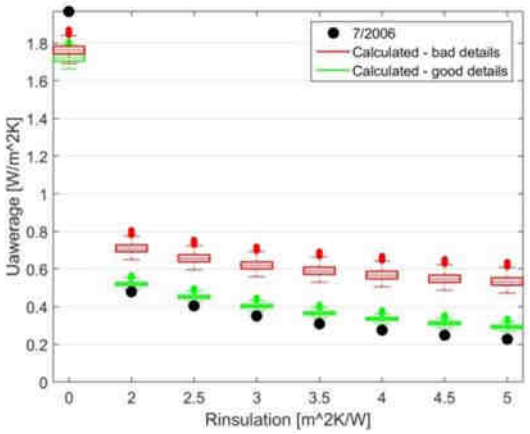

Fig. 361. – aerated clay brick, external insulation, window 3

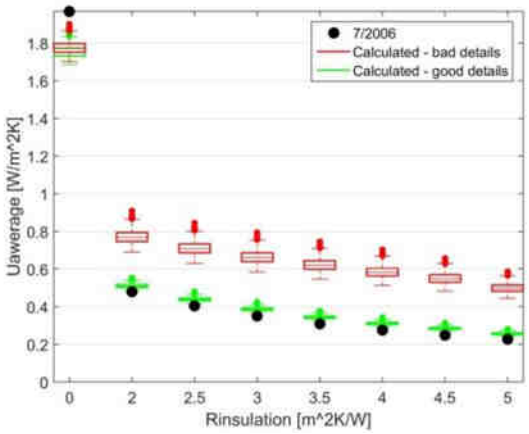

Fig. 362. – aerated clay brick, external insulation, window 4

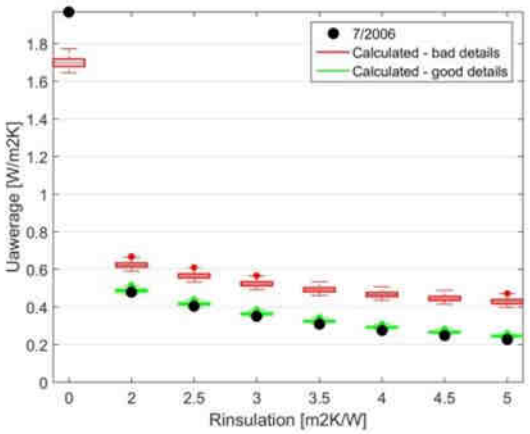

Fig. 363. – aerated clay brick, external insulation, no windows

C.3.2.2.2 Solid clay brick masonry – External insulation

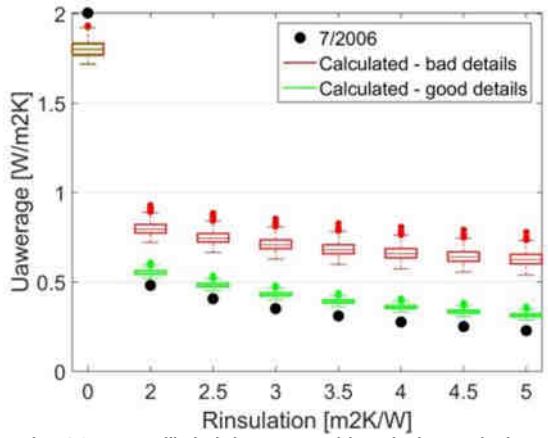

Fig. 364. – solib brick, external insulation, window 1

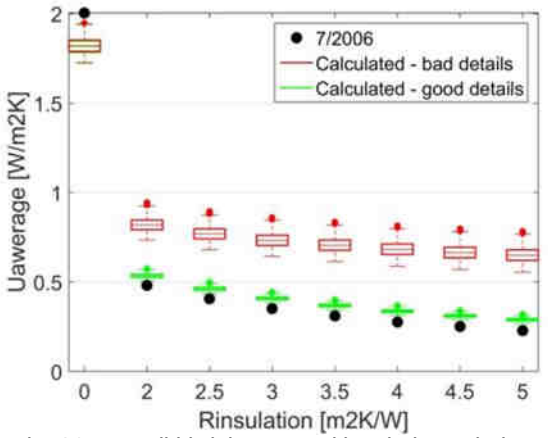

Fig. 365. – solid brick, external insulation, window 2

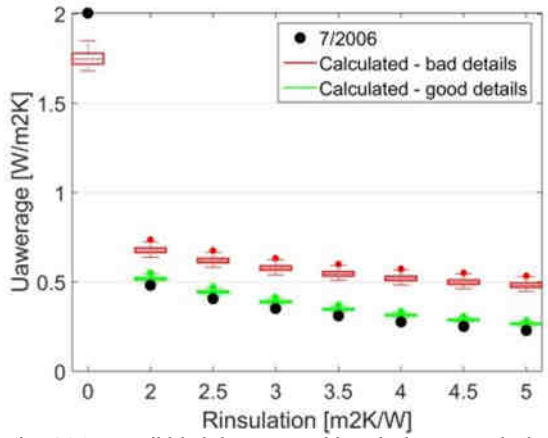

Fig. 366. – solid brick, external insulation, no windows

C.3.3 Ca. 1960' type plan of urban apartment buildings built with prefabricated wall blocks

C.3.3.1 Percentage errors

C.3.3.1.1 No insulation – good details

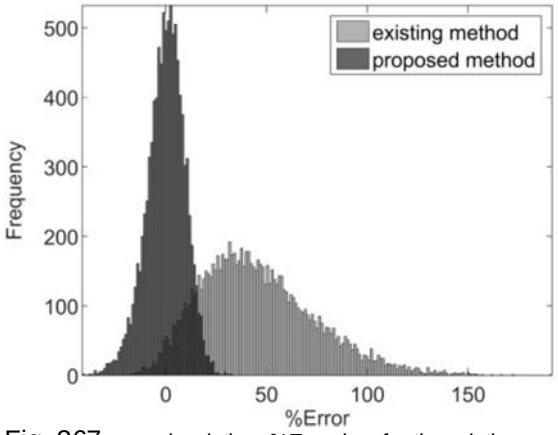

Fig. 367. – no insulation, %Error in χ for the existing an proposed calculation method

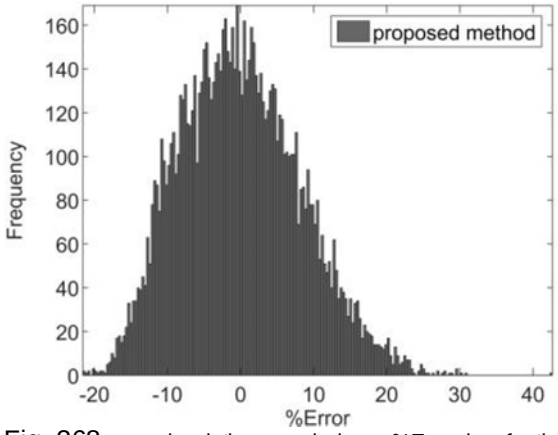

Fig. 368. – no insulation, no windows, %Error in χ for the proposed calculation method

C.3.3.1.2 External insulation – good details

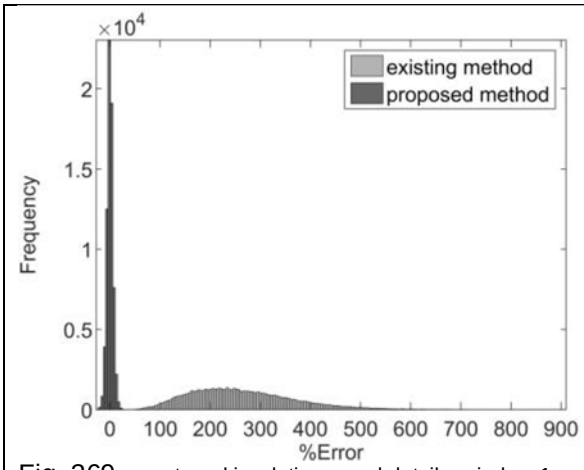

Fig. 369. – external insulation, good details, window 1, %Error in χ for the existing an proposed calculation method

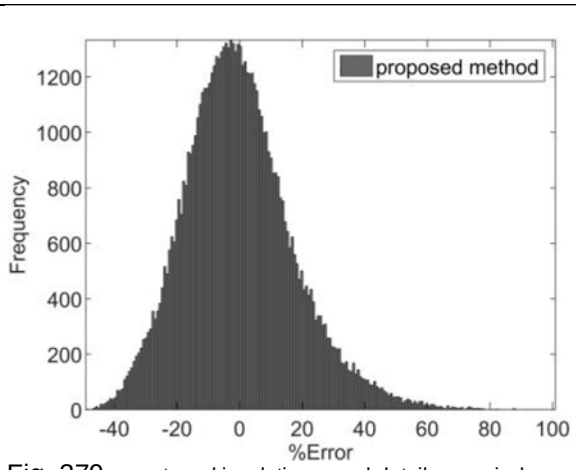

Fig. 370. – external insulation, good details, no windows, %Error in χ for the proposed calculation method

C.3.3.1.3 External insulation – bad details

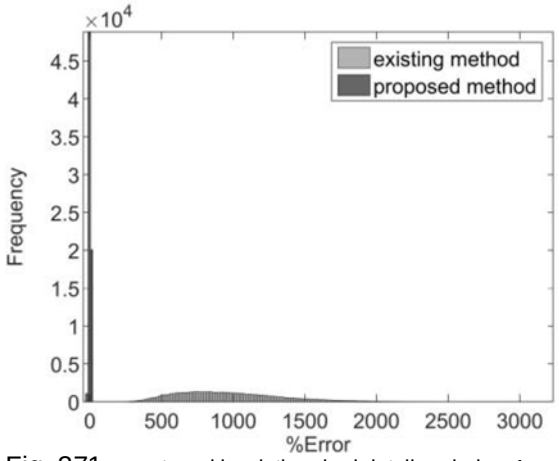

Fig. 371. – external insulation, bad details, window 1, %Error in χ for the existing an proposed calculation method

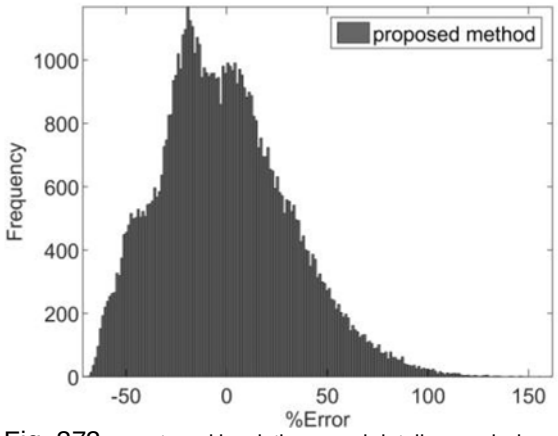

Fig. 372. – external insulation, good details, no windows, %Error in χ for the proposed calculation method

C.3.3.2 Thermal bridge corrected U values of the wall

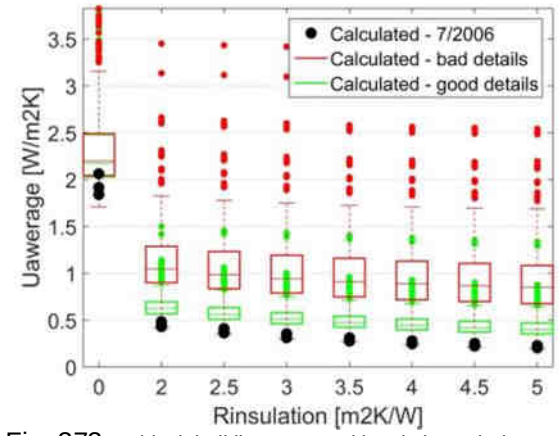

Fig. 373. – block building, external insulation, window 1

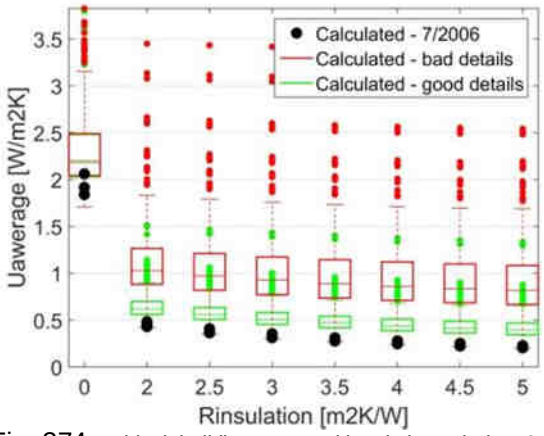

Fig. 374. – block building, external insulation, window 2

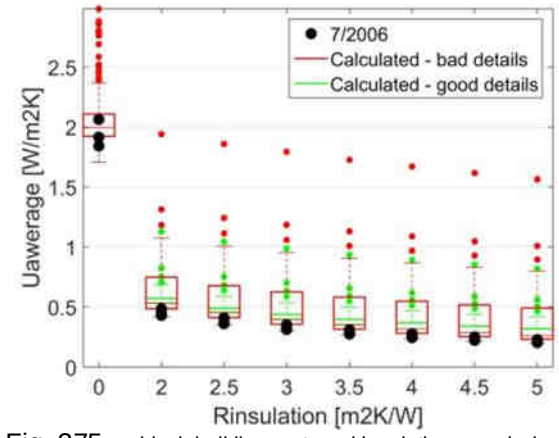

Fig. 375. – block building, external insulation, no windows

D (Appendix D) – EPICAC FVM validation

Validation of EPICAC FVM with the standards EN-ISO 10211 for multidimensional stationary heat conduction and EN 15026 for one-dimensional transient coupled heat and moisture transport

D.1 Introduction

EPICAC FVM is program for the solution of the coupled partial differential equations describing the stationary or transient heat, air and moisture transfer in opaque constructions in one to three spatial dimensions based on the finite volume method. The program's models are based on the work of Künzel [3] as well as my own additions.

Validation is presented for the multidimensional stationary heat transport and the one-dimensional transient coupled heat and moisture transport capabilities of EPICAC FVM based on the relevant sections of the standards EN ISO 10211 [1] and EN ISO 15026 [2] respectively.

D.2 Validation of the multi-dimensional stationary heat conduction calculations based on EN-ISO 10211

The standard EN-ISO 10211 [1] is the harmonized European and international standard describing, among other things, the requirements for computer programs aimed at calculating the thermal transmission and surface temperatures of thermal bridges in building constructions. Annex A of the standard describes 4 test cases for validating the accuracy of such programs: two for 2-dimensional and two for 3-dimensional geometries. All commercial or free but widely used thermal bridge simulation tools must pass these tests in order to be described as a "two-" or "tree-dimensional high precision method" according to the standard.

D.2.1 Case 1

Case 1 presents a simple analytical solution for the stationary heat conduction equation (Fourier-equation) in 2-dimensions. The geometry is a square column (or any infinitely long solid body with a square cross section). The boundary conditions are of the Dirichlet or first-type: the value of the temperature is set at the boundaries (i.e. surface temperatures). The analytically derived solution for the temperatures are specified at 28 points of an equidistant rectangular grid. Due to the nature of the problem the solution does not depend of the thermal conductivity of the material the column is made out of or its size. In order for the program to pass the test the calculated temperatures at the specified points must not differ from the standard's values more than 0.1 [°C]. The whole input definition of the standard is showed in Fig. 376.

Since the geometry and the boundary conditions are symmetric it is possible to simulate either the whole square or just one half and setting the symmetry axis as an adiabatic boundary. The latter option was chosen. EPICAC FVM, being based on the finite volume method, calculates the temperatures for the centroid of the individual cells that make out the computational mesh. Therefore one must take care that the mesh is defined in such a way that some elements (i.e. their centers') are placed exactly under the specified check points of the standard. The mesh used for the calculation is presented in Fig. 377 and used 25878 nodes. The boundary conditions are defined as Neumann type boundaries but with infinitesimally small surface heat transfer resistances that achieve the same result as a Dirichlet type. The problem was solved as steady-state with a matrix solver (i.e. not iteratively) to eliminate errors in the solution of the linear algebraic system (discretization errors still remain). The calculation took 1.444 [s] on an Intel Core i5 laptop.

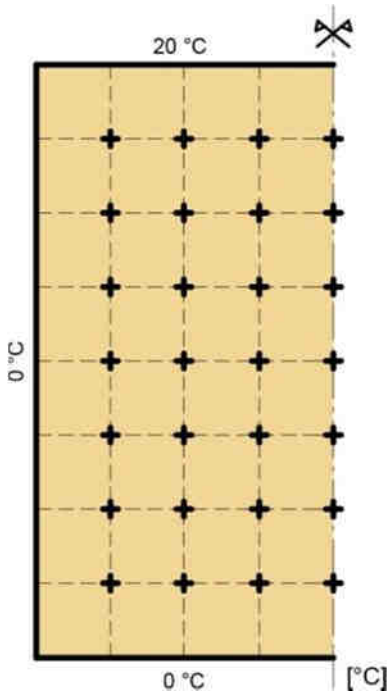

Fig. 376. – the geometry, boundary conditions and the grid of test points defined for case 1

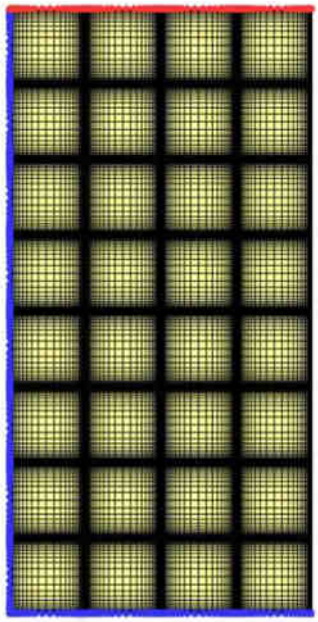

Fig. 377. – the numerical mesh generated for case 1 in EPICAC FVM

The temperature field calculated with EPICAC BE is shown in Fig. 379 and the temperatures at the specified test points are compared to the standard's values in Fig. 378.

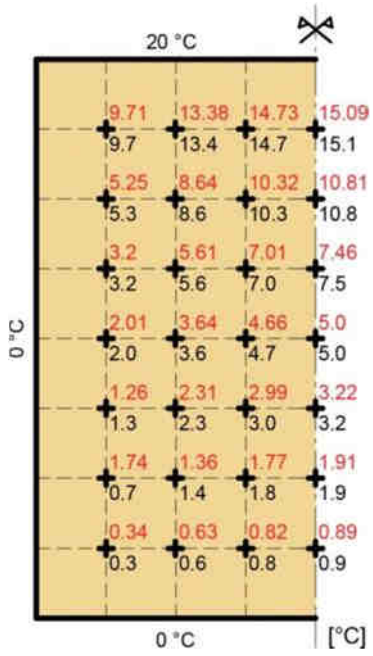

Fig. 378. – the temperatures calculated by EPICAC FVM (red) and the ones given in the standard (black)

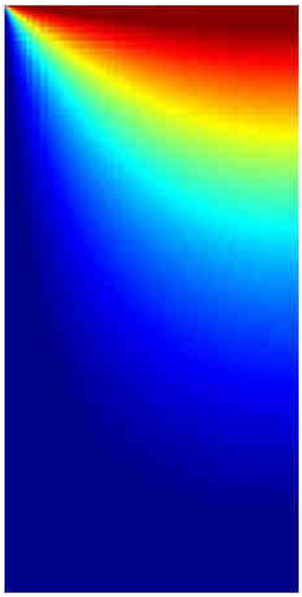

Fig. 379. – the calculated temperature field

The temperatures calculated with EPICA FVM deviate 0.05 [°C] or less from the analytical solution. This falls within the 0.1 [°C] limit set by the standard therefore the test is considered to be fulfilled.

D.2.2 Case 2

Case 2 presents a more realistic two-dimensional heat conduction problem with a reference numerical solution. The task is the calculation of the temperature field in, and the total heat transmission of, a thin-walled aluminum tray lightweight wall filled with thermal insulation and clad with a concrete-like board with a wooden thermal brake. The thermal conductivity of the individual materials, as shown in Fig. 380, differ greatly from one-another. The boundary conditions, shown in Fig. 381, are also more realistic than in the previous case:

- an external boundary with a third or Robin-type BC of θ = 0 [°C] air temperature and a R_s = 0.06 [m^2K/W] heat transfer resistance
- a similar internal BC with θ = 20 [°C] temperature and a R_s = 0.10 [m^2K/W] resistance
- adiabatic (or symmetry) boundary conditions on either end of the wall section.

The test requires the calculation of the temperature at specific points in the wall with a precision of 0.1 [°C] or less and a maximum error in the calculated total heat transmission of 0.1 [W] or less.

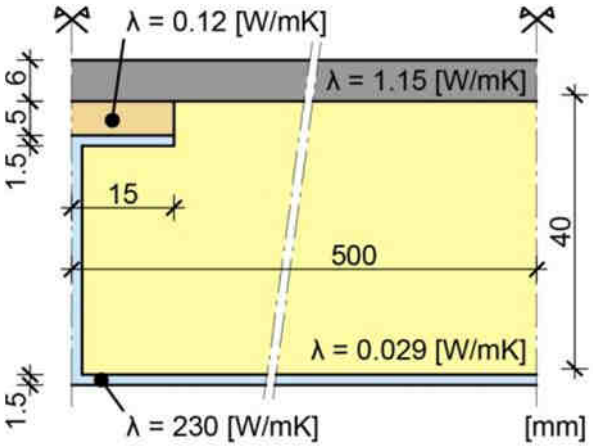

Fig. 380. – the geometry and material properties of case 2

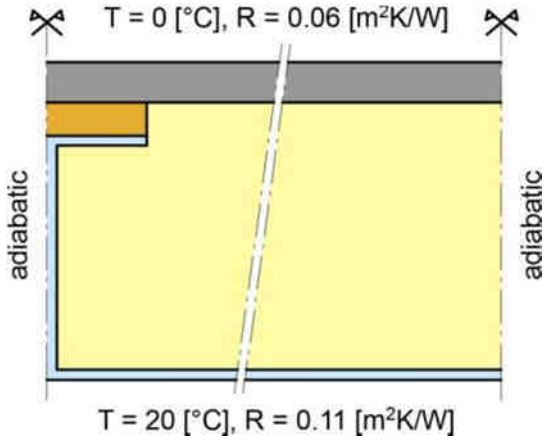

Fig. 381. – the boundary condition for case 2

The problem was meshed in EPICAC BE with a total number of 49910 nodes and was solved as steady-state with a matrix solver (i.e. not iteratively) to eliminate errors in the solution of the linear algebraic system (discretization errors still remain). The calculation took 1.521 [s] on an Intel Core i5 laptop. The temperature field calculated with EPICAC BE is shown in Fig. 383 and the temperatures at the specified test points are compared to the standard's values in Fig. 382.

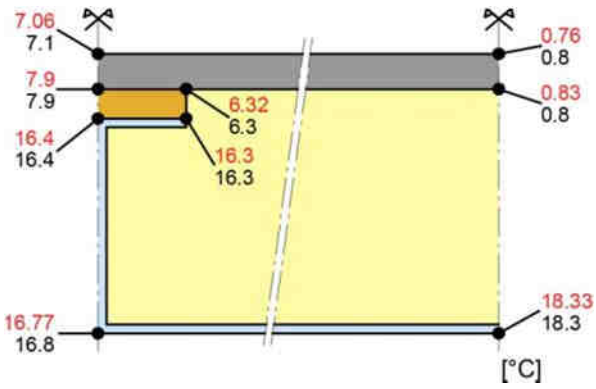

Fig. 382. – the temperatures calculated by EPICAC FVM (red) and the ones given in the standard (black)

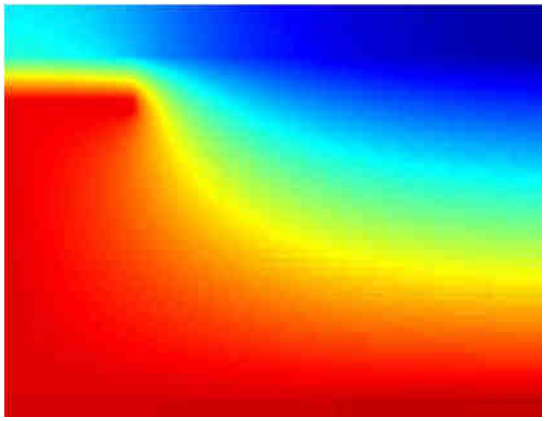

Fig. 383. – part of the calculated temperature field

The temperatures calculated with EPICA FVM deviate 0.04 [°C] or less from the analytical solution. This falls within the 0.1 [°C] limit set by the standard. The total heat transmission of the detail is calculated as 9.492 [W/m] compared to the 9.5 [W/m] specified in the standard which also meets the requirements. The test is therefore fulfilled.

D.2.3 Case 3

Case 3 presents a more or less realistic, although outdated, 3-dimensional building construction detail: the corner of a building with a brick cladded cavity-wall (a sandwich construction without an air gap) around a concrete slab with a cantilever balcony without any thermal brake or external insulation. The dimensions and thermal conductivities are representative of the kind of construction specified. The case defines three distinct boundary conditions, all of them of the third or Robin-type:

- BC 1: the external boundary with $\theta_1 = 0$ [°C] and a surface heat transfer resistance of $R_{s1} = 0.05$ [m^2K/W]
- BC 2: the internal boundary on the top floor with $\theta_2 = 15$ [°C] and $R_{s2} = 0.20$ [m^2K/W]
- BC 3: the internal boundary on the bottom floor with $\theta_3 = 20$ [°C] and $R_{s3} = 0.20$ [m^2K/W]
- all surfaces not assigned with one of them are considered adiabatic

The specified heat transfer resistances do not depend on the direction of the heat flow. The input geometry is summed up in Fig. 384 and the boundary conditions and material properties in Fig. 385 and Fig. 386. The test requires the calculation of the minimum surface temperatures for the two internal boundaries with a maximum error of 0.1 [°C] and the calculation of the thermal coupling coefficients between the individual environments (or boundaries, altogether 3 independent values) with a maximum error of 0.1 [W].

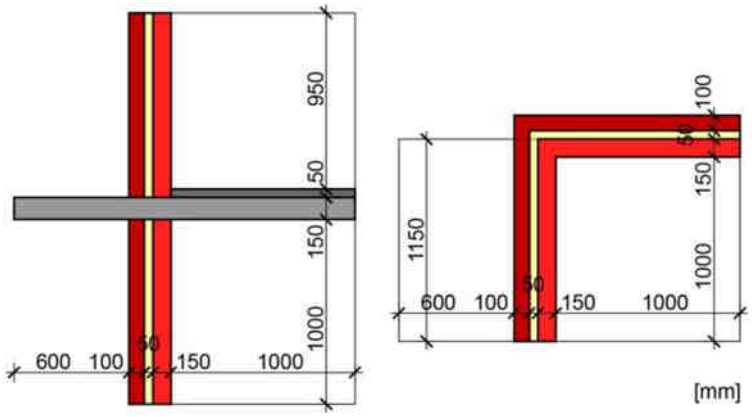

Fig. 384. – the geometry of case 3

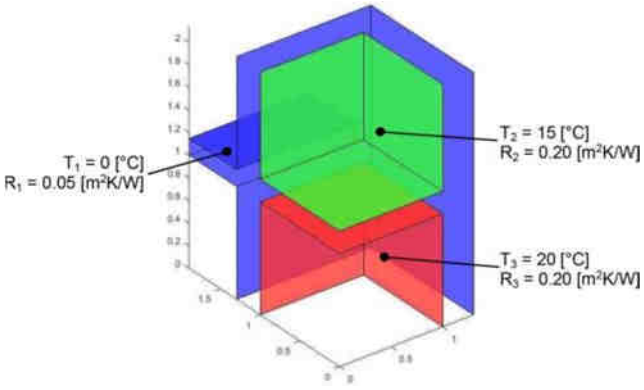

Fig. 385. – the boundary condition definitions of case 3

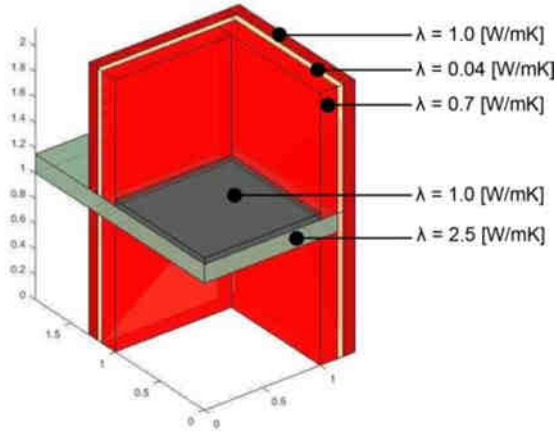

Fig. 386. – the material property definitions of case 3

The detail was meshed in EPICAC BE with a total number of 1508800 nodes and was solved with a steady-state explicit iterative scheme. Because the size of the matrix to be solved is proportional to the third power of the node number a direct matrix solution would very quickly run out of memory and most likely crash MATLAB unless some special solution technique is implemented. For very large matrices the iterative explicit solution technique is usually much faster. The convergence criteria for the iteration was the maximum temperature difference between the last two iterations for all cells with a threshold value of 1e-6 [K]. The calculation took 1973 [s] on an Intel Core i5 laptop.

The temperature field calculated with EPICAC BE (for the surface temperature problem) is visualized in Fig. 387 and Fig. 388 with two characteristic 2-D sections. the lowest surface temperatures for both the top and bottom floor interior boundaries are found in the 3-dimensional corner between the external walls and the slab. The isotherms (or iso-surfaces) going through the top and bottom coldest spots in the corner with the lowest temperatures calculated with EPICAC FVM in red and the temperatures found in the standard in black are showed in Fig. 389 and Fig. 390.

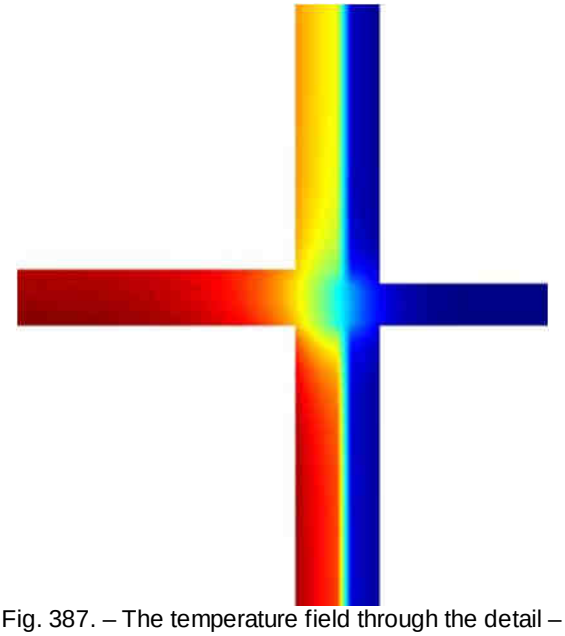

Fig. 387. – The temperature field through the detail – vertical section in the direction of the balcony

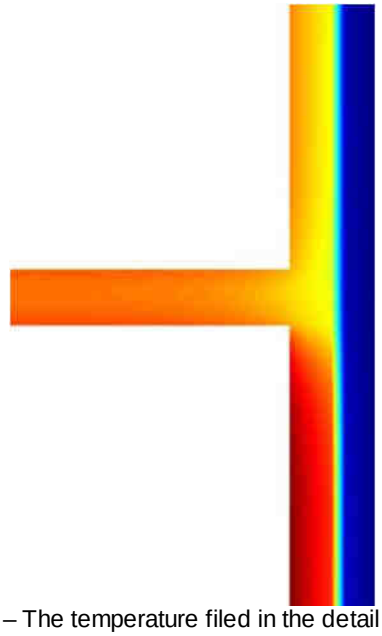

Fig. 388. – The temperature filed in the detail – vertical section perpendicular to the balcony

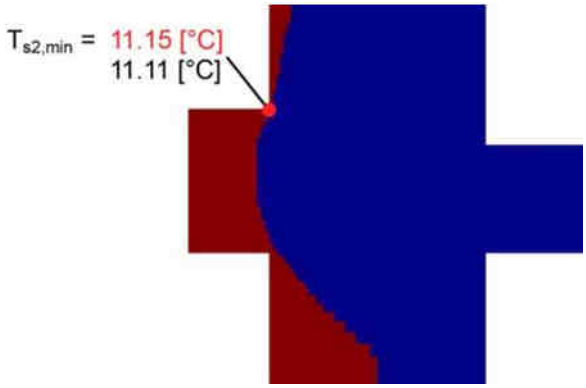

Fig. 389. – the geometry of case 3

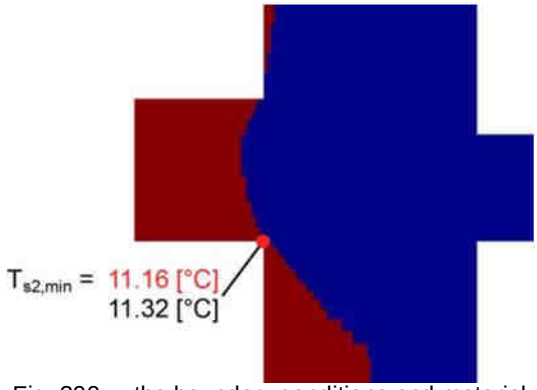

Fig. 390. – the boundary conditions and material properties for case 3

The calculation of the thermal coupling coefficients between any two boundaries in a set of three requires the solution of three heat transfer problems as described in Annex C of the same standard [1]. For each of the three simulations the temperature difference is set as zero between two of the boundaries (e.g. setting their temperatures as 0 [°C]) while setting the third boundary at some other temperature (e.g. 1 or 10 [°C]). The calculated heat transfer rates can be expressed in the following way:

$$\begin{cases} \dot{Q}_{1,0,0} = L_{3D,1-2} \cdot \Delta T_{1-2} + L_{3D,1-3} \cdot \Delta T_{1-3} \\ \dot{Q}_{0,1,0} = L_{3D,1-2} \cdot \Delta T_{1-2} + L_{3D,2-3} \cdot \Delta T_{2-3} \\ \dot{Q}_{0,0,1} = L_{3D,1-3} \cdot \Delta T_{1-3} + L_{3D,2-3} \cdot \Delta T_{2-3} \end{cases} \quad (22)$$

where: $Q_{i,0,0}$ [W] – is the total heat flux between the i[th] boundary and the rest
$L_{3D,i-j}$ [W/K] – is the thermal coupling coefficient between the i[th] and the j[th] boundaries
ΔT_{i-j} [K] – is the temeprature difference between the i[th] and j[th] boundaries

After running the necessary simulations in EPICAC BE and solving the linear system of equations the calculated thermal coupling coefficients (in red) and the reference values given by the standard (in black) are summed up in Table 11.

Environment	L_{3D} - thermal coupling coefficient [W/K]		
	1	2	3
1	-	1.7836/1.781	1.6291/1.624
2	1.7836/1.781	-	2.0957/2.094
3	1.6291/1.624	2.0957/2.094	-

Table 11 – the calculated (red) and the standard's (black) thermal coupling coefficients between the individual boundaries

The temperatures calculated with EPICA FVM deviate less than 0.1 [°C] from the standard and the derived thermal coupling coefficients are all well within the acceptable margin of error (± 0.1 [W]). The test is fulfilled.

D.2.4 Case 4

Case 4 is another 3-dimensional thermal bridge formed by a 50-by-100 [mm] steel rod penetrating a 20 [cm] slab of thermal insulation. The steel rod protrudes far into the internal environment which greatly increases its exposed surface area. The case is numerically demanding because of the dramatically different thermal conductance of the rod and the insulation. The external BC is of the third or Robin-type with a temperature of θ = 0 [°C] and a surface heat transfer resistance of R_s = 0.10 [m^2K/W]. The internal BC is similar but with a temperature of θ = 1 [°C]. The geometry of the case is summed up in Fig. 391, the material properties and boundary conditions in Fig. 392. The test is the calculation of the total heat flow through the detail and the maximum surface temperature on the cold side. the maximum heat flow difference must nod exceed 1% and the temperature difference 0.005 [K].

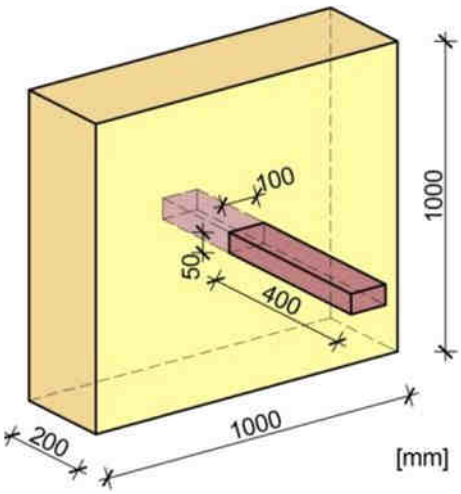

Fig. 391. – the geometry of case 4

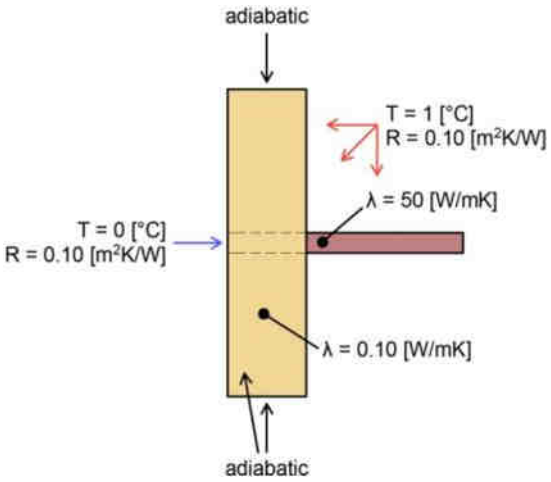

Fig. 392. – the boundary conditions and material properties of case 4

The fact that the problem is symmetric (twice) can be exploited to reduce the computational load and only one quarter of the geometry needs be simulated. The symmetry planes, as well as the other cutoff planes, are set as adiabatic. The mesh created in EPICAC FVM (see Fig. 393 and Fig. 394) used 81286 nodes and the same stationary iterative explicit solver was used as for Case 3. The convergence criteria for the iteration was the maximum temperature difference between the last two iterations for all cells with a threshold value of 1e-8 [K]. The calculation took 1356 [s] on an Intel Core i5 laptop.

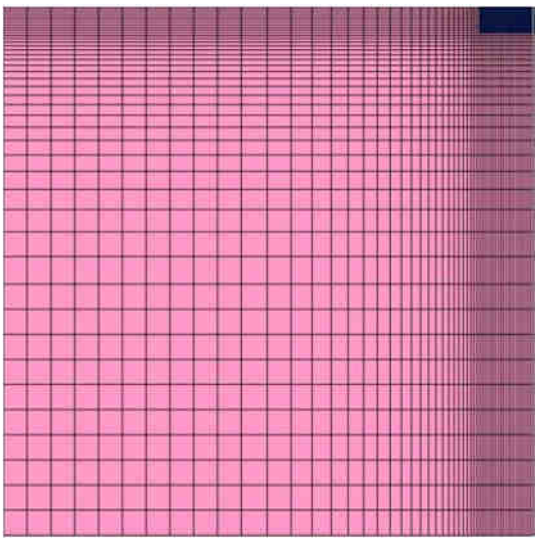

Fig. 393. – the mesh created for case 4

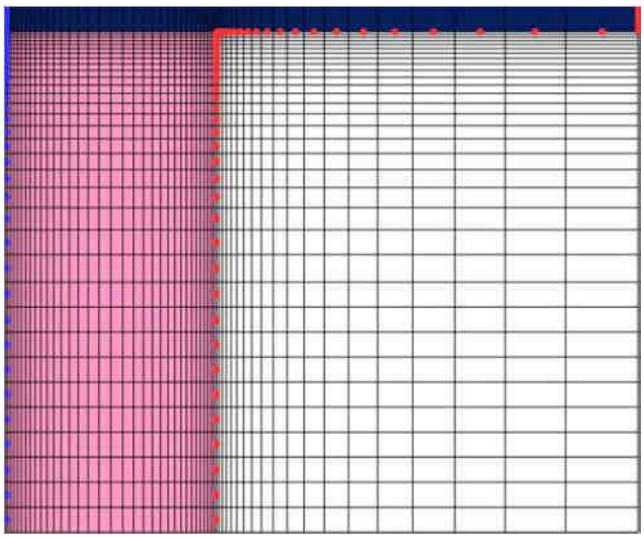

Fig. 394. – the mesh created for case 4

The calculated temperature filed is visualized in Fig. 395 and Fig. 396. The highest surface temperature reported by EPICA FVM on the external face of the detail was 0.8044 [°C] as opposed to 0.805 [°C] in the standard and the calculated total heat transmission 0.538 [W] as opposed to 0.54 [W] in the standard. Both fall within the acceptable margins of error, therefore the test is fulfilled.

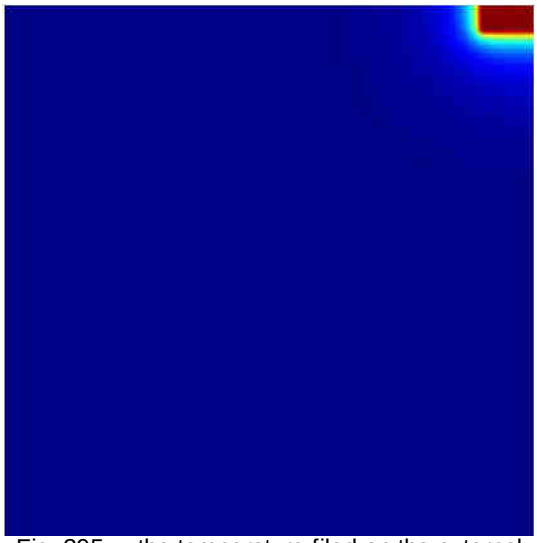

Fig. 395. – the temperature filed on the external face

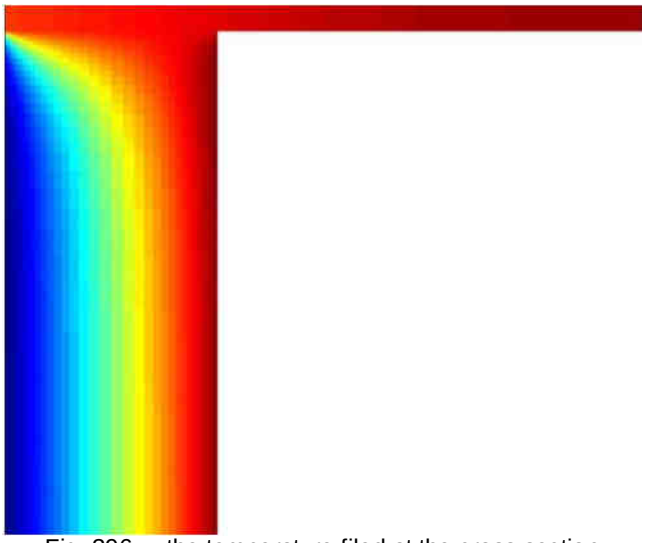

Fig. 396. – the temperature filed at the cross section through the steel rod

D.3 Validation of the one-dimensional transient heat and moisture transport calculations based on EN 15026

EN 15026 [2] is the harmonized European standard describing, among other things, the requirements for computer programs aimed at calculating the transient heat and mass (moisture) transport in solid opaque building constructions. Annex A of the standard describes one test case or benchmark for validating the accuracy of such programs. The test is based on an analytical solution of the coupled heat and mass transport in a homogenous semi-infinite body. The body is in total equilibrium at the beginning but as a result of a step-change in the boundary condition (temperate and relative humidity) transient heat and mass transport is initialized. The standards report the temperature and moisture content profiles of the body at specific times (7, 30 and 365 days after the step-change). The program to be validated needs to match these profiles to within specified margins of error: ± 2.5% of the reported value.

D.3.1 Detailed description of the test case

Geometry:

- a one-dimensional semi-infinite region

The initial condition:

- the whole semi-infinite body is in equilibrium with an initial temperature of $\theta = 20$ [°C] and a equilibrium moisture content corresponding to a relative humidity of $\varphi = 0.5$ [-]

The boundary condition:

- at t=0 [s] the boundary condition changes to $\theta_s = 30$ [°C] and $\varphi_s = 0.95$ [-]
- the surface heat transfer and diffusion resistance is zero
- besides diffusion no additional moisture sources are considered (e.g. driving rain)

Some general data specified by the standard:

- the reference temperature for the material functions is: $T_{ref} = 293.15$ [K]
- the density of water: $\rho_w = 1000$ [kg/m^3]
- the specific gas constant of water vapor: $R_{H2O} = 462$ [J/kgK]

The constant material properties of the semi-infinite body:

- the porosity: $\phi = 0.146$ [-]
- the specific heat capacity of the dry material: $c_{dry} = 850$ [J/kgK]
- the density of the dry material: $\rho_{dry} = 2146$ [kg/m^3]

The analytical material property functions:

- The moisture dependent thermal conductivity of the material:

$$\lambda = 1.5 + \frac{15.8}{1000} w \tag{23}$$

where: λ [W/mK] – the thermal conductivity
w [kg/m^3] – the moisture content of the material

- The moisture content of the material as a function of relative humidity (the material moisture function)

$$w = \frac{146}{\left(1 + \left(-8 \cdot 10^{-8} \cdot R_{H2O} \cdot T_{ref} \cdot \rho_w \cdot \ln(\varphi)\right)^{1.6}\right)^{0.375}} \tag{24}$$

where: w [kg/m^3] – the moisture content of the material
R_{H2O} [J/kgK] – the specific gas constant of water vapor
T_{ref} [K] – the reference temperature
ρ_w [kg/m^3] – the density of water
φ [-] – the relative humidity

- The water vapor diffusivity of the material as a function of the moisture content:

$$\delta_p = \frac{M_w}{RT} \cdot \frac{26.1 \cdot 10^{-6}}{200} \cdot \frac{1 - \frac{w}{146}}{0.503\left(1 - \frac{w}{146}\right)^2 + 0.497} \tag{25}$$

where: δ_p [s] or [kg/msPa] – the vapor diffusivity of the material
M_w [kg/mol] – the molar mass of water
R [J/molK] – the universal gas constant
T [K] – the temperature of the material
w [kg/m^3] – the moisture content of the material

- EPICAC FVM uses the temperature dependent vapor diffusivity of air and the moisture dependent water vapor diffusion resistance factor of the material instead of the diffusivity of the material. This is given as:

$$\mu = \frac{\delta}{\delta_p} = \frac{1.968 \cdot 10^{-7} \cdot (25 + 273)^{0.81}}{101325 \cdot \delta_p} \tag{26}$$

where: μ [-] – the water vapor diffusion resistance factor
δ [s] or [kg/msPa] – the vapor diffusivity of air
δ_p [s] or [kg/msPa] – the vapor diffusivity of the material

Strictly speaking this is only valid for P = 101325 [Pa] and θ = 25 [°C], but the resulting small error is acceptable.

- The liquid conductivity of the material describing it's capillary suction properties:

$$K = \exp\left(\begin{array}{l} -39.2619 + 0.0704\cdot(w-73) - 1.7420\cdot10^{-4}\cdot(w-73)^2 - 2.7953\cdot10^{-6}\cdot(w-73)^3 \\ -1.1566\cdot10^{-7}\cdot(w-73)^4 + 2.5969\cdot10^{-9}\cdot(w-73)^5 \end{array}\right) \quad (27)$$

where: K [s/m] – the liquid conductivity
w [kg/m^3] – the moisture content of the material

This value needs to be converted into the moisture diffusivity EPICAC FVM uses. This is done using the following equation based on the work of (x):

$$D_w = -K\frac{\partial p_{suc}}{\partial w} \quad (28)$$

where: D_w [m^2/s] – the moisture diffusivity
K [s/m] – the liquid conductivity
p_{suc} [Pa] – the suction pressure
w [kg/m^3] – the moisture content of the material

The derivative in equation (x) is the inverse of the moisture content function as defined based on capillary suction (which is also given in the standard). Therefore the equation for the moisture diffusivity can be derived as:

$$D_w = 0.125\cdot10^8\left(\left(\frac{146}{w}\right)^{\frac{1}{0.375}} - 1\right)^{0.625} \quad (29)$$

where: D_w [m^2/s] – the moisture diffusivity
w [kg/m^3] – the moisture content of the material

The acceptable range for the results given by the standard is summed up in tables (x) and (x) for the temperature and moisture content respectively.

day	x=0.5		x=1		x=1.5		x=2.0		x=2.5		x=3.0		x=4.0		x=5.0	
	min.	max.	min.	max.	min.	max.	min.	max.	min.	max.	min.	max.	min.	max.	min.	max.
7	26,4	26,9	23,6	24,1	21,7	22,2	21,1	20,5	20,0	20,5	19,8	20,4	19,8	20,3	19,8	20,3
30	28,1	28,6	26,5	27,0	25,0	25,5	23,7	24,3	22,7	23,2	21,8	22,3	20,7	21,2	20,1	20,6
365	29,2	29,8	28,8	29,3	28,3	28,8	27,8	28,4	27,4	27,9	26,9	27,4	26,0	26,6	25,2	25,7

Table 12 – the standard's range of acceptance for the temperature distribution in the body

day	x=0.01		x=0.02		x=0.03		x=0.04		x=0.05		x=0.06		x=0.08		x=0.10	
	min.	max.	min.	max.	min.	max.	min.	max.	min.	max.	min.	max.	min.	max.	min.	max.
7	50.2	54,5	41,3	45,6	40,8	45,1	40,8	45,1								
30	81,0	85,3	51,1	55,3	43,6	47,9	41,5	45,7	40,9	45,2	40,8	45,1	40,8	45,1		
365	117,5	121,8	104,4	180,7	88,7	93,0	75,6	77,9	62,8	67,1	55,7	60,0	47,9	52,2	44,1	48,4

Table 13 – the standard's range of acceptance for the moisture distribution in the body

D.3.2 Modeling in EPICAC FVM

EPICAC FVM uses tabulated data to read the material properties it needs therefore the analytical functions presented earlier were only used to derive a materials input datafile. The program is not able to model an actual semi-infinite region so a sufficiently large but finite domain was defined instead so that the moisture and temperature wave initiated by the step-change at the boundary would have no time to reach the other side by the end of the simulated time period. The width of the simulated domain was set to 72 [m] with a very fine mesh at the boundary (around 1.5 [mm]) which first slowly and then more rapidly expands towards the inner side to reduce the node count. The final mesh is shown in Fig. 397 and the temperature field at the end of the simulation in Fig. 398. Since the standard only requires the temperature distribution to be reported up to a depth of 5 [m] a possible slight truncation of the geometry at the extreme end of the domain will not effect the results too much. The moisture wave only penetrates the material to a depth of around 0.1 [cm] during the entire 375 [day] length of the simulation so it remains in the densely meshed region (see Fig. 399 and Fig. 400). Altogether only 124 nodes were needed for the mesh.

The boundary with the step-change was defined as third or Robin-type with a temperature of $\theta = 30$ [°C] and a surface heat transfer resistance of R_s = 1e-10 [m^2K/W] and a surface water vapor transfer coefficient of β = 1e10 [kg/m2sPa] to mimic a Dirichlet BC. The other side of the domain is defined as adiabatic.

The instationary calculation used a time step of 1 [h] and a full implicit solution scheme for both the temperature and moisture transport matrices. Within a single time step an iterative scheme with up to 20 cycles is used to resolve the coupling between the heat and moisture transport. The convergence criteria for these iterations are the maxim temperature and relativity differences between the last two steps with threshold values of $\Delta T_{max} \leq$ 1e-5 [K] and $\Delta \varphi_{max} \leq$ 1e-3 [-]. The calculation took 85.4 [s] on an Intel Core i5 laptop.

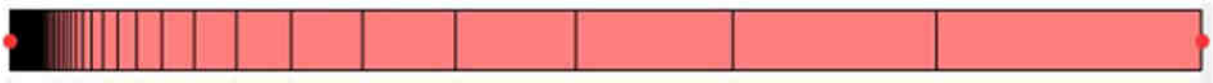

Fig. 397. – the entire simulated 1-dimensional domain and the mesh

Fig. 398. – the temperature filed on the external face

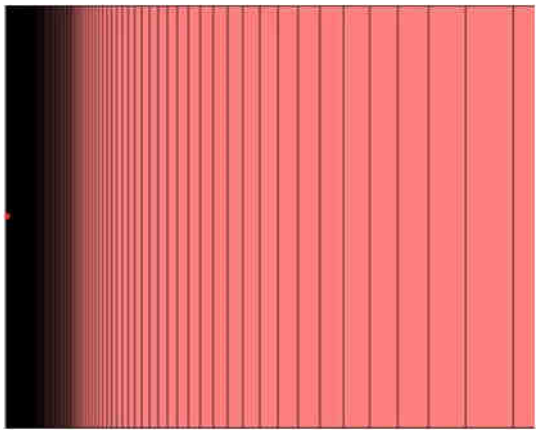

Fig. 399. – the temperature filed on the external face

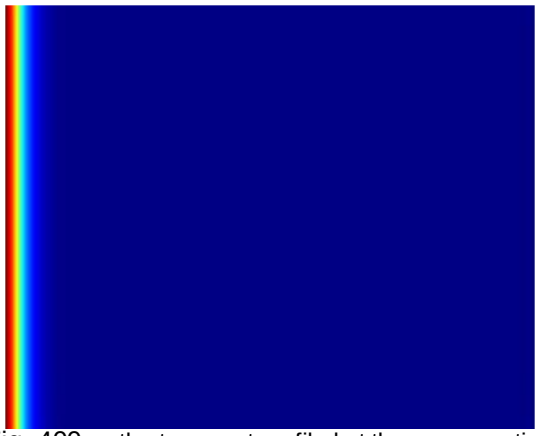

Fig. 400. – the temperature filed at the cross section through the steel rod

D.3.3 Results and conclusions

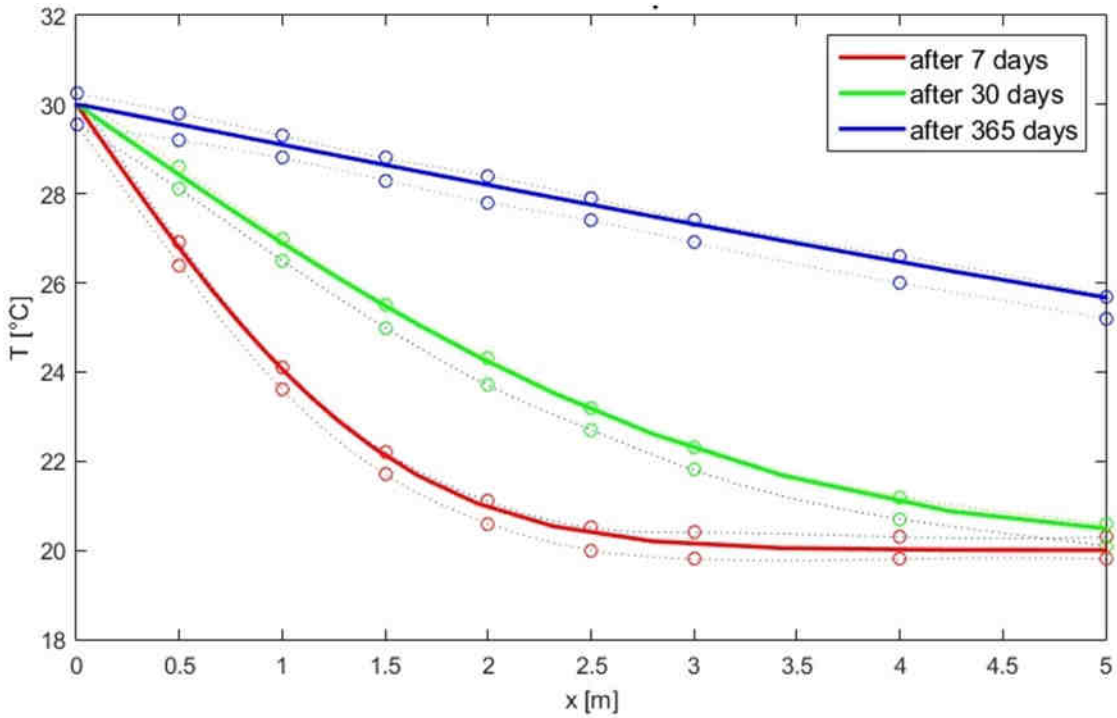

Fig. 401. – the calculated temperature distribution in the body plotted against the range of acceptance specified by the standard

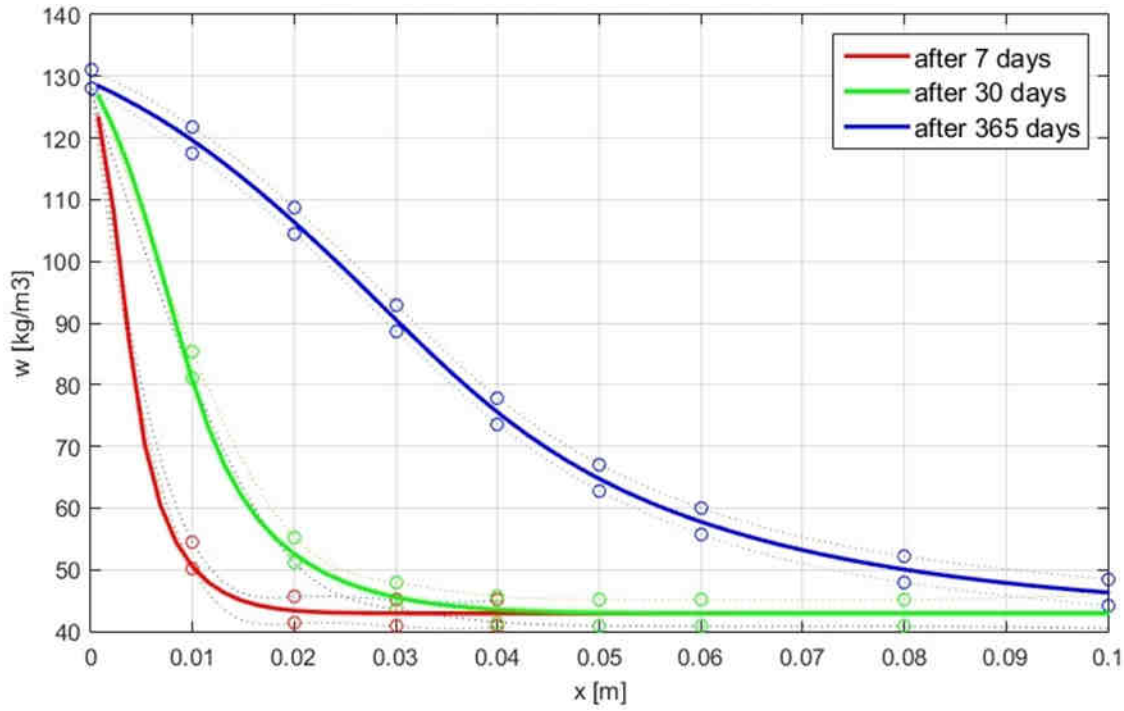

Fig. 402. – the calculated moisture distribution in the body plotted against the range of acceptance specified by the standard

The temperature field (Fig. 401) and moisture filed (Fig. 402) calculated with EPICAC FVM both fall within the preset limits of the standard for all three instances and for every position, therefore the programs fulfills the requirements of the standard.

D.4 References

[1] EN ISO 10211 (2011) Thermal bridges in building construcions – Heat flows and surface temperatures – Detailed calculations

[2] EN 15026 (2007) Hygrothermal performance of building components and building elements. Assessment of moisture transfer by numerical simulation.

[3] Künzel, H. M. (1994) Verfahren zur ein- und zweidimensionalen Berechnung des gekoppelten Wärme- und Feuchtetransports in Bauteilen mit einfachen Kennwerten, PhD Dissertation, Lehrstuhl für Bauphysik, Universität Stuttgart, Stuttgart, Germany, e-print: http://www.ibp.fraunhofer.de/content/dam/ibp/de/documents/hk_dissertation_tcm45-30727.pdf

E (Appendix E) – EPICAC BE validation

Validation of EPICAC BE with the International Energy Agency Simulation Test (BESTEST) and Diagnostic Method

The BESTEST suite of test cases is a widely known and used method for the validation of dynamic building energy simulation engines via cross-comparison. Such programs are very complicated with scores of sub-models and algorithms, modeling assumptions and input parameters which make it very difficult to ascertain their overall accuracy. The use of simple analytical solutions and the use of real life measurement data for validation purposes are equally limited in their scope. Analytical solutions are extremely hard to calculate for even the most rudimentary of cases and real life measurement are prohibitively expensive and hard to carry out. The BESTEST suite of dynamic building energy simulation case, originally created by the International Energy Agency in 1995 (see: [4]), defines a small and somewhat simplified (but not excessively so) number of test cases for which simulation results of several simulation programs are presented. These result were created and submitted by professionals and utilize the modelling capabilities of their respective programs to their full extent and thus form a basic data set to which new results can be compared. It must be emphasized that since this dataset only contains simulation results itself it can't be used for a 100% accurate validation. But even such data is useful for assessing the physical plausibility of the outputs of new simulation software, to check their sensitivity to changes in the inputs or modelling assumptions, to recheck programs after major modifications to the algorithms and for general debugging and software development purposes. The original BESTEST test suite was since incorporated into the ANSI/ASHRAE Standard 140 [5].

The BESTEST suite contains three main groups of test cases of different complexity and purpose, which are:

- The **qualification cases**: cases 600-650 for low-mass buildings and case 900-990 for high-mass buildings. These represent realistic scenarios for testing the overall simulation program as it would be used in everyday practice.
- The **diagnostic cases**: cases 195-320, cases 395-440 and cases 800 and 810. These cases are purposefully simplified to reduce the possible interactions between the various physical phenomena that are hard to track. They are intended to isolate individual sub-models and possible bugs in the programs that lead to erroneous results. The cases 195-320 are the most simple ones, but as some programs don't allow the user to 'dumb them down' sufficiently another set – cases 395-400 – of more complicated tests is also provided.
- The **special cases**: case 960 is for testing the modeling of solar gains through an attached sunspace (winter-garden) and case 990 for testing the more detailed calculation of heat losses through a floor slab connected to the ground. The cases 600FF, 650FF, 900FF and 950FF are the same as their regular qualification case counterparts, but without any mechanical heating or cooling to check the programs capability to calculate free floating internal temperatures.

All cases are based on the same location and overall building shape with some modifications, such as glazing area, orientation, shading surfaces etc. A brief introduction of the cases is found in section E.1 and a summary of the modeling options used in EPICAC BE in section E.2. For the validation of the EPICAC BE program all the qualification cases as well as the diagnostic cases 195 through 395 were performed. Cases 960 and 990 were left out as the modeling of sunspaces and ground contact was not an immediate goal for the program in this work, and test cases 400-440 and 800-810 were not required for the validation as the qualification test were already met as well as the basic set of test problems.

The simulation programs originally used to compile the BESTEST dataset were:

- ESP-RV8 (Strathclyde University, UK),
- BLAST-3.0-193 (CERL, USA),
- DOE2.1D 14 (LANL/LBL, USA),
- SERIERS/SUNCODE 5.7 (NREL/Ecotope, USA),
- SERIRES 1.2 (NREL/BRE, USA/UK),

- S3PAS (University of Seville, Spain),
- TRNSYS 13.1 (University of Wisconsin, USA),
- TASE (Tampere University, Finland).

These programs represented the state of the art in 1995 but for certain cases there are significant discrepancies between their results. To account for the 20 years that passed since the original publication of BESTEST we also added data from more recent programs to the dataset. We chose the validation data from the programs EnergyPlus 1.1 [6], Design Builder/EnergyPlus 8.1 [7] and IES ApacheSim 5.2 [8] as these can be regarded as a 'industry standard' in dynamic building energy simulations.

The data used for the evaluation of BESTEST results are the annual total heating energy demand, the annual total cooling energy demand, the peak heating energy demand and the peak cooling energy demand. For the 4 cases with free floating temperature the energy used is obviously zero and the zone air temperature is checked instead for a given specific day of the year. Not all programs reported results for all the test cases due to modeling limitations.

E.1 The description of the test cases

E.1.1 Site and climate

All BESTEST test cases are defined with the same location: Denver, Colorado, USA. The local weather is cold and clear in the winter and hot and dry in the summer. A short description of the site and the local climate, an excerpt from the original BESTEST documentation ([4] Table 1-3.), is presented in Table 14Table 14 – Site and climate summary. The weather data necessary for the calculations is provided with a weather file (DRYCOLD.TMY) of the 'Typical Meteorological Year' format. This is a concatenation of shorter measurement periods to form a whole year long dataset that is close to a statistical average for each month as well as the whole year. The temporal resolution is hourly and based on the local solar time. The main meteorological parameters contained in the weather file are summed up in Table 15.

Latitude	39.8° North
Longitude	104.9° West
Altitude	1609 [m]
Time Zone	7
Ground reflectivity	0.2
Site	Flat, unobstructed, located exactly at weather station
Mean annual wind speed	4.02 [m/s]
Ground temperature	10 [°C]
Mean annual ambient dry-bulb temperature	9.71 [°C]
Minimum annual ambient dry-bulb temperature	-24.39 [°C]
Maximum annual ambient dry-bulb temperature	35.00 [°C]
Maximum annual win speed	14.89 [m/s]
Heating degree days (base 18.3 [°C])	3636.2 [°C-days]
Cooling degree days (base 18.3 [°C])	487.1 [°C-days]
Mean annual dew point temperature	-1.44 [°C]
Mean annual humidity ratio	0.0047
Global horizontal solar radiation annual total	1831.82 [kWh/m^{2}a]
Direct normal solar radiation annual total	2353.85 [kWh/m^{2}a]
Direct horizontal solar radiation	1339.48 [kWh/m^{2}a]
Diffuse horizontal solar radiation	492.34 [kWh/m^{2}a]

Table 14 – Site and climate summary

Field / description	unit
wind direction	[°]
wind speed	[m/s]
precipitation	[mm/h]
atmospheric pressure	[Pa]
ambient dry-bulb temperature	[°C]
relative humidity	[%]
dew point temperature	[°C]
global solar irradiation incident on a horizontal plane	[W/m^2]
diffuse solar irradiation incident on a horizontal plane	[W/m^2]
solar direct normal irradiation	[W/m^2]
solar direct irradiation incident on a horizontal plane	[W/m^2]
illuminance on a horizontal plane	[Lux]
longwave atmospheric counterradiation incident on a horizontal plane	[W/m^2]

Table 15 – meteorological data series presented in the BESTEST climate file (DRYCOLD.TMY)

E.1.2 Building geometry

The basic form of the building is a single room (and single thermal zone) single-floor type with a simple rectangular floorplan and a flat roof. The only two openings – fully glazed fix windows – are either located towards the south (Fig. 403) or towards the east and the west (Fig. 405). Shading is either completely lacking (Fig. 403 and Fig. 405), or provided with fixed horizontal overhangs towards the south (Fig. 404) or a fixed shroud like structure around the eastern an western windows (Fig. 406). The floor of the building is in direct contact with the ground and the surroundings are taken as completely flat with no other structures or vegetation to cast any shadows on the building. The dimensions specified in the figures are taken as both internal and external dimensions therefore the thickness of the constructions is neglected. This is a reasonable simplification because the purpose of BESTEST is a comparison of results for a 'fictional' building not a real geometry and most dynamic building simulation programs are unable to compute multi dimensional heat transfer through thermal bridges anyway.

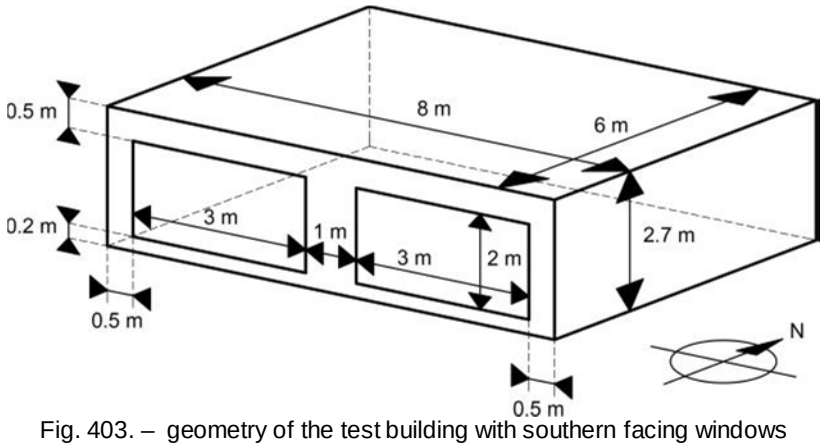

Fig. 403. – geometry of the test building with southern facing windows

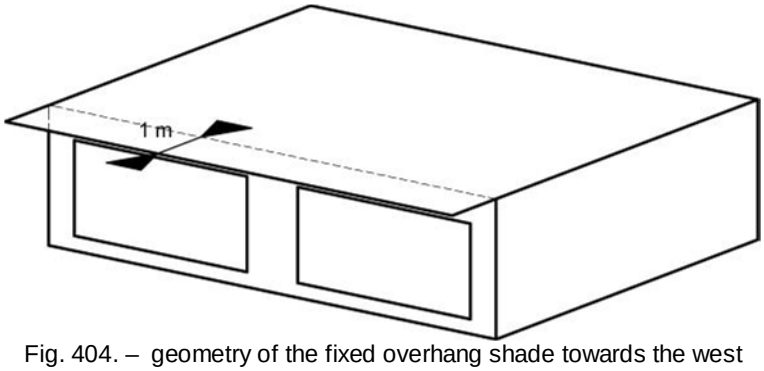

Fig. 404. – geometry of the fixed overhang shade towards the west

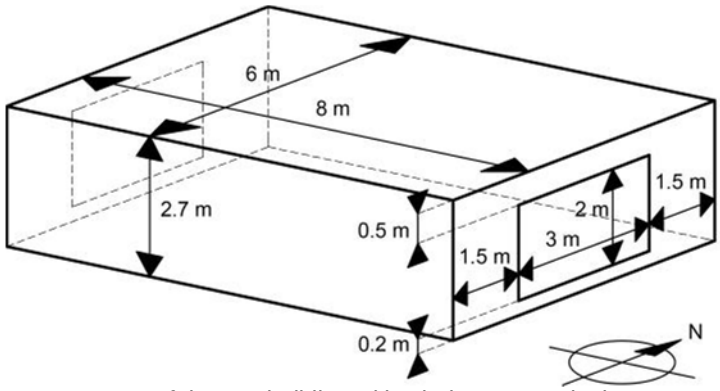

Fig. 405. – geometry of the test building with windows towards the east and the west

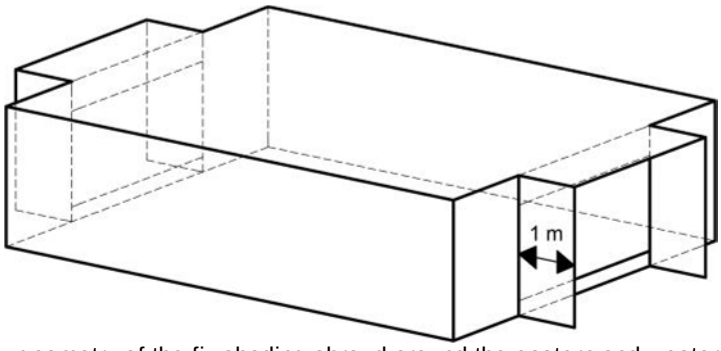

Fig. 406. – geometry of the fix shading shroud around the eastern and western windows

E.1.3 Thermal envelope

E.1.3.1 Opaque constructions

The thermal envelope is only defined with the thermally important layers (moisture transport calculations are not included in BESTEST, therefore vapor barriers and similar layers are not specified). All constructions are assumed completely airtight. A set of low-mass and a separate set of high-mass constructions are used to check for discrepancies in the modelling of thermal inertia.
The low-weight walls (see Table 16) and roof (see Table 18) would in reality contain some kind of wooden or perhaps metal frame which is completely neglected in BESTEST. The thermal insulation is considered to be fully continuous between the internal and external claddings. Like the simplification of the geometrical dimensions this is acceptable as the goal is the simulation of a virtual building. The buildup of the floor is the mot unrealistic (see Table 17). It has a 1 [m] thick thermal insulation layer with a fictional zero thermal mass between the floorboards and the ground to reduce the thermal interaction between the building and the ground to a minimum without actually introducing an adiabatic boundary condition. The reason for this is that the possibilities for detailed ground heat loss calculation in 1995 were very limited and inaccurate due to the lack of sufficient computing power and the authors wanted to eliminate this source of potential error from the comparison.

layer	d [m]	λ [W/mK]	R [m^2K/W]	c_p [J/kgK]	ρ [kg/m^3]
Internal surface coef.	-	-	0.121	-	-
Plasterboard	0.012	0.16	0.075	840	950
Fiberglass quilt	0.066	0.04	1.65	840	12
Wood siding	0.009	0.14	0.064	900	530
External surface coef.	-	-	0.034	-	-
		Σ R	1.944	[m^2K/W]	
		U	**0.514**	**[W/m^2K]**	

Table 16 – Low-mass case: exterior wall (inside to outside)

layer	d [m]	λ [W/mK]	R [m^2K/W]	c_p [J/kgK]	ρ [kg/m^3]
Internal surface coef.	-	-	0.121	-	-
Timber flooring	0.024	0.14	0.179	1200	650
Insulation	1.003	0.04	25.075	-	-
Ground contact	-	-	-	-	-
		Σ R	25.374	[m^2K/W]	
		U	**0.039**	**[W/m^2K]**	

Table 17 – Low-mass case: floor (inside to outside)

layer	d [m]	λ [W/mK]	R [m^2K/W]	c_p [J/kgK]	ρ [kg/m^3]
Internal surface coef.	-	-	0.121	-	-
Plasterboard	0.01	0.16	0.063	840	950
Fiberglass quilt	0.1118	0.04	2.794	840	12
Roofdeck	0.019	0.14	0.136	900	530
External surface coef.	-	-	-	-	-
		Σ R	3.147	[m^2K/W]	
		U	**0.318**	**[W/m^2K]**	

Table 18 – Low-mass case: roof (inside to outside)

For the high-mass cases the external walls (see Table 19) and the timber flooring (see Table 20) are changed to a concrete block masonry with external insulation and a concrete screed respectively. The roof is kept the same (see Table 21).

layer	d [m]	λ [W/mK]	R [m^2K/W]	c_p [J/kgK]	ρ [kg/m^3]
Internal surface coef.	-	-	0.121	-	-
Concrete block	0.10	0.51	0.196	1000	1400
Foam insulation	0.0615	0.04	1.537	1400	10
Wood siding	0.009	0.14	0.064	900	530
External surface coef.	-	-	0.034	-	-
		Σ R	1.952	[m^2K/W]	
		U	**0.512**	**[W/m^2K]**	

Table 19 – High-mass case: exterior wall (inside to outside)

layer	d [m]	λ [W/mK]	R [m^2K/W]	c_p [J/kgK]	ρ [kg/m^3]
Internal surface coef.	-	-	0.121	-	-
Concrete slab	1.13	0.08	0.071	1000	1400
Insulation	1.007	0.04	25.175	-	-
Ground contact	-	-	-	-	-
		Σ R	25.366	[m^2K/W]	
		U	**0.039**	**[W/m^2K]**	

Table 20 – High-mass case: floor (inside to outside)

layer	d [m]	λ [W/mK]	R [m^2K/W]	c_p [J/kgK]	ρ [kg/m^3]
Internal surface coef.	-	-	0.121	-	-
Plasterboard	0.01	0.16	0.063	840	950
Fiberglass quilt	0.1118	0.04	2.794	840	12
Roofdeck	0.019	0.14	0.136	900	530
External surface coef.	-	-	-	-	-
		Σ R	3.147	[m^2K/W]	
		U	**0.318**	**[W/m^2K]**	

Table 21 – High-mass case: roof (inside to outside)

E.1.3.2 Glazing

The windows are considered fully glazed and fixed with no frame elements or dividers. The glazing is a double plane clear float glazing made with 3.175 [mm] glass layers and a 13 [mm] air gap. The BESTEST documentation provides the following table of basic data about the windows' buildup:

property	value
Extinction coefficient of glass	0.0196 [1/mm]
Number of panes	2
Pane thickness	3.175 [mm]
Air-gap thickness	13 [mm]
Index of refraction	1.526 [-]
Normal direct-beam transmittance through one pane in air	0.86156 [-]
Conductivity of glass	1.06 [W/mK]
Conductance of each glass pane	333 [W/K]
Combined radiative and convective coefficient of air gap	6.297 [W/m^2K]
Exterior combined surface coefficient	21[W/m^2K]
Interior combined surface coefficient	8.29 [W/m^2K]
U-value from interior to ambient air	3 [W/m^2K]
Hemispherical longwave infrared emittance of uncoated glass	0.84 [-]
Density of glass	2500 [kg/m^3]
Specific heat capacity of glass	750 [J/kgK]
Curtains, blinds, frames, spacers, mullions, obstructions inside the window	none
Double-pane shading coefficient (at normal incidence)	0.916 [-]
Double-pane solar heat gain coefficient (at normal incidence)	0.787 [-]

Table 22 – Window (glazing) properties specified in BESTEST

A table of angle-of-incidence dependent optical data is also provided but was not used as EPICAC BE is able to calculate all optical and thermal properties itself from the basic definition of the glazing system.

For cases 200-250 an 800 the glazing is replaced with a fictional layer of equivalent thermal properties but no solar transmittance and an exterior solar absorptance equal ton the opaque constructions. This is done for checking the effect of other models first in the diagnostic test cases before introducing large solar gains into the equation.

E.1.4 Additional specifications

E.1.4.1 HVAC systems

The HVAC systems are treated in a very simplified way. Heating and cooling is provided via an idealized system that will always perfectly meet the heating or cooling requirements. The system is assumed to have a 100% efficiency, a 100% convective and 100% sensible load. No plants are modelled and only the ideal heating and cooling loads delivered directly to the thermal zone are counted. The heating and cooling thermostat setpoints are based on the room air temperature and the following settings are used for the different test cases:

- **20/20 or 'bang-bang'**: a constant 20 [°C] setpoint temperature for both the heating and the cooling (the room temperature is held constant)
- **20/27 or 'deadband'**: 20 [°C] setpoint for heating, 27 [°C] for cooling and a free floating room temperature between the two
- **20*/27 or 'setback'**: same as the previous but with nighttime setback of the heating setpoint: 10 [°C] between 23 to 07 (20 [°C] during the day).
- **-/27/V or 'venting'**: no heating and a 27 [°C] setpoint for cooling between 07 and 18 hours. Between 18 and 07 hours the mechanical cooling is turned off and a mechanical nighttime ventilation is used instead with a specified constant volume flow rate.
- **FF or 'free-floating'**: no heating or cooling

The maximum power of both the heating and the cooling is considered basically infinite (10 [kW]) compared to the maximum demands. The volume flow rate of the fan for the nighttime ventilation is taken as a constant 1703.16 [m^3/h].

E.1.4.2 Infiltration

The infiltration is either zero, or specified with a constant air exchange rate of 1 or 0.5 [1/h] throughout the year and during every hour of the day.

E.1.4.3 Internal loads

the internal thermal loads are either zero or specified with a constant 200 [W] value with 60% radiative and 40% convective, 100% sensible load.

E.1.4.4 Surface optical properties

The hemispherical longwave infrared emissivities of the internal and external opaque surfaces are either considered as 0.1 [-] to reduce the longwave infrared heat transfer to a minimum and test convective effect or 0.9 [-] for the more realistic cases. Similarly the shortwave solar absorptance of the opaque surfaces is either 0.1, 0.9 or 0.6 [-] for testing the programs for virtually zero, high and 'normal' levels of solar absorptions.

E.1.5 Summary of all test cases

The precise combination of all the glazing, orientation, shading, setpoint etc. options for the individual test cases is summed up in Table 22 for the low-mass diagnostic cases, in Table 24 for the qualification cases and Table 25 for the additional special test cases. The cases that were not used for the validation of EPICAC BE because they were not relevant or required for this work are highlighted in red.

case	mass	glazing [m^2]	orient.	shade	setpoints [°C]	ε_e [-]	ε_i [-]	α_e [-]	α_i [-]	Q_{int} [W]	ACH [1/h]
195	L	-**	-	-	20/20	0.1	0.1	0.1	-	0	0
200	L	opaque*	S	no	20/20	0.1	0.1	0.1	-	0	0
210	L	opaque	S	no	20/20	0.9	0.1	0.1	-	0	0
215	L	opaque	S	no	20/20	0.1	0.9	0.1	-	0	0
220	L	opaque	S	no	20/20	0.9	0.9	0.1	-	0	0
230	L	opaque	S	no	20/20	0.9	0.9	0.1	-	0	1
240	L	opaque	S	no	20/20	0.9	0.9	0.1	-	200	0
250	L	opaque	S	no	20/20	0.9	0.9	0.9	-	0	0
270	L	12	S	no	20/20	0.9	0.9	0.1	0.9	0	0
280	L	12	S	no	20/20	0.9	0.9	0.1	0.1	0	0
290	L	12	S	yes	20/20	0.9	0.9	0.1	0.9	0	0
300	L	6/6	E/W	no	20/20	0.9	0.9	0.1	0.9	0	0
310	L	6/6	E/W	yes	20/20	0.9	0.9	0.1	0.9	0	0
320	L	12	S	no	20/27	0.9	0.9	0.1	0.9	0	0
395	L	-**	-	-	20/27	0.9	0.9	0.1	-	0	0
400	L	opaque	S	no	20/27	0.9	0.9	0.1	-	0	0
410	L	opaque	S	no	20/27	0.9	0.9	0.1	-	0	0.5
420	L	opaque	S	no	20/27	0.9	0.9	0.1	-	200	0.5
430	L	opaque	S	no	20/27	0.9	0.9	0.6	-	200	0.5
440	L	12	S	no	20/27	0.9	0.9	0.6	0.1	200	0.5

* the glazing is replaced with a fictitious opaque wall with the same U value, no thermal mass and zero solar transmission
** the building has no openings of any kind, all walls are solid

Table 23 – Low-mass diagnostic test cases

case	mass	glazing [m^2]	orient.	shade	setpoints [°C]	ε_e [-]	ε_i [-]	α_e [-]	α_i [-]	Q_{int} [W]	ACH [1/h]
600	L	12	S	no	20/27	0.9	0.9	0.6	0.6	200	0.5
610	L	12	S	yes	20/27	0.9	0.9	0.6	0.6	200	0.5
620	L	6/6	E/W	no	20/27	0.9	0.9	0.6	0.6	200	0.5
630	L	6/6	E/W	yes	20/27	0.9	0.9	0.6	0.6	200	0.5
640	L	12	S	no	20*/20	0.9	0.9	0.6	0.6	200	0.5
650	L	12	S	no	-/27/V**	0.9	0.9	0.6	0.6	200	0.5+v**
900	H	12	S	no	20/27	0.9	0.9	0.6	0.6	200	0.5
910	H	12	S	yes	20/27	0.9	0.9	0.6	0.6	200	0.5
920	H	6/6	E/W	no	20/27	0.9	0.9	0.6	0.9	200	0.5
930	H	6/6	E/W	yes	20/27	0.9	0.9	0.6	0.6	200	0.5
940	H	12	S	no	20*/27	0.9	0.9	0.6	0.6	200	0.5
950	H	12	S	no	-/27/V**	0.9	0.9	0.6	0.6	200	0.5+v**

* heating setpoint with nighttime setback
** automated nightie ventilation instead of cooling during the night

Table 24 – Qualification test cases

case	mass	glazing [m^2]	orient.	shade	setpoints [°C]	ε_e [-]	ε_i [-]	α_e [-]	α_i [-]	Q_{int} [W]	ACH [1/h]
600FF	L	12	S	no	FF	0.9	0.9	0.6	0.6	200	0.5
900FF	H	12	S	no	FF	0.9	0.9	0.6	0.6	200	0.5
650FF	L	12	S	no	FF	0.9	0.9	0.6	0.6	200	0.5+v**
950FF	H	12	S	no	FF	0.9	0.9	0.6	0.6	200	0.5+v**
800	H	opaque*	S	no	20/27	0.9	0.9	0.6	0.6	200	0.5
810	H	12	S	no	20/27	0.9	0.9	0.6	0.6	200	0.5
960	sunspace (winter-garden) test case – not relevant for the current validation of EPICAC BE										
990	detailed ground heat transfer test case – not relevant for the current validation of EPICAC BE										

* the glazing is replaced with a fictitious opaque wall with the same U value, no thermal mass and zero solar transmission

Table 25 – Additional test cases

E.2 Modeling settings in EPICAC BE

The modelling in EPICAC BE followed the specification in the BESTEST document. The opaque constructions were modelled with the help of the EPICAC FVM program, a finite volume method solver for the system of partial differential equations describing heat and mass transfer in opaque constructions. For this validation only the instationery heat conduction options of the program were used. The convective surface heat transfer coefficients were taken from the BESTEST specifications and the radiative heat transfer was calculated by the inbuilt algorithms of the program. The external longwave radiation exchange for all surfaces is computed based on the surfaces' solid angles to the sky, the ground and the terrestrial and atmospheric counterradiation based on the work of Kehrer and Schmidt [9]. The internal longwave radiation exchange is calculated with an exchange matrix derived from numerically calculated view factors between all individual surfaces and their emissivities. The calculation is valid for convex room geometries of arbitrary shape.

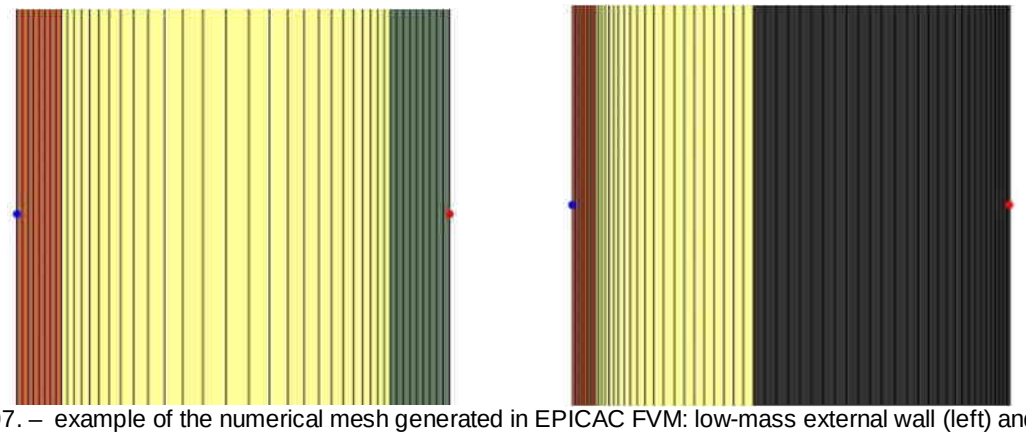

Fig. 407. – example of the numerical mesh generated in EPICAC FVM: low-mass external wall (left) and high-mass external wall (right)

The windows/glazing systems were modelled with EPICAC ISO, a program for the optical and thermal calculation of simple and complex glazing systems. As with almost all glazing design and dynamic building energy simulation programs the thermal mass of the glazing layers is neglected in the calculations.

The diffuse and direct solar radiation incident on a specific surface is calculated with the help of the Perez anisotropic sky model [10]. The effect of the fixed exterior shading elements was modelled by the program with the help of shadings masks precalculated at the beginning of the simulations. These are derived as an average for the discretized surfaces to account for partial shading as well. The corresponding algorithm of EPICAC BE is based on the work of Marsh [11], see Fig. 409. The internal distribution of the transmitted solar load is based on the assumption that all radiation first hits the floor, and the reflections are diffuse and based on the view factors between the floor and the other surfaces.

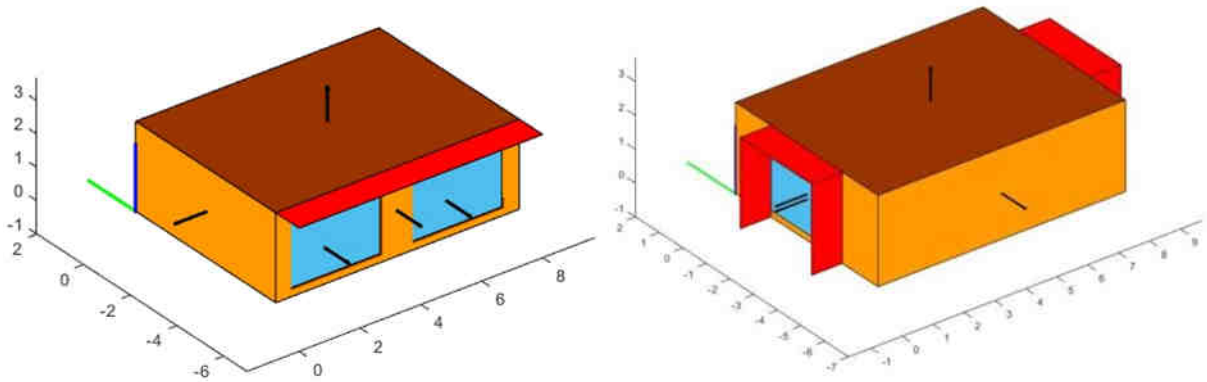

Fig. 408. – the 3D geometry generated by EPICAC BE for test cases 610 (left) and 630 (right)

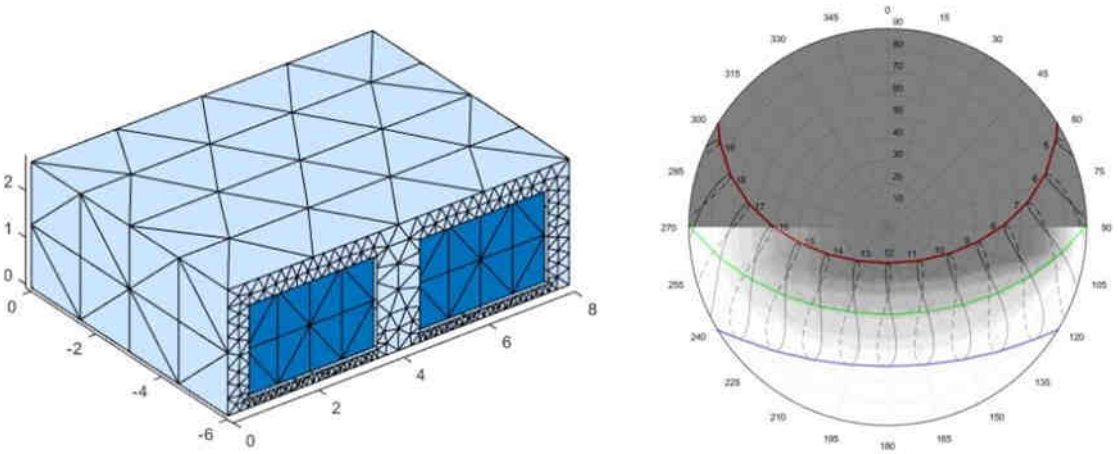

Fig. 409. – the discretization of the surfaces for the shading mask calculations (left) and an example of the calculated shading mask for the western window on the south façade of case 610 (right)

E.3 Results

The comparison of the EPICAC BE results with the 8 programs contained in BESTEST as well ad the additional 3 newer programs (two versions of EnergyPlus and ApacheSim) is summed up in this section. The total and peak annual heating and cooling energy demands for the qualification cases, than the diagnostic cases and finally the room air temperatures for the free floating temperature cases are presented.

E.3.1 Qualification cases

E.3.1.1 Low-mass cases (600-650)

E.3.1.1.1 Case 600

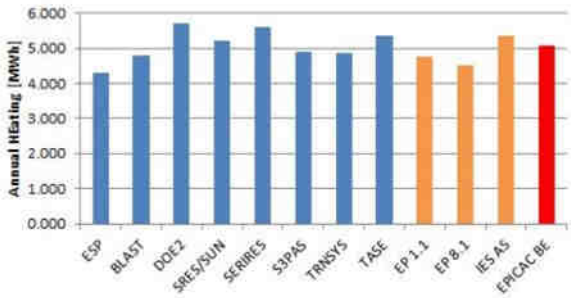

Fig. 410. – Case 600 – annual heating

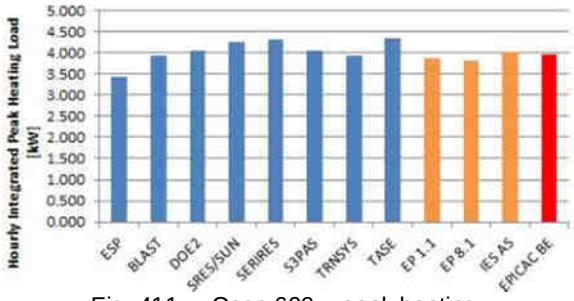

Fig. 411. – Case 600 – peak heating

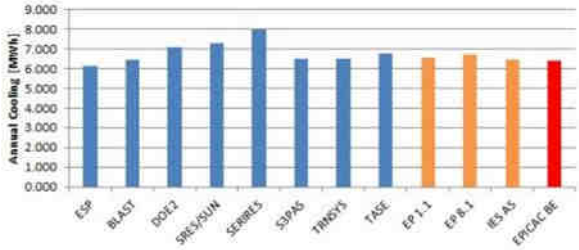

Fig. 412. – Case 600 – annual cooling

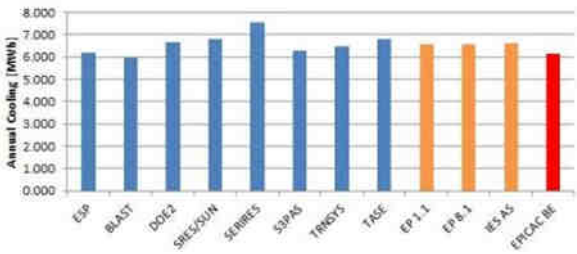

Fig. 413. – Case 600 – peak cooling

E.3.1.1.2 Case 610

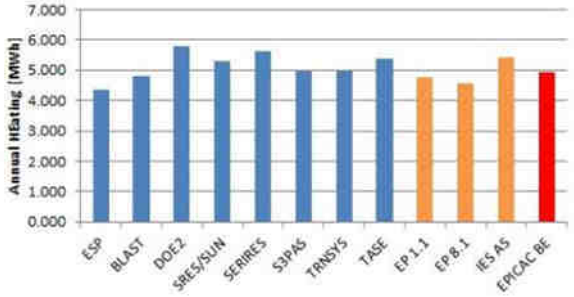

Fig. 414. – Case 610 – annual heating

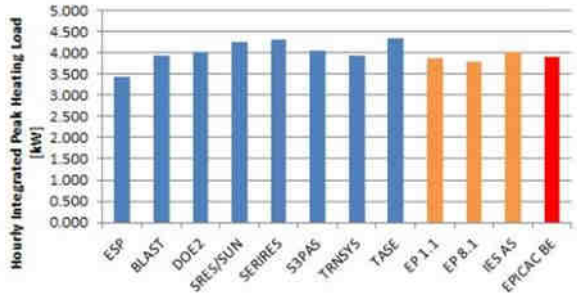

Fig. 415. – Case 610 – peak heating

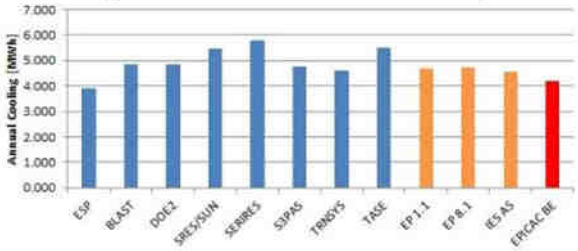

Fig. 416. – Case 610 – annual cooling

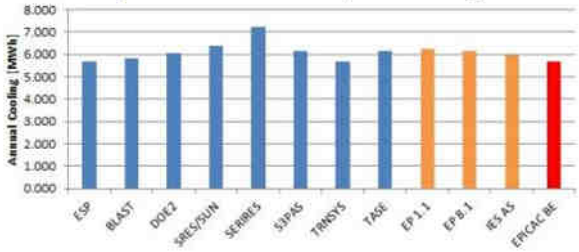

Fig. 417. – Case 610 – peak cooling

E.3.1.1.3 Case 620

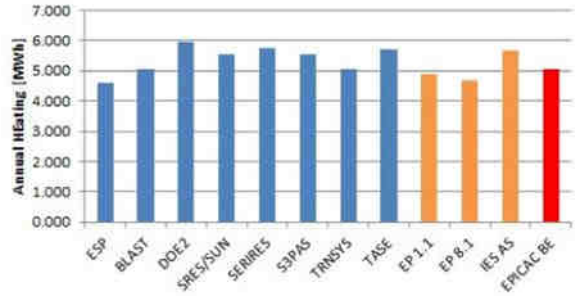

Fig. 418. – Case 620 – annual heating

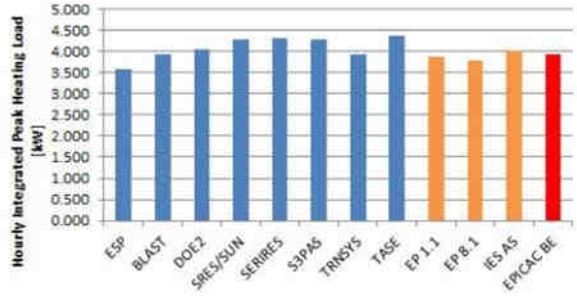

Fig. 419. – Case 620 – peak cooling

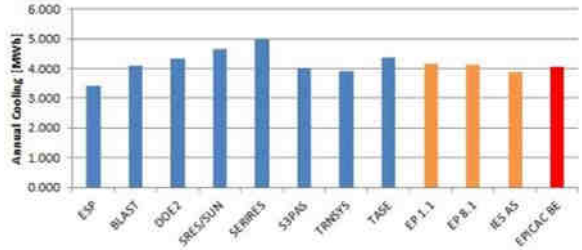

Fig. 420. – Case 620 – annual cooling

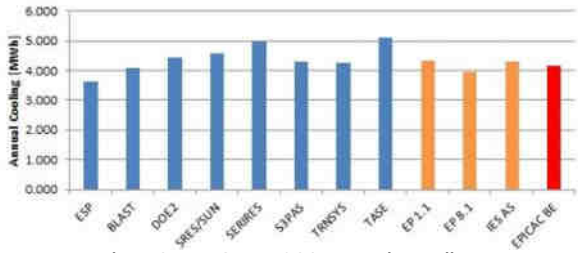

Fig. 421. – Case 620 – peak cooling

E.3.1.1.4 Case 630

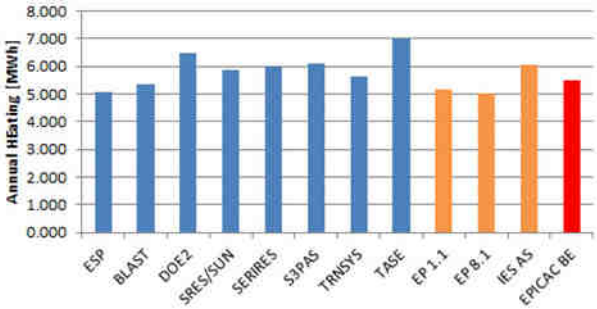

Fig. 422. – Case 630 – annual heating

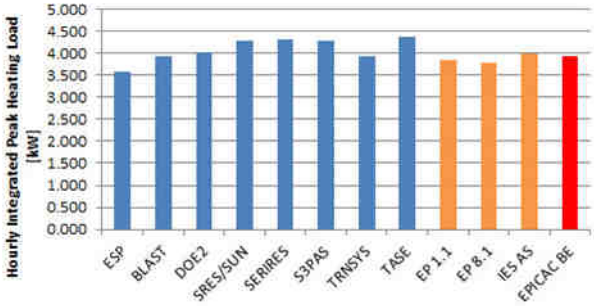

Fig. 423. – Case 630 – peak heating

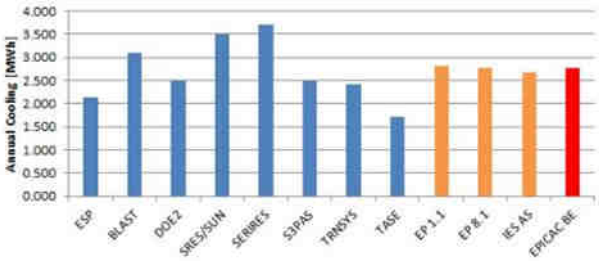

Fig. 424. – Case 630 – annual heating

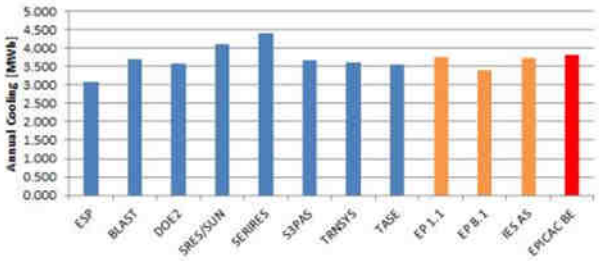

Fig. 425. – Case 630 – peak cooling

E.3.1.1.5 *Case 640*

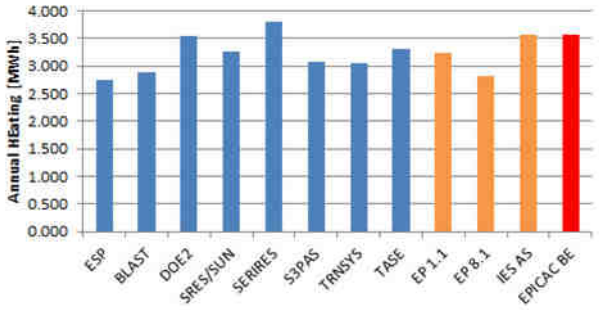

Fig. 426. – Case 640 – annual heating

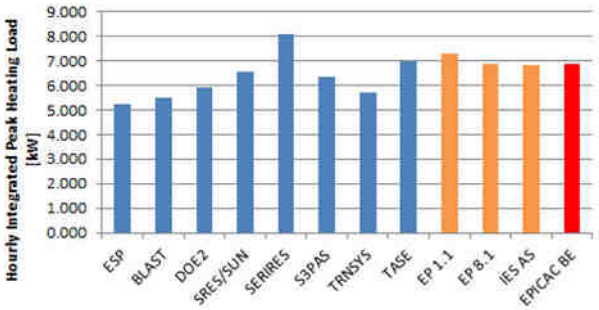

Fig. 427. – Case 640 – peak heating

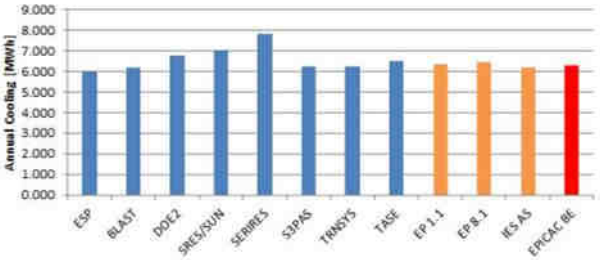

Fig. 428. – Case 640 – annual cooling

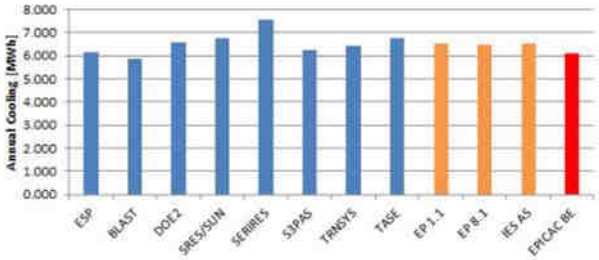

Fig. 429. – 640 – peak cooling

E.3.1.1.6 *Case 650*

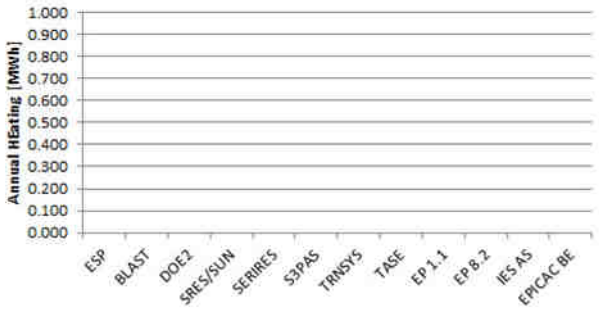

Fig. 430. – Case 650 – annual heating

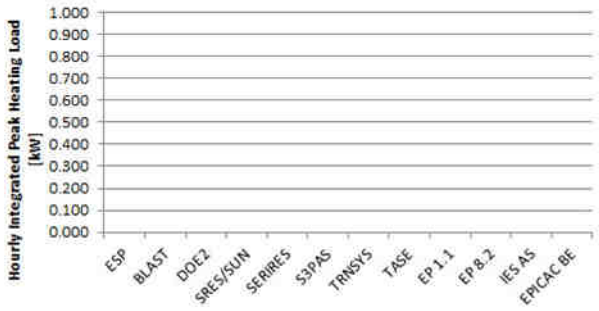

Fig. 431. – Case 650 – peak heating

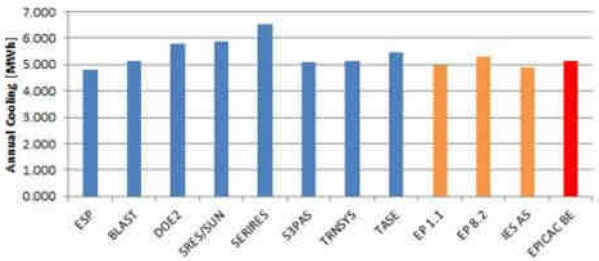

Fig. 432. – Case 650 – annual cooling

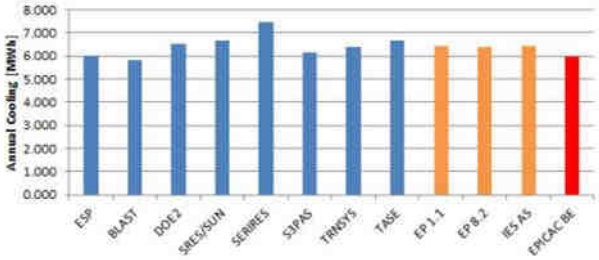

Fig. 433. – Case 650 – peak cooling

E.3.1.2 High-mass cases (900-950)

E.3.1.2.1 Case 900

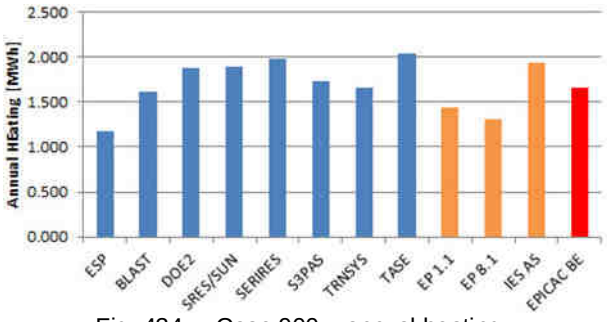

Fig. 434. – Case 900 – annual heating

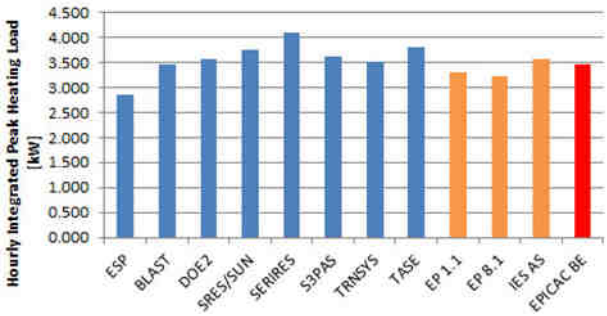

Fig. 435. – Case 900 – peak heating

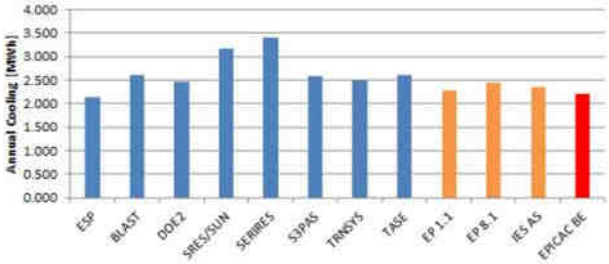

Fig. 436. – Case 900 – annual cooling

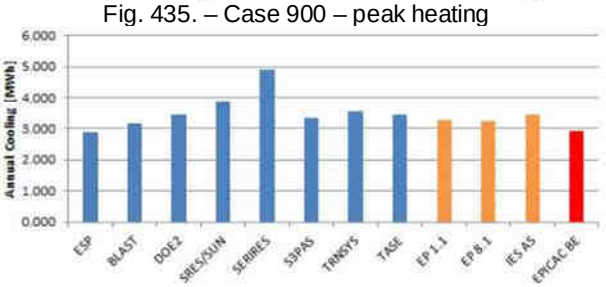

Fig. 437. – Case 900 – peak cooling

E.3.1.2.2 Case 910

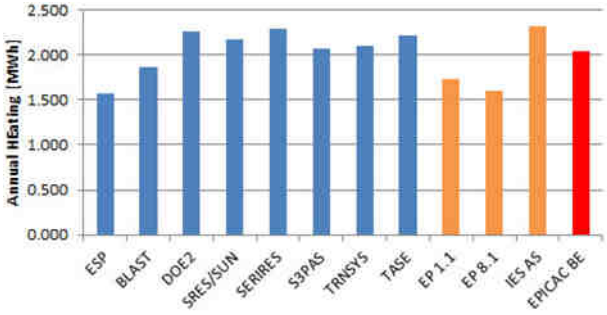

Fig. 438. – Case 910 – annual heating

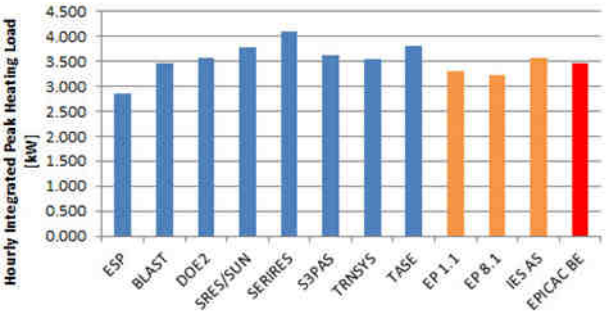

Fig. 439. – Case 910 – peak heating

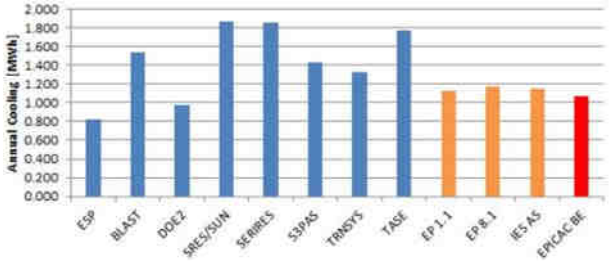

Fig. 440. – Case 910 – annual cooling

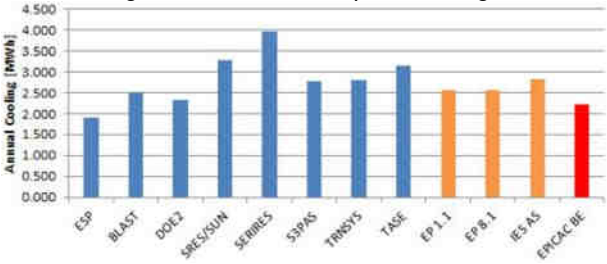

Fig. 441. – Case 910 – peak cooling

E.3.1.2.3 Case 920

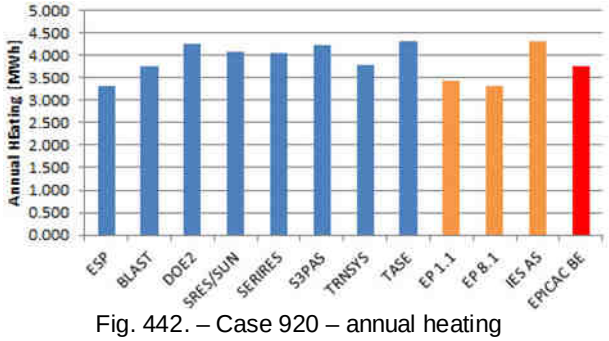

Fig. 442. – Case 920 – annual heating

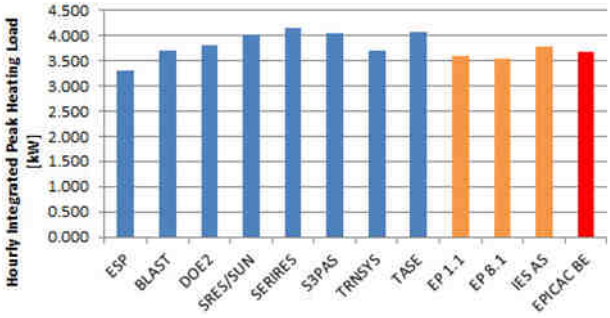

Fig. 443. – Case 920 – peak heating

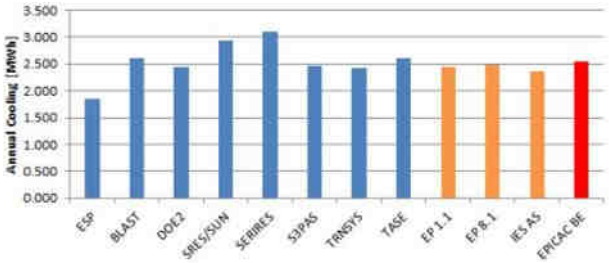

Fig. 444. – Case 920 – annual cooling

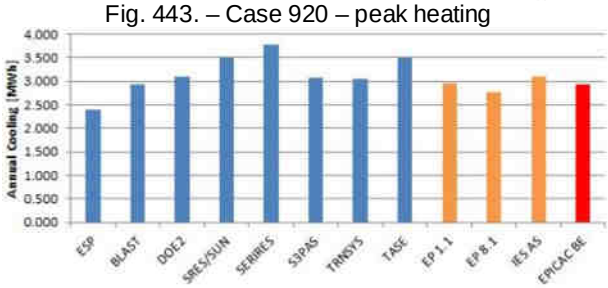

Fig. 445. – Case 920 – peak cooling

E.3.1.2.4 Case 930

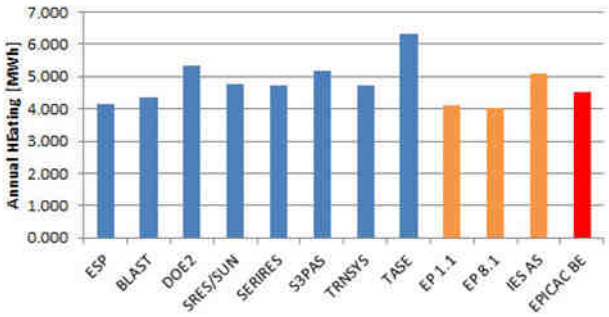

Fig. 446. – Case 930 – annual heating

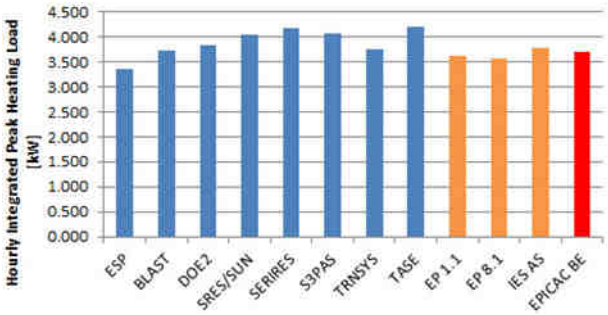

Fig. 447. – Case 930 – peak heating

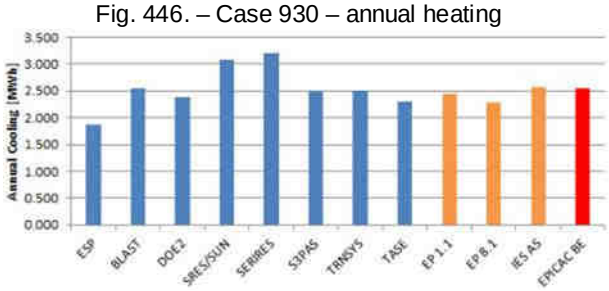

Fig. 448. – Case 930 – annual cooling

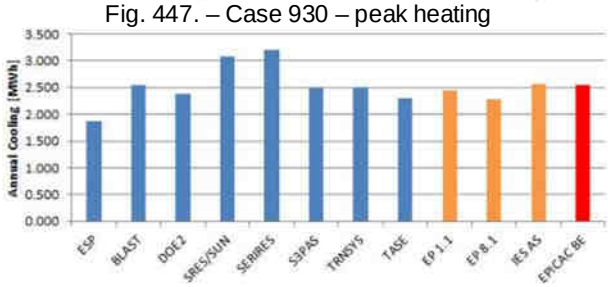

Fig. 449. – Case 930 – peak cooling

E.3.1.2.5 Case 940

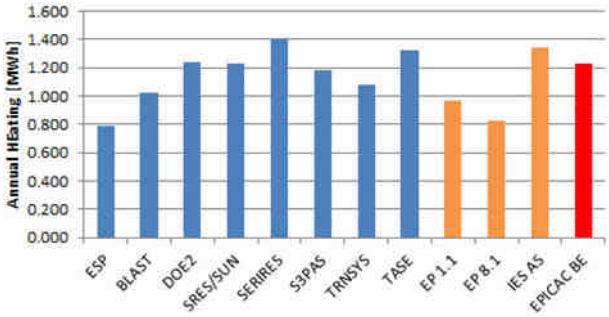

Fig. 450. – Case 940 – annual heating

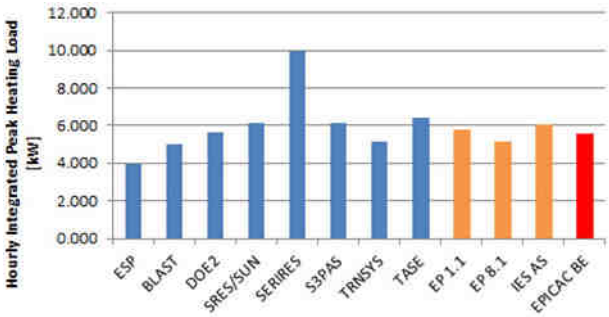

Fig. 451. – Case 940 – peak heating

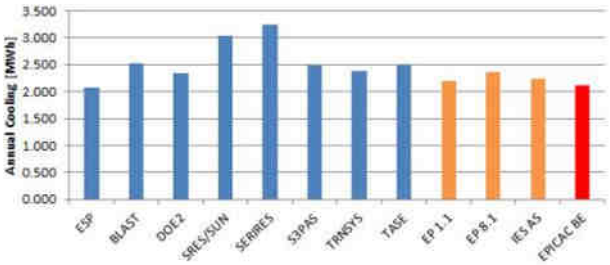

Fig. 452. – Case 940 – annual cooling

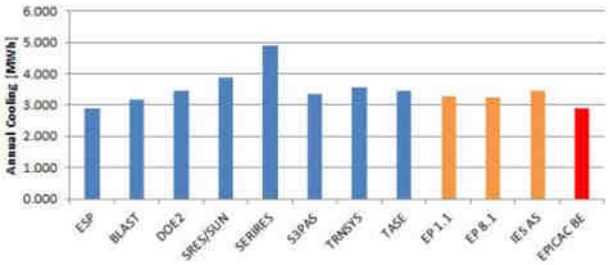

Fig. 453. – Case 940 – peak cooling

E.3.1.2.6 *Case 950*

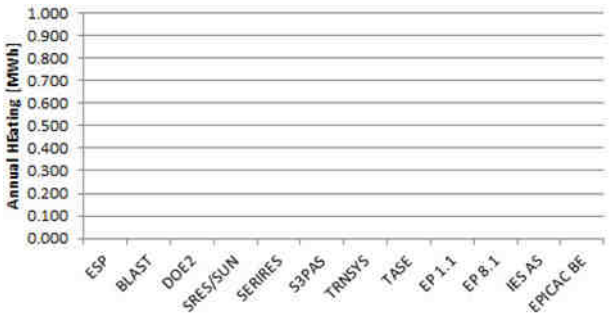

Fig. 454. – Case 950 – annual heating

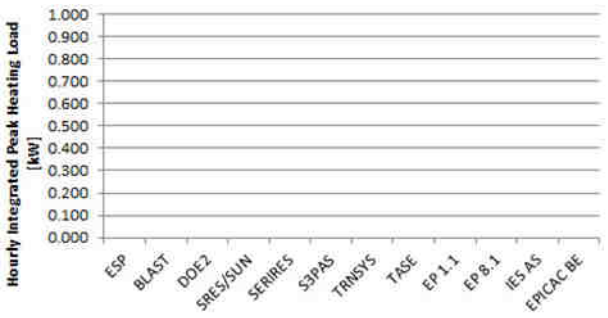

Fig. 455. – Case 950 – peak heating

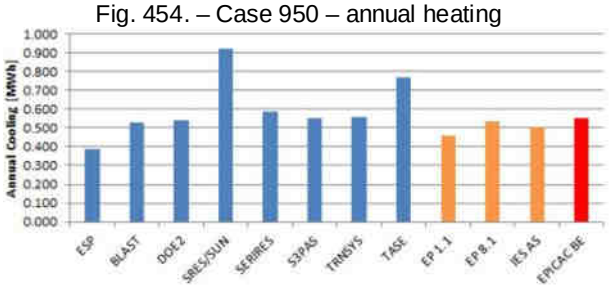

Fig. 456. – Case 950 – annual cooling

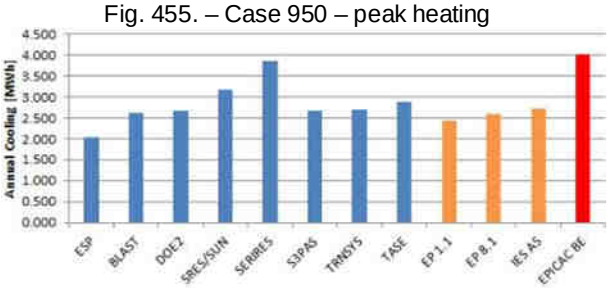

Fig. 457. – Case 950 – peak cooling

E.3.2 Diagnostic test cases

E.3.2.1 *Cases 195*

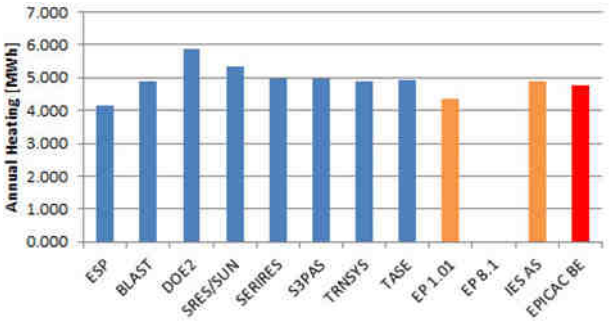

Fig. 458. – Case 195 – annual heating

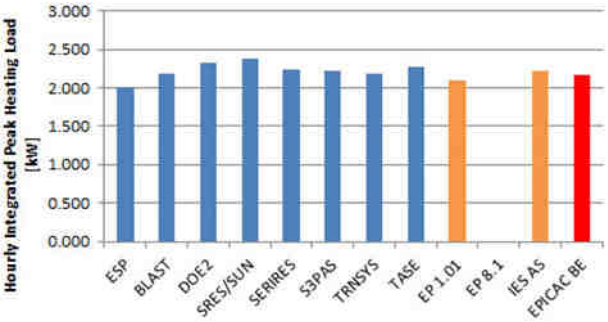

Fig. 459. – Case 195 – peak heating

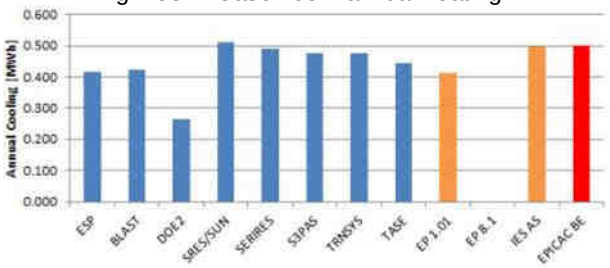

Fig. 460. – Case 195 – annual cooling

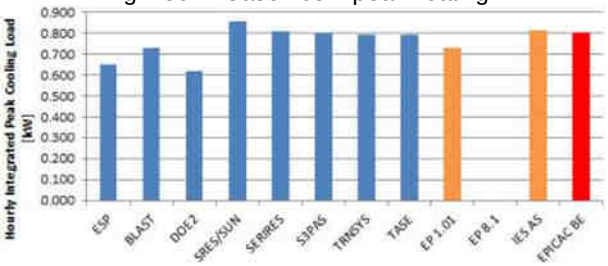

Fig. 461. – Case 195 – peak cooling

E.3.2.2 Cases 200

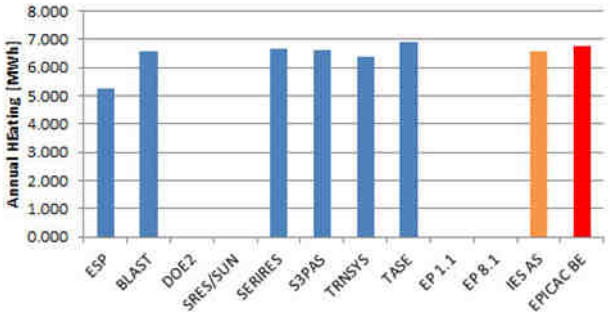

Fig. 462. – Case 200 – annual heating

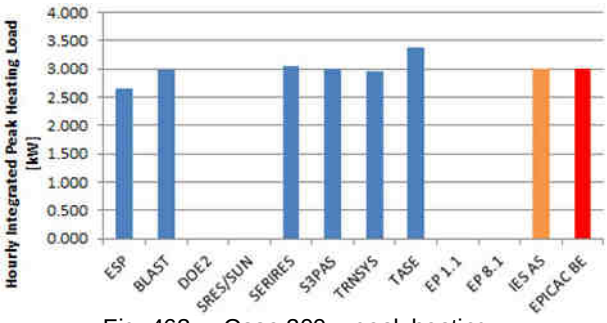

Fig. 463. – Case 200 – peak heating

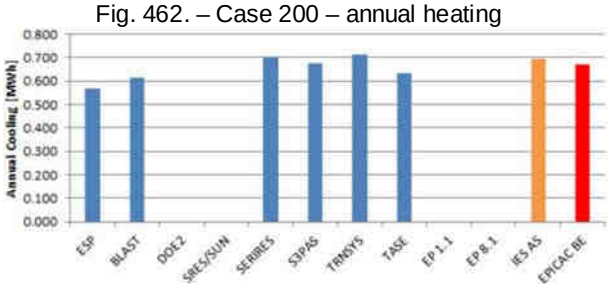

Fig. 464. – Case 200 – annual cooling

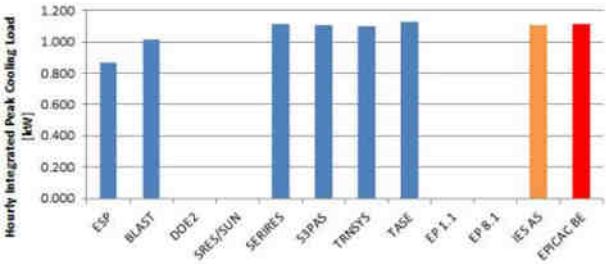

Fig. 465. – Case 200 – peak cooling

E.3.2.3 Cases 210

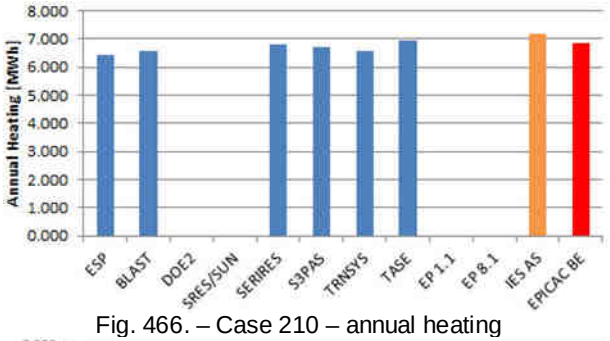

Fig. 466. – Case 210 – annual heating

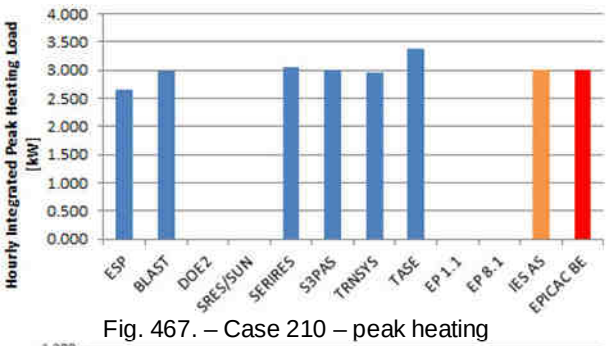

Fig. 467. – Case 210 – peak heating

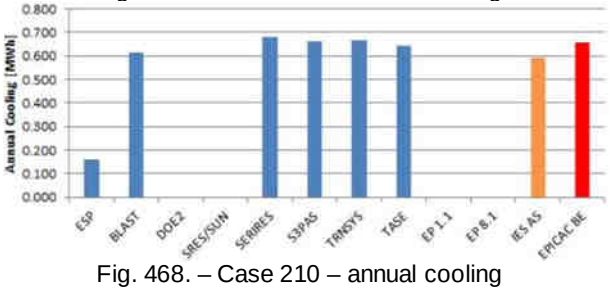

Fig. 468. – Case 210 – annual cooling

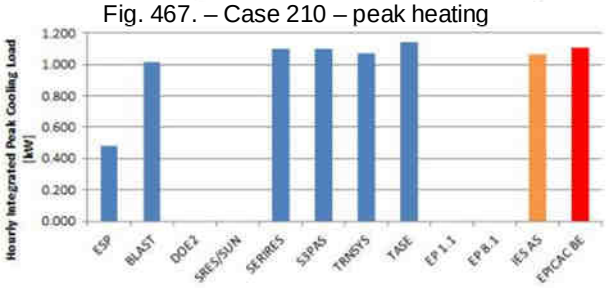

Fig. 469. – Case 210 – peak cooling

E.3.2.4 Cases 215

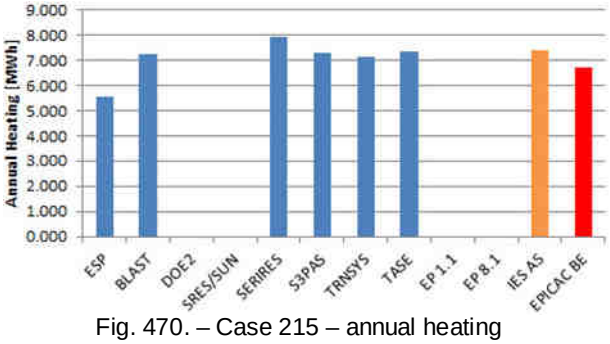

Fig. 470. – Case 215 – annual heating

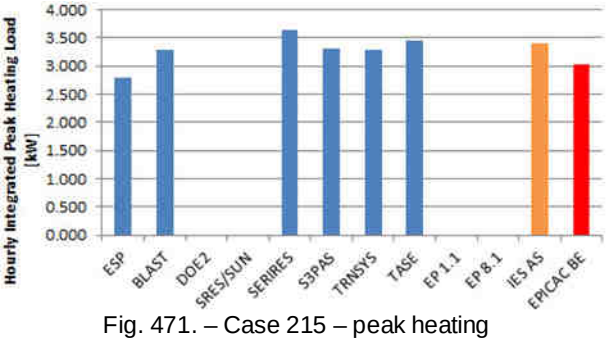

Fig. 471. – Case 215 – peak heating

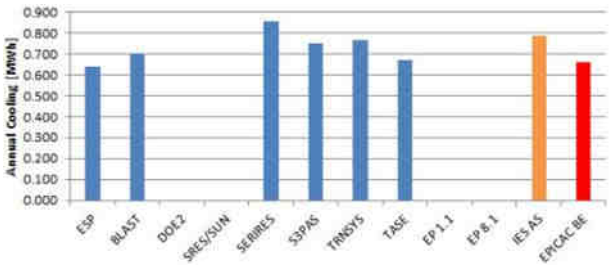

Fig. 472. – Case 215 – annual cooling

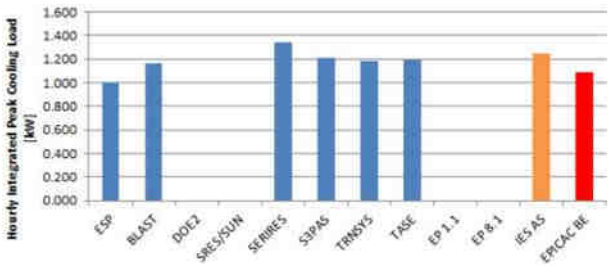

Fig. 473. – Case 215 – peak cooling

E.3.2.5 Cases 220

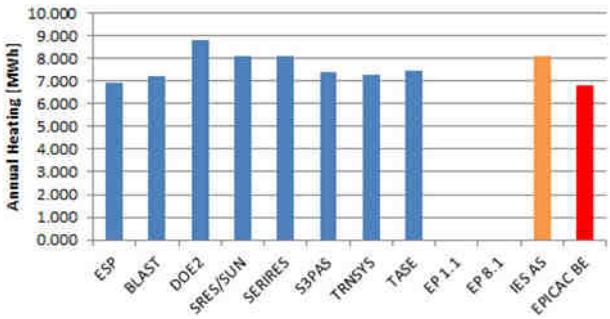

Fig. 474. – Case 220 – annual heating

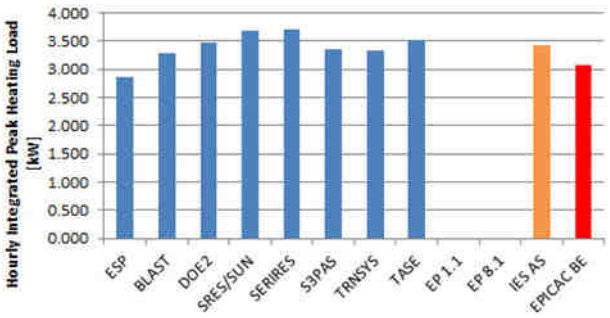

Fig. 475. – Case 220 – peak heating

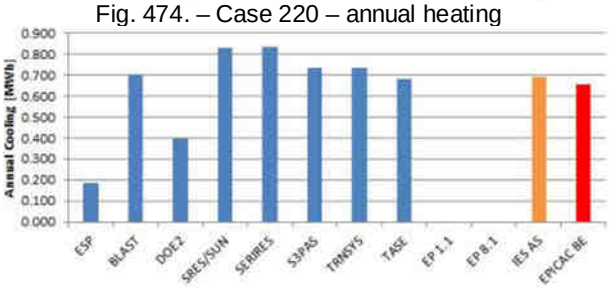

Fig. 476. – Case 220 – annual cooling

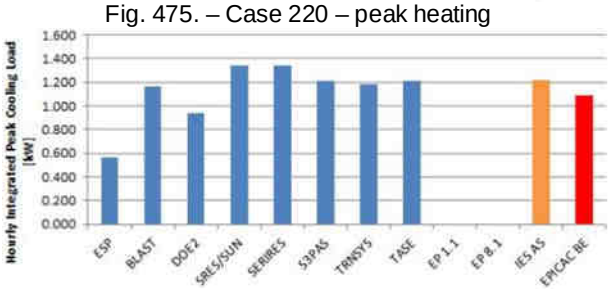

Fig. 477. – Case 220 – peak cooling

E.3.2.6 Cases 230

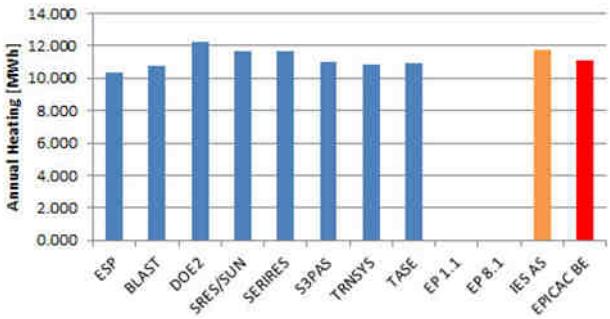

Fig. 478. – Case 230 – annual heating

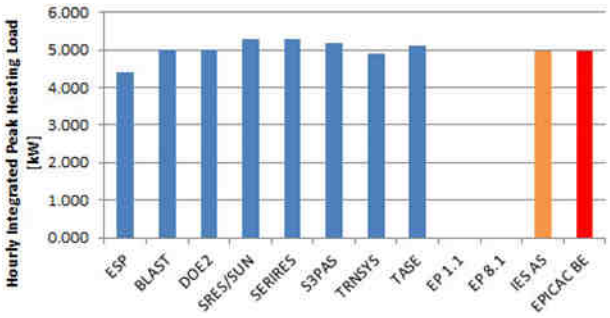

Fig. 479. – Case 230 – peak heating

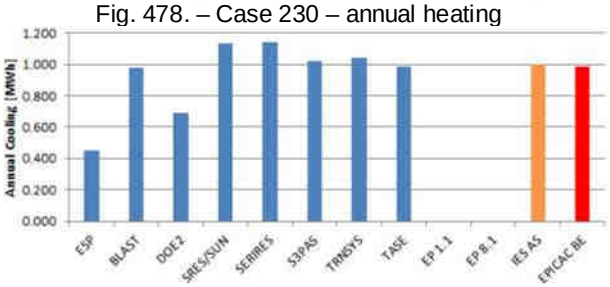

Fig. 480. – Case 230 – annual cooling

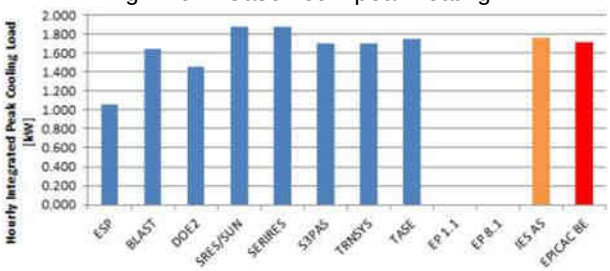

Fig. 481. – Case 230 – peak cooling

E.3.2.7 Cases 240

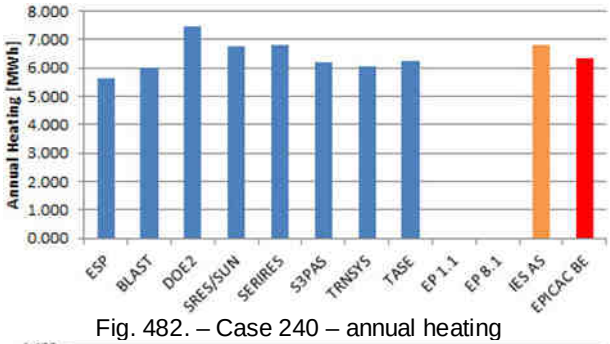

Fig. 482. – Case 240 – annual heating

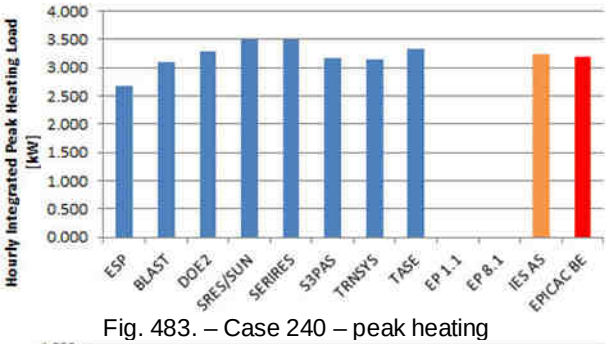

Fig. 483. – Case 240 – peak heating

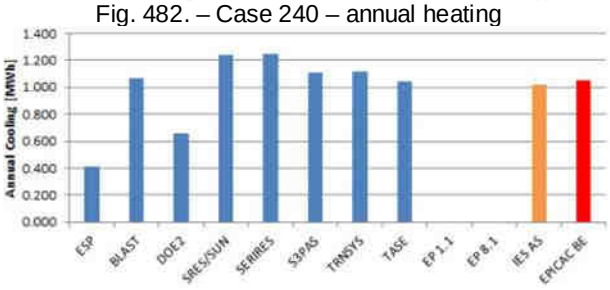

Fig. 484. – Case 240 – annual cooling

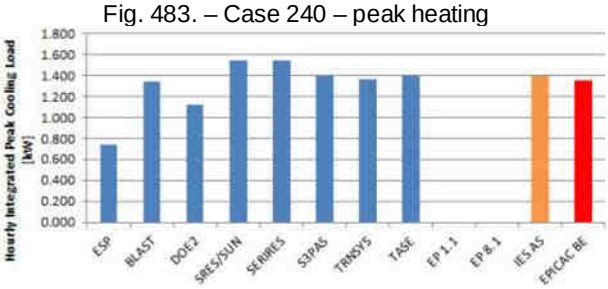

Fig. 485. – Case 240 – peak cooling

E.3.2.8 Cases 270

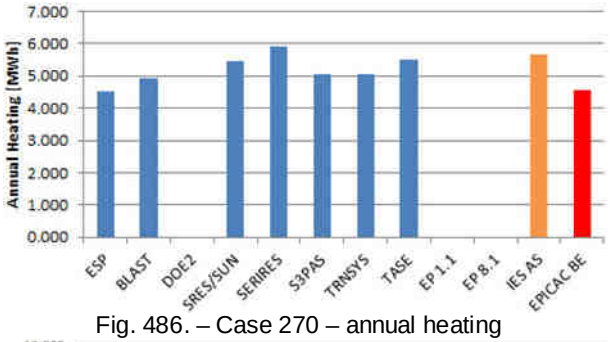

Fig. 486. – Case 270 – annual heating

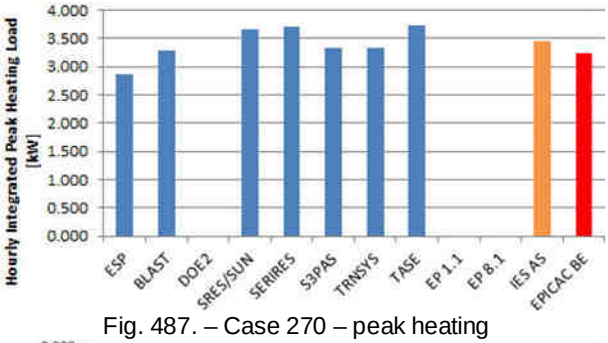

Fig. 487. – Case 270 – peak heating

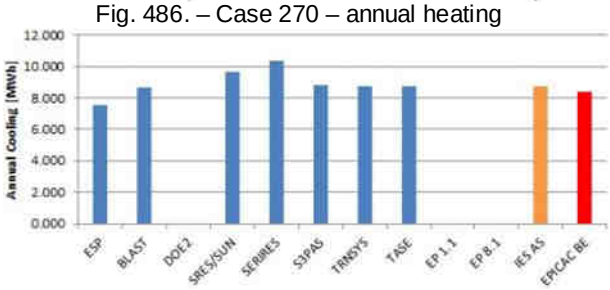

Fig. 488. – Case 270 – annual cooling

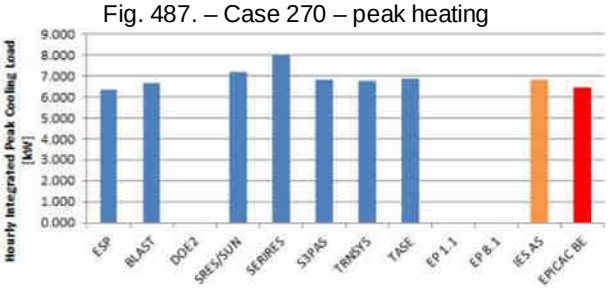

Fig. 489. – Case 270 – peak cooling

E.3.2.9 Cases 280

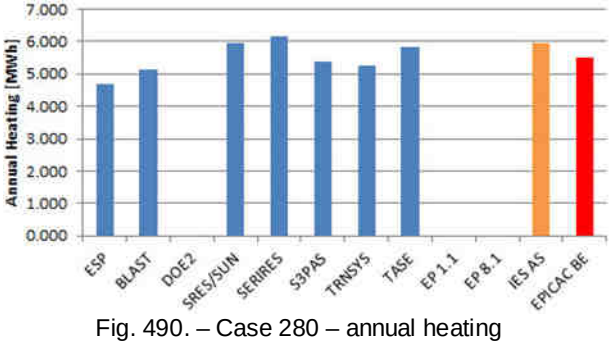

Fig. 490. – Case 280 – annual heating

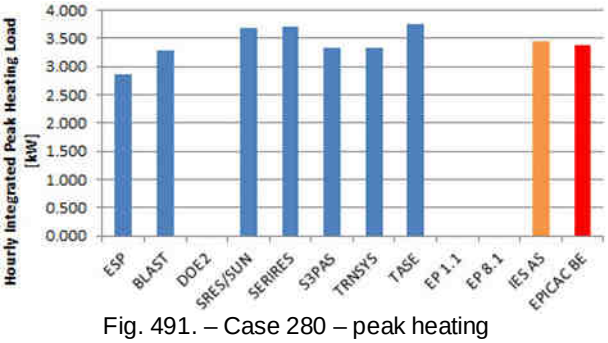

Fig. 491. – Case 280 – peak heating

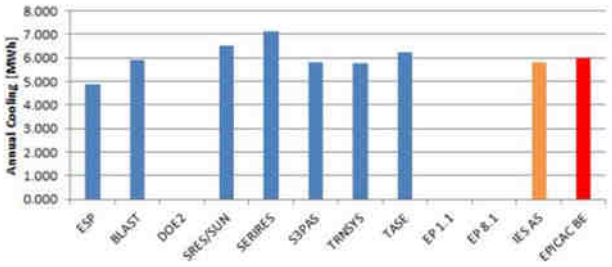

Fig. 492. – Case 280 – annual cooling

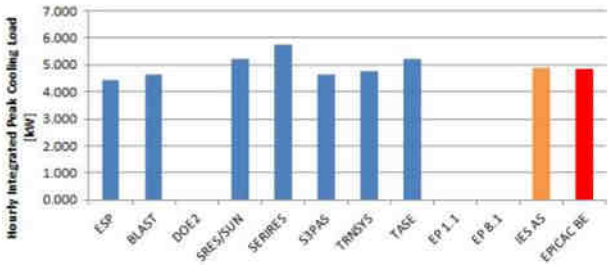

Fig. 493. – Case 280 – peak cooling

E.3.2.10 Cases 290

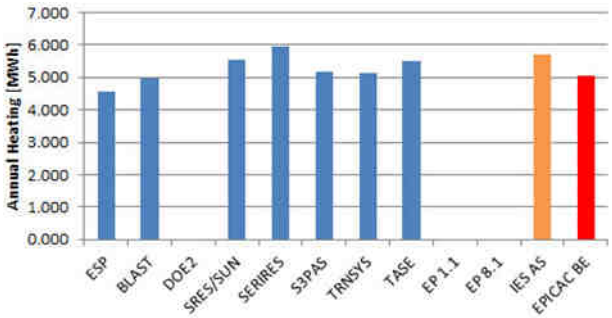

Fig. 494. – Case 290 – annual heating

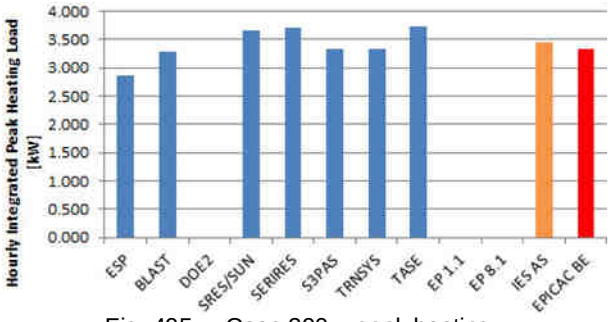

Fig. 495. – Case 290 – peak heating

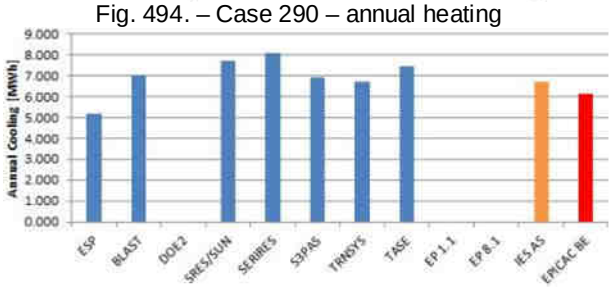

Fig. 496. – Case 290 – annual cooling

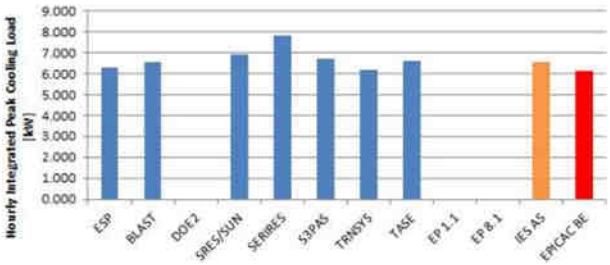

Fig. 497. – Case 290 – peak cooling

E.3.2.11 Cases 300

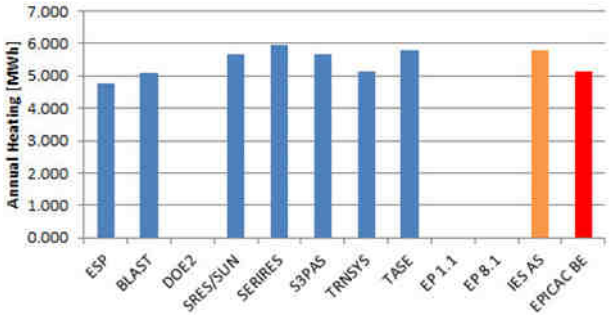

Fig. 498. – Case 300 – annual heating

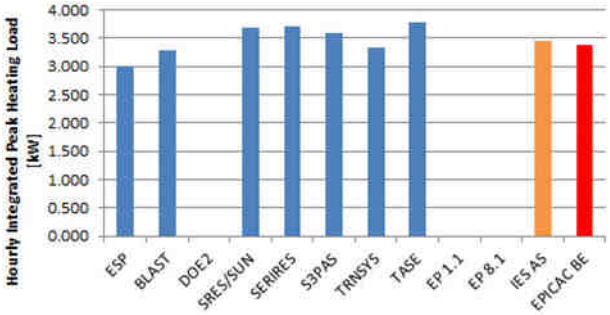

Fig. 499. – Case 300 – peak heating

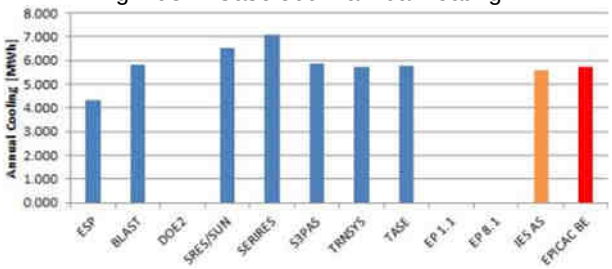

Fig. 500. – Case 300 – annual cooling

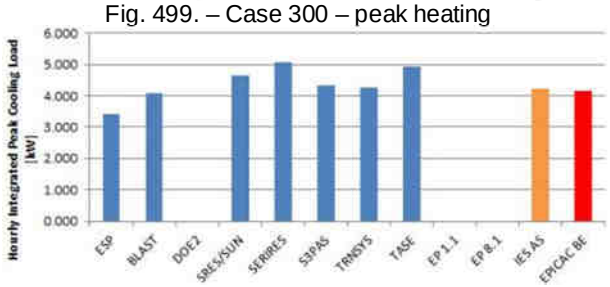

Fig. 501. – Case 300 – peak cooling

E.3.2.12 Cases 310

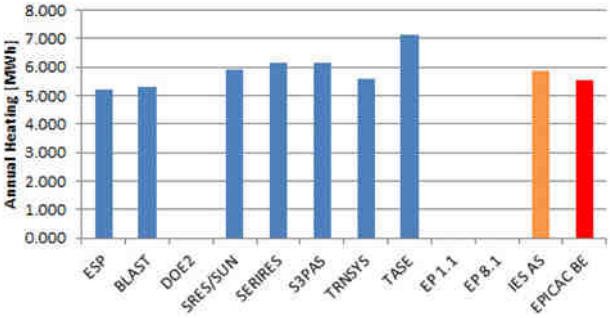

Fig. 502. – Case 310 – annual heating

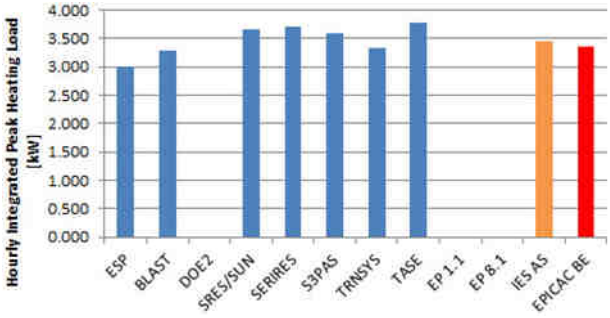

Fig. 503. – Case 310 – peak heating

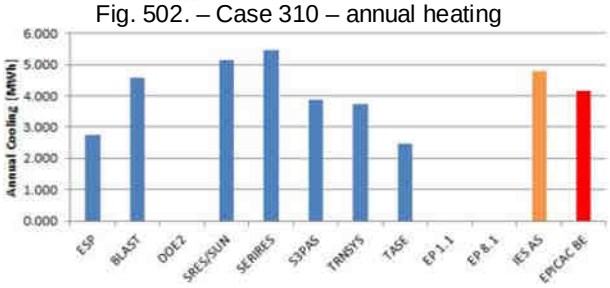

Fig. 504. – Case 310 – annual cooling

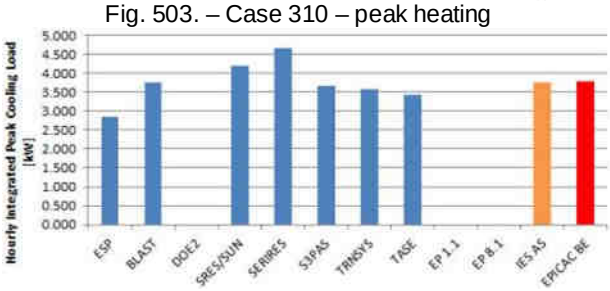

Fig. 505. – Case 310 – peak cooling

E.3.2.13 Cases 320

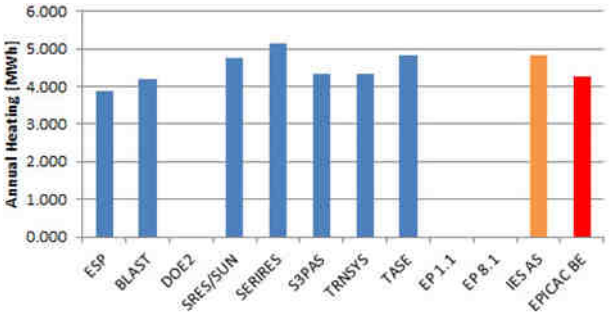

Fig. 506. – Case 320 – annual heating

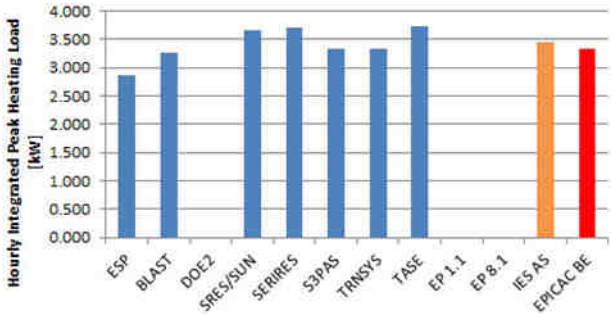

Fig. 507. – Case 320 – peak heating

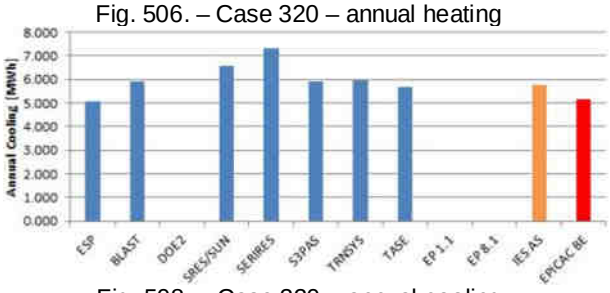

Fig. 508. – Case 320 – annual cooling

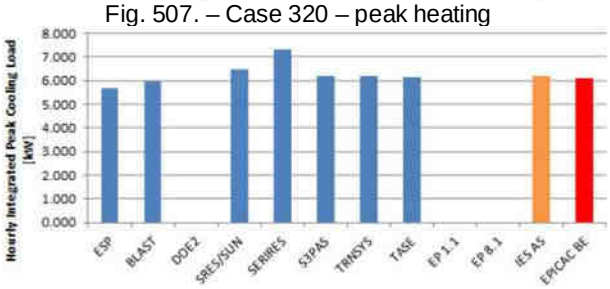

Fig. 509. – Case 320 – peak cooling

E.3.2.14 Cases 395

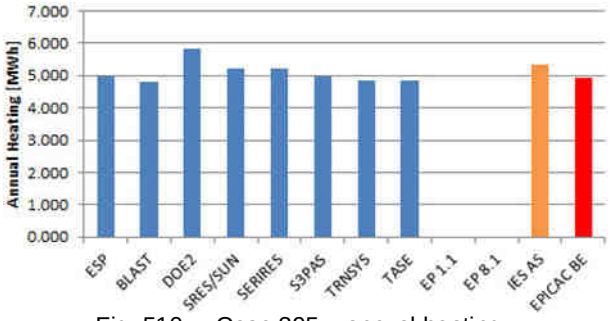

Fig. 510. – Case 395 – annual heating

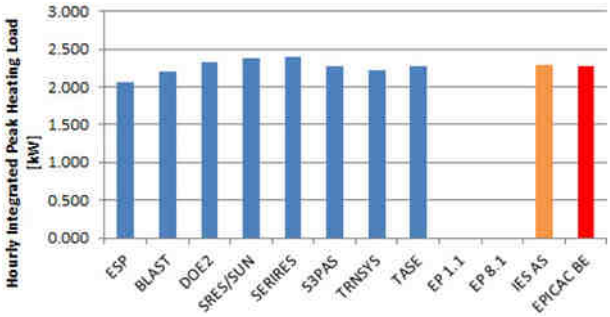

Fig. 511. – Case 395 – peak heating

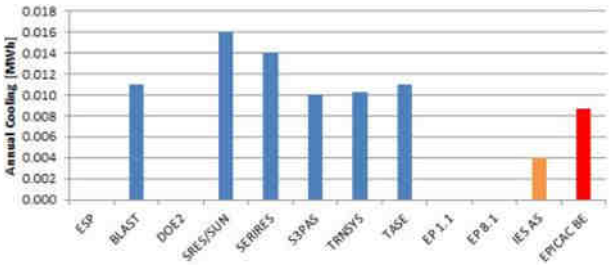

Fig. 512. – Case 395 – annual cooling

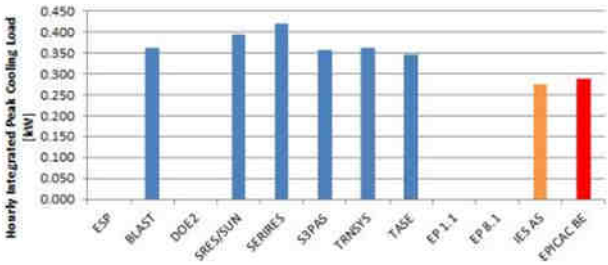

Fig. 513. – Case 395 – peak cooling

E.3.3 Cases with free floating internal temperature

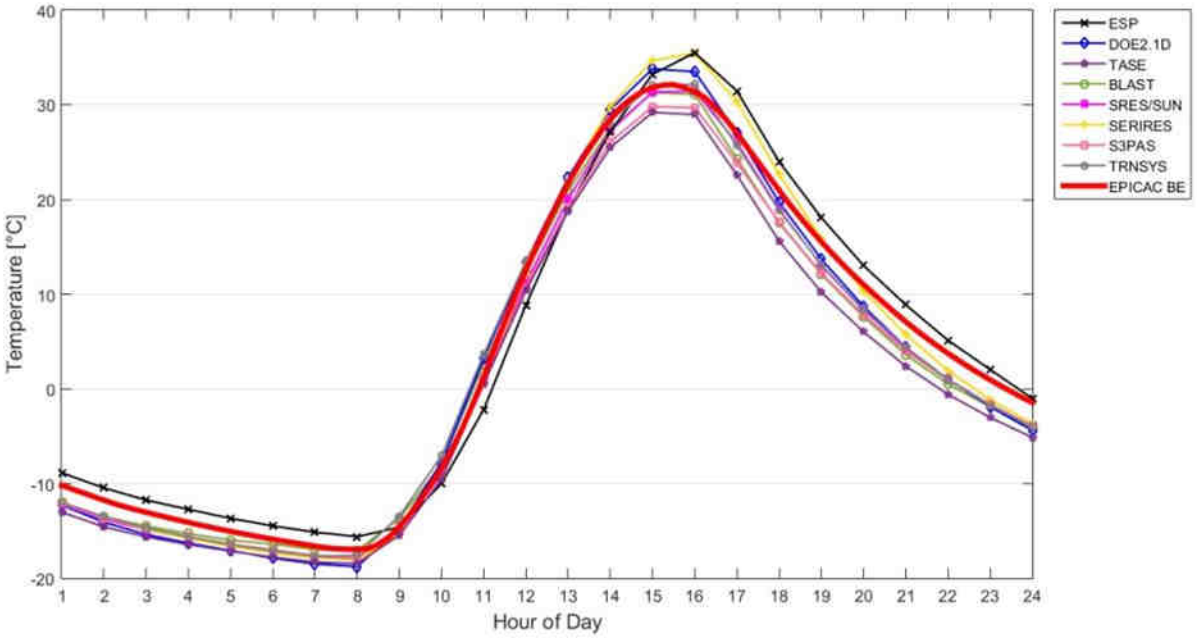

Fig. 514. – Case 600FF – Zone air temperature, clear cold day (January 04)

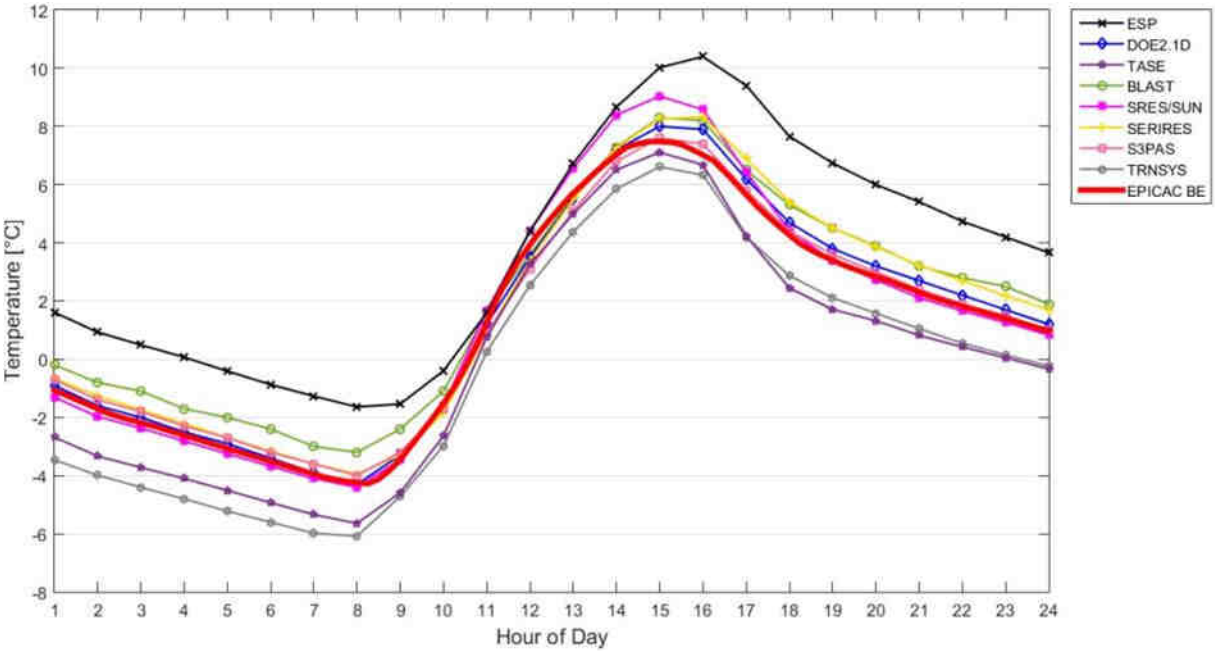

Fig. 515. – Case 900FF – Zone air temperature, clear cold day (January 04)

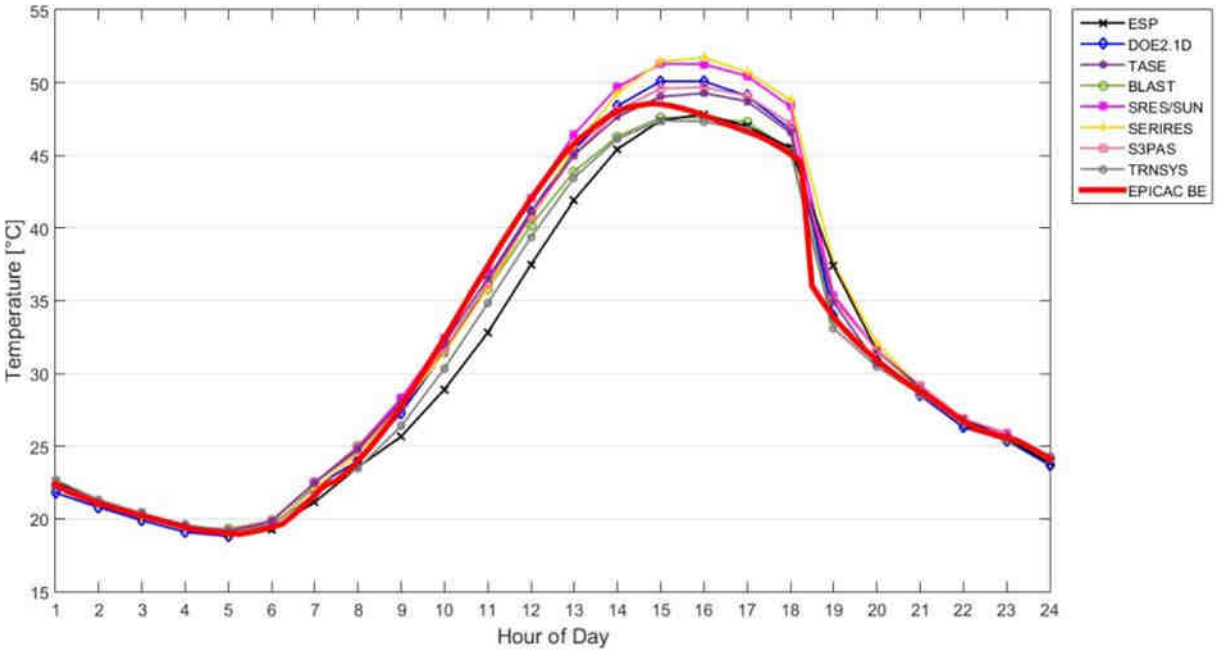

Fig. 516. – Case 650FF – Zone air temperature, clear hot day (July 27)

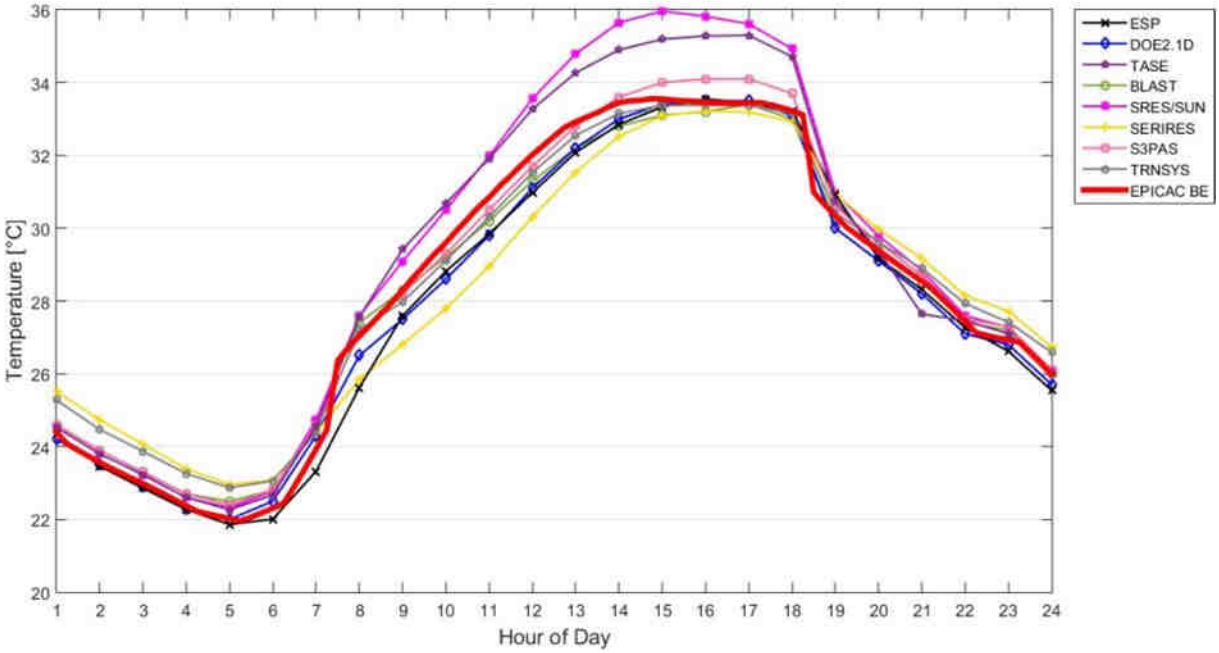

Fig. 517. – Case 950FF – Zone air temperature, clear hot day (July 27)

E.4 Conclusions

EPICAC BE delivered results that were all between the limits of the BESTEST results. The best agreement shown is with the most recent programs EnergyPlus and ApacheSim (data from EnergyPlus is only available for the diagnostic test cases). The accuracy of EPICAC BE for the algorithms and physical phenomena tested for in BESTEST is therefore at least as good as that of the other reference programs.

E.5 References

[4] Judkoff, R.; Neymark, J. (1995) Inetarnational Energy Agency Building Energy Simulation Test (BESTEST) and Diagnostic Method, National Renewable Energy Laboratory, Golden , Colorado, NREL/TP-472-6231

[5] ANSI/ASHRAE Standard 140-2001 (2001) Standard Method of Test for the Evaluation of Building Energy Analysis Computer Programs
[6] Heinriger, R.H., Writte, J.W. (2003) EnergyPlus Testing with ANSI/ASHRAE Standard 140-2001 (BESTEST). EnergyPlus Version 1.1.0.020., Ernest Orlando Lawrence Berkeley National
[7] ANSI/ASHRAE Standard 140-2011 Building Thermal Envelope and Fabric Load Test, DesignBuilder Version 4.2 (incorporating EnergyPlus 8.1.0) (2014)
[8] Gough, M., Rees, C. (2004) Tests performed on ApacheSim in accordance with ANSI/ASHRAE Standard 140-2001, ApacheSim Version 5.2, IES Ltd., Glasgow, UK
[9] Kehrer, M; Schmidt, T. (2008) Radiation Effects On External Surfaces, In: Building Physics 2008 – 8th Nordic Symposium, pp. 207-212
[10] Perez, R., Ineichen, P., Seals, R., Michalsky, J., Stewart, R. (1990) Modeling daylight availability and irradiance components from direct and global irradiance, In: Solar Energy, Vol. 44. (5.), pp. 271–289, DOI: 10.1016/0038-092X(90)90055-H
[11] Marsh, A (2005) The application of shading masks in building simulation, In: Ninth International IBPSA Conference, Montréal, Canada, August 15-15, 2005, pp. 725-732

F (Appendix F) – Window heat balance calculations

F.1 EPICAC BE – Input file example

```
function out = AKA_article_C_6()
%Akadémia - case 007c
%
%glazing: 3*-100-S-100-*3
%   3*mm    hard coated glass - Planibel G 3mm, IGDB 4345
%   83.5mm   air gap
%   33mm     cellular shade
%   83.5mm   air gap
%   *3mm    hard coated glass - Planibel G 3mm, IGDB 4345

%% 1. Header - basic information ----------------------------------------
%%%%%%%%%%%%%%%%%%%%%%%%%%%%%%%%%%%%%%%%%%%%%%%%%%%%%%%%%%%%%%%%%%%%%%%%
%/////////////////////////////////////////////////////////////////////////
%%%%%%%%%%%%%%%%%%%%%%%%%%%%%%%%%%%%%%%%%%%%%%%%%%%%%%%%%%%%%%%%%%%%%%%%
%/////////////////////////////////////////////////////////////////////////
%%%%%%%%%%%%%%%%%%%%%%%%%%%%%%%%%%%%%%%%%%%%%%%%%%%%%%%%%%%%%%%%%%%%%%%%

Input.header.Name='AKA_article_C_6';
Input.header.Notes='Akadémia article - optimal refurbishment';
Input.header.OutputFilename='AKA_article_C_6';
Input.header.DataFolder='c:\BME\PHD\2015-2016-
1\DistributedComputing\Data\';
Input.header.OutputFolder='c:\BME\PHD\2015-2016-
1\DistributedComputing\Output_Article\';
Input.header.TotalHeatedArea=23.36;%[m2]
Input.header.TotalHeatedVolume=23.36*5.71;%[m3]

%% 2. Simulation Settings -----------------------------------------------
%%%%%%%%%%%%%%%%%%%%%%%%%%%%%%%%%%%%%%%%%%%%%%%%%%%%%%%%%%%%%%%%%%%%%%%%
%/////////////////////////////////////////////////////////////////////////
%%%%%%%%%%%%%%%%%%%%%%%%%%%%%%%%%%%%%%%%%%%%%%%%%%%%%%%%%%%%%%%%%%%%%%%%
%/////////////////////////////////////////////////////////////////////////
%%%%%%%%%%%%%%%%%%%%%%%%%%%%%%%%%%%%%%%%%%%%%%%%%%%%%%%%%%%%%%%%%%%%%%%%

Input.settings.plotplots=1;
Input.settings.saveobj=1;
Input.settings.Mode='climatefile';%climatefile,sizing
Input.settings.ZoneScheme='analytical';%Euler,TOB,analytical
Input.settings.ShadeMode=1;%precalculated Shading Masks
Input.settings.SkyDomeDelta=2;%[°] - resolution of sky dome subdivision for
Shading Mask calculation
Input.settings.VentMode=3;%empirical single-sided ventilation model
Input.settings.Ground=1;%ground contact calculation mode
Input.settings.GroundT=10;%[°C] - constant ground temperature
Input.settings.Warmup=1;%0 - no Warmup calculation, 1 - do warmup
calculation
Input.settings.IntSolDistr=2;%Internal Solar Distribution caclulation mode,
2 - view factor weighted
Input.settings.IntLwRadMethod=2;%detailed exchange matrix

%% 3. Simulation Time ---------------------------------------------------
%%%%%%%%%%%%%%%%%%%%%%%%%%%%%%%%%%%%%%%%%%%%%%%%%%%%%%%%%%%%%%%%%%%%%%%%
%/////////////////////////////////////////////////////////////////////////
%%%%%%%%%%%%%%%%%%%%%%%%%%%%%%%%%%%%%%%%%%%%%%%%%%%%%%%%%%%%%%%%%%%%%%%%
```

```
%//////////////////////////////////////////////////////////////////////////
%%%%%%%%%%%%%%%%%%%%%%%%%%%%%%%%%%%%%%%%%%%%%%%%%%%%%%%%%%%%%%%%%%%%%%%%

Input.time.dt=15*60;%[s]
Input.time.t0=0;%[s]
Input.time.tend=60*60*24*365;%[s]
Input.time.UTC=+2;%[h] hours from GMT, Eastern European Timezone +1

%% 4. Location ---------------------------------------------------------
%%%%%%%%%%%%%%%%%%%%%%%%%%%%%%%%%%%%%%%%%%%%%%%%%%%%%%%%%%%%%%%%%%%%%%%%
%//////////////////////////////////////////////////////////////////////////
%%%%%%%%%%%%%%%%%%%%%%%%%%%%%%%%%%%%%%%%%%%%%%%%%%%%%%%%%%%%%%%%%%%%%%%%
%//////////////////////////////////////////////////////////////////////////
%%%%%%%%%%%%%%%%%%%%%%%%%%%%%%%%%%%%%%%%%%%%%%%%%%%%%%%%%%%%%%%%%%%%%%%%

Input.location.RelNorth=-8;%[°] - angle between the north and the building
y axes
Input.location.Latitude=47.26;%[°] - szélesség (északi pozitív)
Input.location.Longitude=19.11;%[°] - hosszúság (keleti pozitív)
Input.location.Altitude=140;%[m]
Input.location.terrain='urban';%type of the surrounding terrain for wind
speed correction
Input.location.Hbuilding=22;%[m] - the height of the building
Input.location.Cp=[0.8, -0.04, -0.11, -0.11];%Cp1(fi=0) Cp2(fi=180)
Cp3(fi=90) Cp4(fi=270)
Input.location.Albedo=0.2;%[-]
Input.location.Horizon.Input=...
    [0 360;...
    5 5];
Input.location.eps_ground=0.9;%[-] - ground longwave infrared emissivity
Input.location.rho_ground=0.1;%[-] - ground longwave infrared reflectivity

%% 5. Numerical Controls -----------------------------------------------
%%%%%%%%%%%%%%%%%%%%%%%%%%%%%%%%%%%%%%%%%%%%%%%%%%%%%%%%%%%%%%%%%%%%%%%%
%//////////////////////////////////////////////////////////////////////////
%%%%%%%%%%%%%%%%%%%%%%%%%%%%%%%%%%%%%%%%%%%%%%%%%%%%%%%%%%%%%%%%%%%%%%%%
%//////////////////////////////////////////////////////////////////////////
%%%%%%%%%%%%%%%%%%%%%%%%%%%%%%%%%%%%%%%%%%%%%%%%%%%%%%%%%%%%%%%%%%%%%%%%

Input.num.ZoneMaxIter=20;% maximum number of iterations for the zone air
heat balance
Input.num.ZoneTCC=1e-2;%[K] - convergence criteria for the zone air heat
balance calculation
Input.num.WarmupDayMax=40;%[d] - maximum number of warmup days
Input.num.WarmupDayMin=6;%[d] - minimum number of warmup days
Input.num.WarmupMaxTDelta=0.5;%[K] - Warmup convergence check - maximum
temperature Delta T
Input.num.WarmupMinTDelta=0.5;%[K] - Warmup convergence check - minimum
temperature Delta T
Input.num.WarmupQtol=0.005;%[%] - Warmup load convergence tolerance

%% 6. Climate Data -----------------------------------------------------
%%%%%%%%%%%%%%%%%%%%%%%%%%%%%%%%%%%%%%%%%%%%%%%%%%%%%%%%%%%%%%%%%%%%%%%%
%//////////////////////////////////////////////////////////////////////////
%%%%%%%%%%%%%%%%%%%%%%%%%%%%%%%%%%%%%%%%%%%%%%%%%%%%%%%%%%%%%%%%%%%%%%%%
%//////////////////////////////////////////////////////////////////////////
%%%%%%%%%%%%%%%%%%%%%%%%%%%%%%%%%%%%%%%%%%%%%%%%%%%%%%%%%%%%%%%%%%%%%%%%

Input.climate.FilePath='Climate\Budapest.wac';
```

```
%% 7. Constructions ------------------------------------------------------
%%%%%%%%%%%%%%%%%%%%%%%%%%%%%%%%%%%%%%%%%%%%%%%%%%%%%%%%%%%%%%%%%%%%%%%%
%/////////////////////////////////////////////////////////////////////////
%%%%%%%%%%%%%%%%%%%%%%%%%%%%%%%%%%%%%%%%%%%%%%%%%%%%%%%%%%%%%%%%%%%%%%%%
%/////////////////////////////////////////////////////////////////////////
%%%%%%%%%%%%%%%%%%%%%%%%%%%%%%%%%%%%%%%%%%%%%%%%%%%%%%%%%%%%%%%%%%%%%%%%

%::::::::::::::::::::::::::::::::::::::::::::::::::::::::::::::::::::::::
%% 7.1. D1.................................................................
%.........................................................................
%% 7.1.1. Z1_WestWall
i=1;
Input.constr.D1(i).Name='WestWall';
Input.constr.D1(i).Type='ExtrWall';
Input.constr.D1(i).InputType=2;%Input structure
Input.constr.D1(i).InputFilePath=[];
Input.constr.D1(i).InputStruct=D1InputGen_KulsoFalElsoEmelet();
Input.constr.D1(i).MatFilePath=[];
Input.constr.D1(i).MatStruct=MatdataGen();
Input.constr.D1(i).A=4.06*5.71;%[m2]
Input.constr.D1(i).Azimuth=270;%[°] from north towards the east
Input.constr.D1(i).Inclination=90;%[°C] from the horizontal
Input.constr.D1(i).Depth=0;%[m] - depth in ground for ground contact
calculation
Input.constr.D1(i).Vertices=[...
    -5.9586,-0.0181, 0;...
    -5.7602,-4.0766,0;...
    -5.7602,-4.0766,5.71;...
    -5.9586,-0.0181,5.71;...
    -5.9586,-0.0181, 0];
Input.constr.D1(i).BC1Air=0;            %BC 1 - air connection
Input.constr.D1(i).BC1IR=0;             %BC 1 - IR connection
Input.constr.D1(i).BC1Sol=1;            %BC 1 - Direct solar gain from the
Input.constr.D1(i).BC1Shade=0;          %BC 1 - Shading
Input.constr.D1(i).BC1Ground=0;         %BC 1 - Ground contact
Input.constr.D1(i).BC1FluxDir=1;        %BC 1 - heat flux direction – hor.
Input.constr.D1(i).BC2Air=1;            %BC 2 - air connection
Input.constr.D1(i).BC2IR=1;             %BC 2 - IR connection
Input.constr.D1(i).BC2Sol=0;            %BC 2 - Direct solar gain from the
Input.constr.D1(i).BC2Shade=0;          %BC 2 - Shading
Input.constr.D1(i).BC2Ground=0;         %BC 2 - Ground contact
Input.constr.D1(i).BC2FluxDir=1;        %BC 1 - heat flux direction – hor.

%.........................................................................
%% 7.1.2. Z1_SouthWall
i=2;
Input.constr.D1(i).Name='Z1_SouthWall';
Input.constr.D1(i).Type='PartWall';
Input.constr.D1(i).InputType=2;%Input structure
Input.constr.D1(i).InputFilePath=[];
Input.constr.D1(i).InputStruct=D1InputGen_Valaszfal1();
Input.constr.D1(i).MatFilePath=[];
Input.constr.D1(i).MatStruct=MatdataGen();
Input.constr.D1(i).A=5.9524*5.71;%[m]
Input.constr.D1(i).Azimuth=180;%[°] from north towards the east
Input.constr.D1(i).Inclination=90;%[°C] from the horizontal
Input.constr.D1(i).Depth=0;%[m] - depth in ground for ground contact
calculation
Input.constr.D1(i).Vertices=[...
    -5.7602,-4.0766,0;...
    0.1851,-3.7860,0;...
```

```
    0.1851,-3.7860,5.71;...
    -5.7602,-4.0766,5.71;...
    -5.7602,-4.0766,0];
Input.constr.D1(i).BC1Air=0;            %BC 1 - air connection
Input.constr.D1(i).BC1IR=0;             %BC 1 - IR connection
Input.constr.D1(i).BC1Sol=0;            %BC 1 - Direct solar gain from the
Input.constr.D1(i).BC1Shade=0;          %BC 1 - Shading
Input.constr.D1(i).BC1Ground=0;         %BC 1 - Ground contact
Input.constr.D1(i).BC1FluxDir=1;        %BC 1 - heat flux direction – hor.
Input.constr.D1(i).BC2Air=1;            %BC 2 - air connection
Input.constr.D1(i).BC2IR=1;             %BC 2 - IR connection
Input.constr.D1(i).BC2Sol=0;            %BC 2 - Direct solar gain from the
Input.constr.D1(i).BC2Shade=0;          %BC 2 - Shading
Input.constr.D1(i).BC2Ground=0;         %BC 2 - Ground contact
Input.constr.D1(i).BC2FluxDir=1;        %BC 2 - heat flux direction – hor.

%.....................................................................
%% 7.1.3. Z1_EastWall
i=3;
Input.constr.D1(i).Name='Z1_EastWall';
Input.constr.D1(i).Type='PartWall';
Input.constr.D1(i).InputType=2;%Input structure
Input.constr.D1(i).InputFilePath=[];
Input.constr.D1(i).InputStruct=D1InputGen_Valaszfal1();
Input.constr.D1(i).MatFilePath=[];
Input.constr.D1(i).MatStruct=MatdataGen();
Input.constr.D1(i).A=3.7905*5.71;%[m]
Input.constr.D1(i).Azimuth=90;%[°] from north towards the east
Input.constr.D1(i).Inclination=90;%[°C] from the horizontal
Input.constr.D1(i).Depth=0;%[m] - depth in ground for ground contact
calculation
Input.constr.D1(i).Vertices=[...
    0.1851,-3.7860,0;...
    0,0,0;...
    0,0,5.71;...
    0.1851,-3.7860,5.71;...
    0.1851,-3.7860,0];
Input.constr.D1(i).BC1Air=0;            %BC 1 - air connection
Input.constr.D1(i).BC1IR=0;             %BC 1 - IR connection
Input.constr.D1(i).BC1Sol=0;            %BC 1 - Direct solar gain from the
Input.constr.D1(i).BC1Shade=0;          %BC 1 - Shading
Input.constr.D1(i).BC1Ground=0;         %BC 1 - Ground contact
Input.constr.D1(i).BC1FluxDir=1;        %BC 1 - heat flux direction – hor.
Input.constr.D1(i).BC2Air=1;            %BC 2 - air connection
Input.constr.D1(i).BC2IR=1;             %BC 2 - IR connection
Input.constr.D1(i).BC2Sol=0;            %BC 2 - Direct solar gain from the
Input.constr.D1(i).BC2Shade=0;          %BC 2 - Shading
Input.constr.D1(i).BC2Ground=0;         %BC 2 - Ground contact
Input.constr.D1(i).BC2FluxDir=1;        %BC 2 - heat flux direction – hor.

%.....................................................................
%% 7.1.4. Z1_NorthWall
i=4;
Input.constr.D1(i).Name='Z1_NorthWall';
Input.constr.D1(i).Type='PartWall';
Input.constr.D1(i).InputType=2;%Input structure
Input.constr.D1(i).InputFilePath=[];
Input.constr.D1(i).InputStruct=D1InputGen_Valaszfal1();
Input.constr.D1(i).MatFilePath=[];
Input.constr.D1(i).MatStruct=MatdataGen();
Input.constr.D1(i).A=5.9586*5.71;%[m]
```

```
Input.constr.D1(i).Azimuth=0;%[°] from north towards the east
Input.constr.D1(i).Inclination=90;%[°C] from the horizontal
Input.constr.D1(i).Depth=0;%[m] - depth in ground for ground contact
calculation
Input.constr.D1(i).Vertices=[...
    0,0,0;...
    -5.9586,-0.0181,0;...
    -5.9586,-0.0181,5.71;...
    0,0,5.71;...
    0,0,0];
Input.constr.D1(i).BC1Air=0;            %BC 1 - air connection
Input.constr.D1(i).BC1IR=0;             %BC 1 - IR connection
Input.constr.D1(i).BC1Sol=0;            %BC 1 - Direct solar gain from the
Input.constr.D1(i).BC1Shade=0;          %BC 1 - Shading
Input.constr.D1(i).BC1Ground=0;         %BC 1 - Ground contact
Input.constr.D1(i).BC1FluxDir=1;        %BC 1 - heat flux direction – hor.
Input.constr.D1(i).BC2Air=1;            %BC 2 - air connection
Input.constr.D1(i).BC2IR=1;             %BC 2 - IR connection
Input.constr.D1(i).BC2Sol=0;            %BC 2 - Direct solar gain from the
Input.constr.D1(i).BC2Shade=0;          %BC 2 - Shading
Input.constr.D1(i).BC2Ground=0;         %BC 2 - Ground contact
Input.constr.D1(i).BC2FluxDir=1;        %BC 2 - heat flux direction – hor.

%.....................................................................
%% 7.1.5. Z1_RoofSlab
i=5;
Input.constr.D1(i).Name='Z1_RoofSlab';
Input.constr.D1(i).Type='PartSlab';
Input.constr.D1(i).InputType=2;%Input structure
Input.constr.D1(i).InputFilePath=[];
Input.constr.D1(i).InputStruct=D1InputGen_Plafon1();
Input.constr.D1(i).MatFilePath=[];
Input.constr.D1(i).MatStruct=MatdataGen();
Input.constr.D1(i).A=23.36;%[m]
Input.constr.D1(i).Azimuth=0;%[°] from north towards the east
Input.constr.D1(i).Depth=0;%[m] - depth in ground for ground contact
calculation
Input.constr.D1(i).Inclination=0;%[°C] from the horizontal
Input.constr.D1(i).Vertices=[...
    -5.9586,-0.0181,5.71;...
    -5.7602,-4.0766,5.71;...
    0.1851,-3.7860,5.71;...
    0,0,5.71;...
    -5.9586,-0.0181,5.71];
Input.constr.D1(i).BC1Air=0;            %BC 1 - air connection
Input.constr.D1(i).BC1IR=0;             %BC 1 - IR connection
Input.constr.D1(i).BC1Sol=0;            %BC 1 - Direct solar gain from the
Input.constr.D1(i).BC1Shade=0;          %BC 1 - Shading
Input.constr.D1(i).BC1Ground=0;         %BC 1 - Ground contact
Input.constr.D1(i).BC1FluxDir=3;        %BC 1 - heat flux direction -
stable stratification
Input.constr.D1(i).BC2Air=1;            %BC 2 - air connection
Input.constr.D1(i).BC2IR=1;             %BC 2 - IR connection
Input.constr.D1(i).BC2Sol=0;            %BC 2 - Direct solar gain from the
Input.constr.D1(i).BC2Shade=0;          %BC 2 - Shading
Input.constr.D1(i).BC2Ground=0;         %BC 2 - Ground contact
Input.constr.D1(i).BC2FluxDir=2;        %BC 2 - heat flux direction -
unstable stratification

%.....................................................................
%% 7.1.6. Z1_FloorSlab
```

```
i=6;
Input.constr.D1(i).Name='Z1_FloorSlab';
Input.constr.D1(i).Type='FloorSlab';
Input.constr.D1(i).InputType=2;%Input structure
Input.constr.D1(i).InputFilePath=[];
Input.constr.D1(i).InputStruct=D1InputGen_Padlo1();
Input.constr.D1(i).MatFilePath=[];
Input.constr.D1(i).MatStruct=MatdataGen();
Input.constr.D1(i).A=23.36;%[m]
Input.constr.D1(i).Azimuth=0;%[°] from north towards the east
Input.constr.D1(i).Depth=1;%[m] - depth in ground for ground contact
calculation
Input.constr.D1(i).Inclination=0;%[°C] from the horizontal
Input.constr.D1(i).Vertices=[...
    -5.9586,-0.0181,0
    -5.7602,-4.0766,0;...
    0.1851,-3.7860,0;...
    0,0,0;...
    -5.9586,-0.0181,0];
Input.constr.D1(i).BC1Air=1;            %BC 1 - air connection
Input.constr.D1(i).BC1IR=1;             %BC 1 - IR connection
Input.constr.D1(i).BC1Sol=0;            %BC 1 - Direct solar gain from the
Input.constr.D1(i).BC1Shade=0;          %BC 1 - Shading
Input.constr.D1(i).BC1Ground=0;         %BC 1 - Ground contact
Input.constr.D1(i).BC1FluxDir=3;        %BC 1 - heat flux direction -
stable stratification
Input.constr.D1(i).BC2Air=0;            %BC 2 - air connection
Input.constr.D1(i).BC2IR=0;             %BC 2 - IR connection
Input.constr.D1(i).BC2Sol=0;            %BC 2 - Direct solar gain from the
Input.constr.D1(i).BC2Shade=0;          %BC 2 - Shading
Input.constr.D1(i).BC2Ground=0;         %BC 2 - Ground contact
Input.constr.D1(i).BC2FluxDir=2;        %BC 2 - heat flux direction -
unstable stratification

%:::::::::::::::::::::::::::::::::::::::::::::::::::::::::::::::::::::::::
%% 7.2. Window ..........................................................
Input.stuff.numWin=1;   %number of windows

%.......................................................................
%% 7.2.1. Z1_Window1 (western facade)
i=1;
Input.constr.Win(i).Name='Western facade window';
Input.constr.Win(i).Mode='ISO';%Mode: 'simple' 'ISO'
Input.constr.Win(i).InputType=2;
Input.constr.Win(i).InputFilePath=[];
Input.constr.Win(i).InputStruct=WinInputGen_Uveg4(Input.header.DataFolder);
Input.constr.Win(i).InputStruct2=WinInputGen_Uveg8b(Input.header.DataFolder
);
Input.constr.Win(i).ControllLogic='default';%switch between window states
Input.constr.Win(i).Parent=1;%ID of the D1 construction

%whole window
Input.constr.Win(i).Aw=0;%[m2] - area of the whole window (use the exterior
dimensions of the frame)
%only specify if using simple model
Input.constr.Win(i).Uw=[1.699   0.888];%[W/m2K] - standard Uw,inst (0/20
[°C], T=Tmr, including installation Thermal Bridges)
%glazed area
Input.constr.Win(i).fg=0.78;%[-] Glazing Area Fraction
Input.constr.Win(i).Ug=[1.759   0.82];%[W/m2K] - standard Ug (0/20 [°C],
T=Tmr)
```

```
Input.constr.Win(i).g=0;%[-] - only specify if using simple model
%frame
Input.constr.Win(i).Af=0;%[W/m2K] - only specify if using simple model
Input.constr.Win(i).Uf=0;%[W/m2K] - only specify if using simple model
%thermal bridges
Input.constr.Win(i).Psi=0;%[W/mK] - only specify if using simple model
Input.constr.Win(i).leg=0;%[m] - only specify if using simple model
%geometry
Input.constr.Win(i).GeomInputMode=2;
Input.constr.Win(i).IntLocalVertices=[...
    1.5996, 0,  0.845;...
    3.7076, 0,  0.845;...
    3.7076, 0,  4.736;...
    1.5996, 0,  4.736;...
    1.5996, 0,  0.845];
Input.constr.Win(i).ExtLocalVertices=[...
    1.6936, 0,  0.92;...
    3.6136, 0,  0.92;...
    3.6136, 0,  3.7;...
    3.4850, 0,  4.18;...
    3.1336, 0,  4.5314;...
    2.6536, 0,  4.66;...
    2.1736, 0,  4.5314;...
    1.8222, 0,  4.18;...
    1.6939, 0,  3.7;...
    1.6936, 0,  0.92];
Input.constr.Win(i).RevealDepth=0.2685;%[m]
Input.constr.Win(i).BC1Air=0;           %BC 1 - air connection
Input.constr.Win(i).BC1IR=0;            %BC 1 - IR connection
Input.constr.Win(i).BC1Sol=1;           %BC 1 - Direct solar gain from the
Input.constr.Win(i).BC1Shade=0;         %BC 1 - Shading
Input.constr.Win(i).BC2Air=1;           %BC 2 - air connection
Input.constr.Win(i).BC2IR=1;            %BC 2 - IR connection
Input.constr.Win(i).BC2Sol=0;           %BC 2 - Direct solar gain from the
Input.constr.Win(i).BC2Shade=0;         %BC 2 - Shading

%::::::::::::::::::::::::::::::::::::::::::::::::::::::::::::::::::::::::::::
%% 7.3. Shading Polygons ..................................................
Input.stuff.numSPoly=0;   %number of Shading Polygons

%.........................................................................
%% 7.3.1. Eastern shading - southern vertical
i=1;
Input.constr.SPoly(i).Name='Eastern shading - southern vertical';
Input.constr.SPoly(i).Vertices=[...
    -11,    0,  0;...
    -11,    0,  5;...
    -11.5,  -7, 5;...
    -11.5,  -7, 0;...
    -11,    0,  0];

%::::::::::::::::::::::::::::::::::::::::::::::::::::::::::::::::::::::::::::
%% 7.4. Thermal Bridges ...................................................
Input.stuff.numTBridgeGroups=1; %number of thermal bride groups

%.........................................................................
%% 7.4.1. Thermal Bridges of Zone 1
i=1;
Input.constr.TBridge(i).L=...%[W/K] - summa(Psii * li)
    0.5*0.2804*(2*5.71)+...%partition wall details
    0.5*0.154*(2*4.6);%slab-to-wall connections
```

```
Input.constr.TBridge(i).Parent=1;

%:::::::::::::::::::::::::::::::::::::::::::::::::::::::::::::::::::::::::
%% 7.5. Flow elements ....................................................
Input.stuff.numFE=3;   %number of flow elements

%.......................................................................
%% 7.5.1. Western window's cracks - bottom
i=1;
Input.constr.FE(i).Name='Western window bottom half';
Input.constr.FE(i).Type='crack';%Mode: 'crack' 'orifice'
Input.constr.FE(i).a=0.5*4.68;%[m3/hPa^2/3] - flow coefficeint V=a*DP^(2/3)
Input.constr.FE(i).n=0.6667;%[-] - flow exponent
Input.constr.FE(i).Z=1.82;%[m] - height above Zone reference
%Input.constr.FE(i).Height=1.95;%[m]
Input.constr.FE(i).H=-0.96;%[m] - height above neutral plane
Input.constr.FE(i).Parent=1;% ID of Parent D1 construction - to get the
azimuth angle
Input.constr.FE(i).BC1Air=0;           %BC 1 - air connection
Input.constr.FE(i).BC2Air=1;           %BC 2 - air connection

%.......................................................................
%% 7.5.2. Western window's cracks - top
i=2;
Input.constr.FE(i).Name='Western window top half';
Input.constr.FE(i).Type='crack';%Mode: 'crack' 'orifice'
Input.constr.FE(i).a=0.5*4.68;%[m3/hPa^2/3] - flow coefficeint V=a*DP^(2/3)
Input.constr.FE(i).n=0.6667;%[-] - flow exponent
Input.constr.FE(i).Z=3.76;%[m] - height above Zone reference
%Input.constr.FE(i).Height=1.95;%[m]
Input.constr.FE(i).H=0.96;%[m] - height above neutral plane
Input.constr.FE(i).Parent=1;% ID of Parent D1 construction - to get the
azimuth angle
Input.constr.FE(i).BC1Air=0;           %BC 1 - air connection
Input.constr.FE(i).BC2Air=1;           %BC 2 - air connection

%.......................................................................
%% 7.5.3. Western window opening
i=3;
Input.constr.FE(i).Name='Western window opening';
Input.constr.FE(i).Type='orifice';%Mode: 'crack' 'orifice'
Input.constr.FE(i).A=2;%[m2] - opening area
Input.constr.FE(i).Cd=0.65;%[-] - discharge coefficient
Input.constr.FE(i).OpeningSchedule=5;%window opening schedule
Input.constr.FE(i).Z=2.27;%[m] - height of opening center above Zone ref.
Input.constr.FE(i).Height=2.7;%[m] - height of the opening
Input.constr.FE(i).Parent=1;% ID of Parent D1 construction - to get the
azimuth angle

Input.constr.FE(i).BC1Air=0;           %BC 1 - air connection
Input.constr.FE(i).BC2Air=1;           %BC 2 - air connection

%% 8. Zone Definitions ---------------------------------------------------
%%%%%%%%%%%%%%%%%%%%%%%%%%%%%%%%%%%%%%%%%%%%%%%%%%%%%%%%%%%%%%%%%%%%%%%%
%/////////////////////////////////////////////////////////////////////////
%%%%%%%%%%%%%%%%%%%%%%%%%%%%%%%%%%%%%%%%%%%%%%%%%%%%%%%%%%%%%%%%%%%%%%%%
%/////////////////////////////////////////////////////////////////////////
%%%%%%%%%%%%%%%%%%%%%%%%%%%%%%%%%%%%%%%%%%%%%%%%%%%%%%%%%%%%%%%%%%%%%%%%

%.......................................................................
```

```
%Zone1
Input.Zone(1).A=23.36;%[m2]
Input.Zone(1).H=5.92;%[m]
Input.Zone(1).Href=8;%[m] reference height of Zone floor above ground level
needed for detailed ventilation calculation
%Input.zone(1).V=0;%manual override, default: A*H
Input.Zone(1).mExtra=0;%[kg]
Input.Zone(1).cExtra=0;%[J/kgK]
Input.Zone(1).HSPSchedule=1;%Heating Setpoint - normal working week heating
Input.Zone(1).CSPSchedule=2;%Cooling Setpoint - normal working week cooling
Input.Zone(1).OccupLoad=100;%[W] Occupancy Load - one person, writing
Input.Zone(1).OccupSchedule=3;%Occupancy Fractional Schedule - office
normal working week occupancy
Input.Zone(1).OccupFracRad=0.5;%[-] - radiant fraction (longwave infrared)
Input.Zone(1).EquipSLoad=5.8;%[W/m2] Equipment Specific Load (for 1m2)
Input.Zone(1).EquipSchedule=4;%Equipment Fractional schedule - office
normal week lighting and plug load
Input.Zone(1).EquipFracRad=0.6;%[-] - radiant fraction (longwave infrared)
Input.Zone(1).LightSLoad=10;%[W/m2] Light Specific Load (for 1m2)
Input.Zone(1).LightSchedule=4;%Lighting Fractional Schedule - office normal
week lighting and plug load
Input.Zone(1).LightFracRad=0.6;%[-] - radiant fraction (longwave infrared)
Input.Zone(1).T0=20;%[°C]
Input.Zone(1).FloorD1ID=6;%the ID of the floor D1 construction

%% 9. HVAC systems ------------------------------------------------------
%%%%%%%%%%%%%%%%%%%%%%%%%%%%%%%%%%%%%%%%%%%%%%%%%%%%%%%%%%%%%%%%%%%%%%%%
%//////////////////////////////////////////////////////////////////////////
%%%%%%%%%%%%%%%%%%%%%%%%%%%%%%%%%%%%%%%%%%%%%%%%%%%%%%%%%%%%%%%%%%%%%%%%
%//////////////////////////////////////////////////////////////////////////
%%%%%%%%%%%%%%%%%%%%%%%%%%%%%%%%%%%%%%%%%%%%%%%%%%%%%%%%%%%%%%%%%%%%%%%%

%::::::::::::::::::::::::::::::::::::::::::::::::::::::::::::::::::::::::::
%% 9.1. Heating ..........................................................
Input.HVAC.heating.Mode='ideal';%Mode:   'none'  'ideal'  'P' 'radiator'
Input.HVAC.heating.Availability=...
    [0 1 1 0 0 0;...
    0 4 15 23 59 59;...
    0 10 15 0 0 0;...
    0 12 31 23 59 59];
%ideal
Input.HVAC.heating.ideal.Qmax=500;% [W/m2] apr. 80 [W/m3]
Input.HVAC.heating.ideal.FracRad=0;%radiative fraction of the heating power

%::::::::::::::::::::::::::::::::::::::::::::::::::::::::::::::::::::::::::
%% 9.2. Ventilation ......................................................

Input.HVAC.ventillation.ACR=0.5;%[1/h]

%::::::::::::::::::::::::::::::::::::::::::::::::::::::::::::::::::::::::::
%% 9.3. Cooling ..........................................................

Input.HVAC.cooling.Mode='ideal';%Mode:   'none'  'ideal'
Input.HVAC.cooling.Availability=...
    [0 4 16 0 0 0;...
    0 10 14 23 59 59];
%ideal
Input.HVAC.cooling.ideal.Qmax=200;%[W/m2] - maximum cooling load of the
system
Input.HVAC.cooling.ideal.FracRad=0;%[-] - fraction of radiation
```

```
%% 10. Schedules ----------------------------------------------------------
%%%%%%%%%%%%%%%%%%%%%%%%%%%%%%%%%%%%%%%%%%%%%%%%%%%%%%%%%%%%%%%%%%%%%%%%
%//////////////////////////////////////////////////////////////////////////
%%%%%%%%%%%%%%%%%%%%%%%%%%%%%%%%%%%%%%%%%%%%%%%%%%%%%%%%%%%%%%%%%%%%%%%%
%//////////////////////////////////////////////////////////////////////////
%%%%%%%%%%%%%%%%%%%%%%%%%%%%%%%%%%%%%%%%%%%%%%%%%%%%%%%%%%%%%%%%%%%%%%%%

%% 10.1. Temperature schedules ..........................................

%Temperature Setpoint Schedules- hourly
%1 - constant 20
%2 - 22 with setback (19)
%3 - constant 18
%4 - constant 26
%5 - constant 99
Input.schedule.Tsp_hourly=...
    [20,    19,     18,     99,     99;...%0-1
    20,     19,     18,     99,     99;...%1-2
    20,     19,     18,     99,     99;...%2-3
    20,     19,     18,     99,     99;...%3-4
    20,     19,     18,     99,     99;...%4-5
    20,     19,     18,     99,     99;...%5-6
    20,     22,     18,     25,     99;...%6-7
    20,     22,     18,     25,     99;...%7-8
    20,     22,     18,     25,     99;...%8-9
    20,     22,     18,     25,     99;...%9-10
    20,     22,     18,     25,     99;...%10-11
    20,     22,     18,     25,     99;...%11-12
    20,     22,     18,     25,     99;...%12-13
    20,     22,     18,     25,     99;...%13-14
    20,     22,     18,     25,     99;...%14-15
    20,     22,     18,     25,     99;...%15-16
    20,     22,     18,     25,     99;...%16-17
    20,     22,     18,     25,     99;...%17-18
    20,     22,     18,     25,     99;...%18-19
    20,     22,     18,     25,     99;...%19-20
    20,     22,     18,     25,     99;...%20-21
    20,     19,     18,     99,     99;...%21-22
    20,     19,     18,     99,     99;...%22-23
    20,     19,     18,     99,     99];  %23-24

%Temperature Setpoint Schedules - daily
%1 - normal working week heating
%2 - normal working week cooling
%3 - xx
%4 - xx
Input.schedule.Tsp_daily=...
    [2,     4,      4,      2;...%Monday
    2,      4,      4,      2;...%Tuesday
    2,      4,      4,      2;...%Wednesay
    2,      4,      4,      2;...%Thursday
    2,      4,      4,      2;...%Friday
    3,      5,      4,      2;...%Saturday
    3,      5,      4,      2];  %Sunday
```

```
%% 10.1. Fractional schedules ........................................

%Fractional Schedules - hourly
%1 - full day off
%2 - full day on
%3 - office occupancy - normal
%4 - office occupancy - light
%5 - office lighting and plug loads - normal
%6 - office lighting and plug loads - light
%7 - office twice daily 5min window opening
Input.schedule.Frac_hourly=...
    [0,     1,      0,      0,      0.05,   0.05,       0;...    %0-1
    0,      1,      0,      0,      0.05,   0.05,       0;...    %1-2
    0,      1,      0,      0,      0.05,   0.05,       0;...    %2-3
    0,      1,      0,      0,      0.05,   0.05,       0;...    %3-4
    0,      1,      0,      0,      0.1,    0.05,       0;...    %4-5
    0,      1,      0,      0,      0.1,    0.05,       0;...    %5-6
    0,      1,      0.1,    0.1,    0.1,    0.1,        0;...    %6-7
    0,      1,      0.2,    0.1,    0.3,    0.1,        0;...    %7-8
    0,      1,      0.9,    0.5,    0.9,    0.3,        0.25;... %8-9
    0,      1,      0.9,    0.5,    0.9,    0.30,       0;...    %9-10
    0,      1,      0.9,    0.5,    0.9,    0.3,        0;...    %10-11
    0,      1,      0.9,    0.5,    0.9,    0.3,        0;...    %11-12
    0,      1,      0.9,    0.5,    0.5,    0.15,       0;...    %12-13
    0,      1,      0.9,    0.5,    0.9,    0.15,       0;...    %13-14
    0,      1,      0.9,    0.1,    0.9,    0.15,       0.25;... %14-15
    0,      1,      0.9,    0.1,    0.5,    0.15,       0;...    %15-16
    0,      1,      0.9,    0.1,    0.5,    0.15,       0;...    %16-17
    0,      1,      0.7,    0,      0.3,    0.05,       0;...    %17-18
    0,      1,      0.4,    0,      0.3,    0.05,       0;...    %18-19
    0,      1,      0.4,    0,      0.3,    0.05,       0;...    %19-20
    0,      1,      0.2,    0,      0.2,    0.05,       0;...    %20-21
    0,      1,      0.2,    0,      0.2,    0.05,       0;...    %21-22
    0,      1,      0.1,    0,      0.1,    0.05,       0;...    %22-23
    0,      1,      0.1,    0,      0.05,   0.05,       0];      %23-24

%Fractional Schedules - daily
%1 - allways off
%2 - allways on
%3 - office normal working week occupancy
%4 - office normal working week lighting and plug loads
%5 - office normal working week window opnening
Input.schedule.Frac_daily=...
    [1, 2,  3,  5   7;...%Monday
    1,  2,  3,  5   7;...%Tuesday
    1,  2,  3,  5   7;...%Wednesay
    1,  2,  3,  5   7;...%Thursday
    1,  2,  3,  5   7;...%Friday
    1,  2,  4,  6   7;...%Saturday
    1,  2,  4,  6   1];  %Sunday
```

F.2 EPICAC BE – Graphical output example

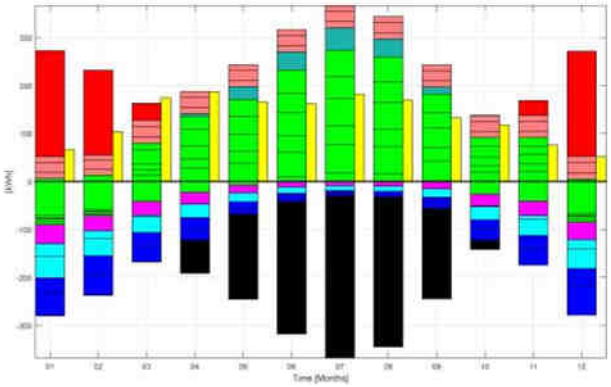

Fig. 518. – Scenario C – Monthly heat balance

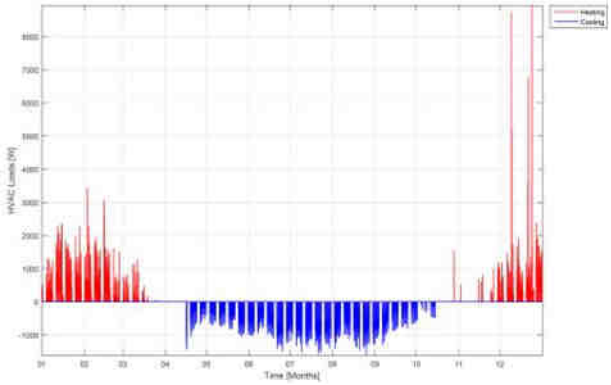

Fig. 519. – Scenario C – HVAC loads

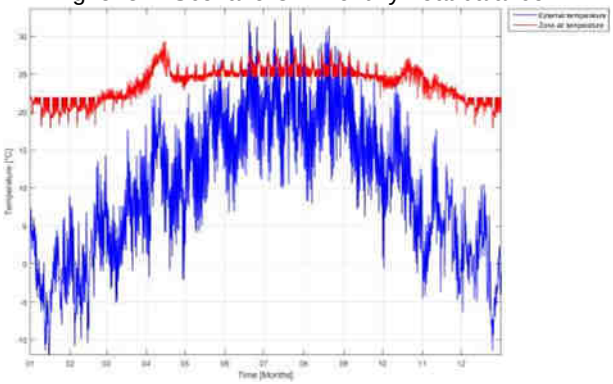

Fig. 520. – Scenario C – T_e, T_{zone}

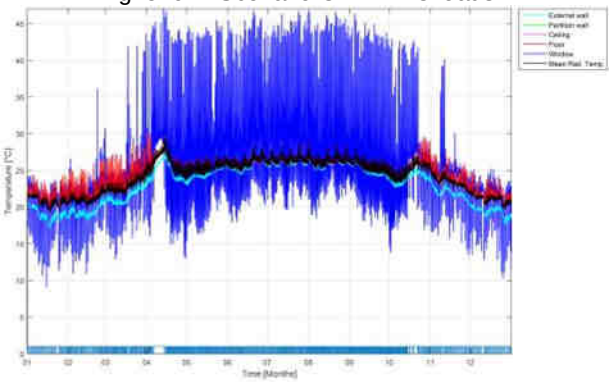

Fig. 521. – Scenario C – T_{si}

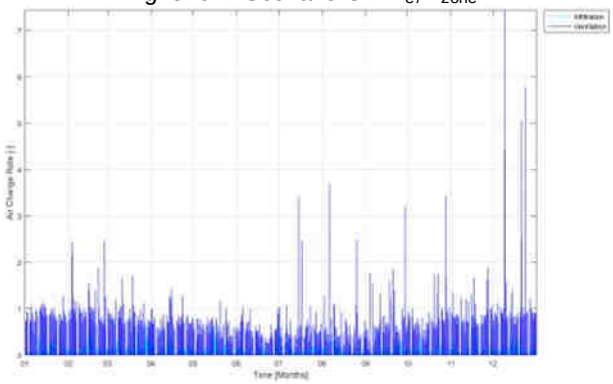

Fig. 522. – Scenario C – ACH

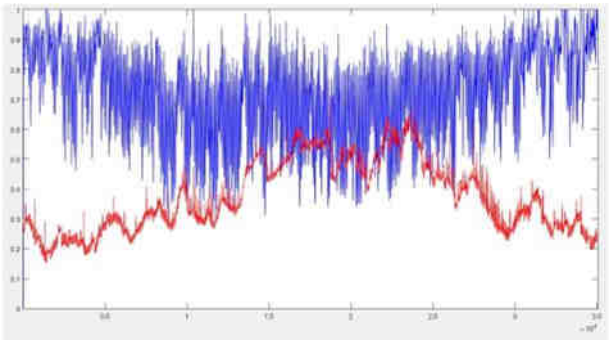

Fig. 523. – Scenario C – Rh_i, Rh_e

F.3 Sensitivity Study

F.3.1 Sensitivity Study 1 – sensitivity to model parameters

No.	parameter	unit	min.	max	distr.
1	$h_{c,e,wall}$ – external convective heat transfer coefficient	[W/m²K]	15	35	uniform
2	α_e – external shortwave absorption coefficient	[-]	0.3	0.8	uniform
3	$h_{c,i,wall}$ – internal convective heat transfer coefficient, walls	[W/m²K]	1.5	4	uniform
4	$h_{c,i,floor}$ – internal convective heat transfer coefficient, floor	[W/m²K]	1	2	uniform
5	$\alpha_{i,floor}$ – internal shortwave absorption coefficient, floor	[-]	0.6	0.8	uniform
6	$h_{c,i,ceiling}$ – internal convective heat transfer coefficient, ceiling	[W/m²K]	3	6	uniform
7	$h_{c,e,window}$ – external convective heat transfer coefficient, window	[W/m²K]	15	35	uniform
8	$h_{c,i,window}$ – internal convective heat transfer coefficient, window	[W/m²K]	1.5	4	uniform
9	ACH – air change rate	[1/h]	0.5	2	uniform
10	Q_{occup} – occupancy load	[W]	50	100	uniform
11	Q_{equip} – equipment load	[W/m²]	4	8	uniform
12	Q_{light} – lighting load	[W/m²]	7	20	uniform
13	T_{hsp} – heating setpoint	[°C]	19	24	uniform
14	$\Delta T_{hsp,night}$ – reduction of heating setpoint during the night	[°C]	0	-4	uniform
15	$\Delta T_{hsp,weekend}$ – reduction of heating setpoint during the weekend	[°C]	0	-4	uniform
16	T_{csp} – cooling setpoint	[°C]	23	28	uniform
17	$\Delta T_{csp,night}$ – reduction of cooling setpoint during the night	[°C]	0	1	uniform
18	$C_{on/off,weekend}$ – cooling on/off during the weekend	yes/no	0	1	digital

Table 26 – sensitivity study 1 –parameter set

rank	No.	parameter	μ	μ*	σ
1	9	ACH	4.84E+00	4.84E+00	5.71E-01
2	13	T_{hsp}	1.86E+00	1.86E+00	4.42E-01
3	12	Q_{light}	-4.25E-01	4.25E-01	2.13E-02
4	14	$\Delta T_{hsp,night}$	4.13E-01	4.13E-01	1.38E-01
5	15	$\Delta T_{hsp,weekend}$	3.78E-01	3.78E-01	1.35E-01
6	8	$h_{c,i,window}$	1.88E-01	1.88E-01	3.82E-02
7	11	Q_{equip}	-1.18E-01	1.18E-01	5.07E-03
8	3	$h_{c,i,wall}$	1.13E-01	1.13E-01	4.80E-02
9	7	$h_{c,e,window}$	8.16E-02	8.16E-02	2.66E-02
10	10	Q_{occup}	-8.05E-02	8.05E-02	3.29E-03
11	1	$h_{c,e,wall}$	6.45E-02	6.45E-02	1.67E-02
12	2	α_e	-5.77E-02	5.77E-02	1.19E-02
13	6	$h_{c,i,ceiling}$	3.38E-02	3.38E-02	1.16E-02
14	4	$h_{c,i,floor}$	-7.20E-03	7.20E-03	5.09E-03
15	16	T_{csp}	-5.80E-03	5.80E-03	5.68E-03
16	5	$\alpha_{i,floor}$	4.90E-03	4.90E-03	1.98E-03
17	18	$C_{on/off,weekend}$	3.00E-04	3.00E-04	2.47E-04

Table 27 – sensitivity study 1 – sensitivity results for Annual Heating

rank	No.	parameter	μ	μ*	σ
1	16	T_{csp}	4.84E+00	4.84E+00	5.71E-01
2	9	ACH	1.86E+00	1.86E+00	4.42E-01
3	12	Q_{light}	-4.25E-01	4.25E-01	2.13E-02
4	18	$C_{on/off,weekend}$	4.13E-01	4.13E-01	1.38E-01
5	2	α_e	3.78E-01	3.78E-01	1.35E-01
6	11	Q_{equip}	1.88E-01	1.88E-01	3.82E-02
7	1	$h_{c,e,wall}$	-1.18E-01	1.18E-01	5.07E-03
8	10	Q_{occup}	1.13E-01	1.13E-01	4.80E-02
9	17	$\Delta T_{csp,night}$	8.16E-02	8.16E-02	2.66E-02
10	3	$h_{c,i,wall}$	-8.05E-02	8.05E-02	3.29E-03
11	8	$h_{c,i,window}$	6.45E-02	6.45E-02	1.67E-02
12	7	$h_{c,e,window}$	-5.77E-02	5.77E-02	1.19E-02
13	5	$\alpha_{i,floor}$	3.38E-02	3.38E-02	1.16E-02
14	4	$h_{c,i,floor}$	-7.20E-03	7.20E-03	5.09E-03
15	6	$h_{c,i,ceiling}$	-5.80E-03	5.80E-03	5.68E-03
16	13	T_{hsp}	4.90E-03	4.90E-03	1.98E-03
17	15	$\Delta T_{hsp,weekend}$	3.00E-04	3.00E-04	2.47E-04

Table 28 – sensitivity study 1 – sensitivity results for Annual Cooling

F.3.2 Sensitivity Study 1b – sensitivity to model parameters, reduced ACH

No.	parameter	unit	min.	max	distr.
1	$h_{c,e,wall}$ – external convective heat transfer coefficient	[W/m²K]	15	35	uniform
2	α_e – external shortwave absorption coefficient	[-]	0.3	0.8	uniform
3	$h_{c,i,wall}$ – internal convective heat transfer coefficient, walls	[W/m²K]	1.5	4	uniform
4	$h_{c,i,floor}$ – internal convective heat transfer coefficient, floor	[W/m²K]	1	2	uniform
5	$\alpha_{i,floor}$ – internal shortwave absorption coefficient, floor	[-]	0.6	0.8	uniform
6	$h_{c,i,ceiling}$ – internal convective heat transfer coefficient, ceiling	[W/m²K]	3	6	uniform
7	$h_{c,e,window}$ – external convective heat transfer coefficient, window	[W/m²K]	15	35	uniform
8	$h_{c,i,window}$ – internal convective heat transfer coefficient, window	[W/m²K]	1.5	4	uniform
9	ACH – air change rate	[1/h]	0.1	1	uniform
10	Q_{occup} – occupancy load	[W]	50	100	uniform
11	Q_{equip} – equipment load	[W/m²]	4	8	uniform
12	Q_{light} – lighting load	[W/m²]	7	20	uniform
13	T_{hsp} – heating setpoint	[°C]	19	24	uniform
14	$\Delta T_{hsp,night}$ – reduction of heating setpoint during the night	[°C]	0	-4	uniform
15	$\Delta T_{hsp,weekend}$ – reduction of heating setpoint during the weekend	[°C]	0	-4	uniform
16	T_{csp} – cooling setpoint	[°C]	23	28	uniform
17	$\Delta T_{csp,night}$ – reduction of cooling setpoint during the night	[°C]	0	1	uniform
18	$C_{on/off,weekend}$ – cooling on/off during the weekend	yes/no	0	1	digital

Table 29 – sensitivity study 1b – sensitivity to model parameters (reduced ACH) – parameter set

rank	No.	parameter	μ	μ*	σ
1	9	ACH	2.59E+00	2.59E+00	3.58E-01
2	13	T_{hsp}	1.35E+00	1.35E+00	2.90E-01
3	12	Q_{light}	-4.03E-01	4.03E-01	2.64E-02
4	14	$\Delta T_{hsp,night}$	2.70E-01	2.70E-01	1.30E-01
5	15	$\Delta T_{hsp,weekend}$	2.59E-01	2.59E-01	1.52E-01
6	8	$h_{c,i,window}$	1.89E-01	1.89E-01	3.35E-02
7	11	Q_{equip}	-1.14E-01	1.14E-01	6.13E-03
8	3	$h_{c,i,wall}$	1.07E-01	1.07E-01	4.10E-02
9	10	Q_{occup}	-7.52E-02	7.52E-02	4.87E-03
10	7	$h_{c,e,window}$	6.82E-02	6.82E-02	2.24E-02
11	1	$h_{c,e,wall}$	5.86E-02	5.86E-02	1.88E-02
12	2	α_e	-5.17E-02	5.17E-02	1.25E-02
13	6	$h_{c,i,ceiling}$	3.10E-02	3.10E-02	9.55E-03
14	16	T_{csp}	-1.13E-02	1.13E-02	6.05E-03
15	4	$h_{c,i,floor}$	-8.31E-03	8.31E-03	3.74E-03
16	5	$\alpha_{i,floor}$	4.04E-03	4.04E-03	1.74E-03
17	18	$C_{on/off,weekend}$	3.99E-04	3.99E-04	2.36E-04
18	17	$\Delta T_{csp,night}$	8.22E-05	8.22E-05	6.13E-05

Table 30 – sensitivity study 1b – sensitivity results for Annual Heating

rank	No.	parameter	μ	μ*	σ
1	16	T_{csp}	-7.15E-01	7.15E-01	5.39E-02
2	9	ACH	-5.13E-01	5.13E-01	9.27E-02
3	12	Q_{light}	2.80E-01	2.80E-01	5.55E-02
4	18	$C_{on/off,weekend}$	1.33E-01	1.33E-01	4.97E-02
5	2	α_e	8.01E-02	8.01E-02	2.29E-02
6	11	Q_{equip}	7.96E-02	7.96E-02	1.44E-02
7	1	$h_{c,e,wall}$	-6.06E-02	6.06E-02	3.14E-02
8	17	$\Delta T_{csp,night}$	5.63E-02	5.63E-02	3.34E-02
9	10	Q_{occup}	5.62E-02	5.62E-02	1.19E-02
10	8	$h_{c,i,window}$	-1.99E-02	1.99E-02	1.07E-02
11	3	$h_{c,i,wall}$	1.77E-02	1.88E-02	1.95E-02
12	7	$h_{c,e,window}$	-1.26E-02	1.26E-02	6.31E-03
13	13	T_{hsp}	1.05E-02	1.05E-02	1.18E-02
14	6	$h_{c,i,ceiling}$	4.01E-03	6.71E-03	8.32E-03
15	5	$\alpha_{i,floor}$	-6.04E-03	6.04E-03	4.82E-03
16	4	$h_{c,i,floor}$	4.29E-03	5.52E-03	4.97E-03
17	14	$\Delta T_{hsp,night}$	2.71E-03	2.71E-03	4.92E-03
18	15	$\Delta T_{hsp,weekend}$	8.22E-05	8.22E-05	6.13E-05

Table 31 – sensitivity study 1b – sensitivity results for Annual Cooling

F.3.3 Sensitivity Study 2 – sensitivity of ventilation and infiltration models

No.	parameter	unit	min.	max	distr.
1	H – building height	[m]	16.5	27.5	uniform
2	c_{p1} – pressure coefficient 1 – windward side	[-]	0.7	0.9	uniform
3	c_{p2} – pressure coefficient 2 – leeward side	[-]	-0.01	-0.1	uniform
4	$c_{p3,4}$ – pressure coefficient 2,3 – tangential	[-]	-0.05	-0.15	uniform
5	a_{window} – window leakage coefficient	[m^3/hm^2Pa]	25.6	38.4	uniform
6	n_{window} – window pressure exponent	[-]	0.6	0.8	uniform
7	y_{above} – height above neutral plane	[m]	0.72	1.2	uniform
8	y_{under} – height under neutral plane	[m]	0.72	1.2	uniform
9	A_{area} – surface area of opening (window)	[m^2]	1.5	2.5	uniform
10	$H_{opening}$ – height of opening (window)	[m]	1.7	2.84	uniform
11	t_{open} – windows opened twice daily for t_{open}	[min]	5	20	uniform
12	T_{hsp} – heating setpoint	[°C]	19	24	uniform
13	$\Delta T_{hsp,night}$ – reduction of heating setpoint during the night	[°C]	0	-4	uniform
14	$\Delta T_{hsp,weekend}$ – reduction of heating setpoint during the weekend	[°C]	0	-4	uniform
15	T_{csp} – cooling setpoint	[°C]	23	28	uniform
16	$C_{on/off,night}$ – cooling on/off during the night	yes/no	0	1	digital
17	$C_{on/off,weekend}$ – cooling on/off during the weekend	yes/no	0	1	digital

Table 32 – sensitivity study 2 – sensitivity of ventilation and infiltration models – parameter set

rank	No.	parameter	μ	μ*	σ
1	12	T_{hsp}	1.35E+00	1.35E+00	1.43E-01
2	11	t_{open}	5.77E-01	5.77E-01	1.27E-01
3	5	a_{window}	4.79E-01	4.79E-01	8.11E-02
4	6	n_{window}	3.06E-01	3.06E-01	7.72E-02
5	14	$\Delta T_{hsp,weekend}$	2.57E-01	2.57E-01	1.36E-01
6	9	A_{area}	2.49E-01	2.49E-01	1.11E-01
7	13	$\Delta T_{hsp,night}$	2.34E-01	2.34E-01	1.46E-01
8	2	c_{p1}	1.80E-01	1.80E-01	4.84E-02
9	1	H	1.49E-01	1.49E-01	4.60E-02
10	10	$H_{opening}$	8.81E-02	8.81E-02	3.73E-02
11	8	y_{under}	-8.49E-02	8.49E-02	2.30E-02
12	3	c_{p2}	-2.94E-02	6.25E-02	6.65E-02
13	4	$c_{p3,4}$	3.23E-02	3.91E-02	5.17E-02
14	15	T_{csp}	-2.48E-02	2.48E-02	5.66E-03
15	17	$C_{on/off,weekend}$	1.27E-03	1.27E-03	3.60E-04
16	16	$C_{on/off,night}$	9.06E-05	9.06E-05	7.50E-05
17	7	y_{above}	-7.89E-10	8.04E-10	1.37E-09

Table 33 – sensitivity study 2 – sensitivity results for Annual Heating

rank	No.	parameter	μ	μ*	σ
1	15	T_{csp}	-8.87E-01	8.87E-01	4.21E-02
2	17	$C_{on/off,weekend}$	2.33E-01	2.33E-01	4.69E-02
3	5	a_{window}	-1.28E-01	1.28E-01	9.45E-03
4	16	$C_{on/off,night}$	8.11E-02	8.11E-02	4.30E-02
5	6	n_{window}	-7.17E-02	7.17E-02	9.06E-03
6	11	t_{open}	-6.81E-02	6.81E-02	1.13E-02
7	2	c_{p1}	-4.89E-02	4.89E-02	8.33E-03
8	1	H	-4.20E-02	4.20E-02	6.99E-03
9	9	A_{area}	-2.70E-02	2.70E-02	8.62E-03
10	12	T_{hsp}	2.56E-02	2.56E-02	8.68E-03
11	8	y_{under}	1.54E-02	1.54E-02	2.26E-03
12	3	c_{p2}	5.76E-03	1.22E-02	1.28E-02
13	4	$c_{p3,4}$	-8.36E-03	9.57E-03	1.22E-02
14	10	$H_{opening}$	-8.83E-03	8.83E-03	2.86E-03
15	13	$\Delta T_{hsp,night}$	7.17E-03	7.17E-03	7.66E-03
16	14	$\Delta T_{hsp,weekend}$	3.96E-03	3.96E-03	3.69E-03
17	7	y_{above}	2.22E-04	2.22E-04	1.15E-04

Table 34 – sensitivity study 2 – sensitivity results for Annual Cooling

rank	No.	parameter	μ	μ*	σ
1	5	a_{window}	1.51E-01	1.51E-01	1.68E-02
2	6	n_{window}	1.04E-01	1.04E-01	2.02E-02
3	2	c_{p1}	5.34E-02	5.34E-02	1.37E-02
4	1	H	4.93E-02	4.93E-02	1.23E-02
5	8	y_{under}	-2.22E-02	2.22E-02	4.34E-03
6	3	c_{p2}	-9.04E-03	1.90E-02	1.99E-02
7	4	$c_{p3,4}$	9.66E-03	1.21E-02	1.56E-02
8	12	T_{hsp}	8.39E-03	8.39E-03	4.01E-03
9	14	$\Delta T_{hsp,weekend}$	1.64E-03	1.64E-03	1.15E-03
10	13	$\Delta T_{hsp,night}$	1.43E-03	1.43E-03	1.46E-03
11	15	T_{csp}	1.69E-04	1.69E-04	7.51E-05
12	11	t_{open}	-1.06E-04	1.06E-04	7.99E-05
13	9	A_{area}	-3.77E-05	3.77E-05	1.39E-05
14	10	$H_{opening}$	-1.14E-05	1.14E-05	5.67E-06
15	17	$C_{on/off,weekend}$	-7.51E-06	7.51E-06	2.53E-06
16	16	$C_{on/off,night}$	-4.78E-07	4.78E-07	4.14E-07
17	7	y_{above}	7.04E-12	7.06E-12	1.47E-11

Table 35 – sensitivity study 2 – sensitivity results for $ACH_{infiltration}$

rank	No.	parameter	μ	μ*	σ
1	11	t_{open}	1.63E-01	1.63E-01	2.97E-02
2	9	A_{area}	6.90E-02	6.90E-02	2.91E-02
3	10	$H_{opening}$	2.33E-02	2.33E-02	9.40E-03
4	12	T_{hsp}	1.39E-02	1.39E-02	5.73E-03
5	14	$\Delta T_{hsp,weekend}$	2.02E-03	2.02E-03	1.23E-03
6	2	c_{p1}	1.99E-03	1.99E-03	9.64E-04
7	3	c_{p2}	-4.59E-04	9.88E-04	1.14E-03
8	1	H	-8.16E-04	8.16E-04	5.66E-04
9	4	$c_{p3,4}$	2.74E-04	4.85E-04	6.14E-04
10	13	$\Delta T_{hsp,night}$	2.93E-04	2.93E-04	3.04E-04
11	15	T_{csp}	2.30E-04	2.30E-04	1.24E-04
12	5	a_{window}	-1.83E-04	1.83E-04	8.11E-05
13	6	n_{window}	-7.14E-05	7.14E-05	3.73E-05
14	8	y_{under}	3.19E-05	3.19E-05	1.31E-05
15	17	$C_{on/off,weekend}$	-1.10E-05	1.10E-05	6.63E-06
16	16	$C_{on/off,night}$	-6.63E-07	6.63E-07	7.20E-07
17	7	y_{above}	9.48E-12	9.50E-12	2.05E-11

Table 36 – sensitivity study 2 – sensitivity results for $ACH_{ventilation}$

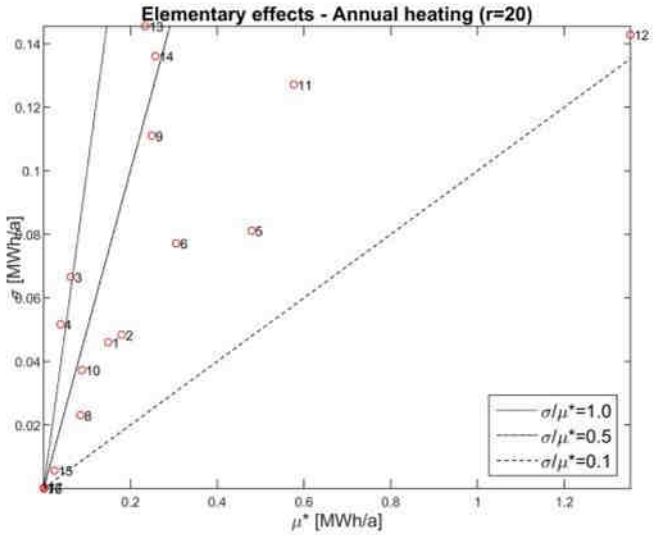

Fig. 524. – sensitivity study 1 – μ*/σ plot – Annual Heating

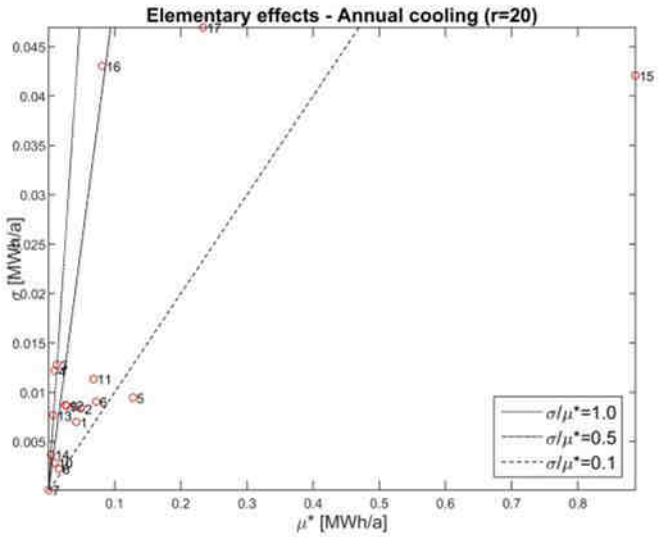

Fig. 525. – sensitivity study 1 – μ*/σ plot – Annual Cooling

F.3.4 Sensitivity Study 3 – sensitivity to model parameters – after refurbishment

No.	parameter	unit	min.	max	distr.
1	$h_{c,e}$ – external convective heat transfer coefficient	[W/m^{2}K]	15	35	uniform
2	α_e – external shortwave absorption coefficient	[-]	0.3	0.8	uniform
3	$h_{c,i,wall}$ – internal convective heat transfer coefficient, walls	[W/m^{2}K]	1.5	4	uniform
4	$h_{c,i,floor}$ – internal convective heat transfer coefficient, floor	[W/m^{2}K]	1	2	uniform
5	$\alpha_{i,floor}$ – internal shortwave absorption coefficient, floor	[-]	0.6	0.8	uniform
6	$h_{c,i,ceiling}$ – internal convective heat transfer coefficient, ceiling	[W/m^{2}K]	3	6	uniform
7	$h_{c,e,window}$ – external convective heat transfer coefficient, window	[W/m^{2}K]	15	35	uniform
8	$h_{c,i,window}$ – internal convective heat transfer coefficient, window	[W/m^{2}K]	1.5	4	uniform
9	a_{window} – window leakage coefficient	[m^3/hm^{2}Pa]	3.15	15.4	uniform
10	Cd – discharge coefficient	[-]	0.6	0.7	uniform
11	t_{open} – windows opened twice daily for t_{open}	[min]	5	15	uniform
12	Q_{occup} – occupancy load	[W]	50	100	uniform
13	Q_{equip} – equipment load	[W/m^2]	4	8	uniform
14	Q_{light} – lighting load	[W/m^2]	7	20	uniform
15	T_{hsp} – heating setpoint	[°C]	19	24	uniform
16	$\Delta T_{hsp,night}$ – reduction of heating setpoint during the night	[°C]	0	-4	uniform
17	$\Delta T_{hsp,weekend}$ – reduction of heating setpoint during the weekend	[°C]	0	-4	uniform
18	T_{csp} – cooling setpoint	[°C]	23	28	uniform
19	$\Delta T_{csp,night}$ – reduction of cooling setpoint during the night	[°C]	0	1	uniform
20	$C_{on/off,weekend}$ – cooling on/off during the weekend	yes/no	0	1	digital

Table 37 – sensitivity study 3 – sensitivity to model parameters after refurbishment – parameter set

rank	No.	parameter	μ	μ*	σ
1	15	T_{hsp}	5.78E-01	5.78E-01	8.69E-02
2	11	t_{open}	3.99E-01	3.99E-01	4.74E-02
3	9	a_{window}	3.73E-01	3.73E-01	5.48E-02
4	14	Q_{light}	-3.40E-01	3.40E-01	3.22E-02
5	13	Q_{equip}	-9.62E-02	9.62E-02	9.39E-03
6	17	$\Delta T_{hsp,weekend}$	9.29E-02	9.29E-02	1.13E-01
7	16	$\Delta T_{hsp,night}$	7.26E-02	7.26E-02	9.22E-02
8	3	$h_{c,i,wall}$	6.86E-02	6.86E-02	2.41E-02
9	12	Q_{occup}	-6.46E-02	6.46E-02	7.57E-03
10	1	$h_{c,e}$	5.89E-02	5.89E-02	2.08E-02
11	2	α_e	-4.05E-02	4.05E-02	8.32E-03
12	8	$h_{c,i,window}$	1.96E-02	1.96E-02	2.69E-03
13	6	$h_{c,i,ceiling}$	1.66E-02	1.66E-02	5.35E-03
14	18	T_{csp}	-1.60E-02	1.60E-02	5.83E-03
15	7	$h_{c,e,window}$	1.02E-02	1.02E-02	2.30E-03
16	5	$\alpha_{i,floor}$	3.80E-03	3.80E-03	1.43E-03

17	4	$h_{c,i,floor}$	-7.18E-04	1.50E-03	1.72E-03
18	20	$C_{on/off,weekend}$	1.71E-04	1.71E-04	8.35E-05
19	19	$\Delta T_{csp,night}$	3.83E-05	3.83E-05	4.10E-05

Table 38 – sensitivity study 3 – sensitivity results for Annual Heating

rank	No.	parameter	μ	μ*	σ
1	18	T_{csp}	-4.00E-01	4.00E-01	4.81E-02
2	14	Q_{light}	3.13E-01	3.13E-01	4.20E-02
3	2	α_e	9.78E-02	9.78E-02	2.69E-02
4	13	Q_{equip}	9.28E-02	9.28E-02	1.56E-02
5	9	a_{window}	-8.72E-02	8.72E-02	2.23E-02
6	1	$h_{c,e}$	-7.70E-02	7.70E-02	3.21E-02
7	12	Q_{occup}	6.19E-02	6.19E-02	8.65E-03
8	20	$C_{on/off,weekend}$	3.25E-02	3.25E-02	1.29E-02
9	11	t_{open}	-2.96E-02	2.96E-02	8.39E-03
10	7	$h_{c,e,window}$	-1.35E-02	1.35E-02	2.63E-03
11	8	$h_{c,i,window}$	1.20E-02	1.20E-02	1.89E-03
12	15	T_{hsp}	8.87E-03	8.87E-03	4.86E-03
13	19	$\Delta T_{csp,night}$	8.68E-03	8.68E-03	5.73E-03
14	3	$h_{c,i,wall}$	-4.88E-03	7.83E-03	7.90E-03
15	4	$h_{c,i,floor}$	-5.69E-03	5.69E-03	2.74E-03
16	17	$\Delta T_{hsp,weekend}$	2.93E-03	2.93E-03	4.48E-03
17	6	$h_{c,i,ceiling}$	2.64E-03	2.64E-03	1.61E-03
18	16	$\Delta T_{hsp,night}$	1.90E-03	1.90E-03	4.13E-03
19	5	$\Delta T_{csp,night}$	-1.57E-03	1.57E-03	5.65E-04

Table 39 – sensitivity study 3 – sensitivity results for Annual Cooling

F.3.5 Sensitivity Study 4 – sensitivity of scenario ranking to model parameters

No.	**parameter**	**unit**	**min.**	**max**	**distr.**
1	$h_{c,e}$ – external convective heat transfer coefficient	[W/m^{2}K]	19.2	28.8	uniform
2	α_e – external shortwave absorption coefficient	[-]	0.48	0.72	uniform
3	$h_{c,i,wall}$ – internal convective heat transfer coefficient, walls	[W/m^{2}K]	2.528	3.792	uniform
4	a_{window} – window leakage coefficient	[m^3/hm^{2}Pa]	3.744	5.616	uniform
5	opening schedule 2*n minutes a day	[min]	12	18	uniform
6	Q_{occup} – occupancy load	[W]	80	120	uniform
7	Q_{equip} – equipment load	[W/m^2]	4.64	6.96	uniform
8	Q_{light} – lighting load	[W/m^2]	8	12	uniform
9	T_{hsp} – heating setpoint	[°C]	20	24	uniform
10	$\Delta T_{hsp,night}$ – reduction of heating setpoint during the night	[°C]	-1	-5	uniform
11	$\Delta T_{hsp,weekend}$ – reduction of heating setpoint during the weekend	[°C]	0	-4	uniform
12	T_{csp} – cooling setpoint	[°C]	23	27	uniform

Table 40 – sensitivity study 4 – sensitivity of scenario ranking to model parameters – parameter set